

**ON THE MECHANISMS
OF NON-PHOTOCHEMICAL QUENCHING
IN PLANTS AND DIATOMS**

Inaugural-Dissertation

zur

Erlangung des Doktorgrades der
Mathematisch-Naturwissenschaftlichen Fakultät
der Heinrich-Heine-Universität Düsseldorf

vorgelegt von

Yuliya Miloslavina

aus Valujki

November 2008

Aus dem Max-Planck-Institut für Bioanorganische Chemie

Gedruckt mit der Genehmigung der
Mathematisch-Naturwissenschaftlichen Fakultät der
Heinrich-Heine-Universität Düsseldorf

Referent: Prof. Dr. A.R. Holzwarth

Koreferent: Prof. Dr. K. Kleinerhans

Tag der mündlichen Prüfung: 28. November 2008

Life is a miracle

*For my dear parents and for you,
with gratitude*

TABLE OF CONTENTS

SUMMARY.....	8
ZUSAMMENFASSUNG.....	11
ABBREVIATIONS AND SYMBOLS.....	14
CHAPTER 1. INTRODUCTION INTO PHOTOSYNTHESIS.....	17
PIGMENTS.....	18
<i>Chlorophylls</i>	18
<i>Carotenoids</i>	19
<i>Binding of pigments</i>	21
THYLAKOID MEMBRANE IN HIGHER PLANTS.....	21
PHOTOSYSTEM I.....	23
PHOTOSYSTEM II.....	25
<i>Photosystem II core</i>	25
<i>PS II supercomplex</i>	26
<i>PS II kinetics</i>	28
<i>Exciton/radical pair equilibrium model</i>	28
<i>Other models</i>	29
CHAPTER 2. INTRODUCTION INTO NON-PHOTOCHEMICAL QUENCHING PROCESSES.....	31
ΔpH	33
XANTHOPHYLL CYCLE.....	33
PSBS PROTEIN.....	35
MAJOR LIGHT-HARVESTING ANTENNA OF PS II (LHC II).....	36
MINOR LIGHT-HARVESTING COMPLEXES.....	38
PRESENT HYPOTHESES FOR THE Q _E QUENCHING MECHANISM.....	39
<i>Zeaxanthin as a direct quencher</i>	39
<i>PsbS as a direct quencher</i>	39
<i>Minor antenna as the site of q_E</i>	40
<i>Conformational change in LHC II</i>	40
<i>PS II RC is the site of q_E</i>	41
NON-PHOTOCHEMICAL QUENCHING IN DIATOMS.....	41
CHAPTER 3. MAIN AIMS OF THE THESIS.....	45
SUMMARY OF OPEN QUESTIONS.....	48

CHAPTER 4. MATERIALS AND METHODS	49
SINGLE PHOTON TIMING.....	49
<i>The principle of single photon timing.....</i>	49
<i>Laser system</i>	52
<i>Detection electronics</i>	52
<i>Data analysis.....</i>	53
PREPARATION AND CHARACTERIZATION OF SAMPLES.....	57
<i>PS II core particles from cyanobacteria</i>	57
<i>PS II enriched membranes (BBYs)</i>	58
<i>LHC II trimers and aggregates.....</i>	59
<i>Arabidopsis thaliana plants.....</i>	60
<i>Fluorescence kinetics.....</i>	62
<i>Diatoms.....</i>	64
CHAPTER 5. CHARGE SEPARATION KINETICS IN PHOTOSYSTEM II CORE PARTICLES.....	67
RESULTS	67
<i>Fluorescence decay kinetics.....</i>	67
<i>Kinetic Modeling.....</i>	69
DISCUSSION	72
<i>Kinetic model.....</i>	72
<i>Trap-limit versus transfer-to-the-trap limit.....</i>	75
CONCLUSIONS	77
CHAPTER 6. ENERGY TRANSFER AND CHARGE SEPARATION KINETICS IN PHOTOSYSTEM II ENRICHED MEMBRANE PARTICLES	79
RESULTS	79
<i>Fluorescence decays and kinetic modeling</i>	79
<i>Theoretical modeling.....</i>	86
DISCUSSION	93
<i>Energy transfer and trapping kinetics.....</i>	94
<i>Comparison with cyanobacterial PS II cores.....</i>	97
<i>Relevance and limitations of the early ERPE model for higher plant PS II.....</i>	99
<i>A “second generation ERPE model”</i>	101
CONCLUSIONS	105
CHAPTER 7. QUENCHING IN ISOLATED LHC II OLIGOMERS.....	107
<i>Pigment content.....</i>	107

<i>Global lifetime analysis of the fluorescence kinetics</i>	108
<i>Target analysis of the kinetics</i>	110
DISCUSSION	114
CHAPTER 8. NON-PHOTOCHEMICAL QUENCHING IN INTACT PLANT LEAVES.....	119
RESULTS.....	120
<i>Fluorescence decays in quenched and unquenched conditions</i>	120
<i>Evidence for the necessity of the additional component</i>	127
<i>Pigment content</i>	130
DISCUSSION	131
<i>Origin and differentiation of the fluorescence components</i>	131
<i>Two sites and mechanisms of non-photochemical quenching</i>	133
CHAPTER 9. QUENCHING IN MINOR ANTENNA MUTANTS.....	137
RESULTS.....	137
<i>Fluorescence decays in quenched and unquenched conditions</i>	137
<i>Target compartment modeling</i>	139
DISCUSSION	143
CHAPTER 10. NON-PHOTOCHEMICAL QUENCHING IN DIATOMS	147
RESULTS AND DISCUSSION.....	147
<i>Fluorescence induction</i>	147
<i>Oxygen evolution and de-epoxidation state</i>	150
<i>Ultrafast fluorescence decay kinetics</i>	152
<i>Global target analysis</i>	153
<i>The NPQ quenching model</i>	160
CHAPTER 11. CONCLUSIONS.....	163
REFERENCES.....	168
LIST OF PUBLICATIONS	187
SPECIAL THANKS	188

SUMMARY

Photosynthetic organisms possess a highly efficient photo-protective apparatus responsible for non-photochemical quenching (NPQ) of the excess excitation energy that helps them to minimize the harmful effects of excess light. The rapidly-reversible part of NPQ, termed qE, is associated with a number of different factors: the pH gradient across the thylakoid membrane, the action of the PsbS protein, the xanthophyll cycle conversion, i.e. de-epoxidation of violaxanthin into zeaxanthin (Zx), conformational changes in the light-harvesting complexes of PS II (LHC II). The exact mechanism of qE is however not known, the quenching sites, their location and molecular origin remain questionable.

These questions are addressed in the thesis by time-resolved fluorescence spectroscopy performed on different levels of organization and physiological state of the photosynthetic apparatus – from isolated pigment-protein complexes to intact leaves. The single photon counting technique was utilized for registering fluorescence emission with picoseconds time resolution and exceptionally high dynamic range and signal-to-noise ratio, allowing a detailed multicomponent analysis of the fluorescence kinetics. For the first time intact plant leaves and diatom cells (*Bacillariophyceae*) were measured *in-vivo* in NPQ state in physiological conditions. The successful analysis and interpretation of the extremely complex fluorescence decay kinetics of the intact system was made possible by combining the knowledge acquired in previous studies, reviewed in the introductory part of the thesis, together with the preliminary investigations in this work, performed on isolated PS II cores, PS II enriched thylakoid membranes, and isolated LHC II in different aggregation states.

The gathered experimental data were thoroughly treated by applying a kinetic modeling (target analysis) approach in order to gain insight into the biophysical parameters (energy and electron pathways, transfer and decay rate constants, species spectra that reveal the molecular nature of the fluorescence-emitting components). Different kinetic models suitable for each particular experimental system were designed and applied to fit the data. In addition, in some instances theoretical modeling was applied, which reveals the contributions of the various intermediates to specific apparent lifetimes and allows to estimate the time dependence of the populations of the intermediates.

Considerable similarities in the early electron transfer rates of PS II reaction centres (RCs, without antenna), cyanobacterial PS II cores (with core antenna), and a higher plant PS II enriched membranes (with core and peripheral antenna) were found. The

energy transfer rates scale with increase in the antenna size. Thus the dynamics of the initial photochemical steps of PS II could be implemented in the model describing the *in-vivo* fluorescence as well.

Fluorescence time-resolved kinetics was measured *in vivo* from leaves of *Arabidopsis* in unquenched dark-adapted states with open and closed RCs (F_0 and F_{max} , respectively) and compared to the kinetics measured under quenched light-adapted condition (F_{NPQ}). The data were fit using a kinetic compartment model combining the previously investigated energy and electron transfer dynamics in PS II and PS I. The results of the kinetic modeling revealed two principal changes in the fluorescence kinetics, signifying the generation of NPQ: 1) appearance of a new far-red-enhanced fluorescence component functionally disconnected from either PS I or PS II and that was shown to originate from peripheral LHC II detached from PS II; 2) increase of the non-photochemical deactivation rate (k_D) that is a direct measure of NPQ in the PS II-attached antenna. Thus, NPQ was found to consist of two separate mechanisms and sites of action, termed quenching site 1 and 2 (Q1 and Q2), respectively. These two quenching sites were further investigated by analyzing the fluorescence kinetics in different *Arabidopsis* mutants lacking different components of the photosynthetic apparatus and also by comparison with isolated LHC II *in vitro*.

The spectral features of the fluorescence of disconnected LHC II were reminiscent of the fluorescence of LHC II oligomers *in vitro*, therefore it was proposed that the Q1 site of quenching represents detached and oligomerized LHC II. Thus the NPQ-associated additional fluorescence component serves as a spectroscopic marker for the formation of LHC II oligomers *in vivo*. It is characterized by a spectrally broad and a strongly far-red enhanced fluorescence spectrum. The far-red emitting state is proposed to be an emissive Chl-Chl charge transfer state. The Q1 site of quenching was missing in the *Arabidopsis* mutant *npq4* lacking PsbS protein but was enhanced in the PsbS overexpressing mutant (*L17*), therefore it was concluded that the role of PsbS in NPQ is to mediate the detachment and oligomerization of LHC II.

The increase of the k_D constant was not observed in the *Arabidopsis* mutant *npq1* lacking Zx but was present in both *npq4* and *L17*. Therefore the Q2 site is strictly dependent on Zx availability and does not depend on the action of PsbS. A study of minor antenna knock-out mutants – koCP24, koCP26 and koCP24/koCP26 revealed further details of the Q2 mechanism – CP24 is the most crucial minor antenna complex for the Q2 quenching, whereas CP26 does not take part in it.

In conclusion of the results obtained from the time-resolved fluorescence analysis of intact leaves, a new model of the qE mechanism in higher plants was developed. It describes the location and molecular origin of the two quenching sites that work independently and complement each other.

The research work on NPQ was extended to cover diatoms that represent a major part of the phytoplankton. We aimed to find differences in the NPQ mechanism in diatoms since they have a different structure of the thylakoid membrane, and completely different antenna compared to higher plants. Surprisingly, despite of the differences, the diatoms *Phaeodactylum tricornutum* and *Cyclotella meneghiniana* operated the same qE mechanism with the same two quenching sites. As a result of the analysis of the diatom fluorescence kinetics under quenched and unquenched conditions, a model for the NPQ in diatoms was presented. According to this model there are two subpopulations of the light-harvesting antenna (fucoxanthin-chlorophyll-binding protein, FCP). The Q1 site of quenching is located in FCP subpopulation II which is detached from PS II and oligomerized under high light intensities. The Q2 site takes place in FCP subpopulation I, which is attached to PS II. Regardless of what type of antenna the photosynthetic organisms possess, they seem to utilize the same NPQ mechanisms which turn out to have universal character.

ZUSAMMENFASSUNG

Photosynthetische Organismen verfügen über eine hocheffiziente Einheit, die für die nicht-photochemische Löschung ("Non-Photochemical Quenching", NPQ) der überschüssigen Anregungsenergie verantwortlich ist und dazu dient, die schädlichen Wirkungen der überschüssigen Lichtenergie zu minimieren. Der hochreversible Teil des NPQ, das sogenannte „qE-Löschen“, wird mit unterschiedlichen Faktoren in Verbindung gebracht: Der pH-Gradient über der Thylakoidmembran, die Funktion des PsbS Proteins, die Konversion des Xanthophylls, d.h. die Deepoxidierung von Violaxanthin zu Zeaxanthin (Zx) und die Konformationsänderungen in den Lichtsammelkomplexen (LHC II) des Photoystems II (PS II). Der genaue Mechanismus des qE-Löschens ist jedoch nicht bekannt und sowohl die Lokalisierung als auch der molekulare Ursprung werden kontrovers diskutiert.

Diesen Fragestellungen wird in der vorliegenden Arbeit mittels zeitaufgelöster Fluoreszenzspektroskopie nachgegangen, wobei als photosynthetische Systeme sowohl isolierte Pigment-Protein-Komplexe als auch intakte Pflanzenblätter betrachtet wurden. Hierzu wurde die Single-Photon-Timing-Methode verwendet, welche die Messung von Fluoreszenzemissionen im Pikosekunden-Zeitbereich mit einer außergewöhnlich hohen Dynamik sowie einem hohen Signal-Rausch-Verhältnis erlaubt und dadurch eine detaillierte Multikomponentenanalyse der Fluoreszenzkinetiken ermöglicht. Zum ersten Mal wurden intakte Pflanzenblätter und Diatomeen (*Bacillariophyceae*) unter physiologischen Bedingungen *in-vivo* im NPQ-Zustand gemessen. Die Analyse und Interpretation der hochkomplexen Fluoreszenzkinetiken intakter Systeme wurde ermöglicht durch die Kombination von Erkenntnissen früherer Arbeiten (vgl. Einleitung) mit den im Rahmen dieser Arbeit durchgeführten Untersuchungen an isolierten PS II Kern-Komplexen, an mit PS II angereicherten Thylakoidmembranen und an isolierten LHC II in verschiedenen Aggregationszuständen.

Die Auswertung der experimentellen Daten erfolgte unter Verwendung von Kinetik-Modellierungsansätzen („Target Analysis“) mit dem Ziel, biophysikalische Parameter wie beispielsweise die Energie- und Elektronentransferwege, Transfer- und Zerfallgeschwindigkeitskonstanten sowie Spektren, welche die molekulare Natur der fluoreszierenden Komponenten wiedergeben, zu erhalten. Unterschiedliche Kinetikmodelle wurden entsprechend des dem jeweiligen Experiment zugrunde liegenden Systems entwickelt und zur numerischen Anpassung an die Daten angewendet. Zusätzlich wurden in einigen Fällen theoretische Modellierungen

durchgeführt, um die einzelnen Beiträge verschiedener Intermediate zu spezifischen Lebensdauern zu erhalten und um eine Abschätzung der zeitabhängigen Populationen der einzelnen Intermediate zu ermöglichen.

Bemerkenswerte Ähnlichkeiten der Elektronentransferraten in PS II Reaktionszentren ("RCs", ohne Antenne), in PS II Kern-Komplexen von Cyanobakterien (mit Kernantenne) und in Membranen, die mit dem PS II höherer Pflanzen angereichert waren (mit Kern- und peripherer Antenne), wurden festgestellt. Die Energietransferraten skalieren mit der Zunahme der Antennengröße. Die Dynamiken der ersten photochemischen Schritte im PS II konnten in das Modell implementiert werden, wodurch auch die Beschreibung der *in-vivo*-Fluoreszenz möglich wurde.

Es wurden die zeitaufgelösten Fluoreszenzkinetiken von Arabidopsis-Blättern *in vivo* im nicht-gelöschten, dunkel-adaptierten Zustand sowohl mit offenen als auch geschlossenen Reaktionszentren (F_0 bzw. F_{max}) gemessen und mit den unter gelöschten licht-adaptierten Bedingungen gemessenen Kinetiken (F_{NPQ}) verglichen. Die Daten wurden unter der Verwendung von Kompartiment-Kinetikmodellen, welche die zuvor untersuchten Energie- und Elektronentransferdynamiken in isolierten PS II und PS I kombinieren, gefittet. Die Ergebnisse der Kinetikmodellierungen zeigen hauptsächlich zwei Veränderungen in den Fluoreszenzkinetiken, welche die Bildung von NPQ aufzeigen: 1) Auftreten einer neuen fernrot-verstärkten Komponente, die funktionell sowohl vom PS I als auch vom PS II abgekoppelt ist und wie gezeigt wurde im peripheren Lichtsammelkomplex LHCII, das vom PS II abgekoppelt ist, entsteht; 2) Anstieg der NPQ-Deaktivierungsrate (k_D), die ein direktes Maß für das NPQ in den angekoppelten Antennen darstellt. Daher erfolgt das NPQ mit zwei verschiedenen Mechanismen an zwei verschiedenen Orten der Löschung, die Löschung 1 bzw. Löschung 2 (Q1 und Q2) genannt werden. Diese zwei Orte der Löschung wurden weiter untersucht sowohl durch die Analyse der Fluoreszenzkinetiken verschiedener *Arabidopsis*-Mutanten, bei denen verschiedene Komponenten der photosynthetischen Einheit fehlten, als auch durch Vergleich mit isolierten LHCII *in vitro*.

Die spektralen Merkmale der Fluoreszenz von abgekoppelten LHC II ähnelten den Merkmalen der *in vitro* Fluoreszenz von LHC II Oligomeren. Aus diesem Grund wurde vorgeschlagen, dass die Löschung 1 durch den abgekoppelten und oligomerisierten LHC II dargestellt wird. Folglich dient die zusätzliche, mit dem NPQ verknüpfte Fluoreszenzkomponente als spektroskopischer Marker für die Bildung von LHC II Oligomeren *in vivo*. Charakteristisch hierfür ist ein spektral breites, im Fernrot verstärktes Fluoreszenzspektrum. Es wird angenommen, dass dieser im fernroten

Bereich emittierender Zustand ein Chl-Chl-Ladungstransferzustand ist. Die Löschung 1 wurde in der *Arabidopsis* Mutante *npq4*, das kein PsbS besitzt, nicht beobachtet, trat jedoch verstärkt in der Mutante mit überexprimierten PsbS Protein (*L17*) auf. Aus diesem Grund wurde die Schlussfolgerung gezogen, dass die Funktion des PsbS im NPQ-Zustand die Abkopplung und Oligomerisierung von LHCII unterstützt.

Die Zunahme der k_D Konstante wurde in der *Arabidopsis* Mutante *npq1*, das kein Zx aufweist, nicht beobachtet, jedoch sowohl in *npq4* als auch in *L17*. Folglich ist die Löschung 2 vom Vorhandensein des Zx abhängig, jedoch nicht von der Funktion des PsbS. Die Untersuchung von Minor-Knock-out-Mutanten - koCP24, koCP26 sowie koCP24/koCP26 zeigten weitere Details des Q2-Mechanismus: CP24 ist der entscheidende Minor-Antennenkomplex für die Q2-Löschung, während CP26 nicht daran beteiligt ist.

Den Ergebnissen der Analyse der zeitaufgelösten Fluoreszenz intakter Blätter zufolge wurde ein neues Modell für den qE-Mechanismus höherer Pflanzen entwickelt. Dieses Modell beschreibt sowohl die Lokalisierung als auch den molekularen Ursprung der zwei Orte der Löschung, welche unabhängig voneinander und komplementär zueinander arbeiten.

Die Forschungsarbeit an NPQ wurde auf Diatomeen, die einen Hauptbestandteil des Phytoplanktons darstellen, ausgedehnt. Hierbei bestand die Zielsetzung darin, Unterschiede im NPQ Mechanismus in Diatomeen zu finden, da diese eine unterschiedliche Struktur der Thylakoidmembran und im Vergleich zu höheren Pflanzen eine völlig andere Antenne aufweisen. Überraschenderweise folgen die Diatomeen *Phaeodactylum tricornutum* und *Cyclotella meneghiniana* trotz der bestehenden Unterschiede demselben qE-Mechanismus mit gleichen Orten der Löschung. Der Analyse der Fluoreszenzkinetiken von Diatomeen unter licht- sowie dunkel-adaptierten Bedingungen folgend wurde ein NPQ-Modell für Diatomeen vorgelegt. In diesem Modell gibt es zwei Subpopulationen der lichtsammelnden Antenne (Fucoxanthin-Chlorophyll bindendes Protein, FCP). Der Q1-Löschungsort befindet sich in der FCP Subpopulation II, die vom PS II abgekoppelt ist und unter hohen Lichtintensitäten oligomerisiert wird. Der Q2-Löschungsort befindet sich in der FCP Subpopulation I, die an das PS II angegliedert ist. Unabhängig davon, welchen Antennentyp die photosynthetischen Organismen aufweisen, scheinen diese denselben NPQ-Mechanismus zu folgen, welcher einen universellen Charakter aufzeigt.

ABBREVIATIONS AND SYMBOLS

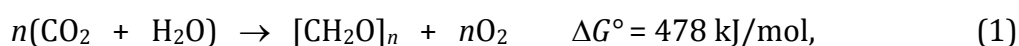
Ax	antheraxanthin
BBY	photosystem II-enriched grana membrane fragments, isolated according to Berthold, Babcock and Yocum
BChl	bacteriochlorophyll
β -DM	<i>n</i> -dodecyl- β -D-maltoside
Car	carotenoid
Chl	chlorophyll
CS	charge separation
DAS	decay-associated (emission) spectrum
DEP	diatoxanthin epoxidase
DES	deepoxidation state
DCMU	3-(3',4'-dichlorophenyl)-1,1-dimethylurea
Ddx	diadinoxanthin
Dtx	diatoxanthin
Dtx	diadinoxanthin/diatoxanthin cycle
Δ pH	transthylakoid proton gradient
EET	excitation energy transfer
ERPE	exciton/radical pair equilibrium model
F ₀	fluorescence from open PS II reaction centre particles in dark-adapted state
FCP	fucoxanthin-chlorophyll-binding protein
Fd	ferredoxin
F _{max}	fluorescence from closed PS II reaction centre particles in dark-adapted state
F _{NPQ}	fluorescence from closed PS II reaction centre particles in light-adapted state
HEPES	2-[4-(Hydroxyethyl)-1piperazinyl] -ethanesulfonic acid
HL	high light
ISC	intersystem crossing
LHC	light-harvesting complex
LHC I	light-harvesting complex I of PS II
LHC II	light-harvesting complex II of PS II
LL	low light
Lut	lutein
MES	2-(N-morpholino)-ethanesulfonic acid
MGDG	monogalactosyldiacylglycerol
NPQ	non-photochemical quenching
Nx	neoxanthin
OEC	oxygen-evolving-complex
Pheo	pheophytin
PQ	plastoquinone
PS	photosystem

PS I	Photosystem I
PS II	Photosystem II
qE	fast reversible component of non-photochemical quenching
RC	reaction centre
RP	radical pair
SA(E)S	species-associated (emission) spectrum.
SPT	single-photon timing
VAZ	violaxanthin/antheraxanthin/zeaxanthin
VDE	violaxanthin-de-epoxidase
Vx	violaxanthin
w.t.	wild type
XC	xanthophyll cycle
ZEP	zeaxanthin epoxidase
Zx	zeaxanthin

Chapter 1

INTRODUCTION INTO PHOTOSYNTHESIS

The essence of photosynthesis is the transformation of light energy into a biochemically available form of energy that leads to the synthesis of organic compounds in cells of photosynthetic organisms. Photosynthesis is one of the most important processes for mankind. In addition to providing us with air to breathe and fossil fuels as an energy source, it is the major nutritional basis of life on Earth and has generated an ozone layer that protects the life on the planet's surface from lethal UV radiation. Photosynthesis provides a large storage of free energy as compared to the starting materials (CO_2 and H_2O). The basic equation is:



where $(\text{CH}_2\text{O})_x$ represents carbohydrates. The solar radiation is needed to overcome the activation barriers of the chemical transformations in the early light-driven steps and to provide the overall free energy for the dark reactions.

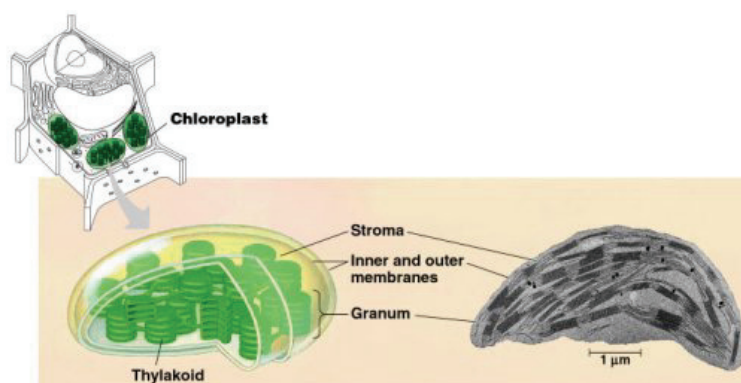


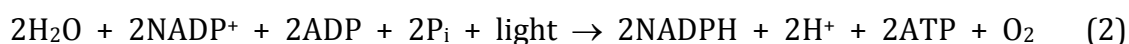
Figure 1.1: Schematic view of a plant cell containing chloroplasts with their thylakoid membranes (green).

Photosynthesis in most photosynthetic organisms is located in special organelles called chloroplasts (Figure 1.1). Chloroplasts from higher plants are usually 3-10 μm in diameter with a thickness of 1-4 μm . The chloroplast envelope consists of two membranes with slightly differing lipid composition spaced 2-10 nm apart. The outer membrane is highly permeable for small molecules, while the inner membrane contains special transporter proteins for selective transfer of certain metabolites into the chloroplast. The interior of the chloroplast is composed of the third, highly structured thylakoid

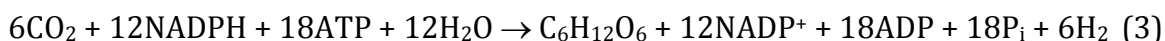
membrane. It forms stacked regions, known as *granum*, and non-stacked regions – the *stroma lamellae*. The aqueous space that surrounds the thylakoid membrane is called *stroma*, while the space enclosed by thylakoids is called *lumen*.

Two types of photosynthetic reactions occur in chloroplasts. *Light reactions* (light driven) take place inside of the thylakoid membrane; they provide the high energy compounds that are required to drive the *dark reactions* of the Calvin-Benson cycle, which is responsible for the carbon dioxide fixation. Dark reactions are not directly driven by light and occur both in the light and in the dark, in *stroma*. These reactions can be summarized as follows:

Light reactions:



Dark reactions:



Since the present work is restricted to the study of specific light-dependent mechanisms, in the following only these are discussed in detail.

Light reactions occur via the following steps: first, light is absorbed by chlorophylls of the light-harvesting antenna creating excited states. The excitation energy migrates to the reaction centres, where charge separation occurs. These primary charges are transferred to secondary donore and acceptors and finally stabilized by creation of stable chemical products.

Chl a X: CH=CH₂ Z: CH₃

Chl b X: CH=CH₂ Z: CHO

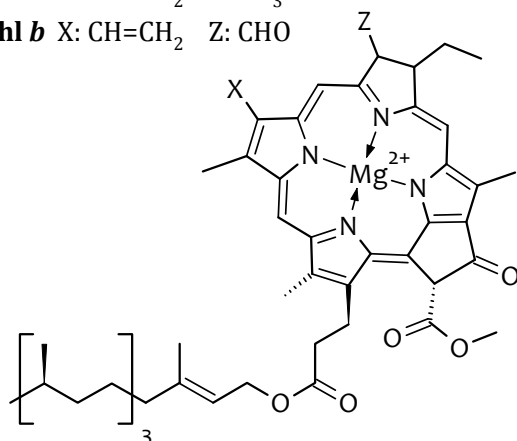


Figure 1.2: Structure of chlorophylls.

PIGMENTS

Chlorophylls

The first step in photosynthesis is the absorption of light by protein-embedded pigment molecules, mostly chlorophylls. The name “chlorophyll” is derived from Greek: *chloros* = green and *phyllon* = leaf. Chlorophyll (Chl) is structurally a substituted tetrapyrrole, the

four nitrogen atoms of which are coordinated by a magnesium atom (see Figure 1.2). Chls are very effective photoreceptors due to a network of conjugated double bonds. A long ester chain helps them to anchor in their surrounding proteins by hydrophobic interactions. There are different forms of Chl known in nature. Higher plants possess Chl *a* and Chl *b*. They have very strong absorption bands in the visible region of the spectrum, where the solar output reaching the earth is also maximal.

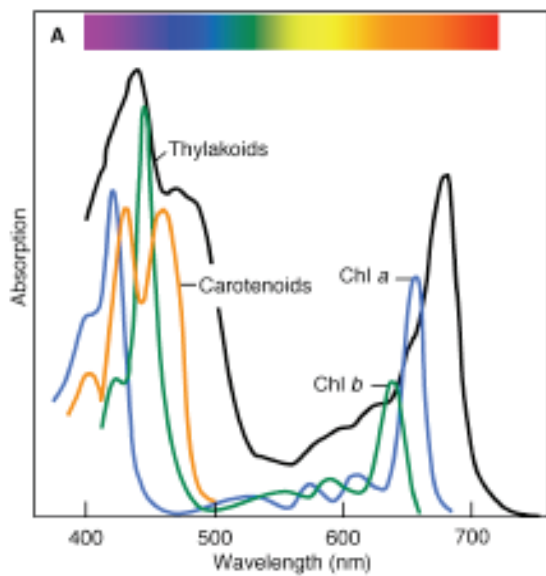


Figure 1.3: The photosynthetic pigments of higher plants. Absorption spectra of Chl *a*, Chl *b* and Cars in non-polar solvents. Upon association with proteins the spectroscopic properties of the pigments are altered as compared to the absorption spectrum of a thylakoid (black curve).

The absorption spectra of Chl *a* and Chl *b* do not completely overlap (Figure 1.3), which increases the spectral range over which light is absorbed, thus increasing the efficiency of light-harvesting. In the blue/violet part of the spectrum an absorption band appears due to the Soret transitions. The maxima are around 430-460 in Chl *a* and Chl *b*, respectively. The red-most band represents the Q_y transition which peaks around 640 and 670 nm in Chl *b* and Chl *a*, respectively. Less obvious from the spectrum is the weak Q_x transition that appears around 580-640 nm which is masked by the Q_y vibronic bands. The strong absorption of both red and blue/violet light by Chls causes the green colour of most plants. The

gap in green light absorbance is filled to some degree by the *carotenoids*.

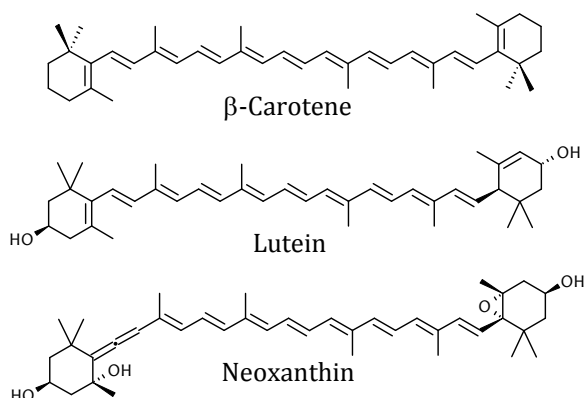
Carotenoids

Carotenoids (Cars) are organic pigments that are naturally occurring in many photosynthetic organisms. Cars belong to the category of tetraterpenoids (i.e. they contain 40 carbon atoms). Cars are also isoprenoids due to their carbon isoprene units assembled and modified in different ways (see Figure 1.4).

There are over 600 Cars known in nature. They are divided into two classes:

- **Xanthophylls** (from Greek: *xanthos* = yellow, *phyllon* = leaf) – Cars containing oxygen, such as lutein, neoxanthin, violaxanthin and zeaxanthin.

- **Carotenes** – oxygen free Cars, typically containing only carbon and hydrogen, such as α - or β -carotenes.



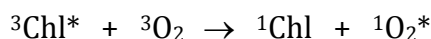
The spectroscopic properties of Cars are mostly determined by the conjugated π -electrons of the polyene chain. They absorb blue light. Each double bond reduces the energy required for electrons to move to higher energy states, allowing the molecule to absorb visible light of progressively longer wavelengths.

Figure 1.4: The structure of Cars involved in photosynthesis in plants.

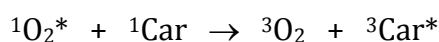
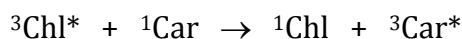
In photosynthetic organisms, Cars play a vital role in the photosynthetic reaction centre.

First, they participate in the energy-transfer process (Mimuro and Katoh 1991): Cars absorb in the wavelengths where Chls do not absorb and transfer the energy to them. Second, they participate in structure stabilization and assembly of protein complexes in the thylakoid membrane (Paulsen et al. 1993, Plumley and Schmidt 1987). However, the most important function of Cars is to protect the system from Chl triplets and singlet oxygen. Cars are able to quench the triplets directly due to their very low triplet energy levels as well as to deactivate the resulting aggressive oxygen species, such as singlet oxygen (Peterman et al. 1997), converting the excess absorbed energy into heat (for an overview see Smith 1991). The reactions involved in photodestruction and protection can be summarized as follows:

- Generation of singlet oxygen and destructive reactions:



- Protection against singlet oxygen and triplet Chl:



Binding of pigments

Chls and Cars are the light harvesting pigments in higher plants. They must be held at a certain range of optimal distances and orientations to each other and to the reaction centres. Thus almost all known antenna systems are pigment-protein complexes. The proteins both hold the pigments in a defined position and provide the possibility of fine-tuning their absorption properties by specific pigment-protein interactions. All Chls and Cars are attached non-covalently to the proteins. The connection might be either by way of weak ligand-metal interactions of the central Mg to nucleophilic amino acid side chains (often histidine (Jordan et al. 2001, Liu et al. 2004)), or by other non-covalent interactions such as hydrogen bonding, π - π -interactions or hydrophobic interactions with their long ester side chains (Jordan et al. 2001, Liu et al. 2004, Remelli et al. 1999, Smith 1991).

THYLAKOID MEMBRANE IN HIGHER PLANTS

Pigment-protein complexes involved in the light reactions of the photosynthesis machinery are embedded into the thylakoid membrane. There are four main protein complexes in higher plants: photosystem II (PS II), responsible for water splitting; photosystem I (PS I), responsible for NADP⁺ reduction; ATP synthase that produces ATP at the expense of the proton motive force (pmf) formed by the light-driven electron-transfer reactions, and the cytochrome (cyt) *b₆f* complex, which mediates electron transport between PS II and PS I and converts the redox energy into part of the proton gradient used for ATP formation (see Figure 1.5).

The protein complexes are distributed unevenly in the thylakoids: PS I is located in the stroma lamellae while PS II is found almost exclusively in the grana (Danielsson et al. 2006). The ATP-ase is located in the stroma lamellae and grana margins, and the cyt *b₆f* complex is found in grana and stroma lamellae (Albertsson 2001, Trissl and Wilhelm 1993) (see Figure 1.6).

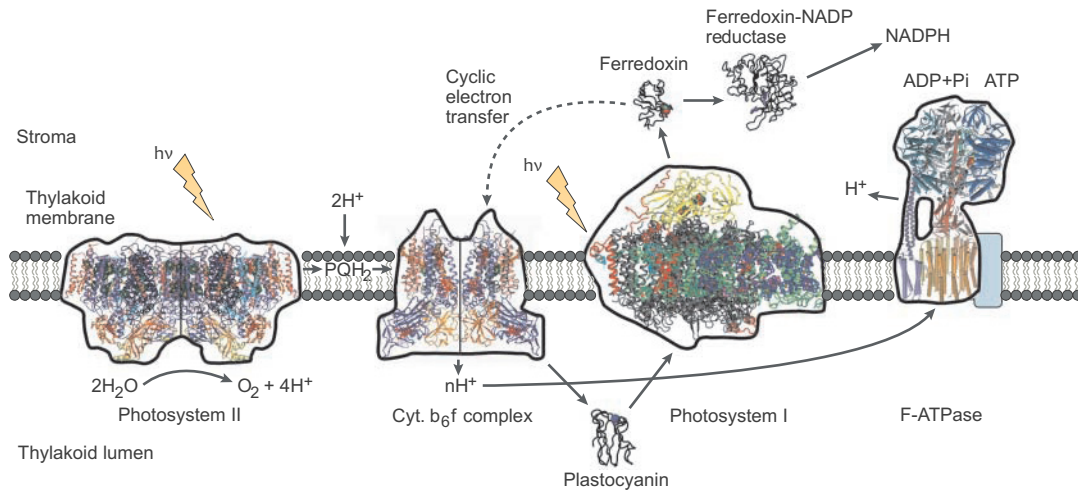


Figure 1.5: The architecture of the thylakoid membrane complexes and soluble proteins based on the figure from (Nelson and Ben-Shem 2004).

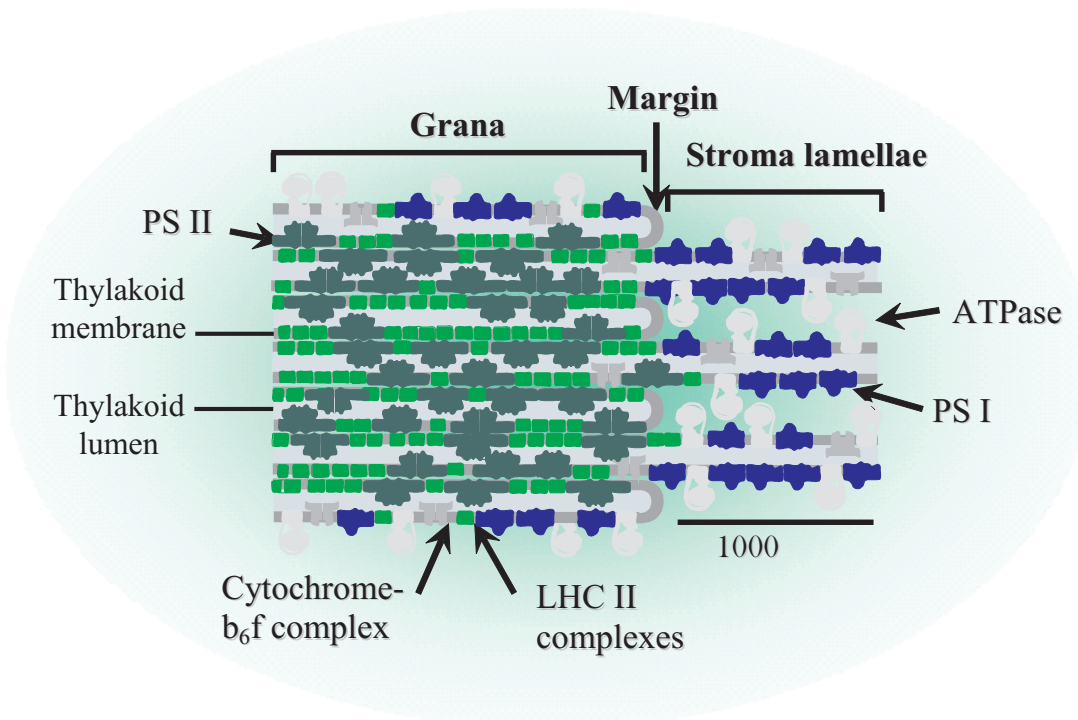


Figure 1.6: Organization of thylakoid membrane in higher plant chloroplasts. The figure is based on (Dekker and Boekema 2005).

Both photosystems consist of a core and antenna complexes. The core contains the reaction centre (RC) with the Chl *a* pair P680 (Primary electron donor absorbing at 680 nm) in PS II and P700 in PS I. The antenna or light-harvesting complexes (LHC) are composed of Chl-Car binding proteins, which are encoded by the nuclear genome and are named Lhca and Lhcb, for the antenna of PS I and PS II, respectively (Jansson 1999).

PHOTOSYSTEM I

Photosystem I (PS I) of higher plants is a monomeric supramolecular pigment-protein complex. The PS I core and its peripheral antennae create two distinct, loosely-associated moieties. Four Chl *a/b* binding proteins of PS I (Lhca1 – Lhca4) are arranged as two heterodimers organised in a form of a half-moon-shaped belt (Amunts et al. 2007, Morosinotto et al. 2005) (see Figure 1.7). The PS I supercomplex contains 168 Chls, 2 phylloquinones, 3 Fe₄S₄ clusters and according to Jolley et al. (2005) over 20 Cars. Despite of the complexity of the PS I organization, it is extremely efficient: almost every photon absorbed by the PS I complex is used to drive electron transport. It is remarkable that PS I exhibits a quantum yield of near unity (Trissl and Wilhelm 1993).

The components of the electron transport chain, P₇₀₀, A₀, A₁, F_X, F_A, and F_B, were first identified spectroscopically during the last half-century (Brettel 1997). They are coordinated by the two large subunits of the PS I core, PsaA and PsaB (Figure 1.7). Excitation energy driven to the reaction centre leads to a charge separation step in which the primary electron donor P700 reduces the primary electron acceptor A₀ (also Chl *a*). In the following steps the electron is transferred to A₁, a phylloquinone in most organisms, and then to a chain of interpolypeptide Fe-S clusters, F_X, F_A and finally F_B, which reduces the water-soluble protein complex ferredoxin (Fd). The electrons of two molecules of reduced ferredoxin are used by Fd: NADP⁺ oxidoreductase (FNR) for converting NADP⁺ to NADPH. The electrochemical proton gradient generated by the light reactions is used by the ATP synthase to synthesize ATP from ADP and Pi. The next step of photosynthesis is the consumption of NADPH and ATP for the assimilation of CO₂ in the Calvin-Benson cycle, resulting in the formation of carbohydrates (*cf.* Eq. 3).

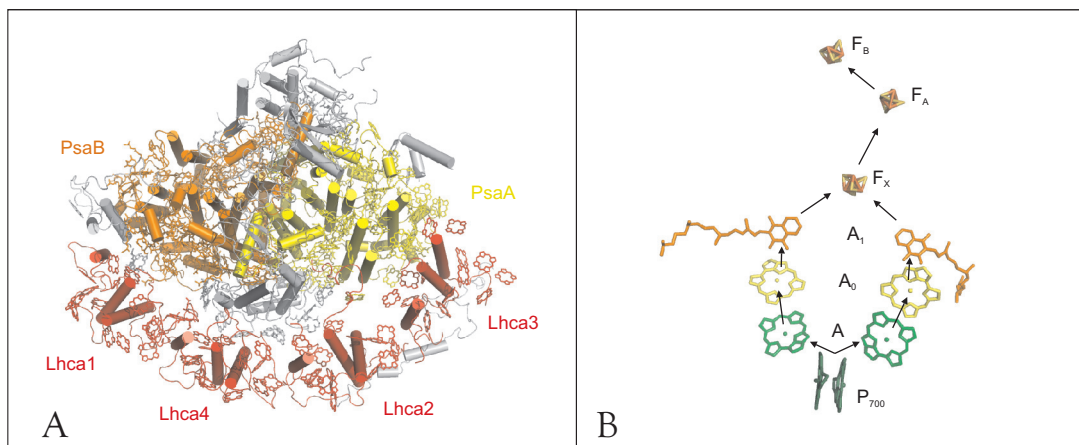


Figure 1.7: Structure of Photosystem I. A: View from the stromal side highlighting the main subunits PsaA and PsaB, containing the reaction centre, and the attached peripheral antenna complexes Lhca1-4 (Amunts et al. 2007). B: Structural arrangement of the electron transfer chain cofactors and electron pathways in the reaction centre (Jordan et al. 2001). The figure is prepared in Pymol (DeLano and Lam 2005).

In addition to the bulk antenna Chls PS I contains also a small number of “red” Chls with shifted absorption bands because of pigment-protein interactions or tighter pigment-pigment interactions due to dense Chl packing in PS I (Croce et al. 2006, Croce et al. 2007, Jennings et al. 1998). These pigments, even though in minority, contribute significantly to the spectroscopic features of PS I. The influence of few “red” Chls on the total trapping kinetics is ~ 4 times larger than the total antenna extension by peripheral antenna complexes (Slavov et al. 2008).

A fluorescence time-resolved study of Slavov et al. (2008) demonstrated trap-limited kinetics in the PS I cores and intact PS I particles from *Arabidopsis thaliana* (Figure 1.8). No “red Chls” were found in the PS I-core particles, while two “red” Chl compartments are located in the PS I intact complex that differ in the type of their EET kinetics and thus can be attributed to differences in their physiological role. The observed two “red” Chl compartments can be attributed to the low-energy forms found in Lhca3 and Lhca4 (Slavov et al. 2008).

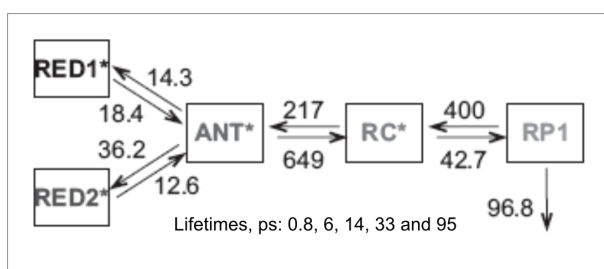


Figure 1.8: Kinetic model for the intact PS I kinetics resulting from target analyses {Slavov, 2008 27922 /id}. Rate constants are given in ns⁻¹. Lifetimes resulting from the model are shown at the bottom.

PHOTOSYSTEM II

Photosystem II core

PS II is a multisubunit supercomplex embedded in the thylakoid membranes of higher plants, algae, and cyanobacteria. PS II is the only biological system known that is capable of oxidizing water to molecular oxygen, and it has been studied extensively. The X-ray structures of the PS II complexes from several cyanobacteria have been reported recently at resolution 3.0-3.8 Å. (Barber et al. 2004, Biesiadka et al. 2004, Ferreira et al. 2004, Kamiya and Shen 2003, Loll et al. 2005a, Zouni et al. 2001). In the native state PS II cores occur as dimers (Rögner et al. 1996). The monomeric PS II core unit is made up of at least 21 protein subunits. The largest subunits carrying Chl pigments are the centrally located D1 and D2 proteins. They contain the RC cofactors, i.e. four Chls [the two primary P_{D1} , P_{D2} and two accessory Chls (Chl_{accD1} and Chl_{accD2})], 2 Pheo, and two quinone molecules (Q_A and Q_B). This arrangement forms a pseudo C_2 symmetry axis. On both sides of the RC two additional antenna Chls (the so-called peripheral, Chl_{D1} and Chl_{D2} , molecules) are localized, approx. 25 Å apart from the pigments of the electron transfer chain. The cofactors P_{D1} , Chl_{accD1} , and $Pheo_{D1}$ constitute the active D1 branch carrying out electron transfer to the quinone Q_A , whereas the pseudo-symmetric D2 branch is not active in primary electron transfer but in photoprotection of the RC (Martinez-Junza et al. 2007).

The PS II core complex contains further two large subunits, CP43 and CP47 (Chl proteins with apparent molecular mass of 43 and 47 kDa, respectively), referred to as core antenna. They carry 13 and 16 Chl *a* antenna molecules, respectively, organized in two layers located near the cytoplasmic and the luminal sides of the membrane (Figure 1.9). The initial processes of energy conversion in PS II are absorption of light in the antenna, followed by energy transfer to a special pair of Chls in the PS II-RC, P680. Upon receiving the excitation an electron is released from P680 and transported to the other side of the thylakoid membrane, where it is donated to a plastoquinone (PQ) molecule. After receiving a second electron from the next photocycle of P680, Q_B takes up two protons (H^+) from the stromal space to form plastoquinol (PQH_2), which diffuses into the membrane towards the Cyt *b₆f* complex. $P680^+$ is a very strong oxidant, which extracts electron from water, leading to the formation of O_2 , the release of protons in the inner thylakoid space and the return of P680 to the neutral state. Water-splitting takes place at a tetranuclear manganese complex (see Renger and Holzwarth 2005 for a recent review

on electron-transfer processes in PS II). Between PS I and PS II electrons flow through the Cyt *b₆f* complex. As the plastoquinol reaches this complex it is oxidized: two electrons are transferred through the Cyt *b₆f* complex to plastocyanin and two protons are released into the inner thylakoid space. The resulting plastoquinone is recycled to PS II. In addition, the Cyt *b₆f* complex pumps another pair of protons across the membrane.

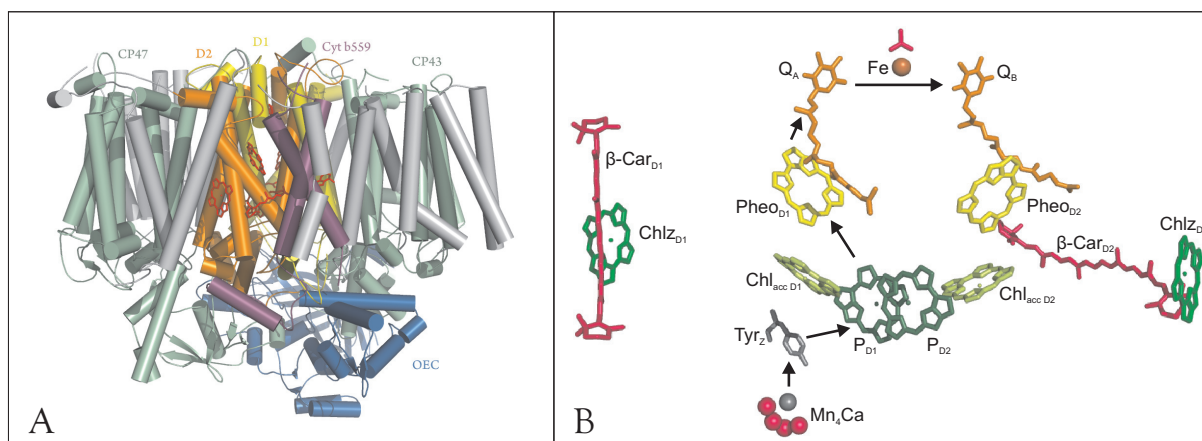


Figure 1.9: Photosystem II. A: Side view of the protein structure of cyanobacterial PS II (Loll et al. 2005a). The main subunits of the reaction centre D1 and D2, the core antenna complexes CP43, CP47, and the subunits of cyt *b₅₅₉* and the oxygen-evolving complex are indicated in colour. The reaction centre cofactors are also shown (in red). B: Structural arrangement of the cofactors involved in the primary reactions of PS II and pathway of electron transfer (arrows). The figure was prepared with PyMol (DeLano and Lam 2005).

It has been possible to isolate a pigment–protein complex, called the **D1/D2-cyt-b₅₅₉** unit, which carries a large part of the RC cofactors, i.e., the 4 Chls, the 2 Pheo, and the two peripheral pigments Chl_{ZD1} and Chl_{ZD2}, and can be considered as the minimal functional RC complex (Danielius et al. 1987, Satoh and Nanba 1987). The D1/D2-cyt-b₅₅₉ complex has, however, lost the two functional quinones and the non-heme iron. Thus it is only capable of performing electron transfer up to Pheo.

PS II supercomplex

The main difference between the organization of the PS II complex of cyanobacteria and higher plants is in the light-harvesting system. Higher plants possess a unique trans-membrane light-harvesting complex whereas in cyanobacteria it is substituted by a large extra membrane on water-soluble phycobilisome antenna complex, which is attached to the cytoplasmic side of the cyanobacterial PS II complex.

Two specific preparations have been very useful in attempts to elucidate the kinetics and function of PS II. The first is the PS II core complex described above. The second one is a preparation of PS II enriched higher plant membranes, called BBY, after Berthold, Babcock and Yocum who reported it first (Berthold et al. 1981). It contains all the components of the PS II core plus the peripheral minor (CP24, CP26, CP29) and major LHC II antenna complexes, which are discussed below. The antenna size increases from 35 Chl *a* per P680 in the PS II core preparation (Loll et al. 2005b) to 230-270 Chl *a* + Chl *b* per P680 in BBY particles (Dekker and Boekema 2005, Yakushevskaya et al. 2001).

The first investigation into the detailed structure of a complete PS II-LHC II complex was done by electron microscopy and image analysis (Rogner 1987 (Barber et al. 1998, Boekema et al. 1999b, Boekema et al. 1999a, Yakushevskaya et al. 2003). These studies revealed the presence of supercomplexes consisting of a dimeric PS II core complex, designated as “C” and trimeric LHC II complexes in three different binding positions. These

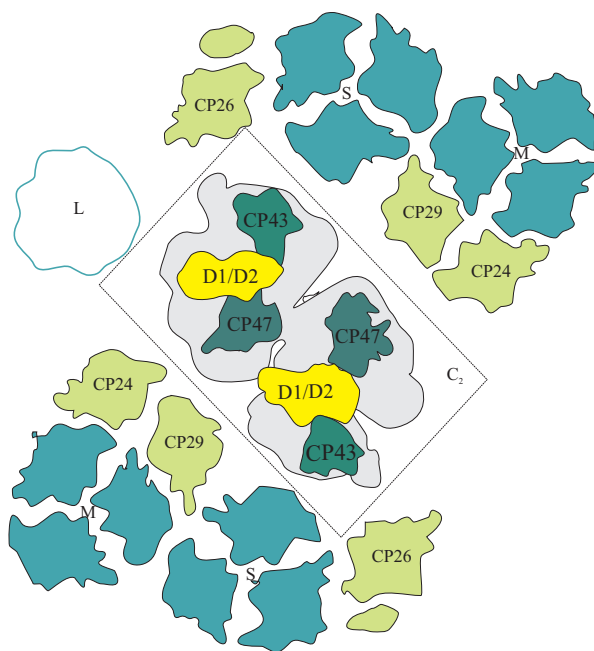


Figure 1.10: Schematic presentation of PS II supercomplex (from {Dekker, 2005 25453 /id}. Additionally to the PS II dimer core it has small (S), middle (M) and sometimes large (L) PS II complexes and minor antenna: CP24, CP26 and CP29.

positions were named S, M and L in the case of higher plants, in which they refer to “strongly”, “moderately” and “loosely” bound trimeric LHC II complex, respectively (Boekema et al. 1999b). Several combinations of attached LHC II complexes have been found and named in a way that the number of attached LHC II is indicated. Among them there are C_2S_2 , C_2S_2M , $C_2S_2M_2$, $C_2S_2M_2L$ supercomplexes. The latter type is depicted in Figure 1.10. The recent electron microscopy work (Yakushevskaya et al. 2001) on *A. thaliana* showed that the “L” type occurs very rarely in preparations from this plant, so our further analysis of *Arabidopsis* considers generally the $C_2S_2M_2$ structure.

PS II kinetics

The energy transfer and charge separation kinetics in intact PS II core particles were studied first about two decades ago by time-resolved fluorescence and transient absorption with a resolution of ~ 10 ps (Nuijs et al. 1986, Schatz et al. 1987, Schatz et al. 1988). Dominant lifetime components from open RCs (i.e., the F_0 state) were observed in the range from 35 ps (Nuijs et al. 1986) to 60-80 ps (Schatz et al. 1987), depending on the method used, and were ascribed to antenna trapping by primary charge separation and ~ 300 -500 ps, which was assigned to the secondary electron transfer to the quinone acceptor Q_A (Nuijs et al. 1986, Schatz et al. 1987, Schatz et al. 1988). These data subsequently gave rise to the development of a kinetic “compartment” model for the early energy – and electron-transfer processes in PS II cores, which became known as the *exciton/radical pair equilibrium model* (ERPE model) (Schatz et al. 1988).

Exciton/radical pair equilibrium model

The ERPE model has been used extensively in the field to analyze and explain a wide range of phenomena related to the kinetics of the early processes in PS II such as radical pair formation, its dependence on the redox states of the cofactors, and Chl quenching in the antenna and the RC.

The ERPE model implies that internal energy equilibration within the PS II core antennae and from the antennae to the RC should occur on a time scale of a few picoseconds (Schatz et al. 1988), that is, below the ~ 10 ps resolution of the time-resolved experiments at the time (actually an equilibration time of ≤ 3 ps was estimated). It was therefore assumed in the ERPE model that the charge separation would start from an equilibrated excitation state distributed over both the antenna and the RC pigments. Consequently, no details of the energy-transfer processes were considered in the model. This assumption gave rise to a relatively simple and straightforward description of the excited-state dynamics, which resulted in the overall *trap-limited charge separation kinetics* Figure 1.11 (Schatz et al. 1988). [We note here in passing that recently in the literature the typical excited-state equilibration time that was assumed in the derivation of the “exciton/radical pair equilibrium model” was misquoted to be in the range of a few hundreds of femtoseconds (Andrizhiyevskaya et al. 2004) i.e., by an order of magnitude shorter than the ≤ 3 ps value that had actually been assumed (Schatz et al. 1988)].

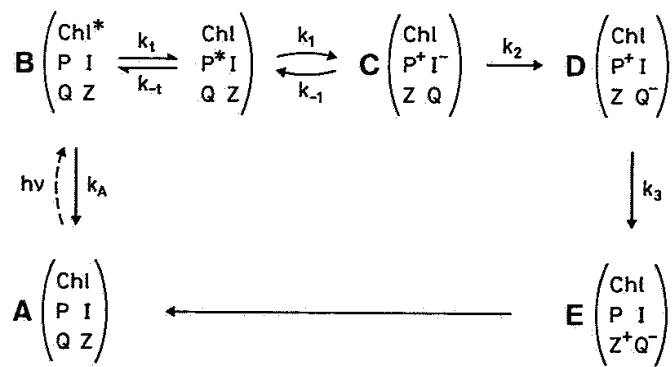


Figure 1.11: ERPE kinetic model of the primary reactions in open PS II. In this scheme the rate constants k_j describe $k_A = k_D + k_{rad}$, the radiationless plus the radiative decay of Chl^{*}; k_t and k_{-t} , the processes of entering and leaving the trap (trapping and detrapping); k_1 , the apparent primary charge separation; k_{-1} , charge recombination to the excited state; k_2 and k_3 , the processes of charge stabilization associated with the relaxation of I⁻ and P⁺ rereduction, respectively [Schatz, 1988 10934 /id].

The other elements of the ERPE model for PS II included an efficient charge recombination process from the first radical pair (RP, compartment "C"), back to the excited states of the RC and the antenna compartment "B"), and thus efficient equilibration between excited states and RP states. The early ultrafast kinetics data suggested a single RP intermediate, assigned to reflect the state P₆₈₀⁺Pheo⁻ (P⁺I⁻), before the electron transfer to Q_A takes place forming the radical pair P₆₈₀⁺Q_A⁻ ("D") (Nuijs et al. 1986, Schatz et al. 1987, Schatz et al.

1988).

On the basis of these interpretations the ERPE model gives rise to a bi-exponential fluorescence decay kinetics, where the faster component reflects the *apparent lifetime* of charge separation from the equilibrated (antenna/RC)* excited state, while the slower component reflects essentially the *apparent electron transfer lifetime* from Pheo to Q_A (Note that *Effective rate constants* of the individual reaction steps are not given by the inverse of the experimental lifetimes (Holzwarth et al. 2006a) which are functions of all rate constants of the system).

Other models

More recently one of the assumptions of the ERPE model, i.e. the rapid energy equilibration between antenna and RC, has been put into question and several papers raised the point that the overall trapping kinetics might be severely limited in particular by energy diffusion to the RC, i.e. a *transfer-to-the-trap limited* model has been proposed (Dekker and van Grondelle 2000, van Amerongen and van Grondelle 2001, Vassiliev et al. 2002). Furthermore a diffusion limitation of the kinetics by the antenna-antenna transfer processes appeared possible based on annihilation data reported for various size complexes of PS II (Barzda et al. 1996) (Bittner et al. 1994, Gillbro et al. 1988) and a more recent fluorescence quenching analysis (Jennings et al. 2000). In particular a very detailed an-

nihilation study by Barzda et al. (Barzda et al. 2001) suggested that inter-monomer transfer in trimeric or larger aggregates of PS II might occur on the time scale of a few tens of ps (van Amerongen and van Grondelle 2001), which could eventually lead to a total energy diffusion time in intact PS II particles of 150-250 ps (Barzda et al. 2001, van Amerongen and van Grondelle 2001). Indeed these antenna equilibration processes have never been probed directly before in intact PS II particles.

More detailed data on the early processes in intact PS II cores with open RCs have recently resolved two RPs before the reduction of Q_A and showed that the primary charge separation – in contrast to previous assignments – starts by an electron transfer step from the accessory Chl to Pheo, leading to the state $\text{Chl}_{\text{acc}}^+\text{Pheo}^-$ (RP1), followed by a secondary electron transfer step from the P_{D1} Chl to $\text{Chl}_{\text{acc}}^+$ forming the state $P_{D1}^+\text{Pheo}^-$ (RP2) (Holzwarth et al. 2006b).

Another controversial discussion that has come up recently concerns the question of whether the rates and the mechanism of the early electron-transfer processes in intact PS II cores and in isolated D1/D2-cyt-b₅₅₉ RCs are identical or not. Whereas the ERPE model estimated very similar intrinsic rate constants for the primary charge separation in intact PS II cores (Schatz et al. 1988) and in D1-D2 RCs (Gatzen et al. 1996), the identity of these processes in the two systems has also been questioned recently (Vasil'ev et al. 2001, Vassiliev et al. 2002) (for recent reviews see refs (Renger and Holzwarth 2005) and (Holzwarth 2004)). In view of these controversies one of the aims of the present work was also to provide new fluorescence kinetic data on intact PS II cores that complement the recent transient absorption kinetics and are suitable for an improved kinetic description of the energy- and electron-transfer processes in PS II. In particular the question of “transfer-to-the-trap-limited” (i.e., diffusion-limited) versus “trap-limited” kinetics is addressed.

Chapter 2

INTRODUCTION INTO NON-PHOTOCHEMICAL QUENCHING PROCESSES

By evolution photosynthetic organisms developed a very efficient apparatus optimized to operate under highly and quickly varying light conditions.

At low-light intensities (e.g. in shade), when PS II RCs are open, i.e. the primary acceptor Q_A is in the oxidized state (ready to accept an electron), photosynthetic organisms convert the absorbed light energy into charge separated states with efficiency exceeding 95%. The yield of photochemistry (Φ_p) in this case is maximal, $\Phi_p = k_p / (k_f + k_d + k_p)$, whereas the yield of fluorescence is at a minimum $\Phi_f = k_f / (k_f + k_d + k_p)$; where Chl *a* fluorescence emission (rate k_f), photochemical (rate k_p) and non-photochemical de-excitation of Chl *a* molecules (rate k_d) compete for the absorbed light energy in a quasi-first order processes.

At high-light intensities (or in full sunlight), much more light is absorbed in the antennae than can be utilized in photosynthetic electron transport. In order to avoid photooxidative damage in the photosystems, photosynthetic organisms dissipate the excess energy by non-photochemical processes, the so-called *non-photochemical quenching* (NPQ) (Barber and Andersson 1992, Horton et al. 1996, Külheim et al. 2002, Niyogi 1999). In this case, the rate of nonradiative energy dissipation k_d increases, whereas the rate k_p and yield of photochemistry decrease. NPQ plays a key role in the life of photosynthetic organisms. It helps them, for example, to cope with natural fluctuations in light intensity, such as passing clouds in a sunny day, without subsequent damage to the photosynthetic apparatus.

Presently two main mechanisms are considered to contribute to NPQ:

– *the energy-dependent mechanism* (Horton et al. 1996), named because of its relation with the energization of the thylakoid membrane. It has been assigned to thermal deactivation of singlet excited Chl ($^1\text{Chl}^*$) in the antenna of PS II (Holt et al. 2005, Horton et al. 1996, Niyogi 1999), thus representing an efficient mechanism to reduce the electron

pressure on the photosynthetic electron transport chain. It is also called “*feedback de-excitation*” or *qE*. This type of quenching can be formed and relaxed on a seconds to minutes timescale.

– *photoinhibition of PS II*, which develops upon prolonged exposure of plants to extreme light-stress conditions and is caused by the light-induced inactivation of the D1 protein in the PS II reaction centre (Aro et al. 1993, Krause 1988, Nishiyama et al. 2006) (Aro et al. 2005, Murata et al. 2007). Although photoinhibition is sometimes considered a protective mechanism, as opposed to permanent damage, the recovery is much longer compared to *qE* – up to several hours, as it involves *de novo* synthesis of the D1 protein and reassembly of the PS II core.

Under most natural conditions, the *qE-mechanism* – which in itself may have different phases – represents the dominating form of energy dissipation in plant photosynthesis and is considered as an easily reversible regulation mechanism. According to the present understanding, the *qE* quenching is correlated with:

- lowering of the thylakoid lumen pH (Horton and Ruban 1999, Jahns et al. 2002, Krause and Jahns 2004, Munekage et al. 2001, Niyogi et al. 1998, Noctor et al. 1991, Takizawa et al. 2007, Wraight and Crofts 1970);
- conversion of violaxanthin (Vx) to zeaxanthin (Zx) via the xanthophyll cycle (Demmig-Adams 1990);
- protonation of the PsbS protein of PS II (Li et al. 2000);
- conformational changes in the antenna of PS II (Horton et al. 2005, Ruban et al. 2007);
- oligomerization of LHC II (Horton et al. 1991).

There exist a number of different hypotheses for the both the location as well as the molecular basis of *qE* quenching. While some reports suggest that *qE* occurs in the PSII RC (see the latest review of Ivanov et al. (2008)), the majority agree that it occurs in LHC II (Horton 1996, Horton and Ruban 1992), where the xanthophyll cycle Cars are bound (Bassi et al. 1993, Peter and Thornber 1991, Ruban and Horton 1994). It has been suggested also that CP26 and CP29, two of the minor PS II antenna components, play a major role in *qE* (Bassi et al. 1993, Crofts and Yerkes 1994, Gilmore et al. 1996, Horton and Ruban 1992, Pesaresi et al. 1997, Walters et al. 1994). At present there is an only general agreement that the site of *qE* is localized in some components of the PS II supercomplex, which consists of the PS II core, the major LHC II antenna and the three minor LHCs:

CP24, C26 and CP29. In the following an introduction to the main proposed mechanisms for qE is given, different hypotheses are highlighted and important questions are pointed out.

Δ pH

In higher-plants' photosynthesis, the energy driving the light-induced electron transfer is stored as an electrochemical gradient of protons, termed the proton motive force (pmf). The total pmf consists of the sum of the membrane potential ($\Delta\psi$) and the proton diffusion potential (Δ pH), and is utilized to drive ATP synthesis (Junesch and Gräber 1991). The acidification of the thylakoid lumen (Δ pH component) slows the oxidation of plastoquinol (PQH₂) at the cyt *b₆f* complex, thus regulating the overall electron transfer rate (Kramer et al. 2003). Moreover Δ pH acts as a key signalling component, regulating light-harvesting efficiency via the qE mechanism (reviewed in (Takizawa et al. 2007) and (Müller et al. 2001)). Quantitative estimates of pmf and lumen pH have been performed by Takizawa et al. (Takizawa et al. 2007): the lumen pH was estimated to range from ~7.5 (under weak light at ambient CO₂) to ~5.7 (under 50 ppm CO₂ and saturating light) within an uncertainty of ~0.5 pH units. The initiation of qE involves two lumen pH-dependent processes, the activation of the xanthophyll cycle and the protonation of PsbS, a PS II protein of unknown location (Gilmore et al. 1998, Li et al. 2004, Müller et al. 2001, Takizawa et al. 2007) (see below).

In isolated thylakoids it is possible to induce qE in darkness by simply lowering the pH of the buffer or by generating Δ pH via ATP hydrolysis and reverse proton pumping by the ATP synthase (Gilmore and Yamamoto 1992, Krieger et al. 1992).

XANTHOPHYLL CYCLE

The role of the xanthophyll cycle (XC) is crucial in the energy-dependent quenching mechanisms. Since 1957, when David Sapozhnikov with his coworkers from Russia first described the light-induced changes in the XC (Sapozhnikov et al. 1957), numerous studies have been performed on the relationships between XC and qE (Demmig-Adams et al.

1996, Demmig-Adams and Adams 1996, Gilmore et al. 1995, Gilmore and Yamamoto 1993, Horton et al. 1996, Kalituho et al. 2007, Pfündel and Bilger 1994, Stroch et al. 2004, Wehner et al. 2006).

Two main types of XC were identified: the violaxanthin/antheraxanthin/zeaxanthin-(VAZ)-cycle in higher plants, green, and brown algae and the diadinoxanthin/diatoxanthin-(Dtx-) cycle in diatoms, dynophytes and other algal groups (Hager and Stransky 1970a, Hager and Stransky 1970b) (see Figure 2.1).

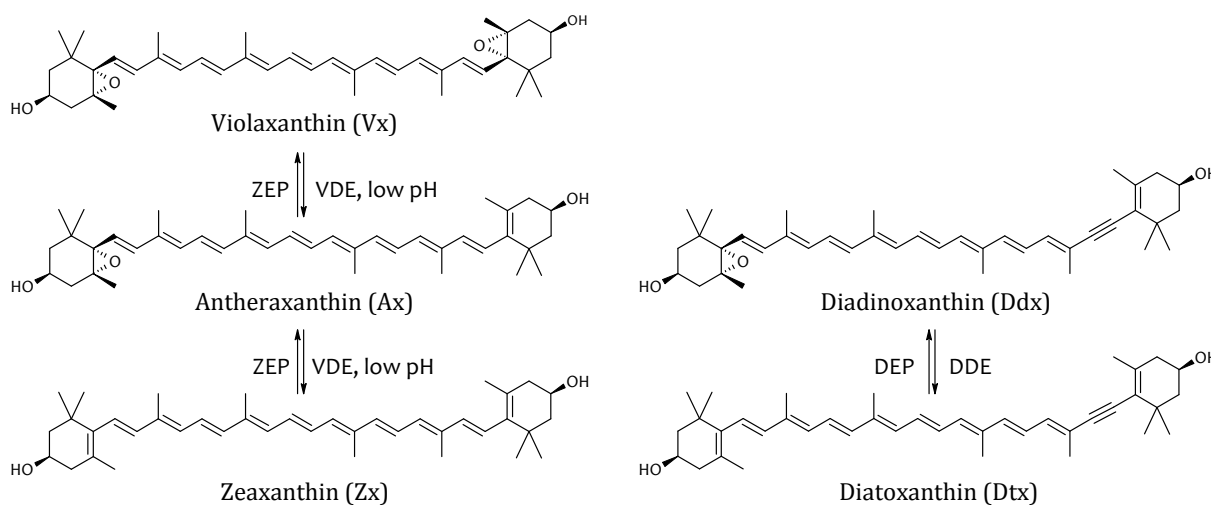


Figure 2.1: The Violaxanthin/Antheraxanthin/Zeaxanthin (VAZ) cycle in plants and Diadinoxanthin/Diatoxanthin (Dtx) cycle in diatoms. HL – high intensity light, LL – low intensity light.

The VAZ cycle involves two steps in which violaxanthin (Vx) is de-epoxidized via antheraxanthin (Ax) into zeaxanthin (Zx) at high light. This reaction is catalysed by the violaxanthin de-epoxidase (VDE), which is located in the thylakoid lumen. VDE is activated when the lumen pH becomes lower than 6.2. It needs ascorbate as a co-substrate to reduce the epoxy group (Bratt et al. 1995, Hager 1969), as well as the presence of the major thylakoid lipid monogalactosyldiacylglycerol (MGDG) (Yamamoto and Higashi 1978), which serves to solubilise xanthophylls and possibly form an inverse hexagonal lipid phase, required for the de-epoxidation (Goss et al. 2005, Wilhelm et al. 2006).

The Zx epoxidase (ZEP, catalyzing the backward reaction sequence Zx to Vx), is located in the chloroplast stroma. It works by a factor of 5-10 slower than VDE (Demmig-Adams et al. 1996). ZEP uses molecular oxygen, NADPH and FAD to put the epoxy groups back into the Cars (Hager and Holocher 1994).

The Dtx cycle involves only one step, diadinoxanthin deepoxidase (DDE) catalyses the conversion of diadinoxanthin (Ddx) into diatoxanthin (Dtx). Similar to the VDE, DDE is

also activated by the acidification of the thylakoid lumen. However, lower amounts of ascorbate (Hager 1969) and MGDG are needed for inducing the Dtx cycle (Goss et al. 2006), the DDE activity can already be observed at neutral pH values of 7.2 (for the review see (Jakob et al. 2001)).

The Dtx epoxidase (DEP) catalyses the back reaction of the Dtx cycle; it also uses oxygen, FAD, and NAD(P)H to re-introduce the epoxy group into the Dtx molecule. However, while ZEP works under high-light illumination with increased rates of pigment conversion, DEP is completely inhibited at such conditions by the build-up of the transmembrane pH gradient (for a review (Wilhelm et al. 2006) and (Mewes and Richter 2002)).

PSBS PROTEIN

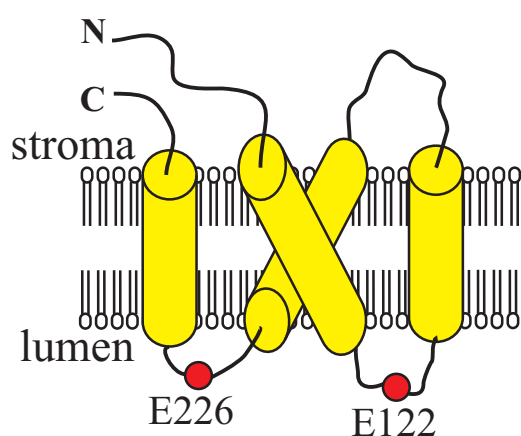


Figure 2.2: Schematic representation of PsbS protein. Amino acids E122 and E226 sensing the lumen pH are marked in red.

Non-photochemical quenching in higher plants is believed to be strictly dependent on the action of the PsbS protein of PS II (Li et al. 2000). Unlike typical light-harvesting complex proteins, PsbS has four rather than three transmembrane helices (Figure 2.1). Protein sequence analysis has shown a high similarity between helix I and helix III and also between helix II and helix IV (Green and Pichersky 1994, Jansson 1999) reflecting the symmetrical topology of the PsbS protein. The two lumen-exposed loops (Kim et al. 1994) are also highly similar,

with two glutamates (E122 and E226) located in the middle of each loop. These two protonatable and lumen-exposed amino acids are the pH sensors in the thylakoid lumen that activate qE (Li et al. 2004). Mutation of E122Q and E226Q inactivates the PsbS function in qE and the mutation of only one of the two glutamates inhibits it only partly (Li et al. 2004).

Recently it has been reported that PsbS can appear in monomeric or dimeric forms in the thylakoid membrane with the dimer-to-monomer conversion reversibly induced by light (Bergantino et al. 2003). According to this work, the PsbS dimer prefers alkaline pH

and connects mainly to the PS II core complexes, while the PsbS monomer is prevalent at acidic pH and preferentially associates with the major light-harvesting complex.

According to Teardo et al. (Teardo et al. 2007) the location of PsbS in the thylakoid membrane is diverse and, moreover, PsbS is laterally mobile. So the PsbS protein is associated either with granal membranes or with stroma lamellae in low or high-intensity light-treated intact leaves, respectively. Kiss et al. (Kiss et al. 2008) provided evidence that PsbS is involved in the macro-organization of PSII antenna.

MAJOR LIGHT-HARVESTING ANTENNA OF PS II (LHC II)

The light-harvesting complex II (LHC II) is the most abundant protein in the thylakoid membrane, playing a crucial role in absorbing light, controlling the structure of the membrane, and in the regulation and adaptation to high light.

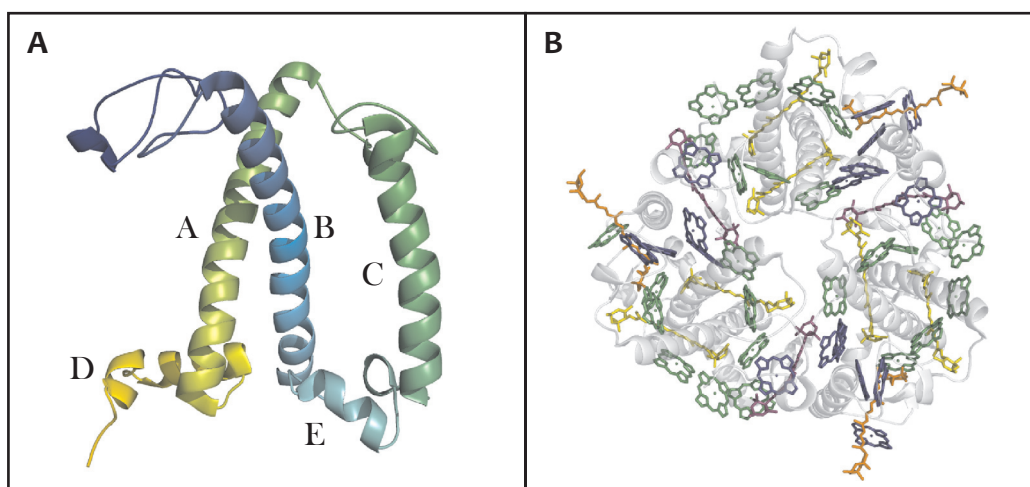


Figure 2.3: A. Localization of α -helices in the LHC II monomer, B. 3D-structure of LHC II-trimer pigments (Liu et al. 2004). The Chls are shown in blue (Chl b) and green (Chl a), Luts are yellow, Nxs are orange and the xanthophyll cycle Cars are violet. Both figures were prepared with PyMol (DeLano and Lam 2005).

Recent analyses of the X-ray structure of the trimeric LHC II from spinach (Liu et al. 2004) at 2.7 Å resolution and pea (Standfuss et al. 2005) at 2.5 Å resolution provided details of the pigment locations and binding sites. A monomeric LHC II (~232 aminoacids) is composed of three transmembrane α -helices, (helices A, B and C) and two short amphipathic helices (helices D and E) on the lumenal part of the membrane (Figure 2.3 A). Helix D connects the C-terminus of the protein with the helix A. The N-Terminus of the

protein lies on the stromal side of the membrane and because of its charge is responsible for grana stacking (Barber 1980) (Standfuss et al. 2005).

The LHCII apoprotein binds 14 Chls, (8 Chl *a* + 6 Chl *b*) and 4 Cars (Figure 2.3 B). The Chls in LHC II are vertically distributed in two layers within the membrane. Inside a monomer the first layer is close to the stromal surface and contains eight Chls, which surround the central helices A and B forming an elliptical ring. The remaining six Chls are arranged in the second layer close to the luminal surface. They form two separate clusters containing four Chls and a Chl *a* – Chl *a* dimer.

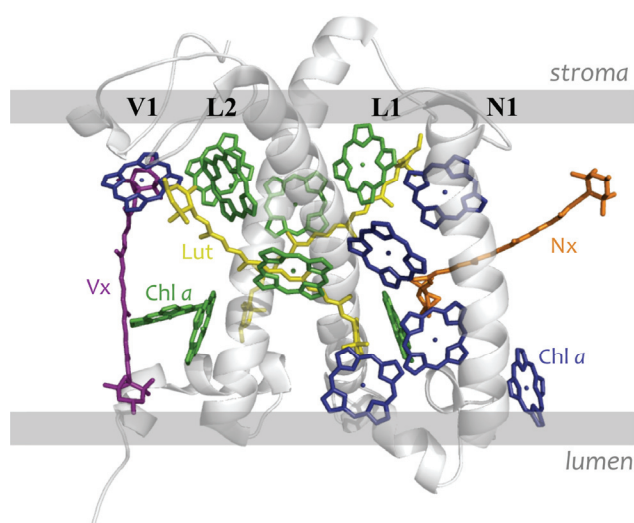


Figure 2.4: Location of the Car-binding sites in the LHC II monomer in the crystal structure of Liu et al. {Liu, 2004 25164 /id /d}.

Depending on the properties and the roles of the Cars, the four different Car-binding sites in PS II antenna proteins are termed (Figure 2.4): L1 (exclusively Lut is bound), L2 (prefers Lut), N1 (prefers Nx) and V1 (prefers Vx). Two lutein molecules (Lut) detected already at 3.4 Å resolution (Kühlbrandt 1994) are located in the groove of the cross helices A and B, also crossing each other (L1 and L2 sites). The N1 site is occupied by 9'-*cis* Neoxanthin (Nx) (Snyder et al. 2004).

It is located in the Chl *b*-rich region around helix C (Croce et al. 1999a). The cyclohexane ring of Nx protrudes from the protein frame into the lipid phase of the membrane. A fourth Car (Vx) is located at the monomer-monomer interface (V1). The pigments on this position have all-*trans* configuration and form an angle of 30° with the membrane normal. It is assumed that pigments of the xanthophyll cycle – violaxanthin (Vx), antheraxanthin (Ax) and zeaxanthin (Zx) bind to this site *in vivo*. Bassi and Caffari (2000) suggest that the V1 site is a source of Vx ready to be converted to Zx under stress conditions.

Equivalent Car-binding sites are suggested in the other LHC II proteins, as they all have a highly conserved secondary structure. However, only binding of Lut to the L1 site is a common feature of all LHC proteins, whereas the occupancy of the other binding sites differs in each member of the antenna subcomplexes (see Morosinotto et al. 2003 for an overview).

MINOR LIGHT-HARVESTING COMPLEXES

The PS II antenna complex is composed of six different polypeptides, Lhcb1-6. The main antenna is LHC IIb, present in trimeric form, as described above (Lhcb1-Lhcb3). The remaining antenna complexes are Lhcb4-6, also known as CP29, CP26 and CP24 (using the old nomenclature based on molecular weights). They are altogether classified as minor antenna (LHC IIa) and they are generally found as monomers. They bind from eight to ten Chl *a* molecules and between 2 and 3 Cars per monomer (Bassi et al. 1993, Caffarri et al. 2007). So far no crystal structure of minor antenna monomers has been reported, but the folding into helices is considered to be similar to the major LHC II. The available data concerning the role of pigment-protein subunits and the role of individual amino acids in the pigment binding and organization of the various cofactors derive from spectroscopic and functional analysis on purified or refolded complexes. Table 2.1 summarizes the pigment content of different Lhcb units.

Table 2.1: Pigment composition of the native (n) and recombinant (r) Lhcb- proteins.

LHC type	Chl <i>a</i>	Chl <i>b</i>	Vx	Lut	Nx	Source
LHC II-monomer	8.5	3.5	0.2	1.8	1.0	Croce et al. (1999b)
rLhcb1	8.5	3.5	0.15	1.85	1	Croce et al. (1999b)
nCP24	2.7	2.3	0.47	0.54	-	Pagano et al. (1998)
rCP24	5	5	0.6	1.5	-	Pagano et al. (1998)
nCP26	6.2	2.8	0.38	1.02	0.61	Croce et al. (2002)
rCP26	6.1	2.9	0.3	1.04	0.76	Croce et al. (2002)
nCP29	5.3	2.7	0.65	1	0.35	Crimi et al. (2001)
rCP29	5.3	2.7	0.5	1	0.4	Crimi et al. (2001)

PRESENT HYPOTHESES FOR THE qE QUENCHING MECHANISM

In the following the main hypotheses present in the literature for the possible quenching mechanisms of NPQ are highlighted.

Zeaxanthin as a direct quencher

In 1994 a “gear-shift” model was proposed by Frank et al. (1994) according to which Zx acts as a direct quencher of excited Chl. Excitation energy transfer from Chl *a* to Zx should be possible, because the first singlet excited electronic state (S1) of Zx is supposed to be lower than the lowest excited state Q_y of Chl (Demmig-Adams 1990, Frank et al. 1994). In contrast the S1 state of Vx is supposed to be above the Q_y level of Chl *a* and thus cannot quench the excited state of Chl *a*. This mechanism occurs in artificial light-harvesting dyads (Berera et al. 2006). This model was questioned by Polivka et al. (2004).

In alternative work femtosecond transient absorption measurements on thylakoid membranes brought evidence for the formation of a Zx cation radical in the PS II antenna (Holt et al. 2005). Thus electron transfer quenching in a Chl/Zx complex with a possible involvement of PsbS was proposed as an alternative mechanism.

PsbS as a direct quencher

This hypothesis implies that PsbS is a quenching site, since it was reported that it binds Zx *in vitro* that gives rise to a strong red shift in the absorption spectrum (Ruban et al. 2002), providing a possible explanation for the absorption change observed at 535 nm when qE is active (Bilger and Björkman 1994, Ruban et al. 1993). The “two xanthophyll binding sites” model (Holt et al. 2004, Li et al. 2004) proposed that protonation of each glutamate residue (E122 and E226) activates a corresponding binding site for de-epoxidized xanthophylls.

However this model was recently disproved by Bonene et al. (2008) whose experiments excluded an interaction between Zx and PsbS. They concluded that the xanthophyll dependence of qE is not due to PsbS but to other pigment binding proteins.

Minor antenna as the site of qE

80% of the xanthophyll-cycle active Cars are bound to the three minor antenna proteins of PS II (Bassi et al. 1993). There is an evidence for qE quenching located in the minor LHCs that is independent of PsbS: in CP26 (Dall'Osto et al. 2005) and in CP29 (Crimi et al. 1998).

Avenson et al. (2008) and Ahn et al. (2008) have recently proposed that generation of the Zx radical cation occurs solely in isolated minor light-harvesting complexes. They suggest that the minor complexes binding Zx are the sites of charge transfer quenching *in vivo*, which is modulated by the trans-thylakoid pH gradient, the PsbS protein, and further by protein-protein interactions.

However, the antisense analysis (Andersson et al. 2001) showed that efficient qE quenching also occurs with deactivated CP29 and CP26, to similar extents as in wild type *Arabidopsis thaliana*.

Conformational change in LHC II

According to this hypothesis Zx acts as an indirect quencher. The acidification of the thylakoid lumen and the de-epoxidation of Vx may induce conformational changes in LHC II resulting in specific Chl-Chl interactions which lead to the formation of a quenching state within the PS II antenna (Horton et al. 2005, Pascal et al. 2005). Fluorescence studies on LHC II crystals have shown that in the crystalline state the LHC II fluorescence is strongly quenched and red shifted (Pascal et al. 2005). The authors suggest one or two Chl pairs to provide a channel for the safe energy dissipation within each of interacting LHC II trimers. The conversion of Vx to Zx during the xanthophyll-cycle is thought to modulate the formation of the dissipative state. It has been shown in the work of Crouchman et al. (2006) that Zx enhances the NPQ quenching but is not absolutely necessary for the process. Therefore Zx is understood as an allosteric regulator which locks-in or favours the conformation in the quenched state but is not necessary for forming it (Crouchman et al. 2006).

Two subhypotheses are related to this model:

- **PsbS is an indirect quencher.** Another recent qE model proposes an indirect role of PsbS (Pascal et al. 2005). According to this model, PsbS interacts with

LHC II in the photosynthetic membrane at low luminal pH, inducing a conformational change that activates Chl-Car binding proteins performing quenching.

- **Lutein is involved.** Femtosecond transient absorption spectroscopy studies on aggregated LHC II *in vitro* resulted in a model in which qE is initiated by a conformational change induced by the light-dependent ΔpH . The change in conformation then enables energy transfer to the L1 in LHC II (Ruban et al. 2007).

PS II RC is the site of qE

An additional Zx-independent mechanism of energy dissipation in the reaction centre (RC) of PSII has been proposed to explain the transient formation of qE upon the transition of dark-adapted leaves to low light (Finazzi et al. 2004).

According to this RC quenching hypothesis, over-reduction of Q_A has been suggested to be a major prerequisite for efficient dissipation of the excess light within the RC of PSII. RC quenching may replace antenna based qE in organisms such as cyanobacteria which lack xanthophyll-cycle-dependent antenna quenching and complement the capacity for antenna quenching under conditions where the enzyme-dependent xanthophyll cycle is thermodynamically restricted (see (Ivanov et al. 2008) for a recent review).

NON-PHOTOCHEMICAL QUENCHING IN DIATOMS

Diatoms (Bacillariophyceae) are unicellular photosynthetic organisms that play a key role in the biochemical cycles of carbon, nitrogen, phosphorus and silica. They have a strong impact on the global climate not only in the ocean, where they are responsible for at least a quarter of global carbon fixation (Falkowski and Raven 1997), but also in the freshwater environment (for a recent review see Wilhelm et al. 2006). Diatoms experience large fluctuations in light intensity due to unpredictable water motions that can vary over several orders of magnitude on a time-scale of minutes (Lavaud et al. 2003). In order to survive the periodic exposure to high excess light intensities, they developed mechanisms to quench the excess energy by non-photochemical processes, presumably by some modification/reorganization in their antenna complexes attached to photosystem (PS) II.

The organization of the thylakoid membrane, the light-harvesting complexes and the pigmentation in diatoms differ from vascular plants and green algae. Diatoms do not contain granal and stromal thylakoids as the vascular plants. They rather contain one homogeneous thylakoid membrane organized in bands of three. According to present knowledge, the antenna proteins of PSI and PSII in diatoms are similar or even identical and they do not differentiate into PSI and PSII antenna nor into minor and major complexes as it is the case in vascular plants (Pyszniak and Gibbs 1992). Besides chlorophyll (Chl) *a*, diatoms contain different Chl *c* species as antenna chromophores, and fucoxanthin as the major light harvesting xanthophyll, which is also responsible for their brown colour.

The proteins of the light-harvesting complexes in diatoms are called fucoxanthin-chlorophyll-binding proteins (FCPs). They are encoded by a conserved family of *fcps* genes of at least six members (Bhaya and Grossman 1993, Eppard and Rhiel 1998). Evidence accumulated on the structural organization of FCPs, showing them to form higher oligomeric states in the species *Cyclotella meneghiniana* and *Phaeodactylum tricoratum* (Büchel 2003, Gundermann and Büchel 2008, Lepetit et al. 2007, Szabó et al. 2008). Two different FCP fractions can be isolated by sucrose density gradient centrifugation, showing distinct oligomerization and pigmentation patterns. A recent study presented evidence that fluorescence quenching in one population of *C. meneghiniana* FCPs depended on the presence of Dtx, while in another it was not affected by Dtx accumulation (Gundermann and Büchel 2008). Regarding the distribution of xanthophyll cycle (XC) pigments, Lepetit and co-workers (2008) could show in *P. tricoratum* that apart from the highly enriched FCPs, a population of Ddx and Dtx is tightly associated with the core complex of both PSI and PSII, and that de-epoxidation takes place in PS I as well.

The main xanthophyll cycle of diatoms is the diadinoxanthin cycle (DdC), but the situation in diatoms is more complex than in vascular plants because diatoms contain both the DdC and the violaxanthin cycle (Lohr and Wilhelm 1999). In the DdC the xanthophyll diadinoxanthin (Ddx) is de-epoxidized into diatoxanthin (Dtx) (Hager and Stransky 1970b) in a one-step reaction.

In the diatom *P. tricoratum* NPQ is assigned to the DdC only (Owens 1986, Ting and Owens 1994). A strict correlation between Dtx content and NPQ was found under most natural conditions in *P. tricoratum* (Lavaud et al. 2002) and it could not be shown that a ΔpH alone induces NPQ (Lavaud and Kroth 2006). However, the proton gradient is needed during the development of Dtx-dependent NPQ, both for the de-epoxidation of Ddx to Dtx and for the activation of the Dtx-dependent NPQ. Once the Dtx-dependent

NPQ has been established, it is stable even in the absence of a proton gradient. These differences suggest a different mechanism of NPQ in diatoms as compared to vascular plants (for a recent review see Horton et al. 2005, Horton and Ruban 2005) because in vascular plants the main part of the NPQ relies on the presence of a ΔpH . A Zx -dependent NPQ without a proton gradient is observed in vascular plants if intact leaves are illuminated with high light for longer time periods (Adams et al. 2001). Recently, evidence for an additional, faster, NPQ mechanism, that is not directly related to the DdC and relaxes rapidly in darkness, was found in the diatom *C. meneghiniana* (Grouneva et al. 2008). This component seems to be missing, however, in *P. tricornutum*. An equivalent to the PsbS protein, which in vascular plants is crucial for NPQ generation and ΔpH sensing (Li et al. 2000), has not been found in the genome of the diatoms *Thalassiosira pseudonana* (Armbrust et al. 2004) or *P. tricornutum* (Oudot-Le Secq et al. 2007). Although the LI818 protein has been suggested to play the role of PsbS in diatoms (Zhu and Green 2008). The search for a functional counterpart of PsbS still remains an open question in the context of NPQ formation in diatoms.

Until now, only slow fluorescence induction kinetics have been used to study NPQ in diatoms. The information gained from such studies is limited as far as the exact location of NPQ within PSII or PSI is concerned. Thus, the main goal of our study is to gain insight into the NPQ characteristics and in particular the locations of NPQ in the photosynthetic complexes of diatoms based on fast fluorescence decay measurements with picosecond resolution. The fluorescence kinetics were measured for both *C. meneghiniana* and *P. tricornutum* in order to understand the differences in NPQ observed for these two diatoms.

Chapter 3

MAIN AIMS OF THE THESIS

From the hypotheses and models of quenching present in the literature (c. f. Chapter 2) it becomes clear that neither the exact location(s) of the quenching site(s) in PS II is known, nor is it clear whether the PsbS protein and Zx cooperate in the same quenching mechanism or whether they operate independently or parallel in different locations and/or with different mechanisms. Thus the most important aim of this thesis is to precisely locate the possibly multiple quenching sites using novel methodology that has not been applied before.

The crucial principle followed in the present work is that the NPQ regulation is a property of the intact plant leaf and intact organism. Thus in order to gain insight into the details of the NPQ regulation it is essential to apply non-invasive methods on intact leaves for the study of these phenomena under conditions close to the physiological ones. This is one of the reasons why Chl fluorescence is commonly used for NPQ characterization. However the traditionally employed methods of measuring slow variations in steady state fluorescence lack the ability to differentiate the signals deriving from various Chl and antenna components of the photosynthetic apparatus. They are also unsuitable to determine the exact contributions of photochemical and non-photochemical quenching (Holzwarth 1988, Holzwarth 1991, Holzwarth 2004). Time-resolved Chl fluorescence kinetics with picosecond resolution is however ideally suited as a non-invasive and direct method to probe the photochemical and non-photochemical energy-dissipating mechanisms in photosynthetic tissue. This method also allows measurements under physiological conditions. The regulation of photosynthetic light-harvesting will thus be addressed in this thesis primarily by applying picoseconds fluorescence measurements on intact plant leaves.

The main difficulty that the intact system presents is its extremely high complexity. This is the principal reason why time-resolved fluorescence has been applied in the past only *in vitro* on isolated parts of the photosynthetic machinery or in a few cases on isolated thylakoids (Gilmore et al. 1995). The complete intact thylakoid membrane contains a vast multitude of absorbing and fluorescing pigments, many of them at overlapping wavelengths, which act together creating a complex kinetic system with many compo-

nents. The analysis of such a system and the proper separation and assignment of its components is only possible applying the in-depth knowledge of the dynamics of the separate pigment-protein complexes, i.e. LHC II, PS II, PS I.

Therefore, the analysis and interpretation of data would have been impossible without preliminary experience received from detailed study of the kinetics on isolated complexes (Holzwarth 2008). The recent reports on PS I kinetics (Holzwarth et al. 2005, Holzwarth et al. 2006a, Ihalainen et al. 2005a, Slavov et al. 2008) and the kinetics of PS II with closed RCs (Martinez-Junza et al. 2008, Szczepaniak et al. 2008) played a decisive role in our analysis. However the kinetics of intact PS II with open RCs was rather controversial. But since the PS II supercomplex is the centre of NPQ we aimed here first to study PS II in different isolated complexes, starting from PS II core from cyanobacteria, continuing with PS II enriched membranes from higher plant and the isolated light-harvesting antenna of PS II in trimeric and oligomeric states. However the main goal was to understand the kinetics in *in-vivo* plants that we could achieve by combining the knowledge from *in-vitro* applying studies.

In combination with ultrafast spectroscopy methods, the molecular biology approach, able to provide transgenic plants in which specific sites or constituents of the photosynthetic machinery are eliminated, will be utilized to resolve the complex puzzle of NPQ. The combined use of these methods should be suitable to unequivocally identify the exact quenching locations in the photosynthetic membrane and their dependence on Zx and PsbS as well as on minor and major PS II antenna. This involves in particular also the identification of the specific roles of Zx and PsbS, major LHCII and minor antenna complexes.

We have chosen *Arabidopsis thaliana* as the principal model organism for our study. This plant has found extremely widespread use in molecular plant science mainly because its complete genome sequence is known and a great number of mutants are available. For our aim, i.e. clarifying the roles of Zx, PsbS and the PS II antenna in NPQ, we found the following *Arabidopsis* mutants particularly useful: *npq1*, which is unable to produce Zx; *npq4*, deficient in the PsbS protein; *L17*, which overexpresses PsbS; and the minor antenna knock-out mutants *koCP24*, *koCP26*, and *koCP24/26*, lacking, respectively CP24, CP26, and both of them. In addition to the antenna mutants of *A. thaliana*, we aimed to investigate the NPQ mechanisms in diatom algae, which completely lack the LHC II antenna, having FCP complexes instead, but are nevertheless capable of rapidly inducible and efficient non-photochemical energy dissipation. We sought to test whether the

quenching processes in diatoms and higher plants have the same or different underlying mechanisms.

After identifying the location of the quenching, in a second step the question of the photochemical quenching mechanisms should be addressed. Time-resolved fluorescence spectroscopy is however not particularly well suited to identify photochemical mechanisms since intermediates that are non-fluorescent may be involved, like e.g. cations/anions of Cars and Chls. Nevertheless important hints on the possible mechanisms can be obtained from the analysis of time-resolved fluorescence spectra etc. This tool will thus be applied as much as possible to get some educated guesses on the mechanisms as well even if it may not give final answers to the photochemical mechanisms.

The following list summarizes the open questions, which were the basis for the experimental work in the thesis.

SUMMARY OF OPEN QUESTIONS

- Is the kinetics in PS II core trap-limited or transfer-to-trap limited?
- What are the differences in the primary kinetics of isolated PS II core, D1/D2-cyt_{b559} RCs and PS II-enriched membranes (BBY particles)?
- Is the exciton/radical pair equilibrium model correct? What are the limitations?
- What are the differences in the rates and energetics of the electron transfer processes between (thermophilic) cyanobacteria and higher plants?
- Is it possible to combine the *in-vitro* results from isolated PS II, PS I and LHC II with the *in-vivo* results from intact leaves? From diatoms?
- Is it possible to link *in-vitro* and *in-vivo* kinetic fluorescence data?
- Where exactly in the photosynthetic apparatus is the location of NPQ?
- What is the role of Zx?
- What is the role of PsbS?
- Do they work together?
- What are the roles of minor and major antenna (LHC II)?
- What are the roles of CP24 and CP26?
- What is (are) the non-photochemical quenching mechanism(s)?
- Which quenching mechanism(s) operate in which part of the photosynthetic apparatus?
- Is the mechanism of qE the same in higher plants and diatoms?
- What is the quenching mechanism in diatoms?
- What are the differences in NPQ behaviour between the two diatoms *C. meneghiniana* and *P. tricornutum*?

Chapter 4

MATERIALS AND METHODS

SINGLE PHOTON TIMING

Fluorescence techniques in general found numerous applications in life sciences since they are highly sensitive, highly selective, nondestructive, and can also be applied easily to strongly scattering materials. The rapid development of time-resolved fluorescence methods starting from the 1970s provided more detailed information, adding a time dimension (Holzwarth 1988, Holzwarth 1995). Single photon timing (SPT, also called time-correlated single photon counting) is one of the most sensitive techniques for recording low-level light signals with picosecond resolution and extremely high precision (Becker 2005) (O'Connor and Phillips 1984). It is indispensable for the kinetic study of photosynthetic light reactions in pigment-protein complexes, cyanobacteria, diatoms and intact leaves.

The principle of single photon timing

The principle of single photon timing stems from the concept of delayed coincidence measurements of radioactive decay originating from nuclear physics. In the SPT experiment the delayed coincidence between an exciting light pulse and the occurrence of the first fluorescence photon is being measured. According to the Ergodic theorem the time distribution of the photon emission from one excited molecule and of the fluorescence from an ensemble of these molecules have the same distribution probability. To measure it as a function of photon time delay the following procedure is used (see Figure 4.1). A pulsed excitation laser beam is split into two parts. One of them excites a photodiode (PD), its electronic pulse determines a reference point. The other part of the beam excites the sample, the emitted photon from which is detected by a photomultiplier tube (PMT). It is normally located after a monochromator in order to be protected from scattered excitation light and to multiply the selected wavelength. PD and PMT forward their electronic pulses to the electronic clock, or time-to-amplitude converter (TAC). It creates a pulse of voltage, the amplitude of which is proportional to the difference between the arrival times of the PD- and PMT-pulses. With the help of an analog-to-digital

converter (ADC) and a multichannel analyzer (MCA) the voltage amplitudes produced by the TAC are converted and stored into channel numbers, where each channel counts the number of emission occurrences within a certain delay time interval. When many (typically millions) detected photons are counted, the computer will contain a histogram of the probability distribution of emitted fluorescence photons across delay times after excitation. The shape of the histogram matches exactly the time course of the fluorescing sample (Figure 4.2)(Holzwarth 1995, Müller 1992).

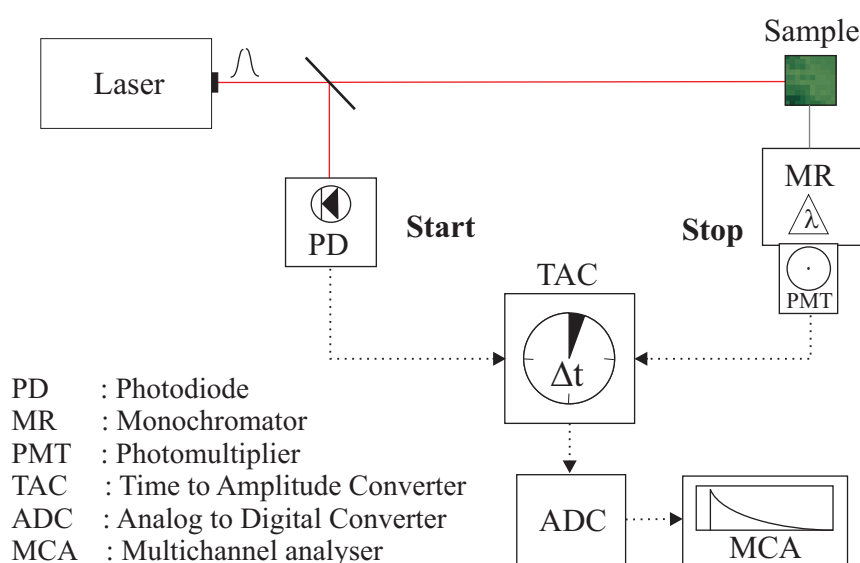


Figure 4.1: Measuring principle of the single-photon-timing.

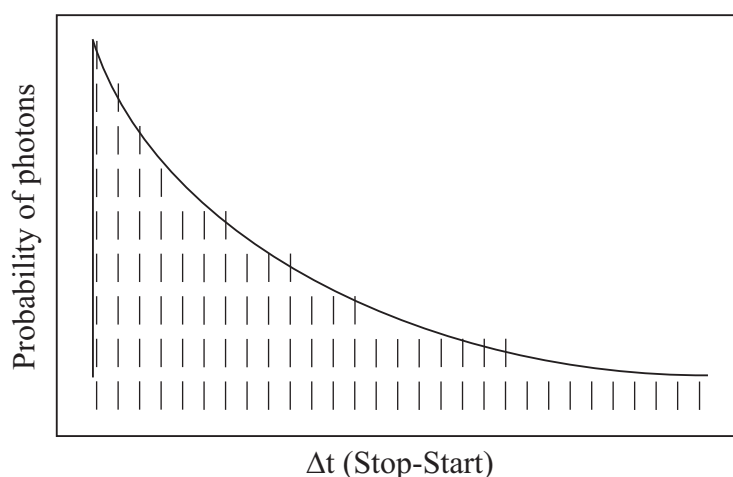


Figure 4.2: Histogram of the distribution of fluorescence photons across delay times after excitation.

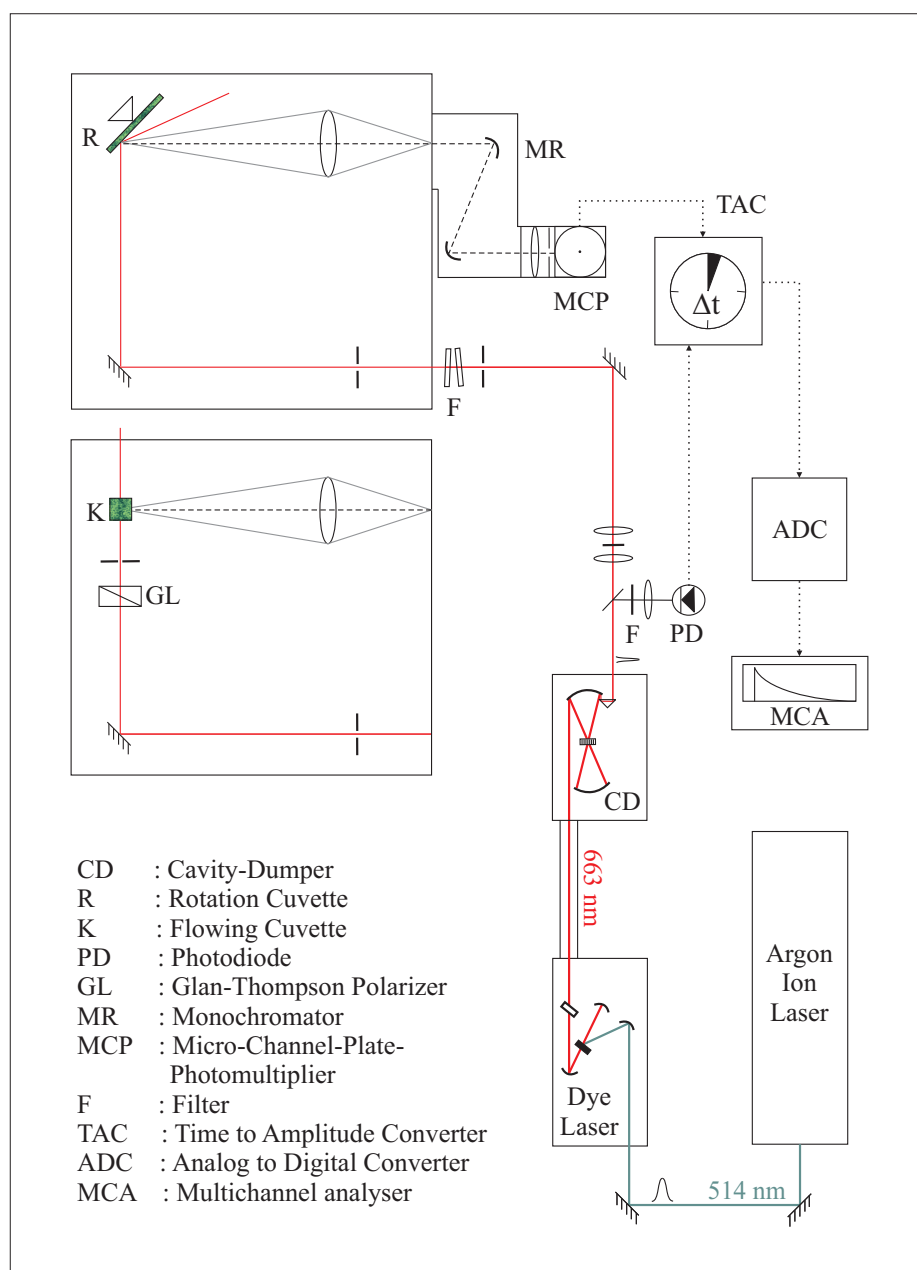


Figure 4.3: Schematic assembly of the single-photon-timing equipment used in this work. Excitation pulses are provided by the dye laser coupled to the cavity dumper. The dye laser is pumped by the argon-ion laser. The optical path of the excitation beam is depicted with a red line. Exiting the cavity dumper the beam passes through a beam splitter, and one part of it is detected by a photodiode that supplies the stop signal to the TAC. The main part of the beam is collimated with lenses and a pinhole and, after passing a set of neutral-density filters to adjust for the desired pulse energy, is directed to the sample compartment and reflected away. Two possible arrangements depending on the type of cuvette, flowing or rotation, are shown. The emitted fluorescence is focused onto the enter slit of a computer-controlled monochromator and the selected wavelength is detected by a MCP photomultiplier. The photomultiplier signal starts the TAC clock. The amplitude generated by the tack (proportional to the time between excitation and detection) is digitized by the ADC and stored into a corresponding time channel by the multichannel analyser.

Laser system

The scheme of the laser system and optical setup used for the measurements is shown in the Figure 4.3. All the details of it are described in (Müller 1992). The core of the SPT-apparatus is a dye laser system providing pulses of picoseconds duration. It consists of the mode-locked argon-ion laser (model 2030 with mode-locker 342A and mode-locker-driver 452, Spectra Physics) and synchronously pumped dye laser (model 375 B, Spectra Physics) that is equipped with cavity-dumper (model 344S with cavity-dump-driver 454, Spectra Physics). As a dye in this work DCM (4-dicyanomethylene-2-methyl-6-p-dimethylaminostyryl-4H-pyran, $C_{19}H_{17}N_3O$) was used, the emission interval of which is 610-710 nm (Brackmann 1986). This laser system allows to reach 1-2 ps time resolution after the deconvolution of signals recorded with a high signal-to-noise ratio. The laser power was 4-6 mW for the cavity dumper repetition rate of 0.8 MHz and 25-30 for 4 MHz. The stability of pulses during the measurements was controlled by an oscilloscope (Tektronix, model 485).

The intensity of the laser pulses was reduced to the required values by two neutral-density filters before entering the light-protected sample box. The geometry of optics in the sample box was set according to the type of measurement. A Glan-Thompson prism situated before the sample improved the vertical polarization purity of the laser beam. The fluorescence photons were detected perpendicular to the excitation direction by a micro-channel-plate photomultiplier with multi-alkali photocathode (R1564U-01, Hamamatsu).

Detection electronics

The power supply (Oltronix A 3.4 k-40R) provides a highly stable voltage for the photomultiplier. The output signal of the photomultiplier is amplified from millivolt- into the volt-range (HP8447 F, Hewlett Packard amplifier) and split into two parts with a Star-splitter. One part of the puls is transformed into a fast rectangular signal by a constant-fraction-discriminator (CFD Model 455 Quad, Tennelec,) in such a way that the triggering time becomes independent of the signal amplitude. The rectangular signals start the time-to-amplitude converter (TAC 862, Tennelec).

The second part of the signal is again amplified (EG&G timing-amplifier, model 574) and analyzed in an energy-discriminator (EG&G TD101/N). Through the pulse transformer it

delivers information to the gate-entrance of the TAC whether the pulse amplitude lies within predetermined limits. Only a relatively small number of photomultiplier pulses will not fulfill this discrimination condition. To minimize the dead time of the system, the TAC works in the “inverse” principle. It means that the laser does not start the TAC, it only stops it. (Becker 2005, Müller 1992).

Data analysis

The measured decay curve $I(t)$ represents a convolution, or folding together, of the real fluorescence decay of the sample $F(t)$ and the instrument response function $P(t')$:

$$I(t) = \int_0^t P(t') \cdot F(t - t') dt' \quad (1)$$

The instrument response function depends basically on the finite duration of the excitation pulse (it is not a δ -shaped excitation) and the final response time of the detection system employed. To overcome this problem the signal of a highly scattering sample (nonfluorescent), the important feature of which is that it responds to the exciting light without delay, was measured under exactly the same optical conditions as the investigated fluorescent sample. As scatterers Ludox¹, colloidal silica, and ultrahigh-temperature-treated milk were used. The signal measured from such a scatterer is usually the direct instrument response (Grinvald and Steinberg 1974, Holzwarth 1995, Müller 1992).

The decay kinetics of photosynthetic complexes has in most cases a multiexponential form. In these cases the decay function $F(t)$ is determined as:

$$F(t, \lambda_{em}) = \sum_{i=1}^n A_i(\lambda_{em}) \cdot \exp(-t / \tau_i) \quad (2)$$

The fluorescence decay function and amplitudes A_i here are not only time-dependent, but also dependent on the emission wavelength (λ_{em}); τ_i presents lifetimes. The analysis

¹ Ludox is a trade mark for an aqueous suspension of silica manufactured by E.I. du Pont de Nemour Co., Wilmington, Delaware, USA.

of measured fluorescence decay $I(t)$ is concentrated mostly on the identification of lifetimes and amplitudes by iterative least-squares fit deconvolution (O'Connor and Phillips 1984). In essence, the procedure consists of calculating a theoretical decay function, $F(t, \lambda_{em})$, according to Eq. 2 and convoluting it with the measured instrument response function $P(t)$ to obtain a theoretical signal $G(t)$. The fitting parameters (amplitudes and lifetimes of the theoretical decay function) are varied to minimize the quadratic deviation χ^2 , which is the criterium for best fit:

$$\chi^2 = \frac{1}{n-p-1} \sum_{i=1}^n \frac{(I_i - G_i)^2}{I_i}, \quad (3)$$

where n is here the total number of data points in the fit, p is the total number of independent fit parameters. The least-square fit procedure is done by the Levenberg-Marquardt algorithm (Marquardt 1963).

The goodness of fit can be evaluated by examining the plot of weighted residuals (r_i). The weighted residual in channel i is calculated from the equation:

$$r_i = \frac{I_i - G_i}{\sqrt{I_i}}. \quad (4)$$

When plotted against channel number, residuals from successful fits should be randomly distributed around zero.

Global analysis

In the global, or “simultaneous” analysis method fluorescence decay data taken at various conditions of emission wavelength, excitation wavelength, temperature, concentration, etc., are analyzed in a combined procedure. The main idea is that certain parameters in fluorescence decay remain constant or change in a defined manner with other independent parameters. Then a combined analysis where several fluorescence decays are linked together becomes possible. It leads to a better accuracy in the values of the extracted parameters and allows the analysis of more complex systems and more closely spaced lifetime components.

The global analysis is focused mostly on the identification of lifetimes and amplitudes (see equation 2). The obtained amplitudes of the decay lifetime components plotted against emission wavelength after correction for stationary spectra (Holzwarth et al. 1985) or detection time produce so called *decay-associated spectra* (DAS) (Holzwarth 1996). In the case when only one emitting species contributes to a given fluorescence lifetime, the corresponding DAS would represent the fluorescence emission spectrum of this species if it were isolated and then measured individually (Holzwarth et al. 1985). The DAS is then identical to the species-associated emission spectrum (SAES), which provides valuable information on the absorption cross-section and hence the antenna sizes of the decay components:

$$A(\lambda_{em}) = k_{rad} \cdot \sigma(\lambda_{exc}) \cdot N \cdot F(\lambda_{em}) \quad (7)$$

where k_{rad} is the radiative rate constant, $\sigma(\lambda_{exc})$ is the extinction or absorption cross-section at the excitation wavelength, $F(\lambda_{em})$ is the shape of the (normalized) fluorescence spectrum, and N is the number of chromophores contributing to the lifetime component. In practice several species having different emission spectra can take part in the observed fluorescence lifetime. In this case the DAS is a linear combination of their SAES. An illustration of that is the energy transfer occurring between two chromophores. This would produce a lifetime component with DAS having a positive maximum at the emission maximum of the donor and a negative maximum corresponding to the acceptor's fluorescence emission maximum.

Important values that one can also get from global analysis are the average lifetime τ_{av} and the relative fluorescence yield φ_i :

$$\tau_{av} = \frac{\sum_i A_i \tau_i}{\sum_i A_i} \quad (5)$$

$$\varphi_i = \frac{A_i \tau_i}{\sum_i A_i \tau_i} \quad (6)$$

Global analysis gives a mathematical description of the measured data, which is not direct information in terms of physical/chemical model. Rather these fitting parameters have to be used to derive the parameters of real interest to the researcher.

Target analysis

The goal of target analysis is to get physically relevant parameters directly, such as species-associated emission and absorption spectra (SAES and SAAS), rate constants (k_i) and concentrations or populations of components (x_i).

It allows to test different kinetic models on raw data and to describe various energy transfer processes between chromophores or chromophore groups. The detailed procedures and interpretations can be found in (Beauregard et al. 1991, Holzwarth 1996, Müller 1992).

The time dependence of concentrations of excited species is found by solving the first order differential equation:

$$\frac{d\vec{X}(t)}{dt} = K \cdot \vec{X}(t) + \vec{B} \cdot I(t), \quad (7)$$

where $\vec{X}(t)$ – ($n \times 1$) vector of concentrations of excited state species,

\vec{B} is a vector of time zero absorbances of species,

$I(t)$ – excitation function,

K is the ($n \times n$) kinetic transfer matrix describing the connectivity of the matrix,

K_{ij} – time constants k_{ij} .

$$K_{ii} = K_{0i} + \sum_{j=1, j \neq i}^n K_{ji}$$

The equation of the time dependence of fluorescence spectra $F(t, \lambda_i)$ is:

$$F(t, \lambda_i) = \sum_{j=1}^n e^{\gamma_j t} \cdot \sum_{m=1}^n S_m(\lambda_i) \cdot (U^{-1} \cdot \vec{B}(\lambda_{exc}))_j \cdot U_{jm}, \quad (8)$$

where γ_j – j^{th} eigenvalue of matrix K , $\gamma_j = -1/\tau_j$,

U – matrix of eigenvectors of K ,

n – number of excited species m ,

$S_m(\lambda_i)$ – SAES for m^{th} species.

These equations completely describe the relationship between the measured decay data as a function of excitation wavelength, emission, the kinetic scheme (quasi first-order kinetics) and the rate constants of the system on the one hand and the SAS on the other hand.

Lifetime distribution analysis

To get information about possible lifetime distributions in complex systems, to determine the main lifetimes contributing to the kinetics and to independently get an idea about whether any of the lifetimes are discrete or distributed, a so-called lifetime distribution analysis (LDA) (Trinkunas and Holzwarth 1996) was applied. LDA was carried out by a home-written program based on an inverse Laplace transform of the kinetic data combined with a Tikhonov regularization (Prokhorenko et al. 2000) using a fixed set of 190 exponential lifetimes ranging from 1 ps to 1.5 ns equally spaced on a logarithmic lifetime scale as the basis function. The algorithm determines the pre-exponential amplitudes only. It works in a similar manner as the calculation of lifetime density maps in transient absorption (Croce et al. 2001, Croce et al. 2003a).

Theoretical modeling

The theoretical modeling of the kinetics was carried out by numerically solving the eigenvalues of the kinetic matrix of the model system (Beauregard et al. 1991) and calculation of the weighted eigenvector matrix (weighted amplitude matrix), the inspection of which reveals the contributions of the various intermediates to specific *apparent lifetimes* and allows to calculate the time dependence of the populations of the intermediates (Beauregard et al. 1991, Müller et al. 2003).

PREPARATION AND CHARACTERIZATION OF SAMPLES

PS II core particles from cyanobacteria

Dimeric PS II core particles from *Thermosynechococcus elongatus* with intact oxygen evolution, kindly provided by J. Sander and Prof. Dr. Matthias Rögner from Ruhr-Universität Bochum, were measured using the above-described SPT apparatus at room temperature and laser repetition rate of 800 Hz. These particles were isolated and purified according to Kuhl et al. (2000) and showed an average oxygen evolution rate of 3200 ($\pm 10\%$) $\mu\text{mol O}_2/\text{mg Chl/h}$. Fluorescence measurements were performed in a buffer of 20 mM MES (pH 6.5), containing 500 mM mannitol and 0.4 mM ferricyanide (to keep the RC in an open (F_0) state). To ensure that no significant amount of closed RCs was present, the sample was kept in a rotating (4000 rpm) cuvette of 1.5 mm path

length with a diameter of 10 cm, which was also oscillated sideways at 66 rpm. Stopping the movement (and thus allowing RCs to close) of the cuvette led to an increase by a factor of 11-12 in the fluorescence intensity. The laser excitation intensity was low enough to ensure that during a single passage of the sample volume through the laser beam the excitation probability for a PSII particle was < 50%.

PS II enriched membranes (BBYs)

Time-resolved fluorescence measurements on the above described apparatus were performed on freshly prepared thylakoids and BBY particles isolated from greenhouse spinach grown for 6 weeks under short day conditions at light intensity of 150 $\mu\text{mol photons m}^{-2}\text{s}^{-1}$ and 20 °C. To ensure low enough laser excitation intensity that allows for the RCs to be kept open and not to be excited twice in a short time, the sample was rapidly pumped (flow rate at $\sim 200\text{-}260$ ml/min) from a large reservoir (200 ml) through a flow cuvette kept at a temperature of 277 ± 1 K. The maximal allowed laser intensities (≤ 0.09 mW on a 1.5 mm diameter spot) for keeping RCs open was calculated from these parameters and then checked experimentally by measuring at several excitation intensities above and below the pre-calculated value in order to ensure that all RCs were open. The actual excitation intensity used in the final measurements corresponded to a probability of < 0.6 for a single PS II unit being excited upon a single passage through the laser beam.

Thylakoid preparation

Thylakoids were prepared from spinach leaves. The leaves were ground in a blender in buffer A (1 mM MgCl_2 , 1 mM MnCl_2 , 10 mM NaCl, 2 mM EDTA, 0.8 mM KH_2PO_4 , 44 mM MES/ NaOH, 0.33 M Sorbitol, 4 g/l BSA, 0.5 g/l Cystein, 0.4 g/l Na-Ascorbate, pH 6.1) and centrifuged for 10 minutes at 5 000 g and 4 °C. The pellet was resuspended in 5 mM MgCl_2 and incubated for 1 minute, then an equal amount of buffer B (5 mM MgCl_2 , 10 mM NaCl, 2 mM KH_2PO_4 , 80 mM HEPES/ NaOH, pH 7.6, 0.66 M Sorbitol) was added and the sample was centrifuged again. The pellet was used for the BBY preparation.

BBY preparation

PS II grana membranes were isolated from thylakoid membranes as described by Berthold et al. (1981) with some modifications by van Leeuwen et al. (1991). The thylakoid pellet was resuspended in a buffer containing 50 mM MES (pH 6.0), 15 mM NaCl, 5 mM MgCl_2 and 1 mM sodium ascorbate to a final concentration of 2.5 mg Chl/ml. Triton X-

100 was added slowly from a stock solution to a final concentration of 20 mg/mg Chl. After 15 min incubation at 4 °C in the dark the suspension was centrifuged for 25 min at 20 000 g. The PSII membrane particles were resuspended in BTS400 buffer consisting of 20 mM BisTris (pH 6.5), 20 mM MgCl₂, 5 mM CaCl₂, and 1 mM MgSO₄ and were centrifuged for 25 min at 20 000 g. This typical preparation will be referred to as BBY-1 throughout the paper. It had a Chl *a/b* ratio of 1.95, corresponding to 3 LHC II trimers per monomeric PS II core. In a second type of preparation (referred to as BBY-2) the PS II membranes were resuspended a second time as described. This preparation (BBY-2) had a higher Chl *a/b* ratio of 2.05, corresponding to 2.0-2.5 LHC II trimers per monomeric PS II core. Finally the PSII membrane particles were resuspended in BTS400 with additional 0.4M sucrose. For the measurements 0.4 mM FeCy was added as an electron acceptor.

EPR measurement

To check for a possible PSI content of the isolated PSII membrane particles the samples were analyzed by EPR spectroscopy as described by Danielsson et al. (Danielsson et al. 2004). The BBY particles were found to contain << 5% of PS I RCs (this corresponds to the detection limit). The measurements were done by Dr. Maurice van Gestel at the MPI für Bioanorganische Chemie.

LHC II trimers and aggregates

LHC II trimers from the *npq1* and *npq2* mutants of *Arabidopsis thaliana* were provided by Dr. Roberta Croce, University of Groningen. Time-resolved fluorescence measurements were performed on the described above SPT-apparatus at room temperature. The sample was slowly pumped through a flowing cuvette. To avoid oxygen in the sample the system was closed and aerated with nitrogen. The LHC II trimers were measured in a buffer containing 10 mM HEPES pH 7.6, 0.06% β -DM and an oxygen scavenging system containing 1.36 mg/ml glucose, 65 μ g/ml glucose-oxidase and 65 μ g/ml catalase. Fluorescence decays did not differ whether detected starting from the longer or shorter wavelength range.

Isolation of lamellar LHC II aggregates

Lamellar LHC II aggregates isolated from wild type spinach were supplied by Dr. Petar Lambrev and Dr. Gy z  Garab from the Biological Research Center in Szeged, and prepared following the procedure described earlier (Lambrev et al. 2007, Simidjiev et al.

1997). The LHC II aggregates isolated by this procedure are organized in lamellar structures with diameter of several μm , Chl *a/b* ratio 1.3 and $\sim 300\mu\text{g}$ lipids/mg Chl.

LHC II trimers preparation

LHC II trimers were isolated from market spinach or from *Arabidopsis thaliana* plants grown under greenhouse conditions. Thylakoids were prepared according to (Bassi et al. 1988). The membranes were washed with 5 mM EDTA and solubilized at a final concentration of 0.5 mg/ml Chl and 0.6% α -DM in 10 mM HEPES. The solubilized material was loaded on a sucrose gradient and centrifuged at 280 000 g for 22 h. The characteristic band of LHC II trimers was harvested with a syringe from the gradient (Caffarri et al. 2001).

Pigment analysis

The pigment content of the isolated LHC II complexes was analyzed by HPLC as described by Gilmore and Yamamoto (1991). The Chl *a/b* and the Chl/Car ratios were determined by fitting the absorption spectrum of the acetone extract with the spectra of pigments in acetone (Croce et al. 2002).

Aggregated LHC II trimers preparation

To achieve aggregation of LHC II trimers the sample was diluted under the cmc of α -DM in a buffer containing 10 mM HEPES, 30 mM MgCl_2 and 100 mM KCl and concentrated by ultrafiltration over a 50 kDa membrane.

***Arabidopsis thaliana* plants**

Arabidopsis thaliana is a small flowering plant naturally found over a large area on Earth. It has an extraordinarily short generation time. Depending on growth conditions (mainly day length) it can be as short as six weeks from seed to seed. *Arabidopsis* is widely used in the laboratories over the world as a model organism. Its genome is one of the smallest plant genomes and was the first plant genome to be sequenced (*Arabidopsis* Genome Initiative, 2000). Because of that a number of different mutants biochemically well characterized are available. Moreover, *Arabidopsis* is well suited for the experiments described in this thesis due to their optical properties (thin leaves). However the small size of their leaves made filling of the cuvettes more difficult and time-consuming.

Different *Arabidopsis* mutants were used for the NPQ investigation and compared with the wild type (ecotype Col-0):

- *npq1* – deficient in VDE, synthesis of Zx is blocked (Niyogi et al. 1998)
- *npq4* – PsbS protein deficient (*psbs-1.3* (Graßes et al. 2002)
- *L17* – PsbS overexpressor (Li et al. 2002a)
- koCP24 – lacking CP24 minor antenna
- koCP26 – lacking CP26 minor antenna
- koCP24/CP26 – lacking both CP24 and CP26 minor antenna

The mutants were provided by Manuela Nilkens and Prof. Dr. Peter Jahns (University of Dusseldorf) except for the minor antenna knock-out mutants, provided by Silvia de Bianchi and Prof. Dr. Roberto Bassi (University of Verona). The plants were grown in soil under short-day conditions (10 h light / 14 h dark) at 20°C and light intensity of 150 $\mu\text{mol photons m}^{-2} \text{s}^{-1}$. Fully developed leaves of 5-6 week-old plants were used for the experiments.

Pigment analysis

Pigments were extracted from leaves with acetone and quantified by reversed-phase HPLC as described (Färber et al. 1997) of three plant genotypes for each condition. Dark-adapted leaves were kept in the dark for at least 10 h (F_{max} conditions). Light-adapted leaves were illuminated for 2 h at light-intensity of 600 $\mu\text{mol m}^{-2} \text{s}^{-1}$ (F_{NPQ} conditions).

Pulse-amplitude-modulated measurements

Fluorescence induction kinetics of variable Chl fluorescence was measured by a pulse-amplitude-modulated (PAM) fluorometer (Walz GMBL, Germany). Saturating pulses of around 4000 $\mu\text{mol photons m}^{-2} \text{s}^{-1}$ were given each 10s for the first 100 s and then each 100 s. The result of the PAM measurement is normally a curve shown in the Figure 4.4. First with a measuring modulated light (ML) of $\sim 1 \mu\text{mol photons m}^{-2} \text{s}^{-1}$ an F_0 state is measured, where the PS II RCs are open. Then a saturating pulsed light (PL) of $\sim 4000 \mu\text{mol photons m}^{-2} \text{s}^{-1}$ is switched on to close PS II RCs and to determine F_{max} conditions. When the actinic light (AL) of $\sim 1000 \mu\text{mol photons m}^{-2} \text{s}^{-1}$ is turned on, the fluorescence is going down to a stable value, called F'_{max} or F_{NPQ} . From the F_{max} and F'_{max} the NPQ value can be calculated (Krause and Jahns 2004):

$$\text{NPQ} = (F_{\text{max}} - F'_{\text{max}}) / F'_{\text{max}}$$

which is typically used to characterize the quenching capacity of a plant.

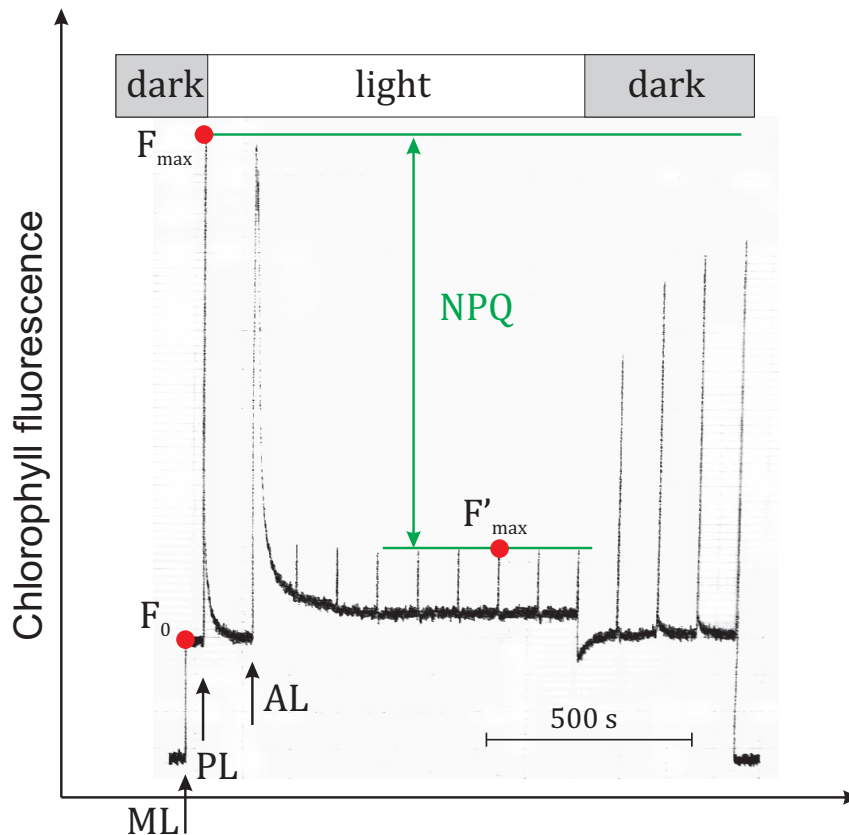


Figure 4.4: Measurement of NPQ with a PAM fluorometer. First F_0 is determined by using a weak measuring light (ML). A saturating pulse (PL) is applied to determine F_{max} . Then NPQ is generated by switching on the actinic light and the NPQ is probed by a series of saturating flashes to induce F'_{max} . The relaxation of NPQ is followed after switching off the actinic light.

Fluorescence kinetics

Fluorescence decays were measured by the described apparatus for single photon timing to high S/N ratio at several wavelengths. Detached plant leaves were held between two glass plates in a rotation cuvette (diameter = 10 cm, Figure 4.5) that was also oscillated sideways (Lissajous scanner, Figure 4.6). Fluorescence was measured in a front face arrangement from the upper side of the leaves. The cuvette was filled with a sucrose solution (0.3 M).



Figure 4.5: Rotation cuvette with *Arabidopsis thaliana* leaves ready for the SPT-measurement.

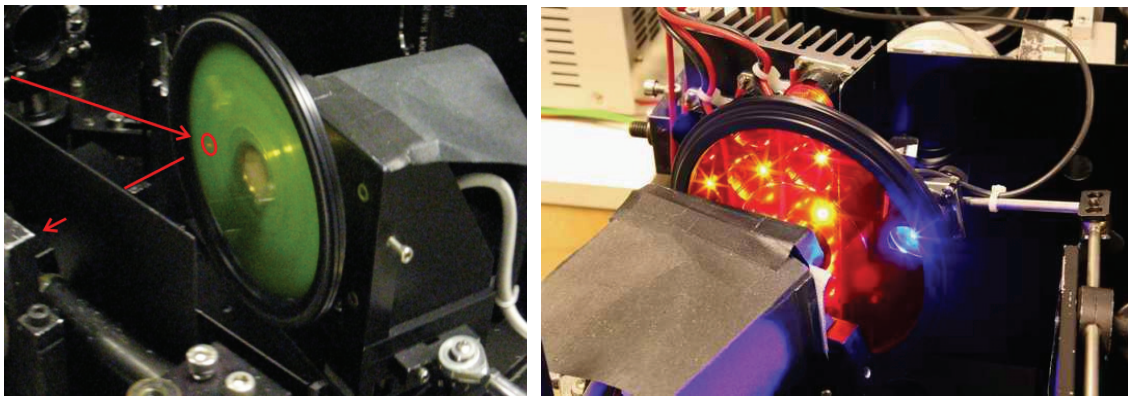


Figure 4.6: Rotation cuvette during the measurement on dark-adapted leaves (left) and on quenched light-adapted leaves (right). The laser spot (the red dot outlined on the left image) is positioned on the cuvette window so that the fluorescence is detected at approx. 45° angle with the excitation. The light path of excitation and detected fluorescence is indicated with arrows. During NPQ measurements (right) the cuvette is continuously illuminated with a red-orange LED array and in addition a high-intensity blue LED is positioned right above the laser spot to ensure closure of the reaction centres.

The measurements were performed in such a way that they characterize the three conditions (F_0 , F_{\max} and F'_{\max}) as much as possible:

1. F_0 was measured in complete darkness after dark-adaptation overnight. The laser frequency was 800 kHz, the rotation speed 1800 rpm with 78 side movements per minute (mpm). Preliminary checks were done to ensure that the PS II RCs are indeed open.
2. For measurements at maximal fluorescence F_{\max} conditions leaves were cut at the stem and dipped immediately in a 45 μM DCMU solution with the main part of the leaf that was later used for measurement exposed to air. The detached leaves were incubated for 14 hours in the DCMU solution in complete darkness (Toth et

al. 2005). For achieving full closure of the PS II RCs during the measurement an additional blue LED light-spot of very low intensity ($\sim 50 \mu\text{mol photons m}^{-2} \text{s}^{-1}$) was applied immediately before detection of the signal. The laser frequency was 4 MHz and the cuvette speed 1300 rpm/78 mpm.

3. Light-adaptation for the F_{NPQ} state was carried out using a mixed array plate of red and amber high intensity light-emitting diodes providing 550-600 $\mu\text{mol photons m}^{-2} \text{s}^{-1}$. Measurements were started after 45 minutes of illumination after stabilization of the quenching. For closing all PS II RCs under quenched F_{NPQ} conditions before entering the measuring light an additional blue high intensity LED was focused on a 1 cm diameter spot right above the fluorescence excitation laser light pulses (1.5 mm diameter). 4 MHz laser frequency was used, the cuvette was rotating at 1800 rpm, fast enough to keep the PS II RCs closed.

To measure DAS at one condition 1-2 hours were needed. The measurement of every wavelength was limited maximally to 15 minutes, to avoid stress in the leaves due to prolonged incubation in the rotating cuvette. For every condition the rotation cuvette with freshly prepared leaves from the same set has been used.

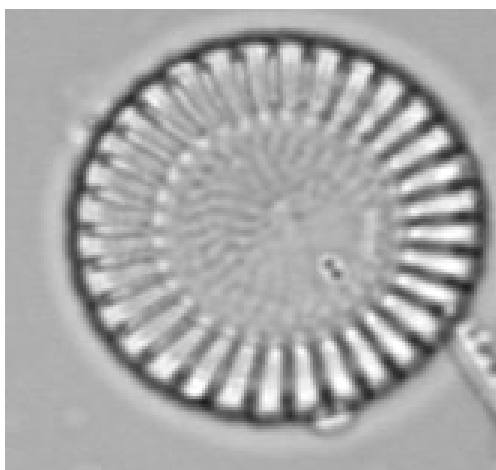


Figure 4.7: *C. meneghimiana* (above) and *P. tricornutum* (below).

Diatoms

Diatoms (Bacillariophyceae) are unicellular photosynthetic organisms responsible for at least a quarter of carbon fixation in the oceans (Falkowski and Raven 1997). They experience large fluctuations in light intensity due to unpredictable water motions that can vary over several orders of magnitude (Lavaud et al. 2003). This makes them an interesting object for studies in non-photochemical quenching. The diatoms *Cyclotella meneghimiana* and *Phaeodactylum tricornutum* (Figure 4.7) having different behaviour under high light illumination were used (Chapter 10).

Diatom material and growing conditions

C. meneghiniana and *P. tricornutum* cells were obtained from Irina Grouneva and Prof. Dr. Christian Wilhelm (University of Leipzig). The diatoms were grown aerobically as a periodic culture in continuously shaken flasks at 20°C with a light to dark cycle of 14:10 h and light intensity of 40 $\mu\text{mol photons m}^{-2} \text{s}^{-1}$. *C. meneghiniana* was grown as an air-bubbled culture in silica-enriched f/2 medium according to Guillard and Lorenzen (1972). *P. tricornutum* was grown without being bubbled in ASP medium according to Provasoli et al. (1957) with modifications introduced by Lohr and Wilhelm (2001). Immediately before measurements cells were concentrated by centrifugation (3500 x g) at 4 °C to Chl *a* contents of 10 mg l⁻¹ for *C. meneghiniana* and 5 mg l⁻¹ for *P. tricornutum*. For all measurements performed in the present study, 10 mM NaHCO₃ was added to the algal cultures to ensure sufficient CO₂-supply during the periods of actinic high light illumination.

Fluorescence kinetics

Time-resolved fluorescence decays were measured by the described SPT apparatus at several wavelengths on a total volume of 500 ml algal suspension under three different conditions, as was the case with Arabidopsis (see above). (1) Ground fluorescence (F_0 , reaction centres open) was measured with dark-adapted cells. (2) Maximal fluorescence F_{max} (reaction centres closed) was measured in dark-adapted cells after addition of 100 μM DCMU. Low light (100 $\mu\text{mol photons m}^{-2} \text{s}^{-1}$ for 1 s) was applied immediately before the algal suspension entered the flow cell for detection of the time-resolved fluorescence signal. In the case of *P. tricornutum* 5 mM of NH₄Cl were applied in addition to DCMU in order to prevent the build-up of NPQ during measurement. (3) For fluorescence measurements in the quenched state (F_{NPQ}), actinic light of 600 $\mu\text{mol photons m}^{-2} \text{s}^{-1}$ was applied to the reservoir. Cells were adapted to this light for at least 30 min prior to data recording in order to reach a stable quenched steady-state fluorescence signal. In this case maximal fluorescence under actinic illumination (F_{max}') was induced by application of a saturating light pulse of 1000 $\mu\text{mol photons m}^{-2} \text{s}^{-1}$ for at least 200 ms immediately before the cells entered the exciting laser beam. Measurements were carried out in a flow-through cuvette (cross-section of 1.5x1.5 mm). Samples were pumped through a system of rubber tubing (Figure 4.8) at a rate of 500 ml min⁻¹, except for F_m measurements, where the speed was adjusted to 50 ml min⁻¹. The algal suspension was constantly stirred during measurements in order to insure a homogenous distribution. The fluorescence decays were analyzed by global target analysis (Holzwarth 1996).

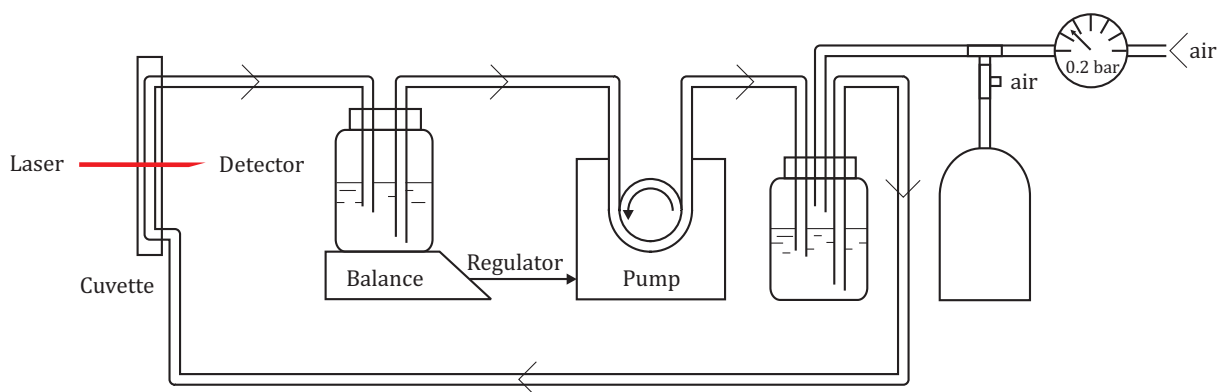


Figure 4.8: Schematic diagram of the flow system for SPT measurements on diatoms. The algal suspension is contained in reservoirs and pumped with a peristaltic pump through the laser beam. Continuity of the flow is achieved by using gas pressure. Two weight limits were preset on a balance. When the suspension reached the low limit, the pump was switched on. When the suspension reached upper limit, the pump was switched off and the gas was pressing the sample away till the lower weight limit.

Fluorescence induction measurements

Fluorescence induction kinetics of variable Chl fluorescence and the development of NPQ were monitored with a PAM fluorometer (Walz GmbH, Effeltrich) on cells adjusted to a Chl *a* content of $2 \mu\text{g ml}^{-1}$. 1.5 ml of algal suspension were measured in a 3 ml glass cuvette. Saturating light flashes ($3500 \mu\text{mol photons m}^{-2} \text{s}^{-1}$) with duration of 800 ms were applied every 10 seconds. The cells were dark-adapted for two minutes before F_{max} was determined.

Oxygen evolution measurements

Oxygen measurements were carried out at $20 \text{ }^\circ\text{C}$ with a Clark-type electrode (MI730, Microelectrodes Inc., Bedford, NH, USA). Respiration was measured for 5 min in darkness, photosynthetic electron transport during 10 min of saturating actinic light ($600 \mu\text{mol photons m}^{-2} \text{s}^{-1}$).

Pigment analysis

Pigment analysis was carried out by HPLC (Waters, Millipore, Eschborn) on a Nucleosil ET 250/8/4, 300-5, C18 column (Macherey & Nagel). Pigments were quantified according to the methods used by Wilhelm et al. (1995) and Lohr and Wilhelm (2001). Dtx content and conversion were monitored before and after 3 h of measurement under F_{NPQ} conditions or 3 hours of darkness (F_0 measurement).

CHARGE SEPARATION KINETICS IN PHOTOSYSTEM II CORE PARTICLES

The analysis of the primary energy- and electron-transfer reactions in intact PS II cores was focused on answering the question whether the kinetics is “trap-limited” or “transfer-to-trap limited” (i.e., diffusion-limited). Recent work (Dekker and van Grondelle 2000, van Amerongen and van Grondelle 2001, Vassiliev et al. 2002) put the old ERPE model under into doubt. It was necessary to verify its validity in detail and to test whether the rates and the mechanism of the early electron-transfer processes in intact PS II cores and in isolated D1/D2-cyt-b₅₅₉ RCs are identical or not. In view of this situation it was important to measure new fluorescence kinetic data on intact PS II cores that complement the recent transient absorption kinetics (Holzwarth et al. 2006b) and were suitable for an improved kinetic modeling of the primary processes in PS II.

RESULTS

Fluorescence decay kinetics

The fluorescence decay kinetics was studied in dimeric PS II core complexes from *T. elongatus* by single-photon timing. An excitation wavelength of 663 nm, located in the blue absorbing edge of the Q_y band of the Chl antenna, was chosen. This excites preferentially the CP43 complex (Groot et al. 1995, Groot et al. 1999). The fluorescence kinetics was measured with a high signal/noise ratio (30000 counts in the peak channel at all wavelengths) at 4 nm intervals in the range from 673 to 701 nm with very low excitation intensity ($<10^{-4}$ absorbed photons/particle/pulse). Extreme care was taken to avoid re-excitation of the same particle before reopening of the RC. Thus, the measured kinetics reflects >99% open RCs (see Chapter 4 for experimental details).

For a good description of the kinetics across the whole wavelength range six lifetimes were required in global analysis over a fitting range of 2 ns [*cf.* Figure 5.1 for the DAS]. The lifetimes with dominant amplitudes were 2, 9, 42, 106, and 332 ps. An additional

lifetime of 2 ns with very small amplitude was also required. The χ^2 value for this global fit was 1.07. Leaving out the shortest lifetime component from the fit worsened the χ^2 value to 1.15 and led to large deviations in the residual plots. Whereas the longer lifetimes, including the ~ 40 ps component, have been resolved earlier in the fluorescence kinetics of intact PS II cores (Schatz et al. 1987, Schatz et al. 1988, Vasil'ev et al. 2001, Vassiliev et al. 2002), the two faster lifetimes of 2 and 9 ps have not been resolved before.

The amplitude of the fastest lifetime component is negative across the whole wavelength range with a minimum around 685 nm and approaches zero near 675 nm. At slightly shorter detection wavelengths positive amplitude was observed for this component. However, we did not include these short-wavelength data in the present fit because below 676 nm we cannot exclude the scattering contribution from the exciting pulse. The amplitudes of all other lifetime components are positive across the whole spectrum with peaks around 680-685 nm, except for the 9 ps component, which is also slightly negative at the longest detection wavelength. The fastest component (~ 2 ps) clearly shows the amplitude feature of an energy-transfer process, and we assign it to a mixture of both energy transfer within the antenna complexes CP43 and CP47 (de Weerd et al. 2002) and to energy transfer from the antenna complexes to the RC, in agreement with recent femtosecond transient absorption data on the same system (Holzwarth et al. 2006b) (*vide infra* for a detailed discussion). All longer lifetime components must be assigned to energy trapping by primary charge separation and to secondary electron-transfer processes, which can be observed in the Chl fluorescence decay due to the charge recombination processes active in PS II (Holzwarth et al. 2005, Schatz et al. 1988). The assignment of the ~ 330 ps process is likely electron transfer from Pheo⁻ to Q_A (Schatz et al. 1988). Strictly speaking, each of the lifetimes, which are the inverse eigenvalues of the kinetic matrix of the system, depends on all rate constants in the system and generally does not reflect the property of a particular excited-state species or radical pair intermediate. For this reason an interpretation in terms of lifetime components can provide at best a qualitative interpretation, and a detailed kinetic modeling is required to get physical insight into the kinetics of the system.

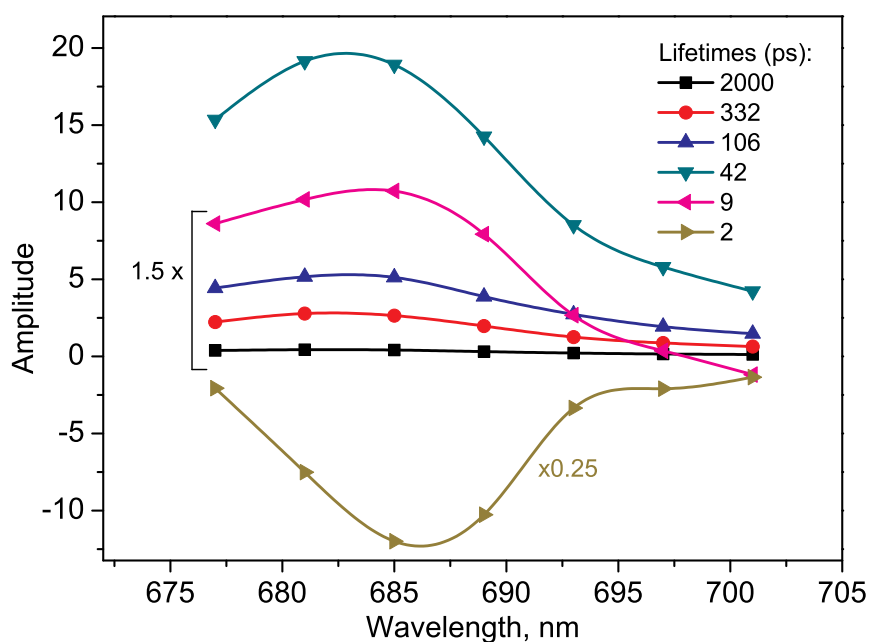


Figure 5.1: DAS of PS II core particles from *T. elongatus* excited at 663 nm as analyzed by global lifetime analysis.

Kinetic Modeling

We applied global compartment modeling to the kinetics testing several different kinetic models on the data. The simplest kinetic scheme that allowed a good description of the experimental data is shown in Figure 5.2 together with the optimal rate constants from a global target modeling. The system contains six compartments, that is, three excited-state compartments (CP43*, CP47*, and RC*) and three radical pair compartments (RP₁–RP₃). RC* stands for the equilibrated excited state of the six pigments comprising the RC. The SAS of the compartments are given in Figure 5.3, and the time-dependence of the populations of the compartments is shown in Figure 5.4. The SAS of radical pairs are zero by definition, because RPs are not fluorescent. Nevertheless, the kinetics of the RP states is observed in fluorescence indirectly by way of the charge recombination fluorescence because the early electron-transfer steps are reversible. This kinetic scheme results in lifetime components of 1.5, 7, 10, 42, and 351 ps. In the modeling two additional free running lifetime components of 111 ps and 2.3 ns of small amplitude were required for a good fit (see Figure 5.5 for the corresponding DAS). Thus, all lifetime components from the global analysis are present in this model. However, the 9 ps lifetime from global analysis is now split into two components of 7 and 10 ps, which would be too close-lying to be resolved in global analysis. The small 2.3 ns component is clearly due to a very small amount of closed RCs in the sample, whereas the origin of the 111 ps component,

which is outside the kinetic scheme shown in Figure 5.2, is unclear at present. Thus, there is possibly room for a slightly extended or more complex model (*vide infra*). Other (simpler) kinetic schemes than the one shown in Figure 5.2 either resulted in a poor fit to the data or did not provide reasonable SAS or both.

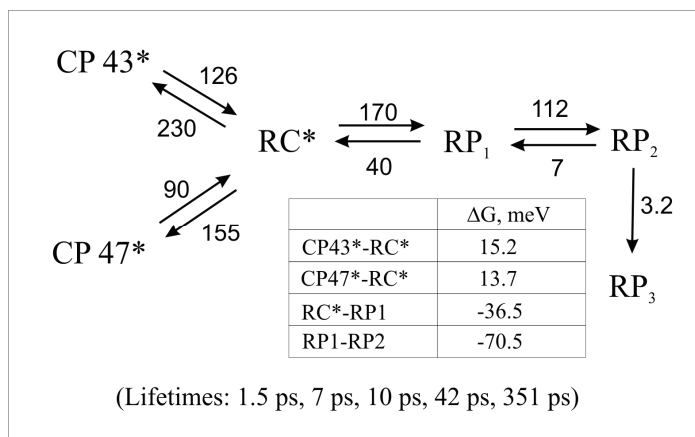


Figure 5.2: Kinetic model for dimeric PS II core particles resulted from target analyses. Rate constants are given in ns^{-1} . Errors of electron-transfer rates are $\pm 10\%$, whereas errors in energy-transfer rates may be up to $\pm 20\%$ due to the lifetime of 1.5 ps being close to the resolution limit of the apparatus. Lifetimes resulting from the model are shown at the bottom. (Inset) Free energy differences ΔG between compartments as calculated from the forward and backward rates of energy or electron transfer.

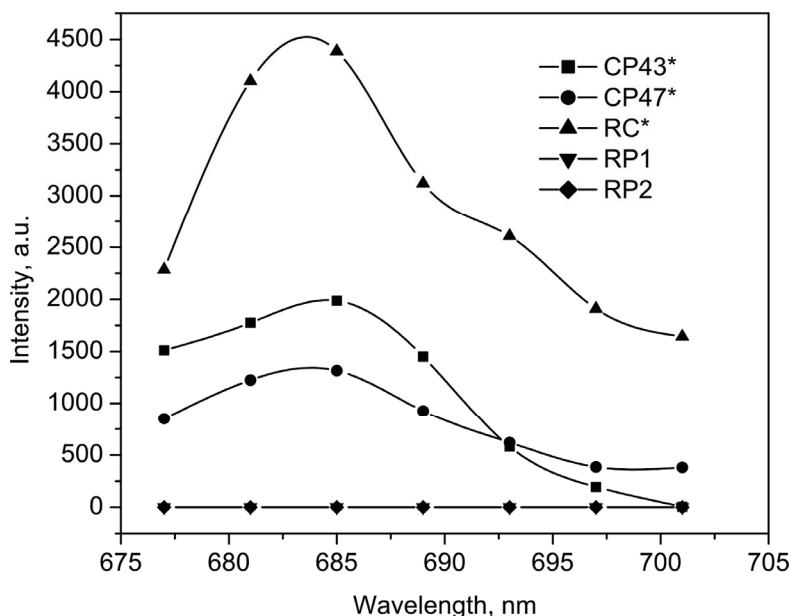


Figure 5.3: SAS resulting from the fit of the kinetic model present in Figure 5.2 to the data.

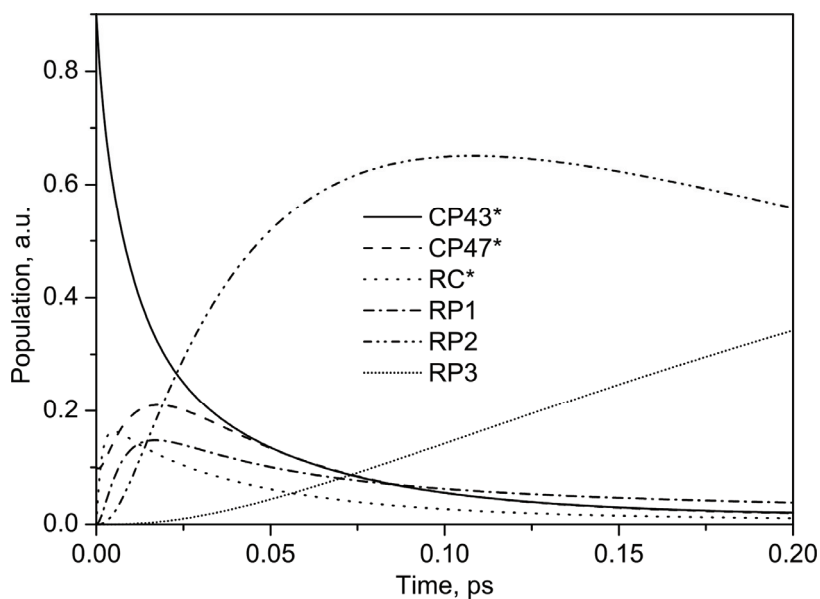


Figure 5.4: Calculated time dependence of populations of the compartments as shown in Figure 5.2.

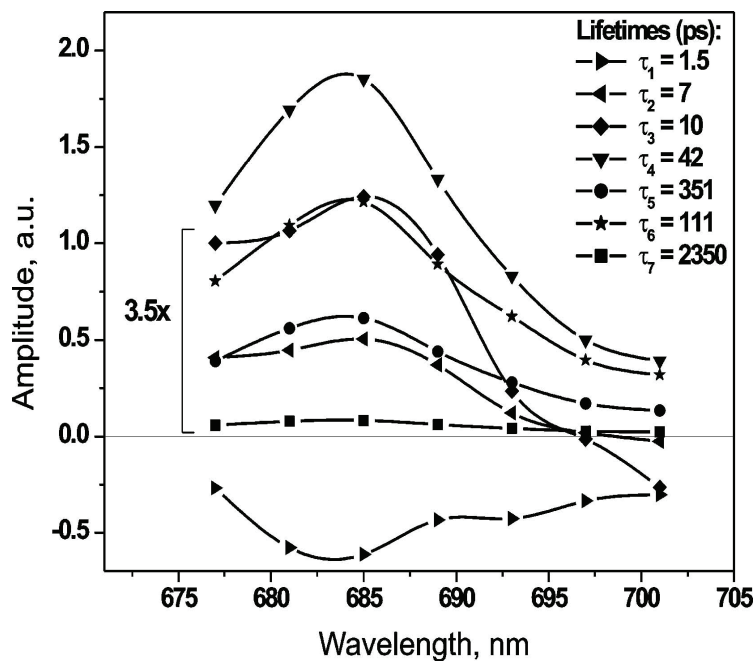


Figure 5.5: DAS from target analysis leading to the kinetic scheme shown in Figure 5.2. Lifetimes τ_1 - τ_5 are those that result from the kinetic model. The 111 and 2350 ps lifetime components are additional free running components outside the kinetic scheme, which are required for a good fit.

DISCUSSION

Kinetic model

The kinetic scheme giving a good fit to the data is analogous to the one found earlier explaining the femtosecond transient absorption data (Holzwarth et al. 2006b). The rate constants for the electron-transfer processes are in fact the same within the error limits as found for transient absorption. Also, the rate constants of energy transfer are very similar, except for a slight difference in the rate constant of forward energy transfer from CP43 to the RC, which is somewhat higher in transient absorption than in the fluorescence model.

The weighted eigenvectors corresponding to the kinetic scheme in Figure 5.2 are given in Table 5.1. This eigenvector matrix allows to assign the origin of the various lifetimes in the model to the physical processes and the compartment kinetics. A negative value indicates a rise of a compartment population, and a positive value indicates decay. Generally, the lifetimes are functions of all rate constants in the model. Thus, there is essentially some contribution of all lifetimes to each of the compartment populations. However, we are looking here only for the amplitudes that make the dominant contributions to the various compartment populations. It can be clearly seen from Table 5.1 that the 1.5 ps lifetime represents primarily the rise of the RC* population; that is, it is the dominant component describing the energy-transfer kinetics from the antennae to the RC besides a very small contribution to the RC* rise by the 7 ps lifetime. Thus, the overall equilibration time between antenna and RC should be in the range of a few picoseconds. The 7 ps component represents primarily the rise of the RP₁ population. It thus reflects the *apparent lifetime* for primary charge separation, which is at least a factor of 5 faster than believed previously (Schatz et al. 1987). The 10 ps component is a mixed component that cannot be assigned exclusively to one process. The energy transfer between the not directly connected CP43 and CP47 antennae makes a strong contribution, as does the rise of RP₁. The 42 ps component is the dominant excited-state decay component (all three excited-state compartments contribute with decay terms to this component), and it also reflects the main rise of the RP₂ population. RP₁ and RP₂ have been identified as representing the radical pair states $\text{Chl}_{\text{accD1}}^+\text{Pheo}_{\text{D1}}^-$ and $\text{P}_{\text{D1}}^+\text{Pheo}_{\text{D1}}^-$, respectively (Holzwarth et al. 2006b). The 351 ps component reflects the rise of the RP trap state, which in analogy with previous data (Holzwarth et al. 2006b, Schatz et al. 1988) represents the state $\text{P}_{\text{D1}}^+\text{Q}_\text{A}^-$.

Table 5.1: Weighted eigenvectors (amplitudes) of the compartments for the kinetic model shown in Figure 5.2.

Compartment	CP43*	CP47*	RC*	RP ₁	RP ₂	RP _{trap}
Exc. vector	0.9	0.1	0	0	0	0
lifetime, ps						
1.5	0.087	0.055	-0.198	0.068	-0.012	5.9·10 ⁻⁵
7	0.076	0.022	-0.009	-0.38	0.297	-0.006
10	0.354	-0.372	0.034	0.102	-0.122	0.004
42	0.352	0.366	0.156	0.144	-1.168	0.158
351	0.031	0.03	0.017	0.065	1.005	-1.143

^aThe time dependence of populations $C_j(t)$ for each intermediate compartment j (top row) follows the equation

$$C_j(t) = \sum_{i=1}^n A_{ij} e^{-t/\tau_i},$$

where A_{ij} represents the elements of the eigenvector matrix and τ_i are the lifetimes given in the left column. Inspection of this matrix allows one to easily deduce the apparent lifetimes and their amplitudes that contribute to the rise (negative amplitude) and decay (positive amplitude) of population of each of the intermediates (compartments). For further details of this presentation see Müller et al. (Müller et al. 2003)

The 111 ps component (contributing ~10% to the relative amplitude) which is outside of the present kinetic model (Figure 5.2) most likely derives also from the intact PS II core system, unless we assume some kind of heterogeneity. If one wants to include such a 111 ps component, the kinetic scheme has to be extended beyond the one shown here. This extended description was done later independently by Szczepaniak et al. (2008). From the expected rate constant of a process giving rise to a 111 ps component (somewhere in the range of 6-9 ns⁻¹) it can be concluded that this is a process occurring after formation of the second radical pair but before the electron transfer to Q_A. Thus might reflect a protein relaxation step after formation of RP₂. Protein relaxation steps have been described for PS II cores and RCs by various authors (Gatzen et al. 1996, Vassiliev et al. 2002).

The important conclusion – and that is the result of all our modeling of more extended kinetic schemes – is, however, that whatever extension in the kinetic scheme is made, it does not change to any significant extent the rate constants of the energy-transfer processes between antenna and RC or the rate constants of the early electron-transfer step(s). Because the focus of this experiment was primarily on the clarification of the trap– versus diffusion-limited model and of the rate constant (and *apparent lifetime*) of the primary charge separation, any further extension of the kinetic scheme would not af-

fect in any way our conclusions (or the rate constants in Figure 5.2 for the processes up to and including the rate constants for the formation of RP_2).

The SAS of the excited states of the antenna complexes CP43 and CP47 have their emission peaks around 685 nm. The emission spectrum (SAS) of the excited RC state in an intact PS II core is resolved here for the first time. It peaks between 683 and 685 nm and has more than twice the amplitude of the SAS of the antenna complexes. The area under an SAS being proportional to the radiative transition probability of the corresponding

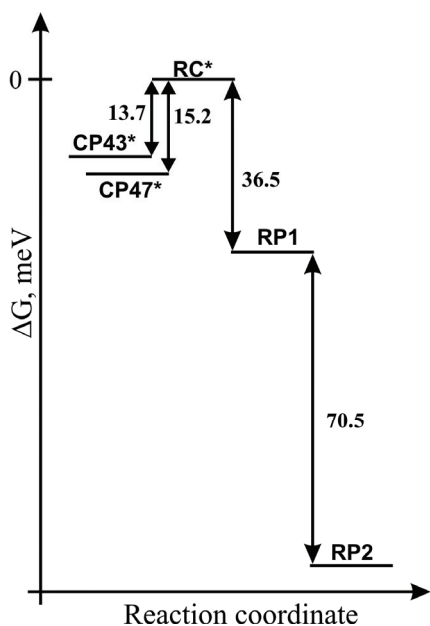


Figure 5.6: Scheme of free energy differences ΔG between the model compartments. The free energy of the RC excited state is used as thermodynamic reference.

state implies that the radiative rate of the RC^* state is by a factor of 2-3 higher than that of the antenna excited states. This higher rate reflects, and is consistent with, the well-known increase of transition probability due to exciton coupling of the lower exciton states of the RC complex (Durrant et al. 1995, Prokhorenko and Holzwarth 2000). It is interesting to compare the SAS of the RC^* state to the one obtained earlier for the isolated D1-D2-cyt- b_{559} complex, which is very similar in shape and also substantially higher in amplitude than the SAS of the peripheral monomeric Chl_z molecules in the D1-D2 RC (Gatzen et al. 1996). Thus, in both the intact PS II cores and the isolated D1-D2 RC the transition probability of the emitting exciton states of the RC is by a factor of 2-3 higher than for monomeric Chl. However, the maximum of the RC emission in intact PS II cores seems to be red-shifted by ~ 2 nm as compared to iso-

lated D1-D2 RCs (Gatzen et al. 1996). It is also worth mentioning that the SAS of the RC shows a pronounced shoulder on the long-wavelength tail around 693 nm, and the spectrum shows substantial amplitude well above 700 nm. It is possible that the long-wavelength tail is caused by emission from low-lying emitting states, either exciton states or even charge-transfer states with significant optical transition probability. The presence of the latter states has recently been proposed for the isolated D1-D2 RC on the basis of exciton calculations (Novoderezhkin et al. 2005).

From the rate constants of forward and reverse electron transfer in Figure 5.2 one can calculate the free energy differences between the excited RC^* state and the radical pairs shown in Figure 5.6. The drop in ΔG for RP_1 is -37 meV and between RP_1 and RP_2 is -71

meV, resulting in a total free energy drop of slightly less than -110 meV for the state RP₂. Thus, the main energy drop occurs in the second electron-transfer process.

Trap-limit versus transfer-to-the-trap limit

The main energy-transfer lifetime between antenna and RC is 1.5 ps, with some small contribution of the 7 ps component to the rise of the RC* population (*vide supra*). In addition, the 10 ps component contributes with a small amplitude to energy equilibration between CP43 and CP47. The overall very fast energy transfer between antenna and RC is reflected in the fact that after antenna excitation the population of RC* reaches its maximal value at ~4-5 ps, whereas the RP₁ state reaches its maximal population after ~15 ps and the RP₂ state after ~100 ps. According to these data the energy transfer between antenna and RC (the transfer to the trap) is not rate-limiting for the overall charge separation process. These results, which resolve for the first time the kinetics of energy transfer between the antenna and the RC directly, are in excellent agreement with the assumptions made previously in the derivation of the ERPE model (Schatz et al. 1988).

The most transparent way of deciding upon the individual contributions of energy transfer (diffusion) and charge separation to the overall trapping process is the average lifetime of the decay of all excited states and their dependence on the rates of energy transfer and charge separation. The total average trapping time $\tau_{\text{tot trap}}$ as derived from theoretical work on energy transfer and trapping (Pearlstein 1982a, van Grondelle and Gobets 2004) is given by a sum of the individual contributions of diffusion within the antenna τ_{diff} , the transfer-to-the-trap (RC) time $\tau_{\text{transfer-to-trap}}$, and the charge separation time τ_{CS} , respectively. Because in our simple compartment model (Figure 5.2) we are not distinguishing between internal antenna diffusion and transfer to the trap processes, the relationship can be simplified to two terms as follows:

$$\tau_{\text{tot trap}} = \tau_{\text{diff}} + \tau_{\text{transfer-to-trap}} + \tau_{\text{CS}} = \tau_{\text{EET}} + \tau_{\text{CS}}$$

Thus, τ_{EET} represents the sum of the intra-antenna diffusion and transfer-to-the-trap times. The contributions of the charge separation time τ_{CS} , on the one hand, and the total energy transfer time τ_{EET} to the total average trapping time, on the other hand, can be calculated easily within the kinetic model of Figure 5.2 by scaling up either the energy-transfer rates or the electron-transfer rates by a factor of >100, respectively. In this way

the contributions of either τ_{EET} or τ_{CS} , respectively, to the total trapping time are negligible and the value of the other term can be obtained. An alternative and equivalent way of obtaining τ_{CS} is to solve the system of differential equations for the kinetic scheme by setting the initial excitation to be entirely located in the RC instead of the antenna.

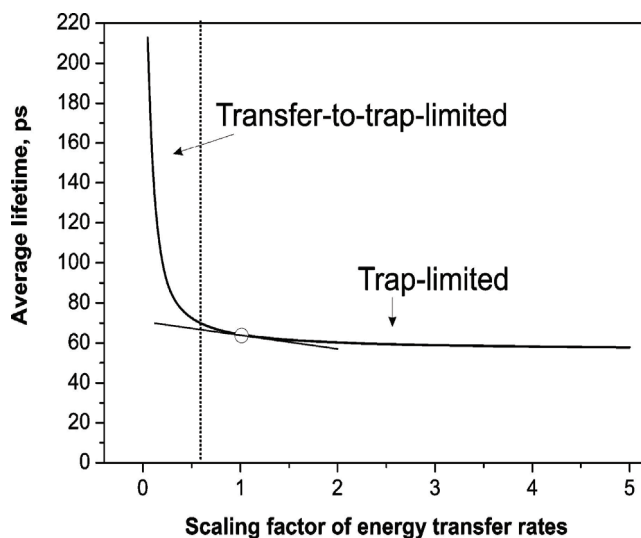


Figure 5.7: Dependence of the excited-state average lifetime $\tau_{\text{tot trap}}$ on the scaling of the energy-transfer rates given in the kinetic model (see Figure 5.2).

In a transfer-to-the-trap-limited kinetics the contribution of τ_{EET} to the total trapping time is the dominant term, whereas in a trap-limited kinetics the τ_{CS} is the dominant term. Thus, in trap-limited kinetics the total trapping time depends only very weakly on the up-scaling of the energy-transfer rates. The dependence of the total trapping time (equivalent to the average excited-state decay lifetime) on the scaling of the energy-transfer rates in our model is shown in Figure 5.7. The scaling factor 1 corresponds to the experimental situation. As expected, the total trapping time depends only very weakly on the up-scaling of the energy-transfer rates, thus indicating a trap-limited overall kinetics for PS II cores. The calculation yields $\tau_{\text{tot trap}} = 65$ ps, $\tau_{\text{EET}} = 9$ ps, and $\tau_{\text{CS}} = 56$ ps. With a ratio of $\tau_{\text{CS}}/\tau_{\text{EET}} \geq 6$ the kinetics in PS II cores is on the extreme trap-limited side.

This result is in vast disagreement with recent conclusions from other groups for the overall trapping kinetics in PS II cores to be transfer-to-the-trap-limited (Vasil'ev et al. 2001, Vassiliev et al. 2002). The conclusions of Vasil'ev et al. claiming a transfer-to-the-trap-limited model result from a huge overestimation of the primary charge separation rate in PS II [rate constants for the primary charge separation process from P_{680} ranging from a minimum of 1400 ns^{-1} (Vasil'ev et al. 2001) to 7000 ns^{-1} (Vassiliev et al. 2002)

were reported] and a pronounced underestimation of the antenna to RC energy-transfer rates (Vasil'ev et al. 2001, Vassiliev et al. 2002). Some of the likely reasons for the inadequacy of their estimated energy- and electron-transfer rates are revealed by their sequential radical pair relaxation model (Vassiliev et al. 2002). In that analysis the assumed intermediates RP_1 to RP_3 as well as the rate constants connecting P_{680}^* and these radical pairs are pure fitting artefacts that have no experimental foundation. This is clearly born out by the fact that the fastest experimentally resolved lifetime component in the Vasil'ev data for PS II cores with open RC was 60 ps. This fastest lifetime can be obtained in their data by completely leaving out RP_1 - RP_3 from the modeling. On the basis of the same arguments their conclusion of a significant radical pair relaxation contribution to the kinetics of PS II cores with open RCs lacks experimental support. We also note that there exists a severe discrepancy between the average lifetime of antenna decay of PS II cores with open RCs (F_0) in the measurements of Vasil'ev (2002), which is 174 ps, and our average fluorescence decay lifetime with open centres of 65 ps (*vide supra*). The discrepancy is primarily caused by the significant contributions of 0.97 and 5 ns components in the fluorescence decay reported by Vasil'ev. These lifetime components according to our analysis are not related to PS II cores with intact open RCs but originate most likely from a contribution of closed RCs and/or damaged PS II particles. A non-negligible contribution of an 1.8 ns component to the fluorescence decay of PS II cores at F_0 – also likely resulting from a contribution of PS II cores with closed RCs – was also found earlier by Schatz et al. (1987). It requires very high sample purity and extreme care in avoiding multiple excitation of RCs closed by previous laser pulses in order to be able to achieve an experimental fluorescence decay that is essentially free of long-lived components in the range of 1 ns or longer.

CONCLUSIONS

The analysis of the present fluorescence kinetic data of PS II cores with open RCs and the analysis of recent femtosecond transient absorption data (Holzwarth et al. 2006b) show that both kinds of data can be described by the same kinetic model. The results presented here confirm the validity of the assumptions regarding energy equilibration made in deriving the earlier ERPE model for the trapping and charge separation kinetics in PS II cores (Schatz et al. 1987, Schatz et al. 1988). However, both the recent transient absorption data and the refined fluorescence kinetics reported here require an exten-

sion of the early ERPE model to include one additional electron-transfer step leading to an additional early radical pair. This first radical pair (RP₁) is the Chl_{acc} D1⁺ Pheo_{D1}⁻ state (Holzwarth et al. 2006b). Formation of this intermediate reflects itself in the fluorescence kinetics by an additional 7 ps component, which was not contained in the early ERPE model. It is particularly gratifying that the same mechanism and also the same rates of the two early electron transfer steps have been found for isolated PS II cores (this work and ref. Holzwarth et al. (2006b)) and for isolated D1-D2-cytb559 RC (Holzwarth et al. 2006b). This finding is in vast contrast to the claim of a ~100-fold difference in the primary charge separation rate constants for isolated PS II RCs, on the one hand, and intact PS II cores, on the other (Vassiliev et al. 2002). In fact an extreme trap-limited kinetics was confirmed for PS II cores by the present experiments (see Holzwarth et al. 2006b, Miloslavina et al. 2006).

ENERGY TRANSFER AND CHARGE SEPARATION KINETICS IN PHOTOSYSTEM II ENRICHED MEMBRANE PARTICLES

The study of the PS II kinetics was extended from the isolated PS II core complexes to PS II enriched thylakoid membranes – i.e. BBY particles. Preparations with two and three LHC II trimers per RC were studied. The main question was the dependence of the kinetics on the antenna size – whether the kinetics remain “trap-limited” with increasing the antenna size or converts to “transfer-to-trap limited”. Another aim was to study and discuss the implications of these data on the validity and limits of the ERPE model, and finally compare the obtained rates and mechanism of electron transfer with those obtained from the isolated PS II cores from *Thermosynechococcus elongatus* in order to reveal any possible differences in the rates and energetics of the electron transfer processes between higher plants and (thermophilic) cyanobacteria. In order to probe the structural validity of the emerging energy transfer and trapping model the experimental study is complemented by theoretical kinetic modeling of the energy transfer processes.

RESULTS

Fluorescence decays and kinetic modeling

Two types of PSII-enriched membrane particles (BBY particles) were studied by single-photon timing – one having about 3 LHC II trimers per monomeric PS II core (BBY-1) and one with about 2–2.5 trimers per core (BBY-2). The fluorescence was excited by pulses with wavelength of 663 nm. Figure 6.1 shows the fluorescence decays near the peak of the fluorescence spectrum at 685 nm. Global multi-exponential analysis of the BBY-1 data requires four lifetime components of 33 ps, 152 ps, 316 ps, and 1.02 ns for a good fit (DAS Figure 6.2 A). The amplitude of the ca. 1 ns component is almost negligible. The corresponding lifetimes for the BBY-2 preparation are 37 ps, 145 ps, and 272 ps, in addition to a small amplitude of a 563 ps component (Figure 6.2 B). The two strongest components have the same spectrum within the error limits while the 33 and 37 ps

components, respectively, have a slightly more red-shifted spectrum. The lifetimes from the global analysis agree well with the lifetime distribution analysis (LDA), which shows three main peaks around 37 ps (small amplitude), 140 ps, and 300 ps, as well as a very weak and relatively broad band around 930 ps (Figure 6.3). This shows that the kinetics can be described by a small number (about 3-4) of discrete exponentials. In the following target analyses we may thus attempt to analyze the kinetics with discrete rate equation models. Several different target models have been tested on the original kinetic data.

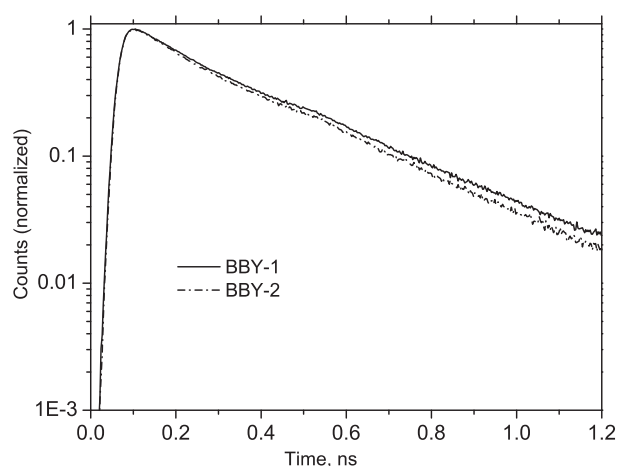


Figure 6.1: Fluorescence decays (on semilogarithmic scale) of BBY-1 and BBY-2 particles with open RCs at the fluorescence peak near 685 nm excited by 663 nm wavelength. See Chapter 4 (Materials and Methods) for details on the preparation.

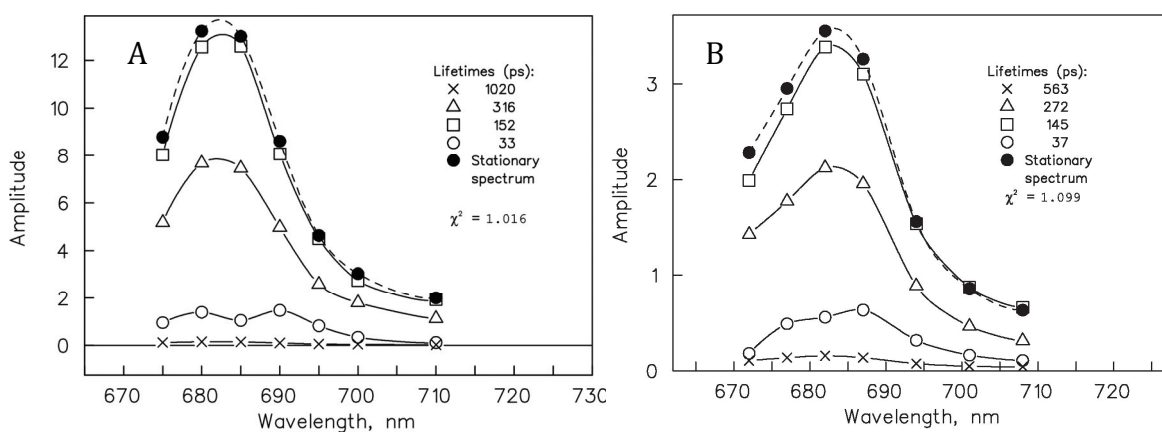


Figure 6.2: DAS and lifetimes from global analysis for the fluorescence of BBY particles with open RCs using 663 nm excitation wavelength. A minimum of 4 lifetimes is necessary for a good fit. The full circles show the stationary fluorescence spectrum. A) BBY-1 particles, B) BBY-2 particles

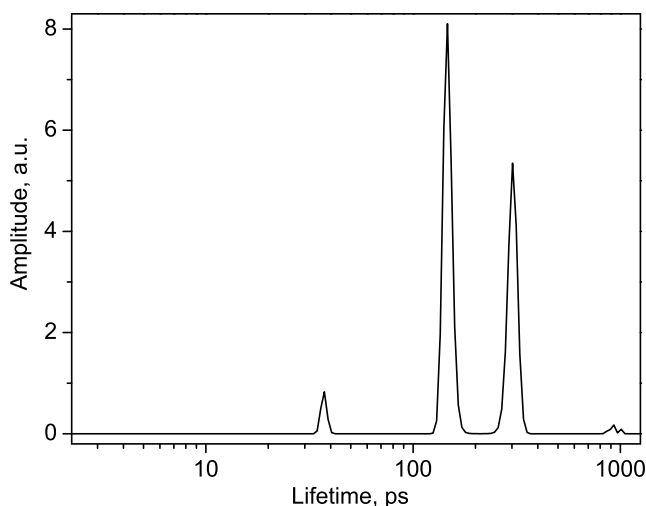


Figure 6.3: Results of the lifetime distribution analysis (LDA) of the fluorescence decay of BBY-1 particles at 685 nm for an excitation wavelength of 663 nm.

Models B-D (Figure 6.4) separate the antenna and RC excited states and explicitly take into account the antenna-RC energy transfer, which goes beyond the simple ERPE model. They furthermore take into account the information regarding the more complex electron transfer mechanism involving two intermediate RPs that has come from the recent study of PS II cores (Holzwarth et al. 2006b, Miloslavina et al. 2006):

- A) A simple bi-exponential PS II model corresponding to the original ERPE model (Schatz et al. 1988) (1 excited state compartment, 2 RP compartments) with two unconnected compartments representing free and/or energetically unconnected Chl forms.
- B) A sequential reversible model with five compartments (1 Ant* and 1 RC* as separate excited state compartments, and three RPs) leading to four-exponential fluorescence, with all rates free-running, plus two unconnected compartments representing free or energetically unconnected Chl forms.
- C) A sequential reversible model with five compartments as described above (B) with the electron transfer rate constants fixed to the values obtained from the recent analysis of the cyanobacterial PS II core data (Holzwarth et al. 2006b) (plus two unconnected compartments).
- D) The same five-compartment model as above with the fast electron transfer rates fixed to the same values as in model C) but allowing for a free-running rate constant for Q_A reduction (i.e. the $RP_2 \rightarrow RP_3$ electron transfer rate).

In the following we describe in detail the results for the BBY-1 preparation. The data for the BBY-2 preparation are essentially identical with respect to the electron transfer rates, but show slightly different lifetimes due to the different Ant to RC energy transfer rates, reflecting the smaller antenna size and the shorter overall decay kinetics for the BBY-2 preparation (*cf.* Figure 6.1). The data for both types of BBY particles are summarized in Table 6.1.

Table 6.1: Total trapping times $\tau_{\text{tot trap}}$, charge separation times τ_{CS} , energy migration times τ_{EET} , and ratio of energy migration to charge separation times for the various models used in the work, all in units of [ps] for BBY-1 and BBY-2 particles. Models A-D correspond to the various compartment models shown in Figure 6.4. Models 1 and 2 correspond to the theoretical modeling results shown in Figure 6.8 for BBY-2 particles and BBY-1 particles, respectively.

	Model	$\tau_{\text{tot trap}}$	τ_{CS}	τ_{EET}	$\tau_{\text{EET}}/\tau_{\text{CS}}$
BBY-1	A	191.2	-	-	-
	B	193.6	88.8	104.8	1.18
	C	192.7	63.7	129.0	2.03
	D	198.9	64.3	134.6	2.09
BBY-2	A	215.1	-	-	-
	B	186.9	41.1	145.8	3.55
	C	182.9	50.7	132.2	2.61
	D	190.3	54.1	136.2	2.52
BBY-2 dimer	1	176.7	87.5	89.2	1.02
BBY-1 dimer	2	199.2	106.8	92.4	0.87

The target analysis results for the BBY-1 preparation are given in Figure 6.4 and Figure 6.5. The simple model A with one, or for a slightly better fit with two unconnected components, gave a satisfactory, though not perfect fit (model A with no unconnected components gave a very unsatisfactory fit and had to be discarded). From our previous experience and from other literature data we had suspected already that the long-lived ~ 1 ns component with rather small amplitude should derive from a small amount of energetically uncoupled Chl-containing pigment compartment (decoupled antenna or free Chl) or from a small amount of closed RCs (Haehnel et al. 1981, Holzwarth et al.

1990, McCauley et al. 1989, McCauley et al. 1990, Nairn et al. 1982, Roelofs et al. 1992). This seems to be indeed the case, since that component could not be made part of any of the models A-D that were tested even if we tried to limit the allowed rate constants severely.

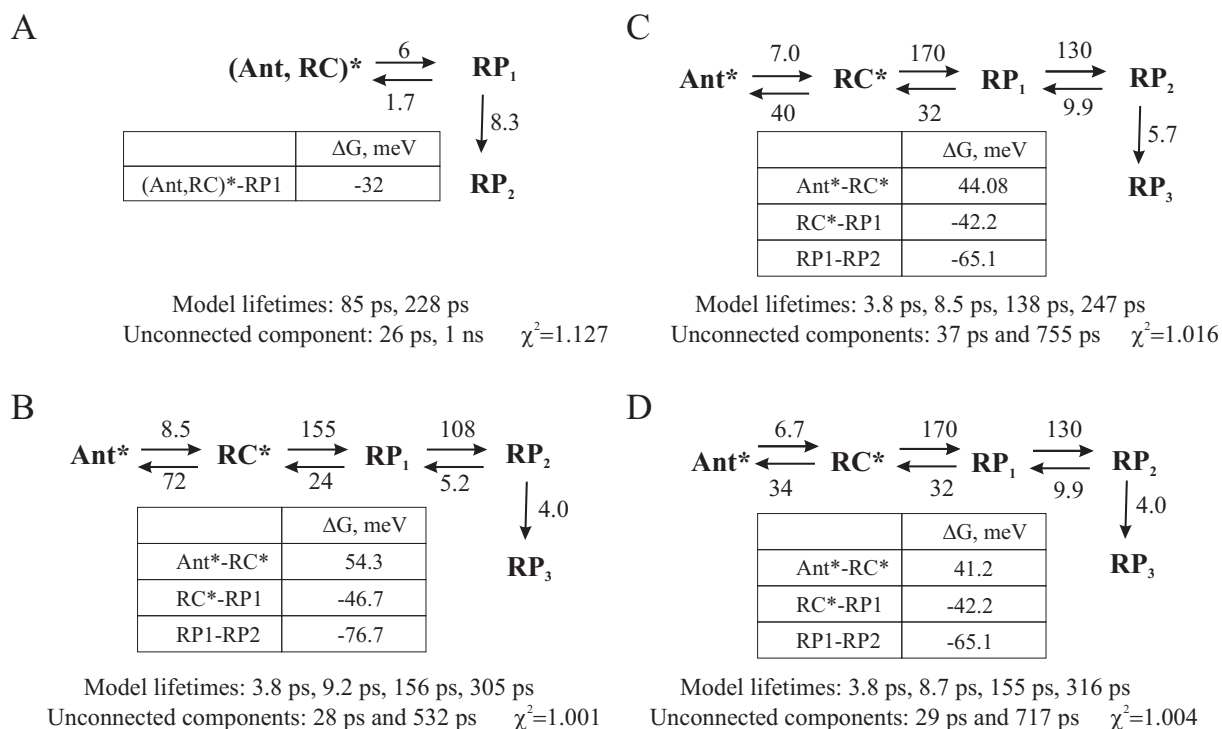


Figure 6.4: Target analyses using different models for the fluorescence decay of BBY-1 particles with open RCs. Two additional lifetimes, not included in the target models, were necessary for a good fit as well. The plots show the kinetic models with rate constants (in ns⁻¹), the resulting lifetimes from the models, and the lifetimes of the additional components. A) Simple ERPE model; B-D) Extended models taking into account the recent findings for a more complex electron transfer mechanism (Holzwarth et al. 2006b). B) Model with free-running rates for the electron and energy transfer processes; C) As in model B but with rate constants of electron transfer processes fixed to the values for cyanobacterial PS II cores from *Thermosynechococcus elongatus* (Holzwarth et al. 2006b); D) as in model C, but with the rate constant for Q_A reduction (RP₂→RP₃) free-running. The insets show the free energy differences ΔG in meV for the reversible reaction steps. The results for BBY-1 as well as BBY-2 particles (not shown in detail) are summarized in Table 6.1

Interestingly it turned out that also the 26-37 ps (depending on the model) component could not be made part of any of the models and always remained outside the target models as an unconnected compartment. The assignment of this component is thus more complex and will be discussed below. For models B-D, which require a four-exponential fluorescence kinetics, lifetimes of ~4 and 9 ps with small amplitudes result from the analysis. The results for models A to D applying various combinations of fixed and free-running rates for the electron transfer processes in the RC are shown in Figure

6.4 A-D providing the rate constants, the model lifetimes, and the lifetimes of the unconnected additional components.

Figure 6.5 shows the time dependence of the populations of the various compartments in the models. In models B-D the relative populations of RC* and of RP₁ are rather small, typically not more than 5%. The largest intermediate population occurs in RP₂, amounting to about 40% at the maximum. The dependence of the average trapping lifetime on the scaling of the energy transfer rates for model B is given in Figure 6.6. Note that for the calculation of the average trapping time we also included the 26-37 ps component, since, as it will be shown below, this component actually derives from intact BBY particles, although it cannot be described within the simple target models A-D. The data for the average trapping times, the charge separation times (calculated for the case when all the excitation starts on the RC (Hemenger et al. 1972, Miloslavina et al. 2006, Pearlstein 1982b)) and the energy migration (diffusion) times calculated according the relationship

$$\tau_{\text{tot trap}} = \tau_{\text{EET}} + \tau_{\text{CS}}$$

where $\tau_{\text{tot trap}}$ is the total average trapping time, τ_{EET} the energy migration time, and τ_{CS} the average charge separation time, are compiled in Table 6.1 for both BBY preparations. As expected from the original decays (Figure 6.1) the BBY-2 preparation shows slightly shorter total trapping times and shorter charge separation lifetimes than the BBY-1 preparation with the larger antenna size. We should note here that both BBY preparations – which we consider to be quite typical for such kind of PS II membrane preparations – have a much lower LHC II content per PS II than the intact thylakoids. Thylakoids isolated from our starting material show a Chl *a/b* ratio of 2.8. Assuming equal total antenna sizes for PS I and PS II in the thylakoids, one can easily estimate 4-4.5 LHC II trimers per PS II monomer (corresponding to antenna sizes for PS II of 230-270 Chls (*a+b*)). This value is in good agreement with many literature data. In contrast, our BBY preparations contain only between 2 and 3 LHC II trimers per PS II. This difference in PS II antenna size between BBY particles and thylakoids is not surprising, given the fact that quite similar procedures are used for the isolation of BBY particles and the isolation of pure LHC II as lamellar aggregates (Simidjiev et al. 1997). This clearly shows that BBY particles must contain a substantially reduced LHC II content as compared to thylakoids.

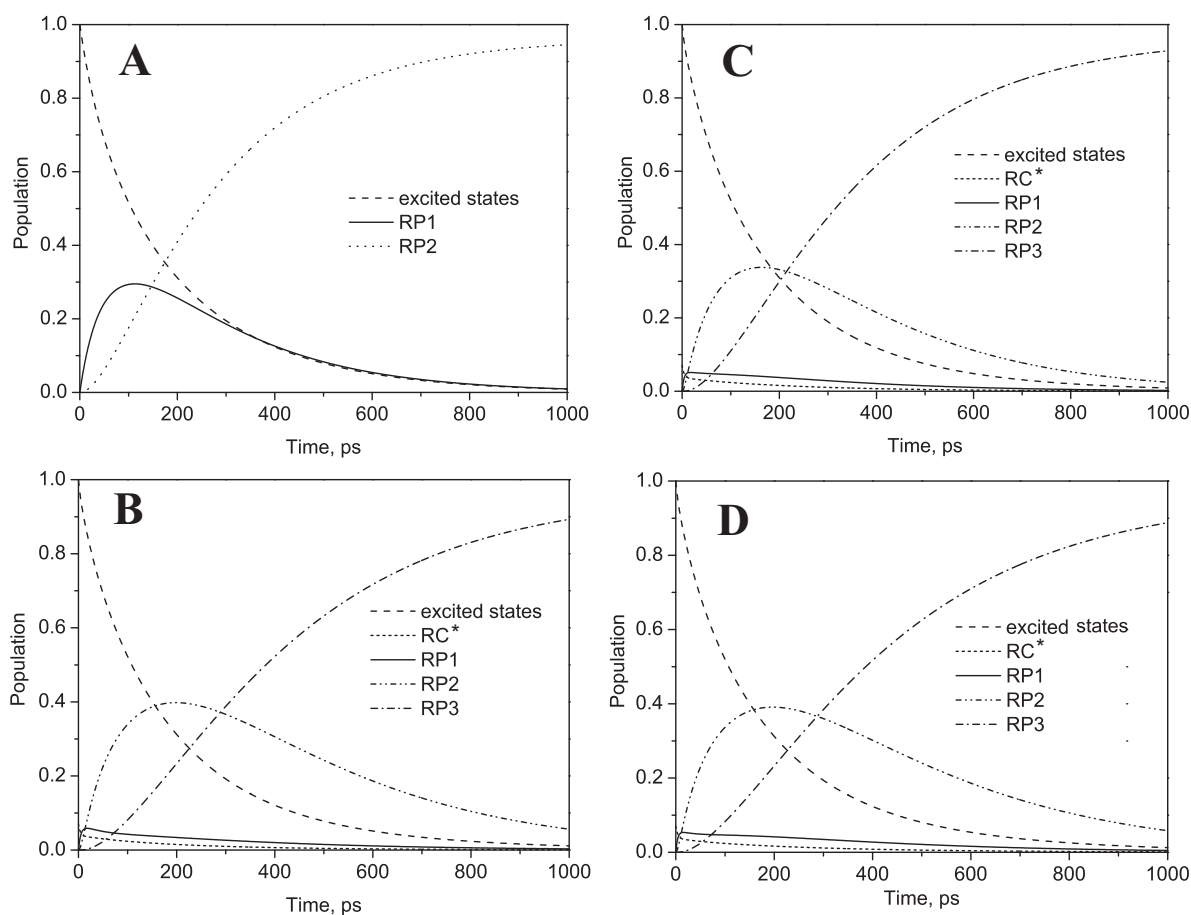


Figure 6.5: Time dependence of populations of excited states (sum of Ant* and RC* populations) and RPs within the target models (Figure 6.4 A-D) for BBY-1 particles. Note that the ca. 26-37 ps component from the target analyses was also included in the calculation of the time dependence of excited state populations.

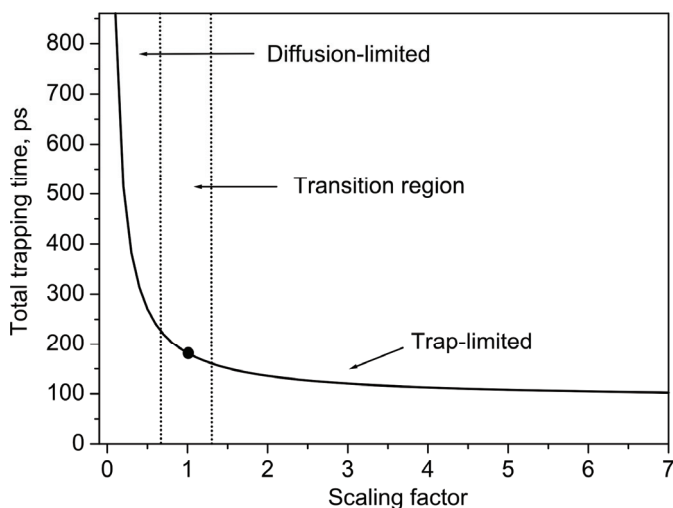


Figure 6.6: Average lifetime of excited state decay for the target model from Figure 6.4 B in dependence on the scaling of the energy transfer rate constants for BBY-1 particles. Note that the ca. 26-37 ps component from the target analysis was also included in the calculation of the average lifetime. A scaling factor of 1 corresponds to the energy transfer rates as obtained from the analysis shown in Figure 6.4 B.

Theoretical modeling

In order to get an estimate of the individual antenna energy transfer rates and also to develop a more detailed picture and to provide an insight into the overall kinetics and possible bottlenecks for energy transfer we performed theoretical modeling of the kinetics. Intra-monomer equilibration of the excited states in LHC II occurs on a time scale of up to ca. 3 ps (Connelly et al. 1997b, Connelly et al. 1997a, Kleima et al. 1997, Salverda et al. 2003, van Amerongen and van Grondelle 2001) and on a similar time scale for the minor complexes CP24, CP26, and CP29 (Cinque et al. 2000, Croce et al. 2003b, Croce et al. 2003a, Gradinaru et al. 1998, Gradinaru et al. 2000, Pascal et al. 1999, Salverda et al. 2003). Thus the energy equilibration between monomeric complexes is limited to Chl *a* to Chl *a* transfer due to the ultrafast intra-monomer Chl *b* to Chl *a* transfer kinetics. Inter-monomer transfer is likely to occur on a significantly slower time scale however and thus the details of the intra-monomer equilibration kinetics can be ignored (Barzda et al. 2001, van Amerongen and van Grondelle 2001). For this reason in our model only the inter-monomer transfer steps are taken into account. Estimates of the inter-monomer transfer times have been obtained from annihilation measurements (Barzda et al. 1996, Bittner et al. 1994). A very detailed recent study resulted in annihilation rates in the range of (16-28 ps)⁻¹, depending on the aggregation state of the LHC II complexes. It has been noted that these values imply an equilibration time of a single excitation per trimer of LHC II of 32 ps (van Amerongen and van Grondelle 2001).

Our kinetic model is based on the following assumption: We assume that the PS II complex from higher plants is dimeric and consists of so-called CSM units (C₂S₂M₂ in a dimer) which results in the kinetic scheme shown in Fig. 7. Additional LHC II trimers may be bound to this minimal complex. Corresponding to the different Chl *a/b* ratios, reflecting about 2-2.5 LHC II trimers per PS II core for the preparation BBY-2 the structural model contains 2 LHC II trimer units per PS II monomer according to the supercomplex proposed by Dekker and Boekema (Dekker and Boekema 2005, Yakushevskaya et al. 2003). The preparation BBY-1, having a Chl *a/b* ratio corresponding to 3 LHC II trimers per PS II monomer, was modeled with a structure containing 3 LHC II trimers per PS II monomer. Since it is not clear where exactly the third LHC II trimer is bound, we attached this additional LHC II trimer functionally to the CP43 complex (Figure 6.7).

similar). We have verified that this assumption is indeed not a critical one and it is justified sufficiently by the fact that in the experimental data no significant spectral equilibration components were present (Figure 6.2). However it is important that the ratio of forward to backward transfer rates is taken properly into account for the different pairs of monomers. This ratio is chosen as the inverse ratio of the number of Chl *a* molecules in each of the monomers involved, which guarantees detailed balance (provided that the average excited state energies, see above, are indeed similar or identical). All initial excitation probabilities for the different compartments have been chosen in a ratio as to reflect the number of Chl *a* pigments in the compartment.

The rate constants of energy and electron transfer within the PS II core have been determined recently (Holzwarth et al. 2006b) and were taken as such except for the second back transfer rate for the electron. This is necessary since the fluorescence decays of the BBY particles in this work were performed at 4-5 °C, whereas the PS II cores data have been recorded at room temperature. Models 1 (for BBY-2 particles) and 2 (for BBY-1 particles) were calculated with two and three LHC II trimers per PS II monomer, respectively. The results are shown in Figure 6.8 (note that we plot the time dependence of the populations of the excited states and the RP states, rather than the fluorescence kinetics at a certain wavelength, since the former is a wavelength independent quantity, in contrast to the latter). We note that in general monomeric PS II models (not shown) resulted in a less satisfactory agreement with the experiment than the dimeric models reported here. The weighted eigenvector matrices (amplitude matrix for populations) together with the resulting model lifetimes are given in Table 6.2 and Table 6.3 for the BBY-2 data and the BBY-1 data, respectively). These tables will be used in the further discussion for an assignment of the origin of the various lifetime components and a comparison with the results of the target models. Inspection of the respective weighted eigenvector matrix and the theoretical lifetimes shows that the calculations predict quite significant amplitudes of lifetimes shorter than 100 ps in both types of BBY particles, in agreement with the experimentally resolved short lifetime of 25-40 ps of 10-15% amplitude.

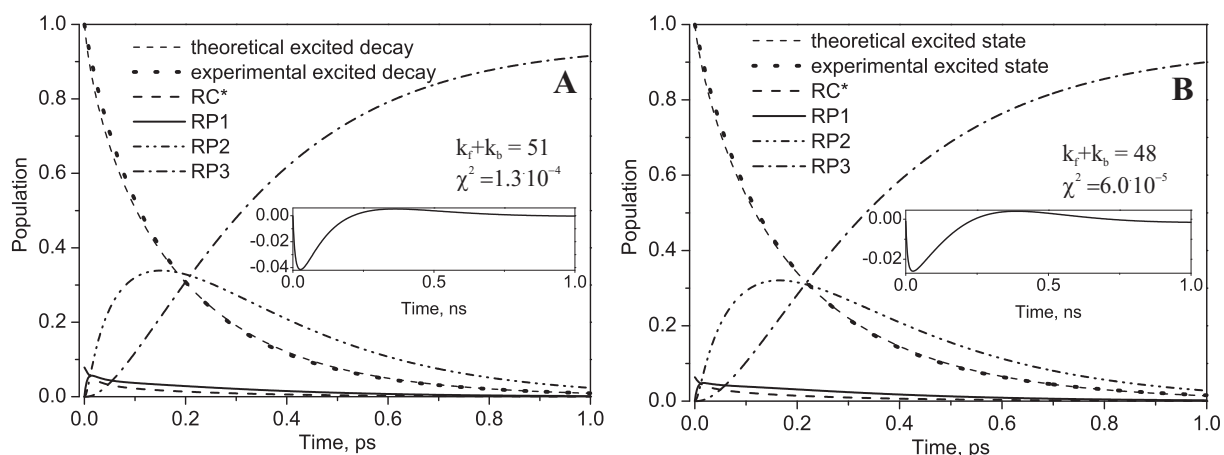


Figure 6.8: Time dependence of populations of excited states and RP intermediates for the theoretical modeling based on structure. 1) for BBY-2 particles and 2) for BBY-1 particles. The insets show the deviations between the theoretical and the experimental excited state decay functions.

The optimal value for the sum of the rate constants of monomer-monomer forward and backward transfer rates was found to be 51 ns^{-1} and 48 ns^{-1} for the BBY-2 and BBY-1 models, respectively. The latter rates correspond to monomer-monomer equilibration times of 18-22 ps. For a single excitation in an LHC II trimer this implies an equilibration time of 12-14 ps. The energy transfer rates are determined very accurately in the models, since small deviations already give rise to a significant worsening of the fit quality. The average trapping times (as calculated on the basis of the excited state populations) are about 200 ps for the BBY-1 preparation and 177 ps for the BBY-2 preparation (see Table 6.1 for a compilation of these values). The corresponding pure charge separation times (calculated for a starting condition where all initial excitation is created on the RC (Miloslavina et al. 2006, van Amerongen et al. 2000)) are 107 and 87 ps for the two preparations.

Figure 6.9 shows the dependence of the average trapping time on the scaling of the energy transfer rates for BBY-2 and BBY-1 (*cf.* Figure 6.8). It follows from these plots that the inter-antenna energy transfer rates for the peripheral antenna are the critical parameters, whereas the average trapping lifetime is basically independent on an increase of the CP47-RC and/or the CP43-RC transfer rates.

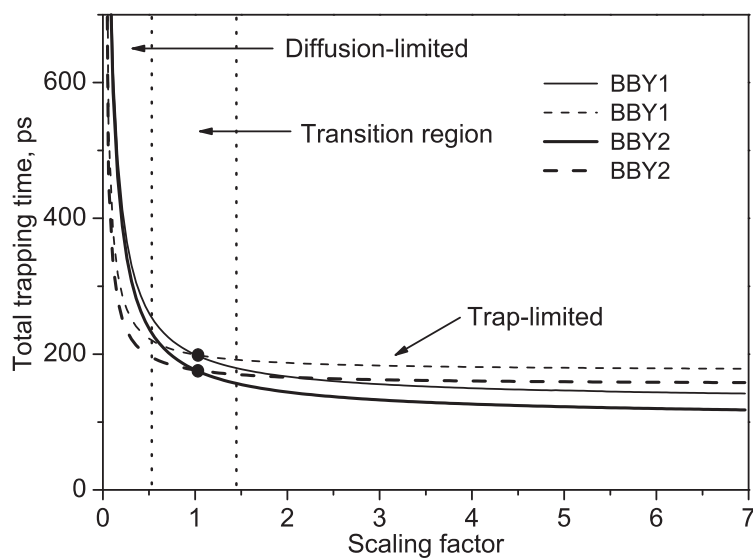


Figure 6.9: Dependence of the average excited state decay lifetime (full lines) on the scaling of all energy transfer rates for the theoretical PS II dimer models for BBY-1 (thin lines) and BBY-2 (thick lines) particles. The dependence of the average excited state decay lifetime on the scaling of the RC-core antenna energy transfer rates only is also shown for comparison (dashed lines). A scaling factor of 1 corresponds to the optimal values for the theoretical dimer models (Figure 6.8).

Table 6.2: BBY-2 model. Table of excitation vector (normalized to 1) and weighted eigenvectors for the lifetimes of the theoretical model. Also shown are the compartment numbering (1-15) as well as the compartment names according to the model shown in Figure 6.7. The second column from left shows the amplitudes for the total excited state decay function (as calculated from the summed eigenvectors of all excited state compartments, including the RC) for each lifetime range (the lifetime ranges which have been combined are shown in the leftmost column).

Compart. #		1	2	3	4	5	6	7	8	9	10	11	12	13	14	15
Compart. name	Exc. states	CP29	LHC II	LHC II	LHC II	CP24	CP47	RC	CP43	CP26	LHC II	LHC II	LHC II	RP1	RP2	RP3
Exc. vector		0.059	0.078	0.078	0.078	0.049	0.157	0.078	0.128	0.059	0.078	0.078	0.078	0.000	0.000	0.000
Lifetimes, ps		Matrix of Weighted Eigenvectors														
1.4	-0.001	0.000	0.000	0.000	0.000	0.000	0.001	-0.005	0.003	0.000	0.000	0.000	0.000	0.002	0.000	0.000
5	0.022	0.007	-0.003	0.000	0.000	0.001	-0.022	0.013	0.036	-0.005	0.003	0.002	-0.011	-0.070	0.024	-0.001
6.1	0.003	-0.008	0.006	-0.001	-0.002	0.003	0.004	-0.001	0.000	0.000	-0.001	-0.003	0.005	-0.019	0.008	0.000
6.6	0.000	0.000	0.000	0.000	0.000	0.000	0.000	0.000	0.000	0.000	0.000	0.000	0.000	0.000	0.000	0.000
8.3	0.000	-0.001	-0.002	0.001	0.000	0.002	-0.001	0.000	0.000	0.001	-0.002	0.002	0.001	0.000	0.000	0.000
8.9	0.001	0.003	0.001	-0.002	0.005	-0.005	-0.007	0.001	0.004	0.000	-0.003	-0.006	0.011	0.003	-0.002	0.000
9.9	0.003	-0.009	-0.002	-0.003	0.007	-0.003	0.006	0.003	0.003	-0.002	0.001	0.006	-0.005	0.007	-0.005	0.000
11	0.000	0.000	0.002	-0.001	0.000	-0.001	0.000	0.000	0.000	0.001	-0.002	0.001	-0.001	0.000	0.000	0.000
13	0.007	-0.002	0.000	0.013	-0.013	-0.008	0.009	0.004	0.005	-0.003	-0.002	0.002	0.002	0.007	-0.007	0.001
17	0.002	-0.004	-0.003	0.006	0.001	-0.002	-0.001	0.001	0.002	0.012	0.002	-0.008	-0.005	0.001	-0.002	0.000
26	0.073	0.016	-0.008	-0.017	0.000	0.020	0.067	0.020	0.020	-0.004	-0.019	-0.019	-0.002	0.022	-0.055	0.008
45	0.060	0.003	-0.012	-0.032	-0.025	-0.003	0.016	0.009	0.014	0.021	0.031	0.018	0.020	0.006	-0.044	0.011
142	0.310	0.020	0.044	0.053	0.048	0.018	0.018	0.002	0.006	0.013	0.028	0.035	0.024	-0.054	-0.642	0.520
246	0.520	0.033	0.055	0.061	0.058	0.029	0.067	0.029	0.034	0.024	0.042	0.048	0.039	0.094	0.726	-1.019

Table 6.3: BBY-1 model. Table of excitation vector (normalized to 1) and weighted eigenvectors for the lifetimes of the theoretical model. Also shown are the compartment numbering (1-18) as well as the compartment names according to the model shown in Figure 6.7. The second column from left shows the amplitudes for the total excited state decay function (as calculated from the summed eigenvectors of all excited state compartments, including the RC) for each lifetime range (the lifetime ranges which have been combined are shown in the leftmost column).

Compart. #		1	2	3	4	5	6	7	8	9	10	11	12	13	14	15	16	17	18	
Compart. Name	Exc. states	CP29	LHC II	LHC II	LHC II	CP24	CP47	RC	CP43	CP26	LHC II	LHC II	LHC II	RP1	RP2	RP3	LHC II	LHC II	LHC II	
Exc. vector		0.048	0.064	0.064	0.064	0.04	0.127	0.064	0.103	0.048	0.064	0.064	0.064	0	0	0	0.064	0.064	0.064	
Lifetimes, ps		Matrix of Weighted Eigenvectors																		
1.4	-0.001	0.000	0.000	0.000	0.000	0.000	0.001	-0.004	0.003	0.000	0.000	0.000	0.000	0.001	0.000	0.000	0.000	0.000	0.000	0.000
4.6	0.017	0.003	-0.001	0.000	0.000	0.001	-0.017	0.013	0.030	-0.003	0.001	0.001	-0.006	-0.043	0.027	-0.001	-0.003	0.001	-0.003	
6.4	0.003	-0.005	0.003	-0.001	-0.001	0.001	0.006	-0.001	-0.001	0.000	-0.001	-0.002	0.004	-0.020	0.018	-0.001	0.000	0.000	0.000	
6.6	0.000	0.001	-0.001	0.000	0.000	-0.001	0.001	0.000	-0.001	0.000	0.000	0.000	0.000	-0.003	0.003	0.000	0.000	0.000	0.000	
8.7	0.000	0.000	-0.002	0.001	0.000	0.001	-0.001	0.000	0.000	0.001	-0.002	0.002	0.001	0.000	0.000	0.000	0.000	0.000	0.000	
9.1	0.001	0.001	0.001	-0.002	0.003	-0.004	-0.001	0.001	0.002	0.000	-0.001	-0.003	0.005	0.003	-0.003	0.000	-0.001	0.001	-0.001	
9.8	0.000	0.000	0.000	0.000	0.000	0.000	0.000	0.000	0.000	0.000	0.000	0.000	0.000	0.000	0.000	0.000	0.000	0.000	0.000	
10	0.001	-0.003	-0.001	-0.001	0.002	-0.001	0.004	0.001	0.001	-0.001	0.001	0.003	-0.003	0.002	-0.004	0.000	-0.001	0.001	-0.001	
11	0.000	0.000	0.001	0.000	0.000	0.000	0.000	0.000	0.000	0.000	-0.001	0.000	0.000	0.000	0.000	0.000	0.000	0.000	0.000	
12	0.000	-0.001	0.000	-0.002	0.003	0.000	-0.002	0.000	0.001	0.000	0.000	0.001	0.000	0.000	0.000	0.000	0.003	-0.004	0.003	
14	0.005	-0.001	0.000	0.010	-0.010	-0.006	0.007	0.003	0.004	-0.002	-0.001	0.001	0.001	0.005	-0.011	0.001	0.002	-0.004	0.002	
18	0.002	-0.002	-0.002	0.004	0.001	-0.001	0.000	0.001	0.002	0.009	0.001	-0.006	-0.003	0.001	-0.003	0.000	0.000	-0.001	0.000	
25	0.039	0.011	-0.004	-0.013	0.000	0.014	0.041	0.011	0.009	-0.002	-0.009	-0.009	0.001	0.012	-0.059	0.008	-0.001	-0.008	-0.001	
45	0.008	0.001	-0.003	-0.009	-0.007	-0.001	0.002	0.001	0.002	0.007	0.012	0.008	0.007	0.001	-0.012	0.003	-0.003	-0.005	-0.003	
74	0.110	-0.002	-0.015	-0.023	-0.019	-0.003	0.012	0.008	0.015	0.006	0.002	-0.004	0.002	0.000	-0.186	0.079	0.038	0.053	0.038	
143	0.235	0.015	0.033	0.040	0.036	0.013	0.010	0.000	0.003	0.009	0.021	0.026	0.017	-0.049	-0.959	0.782	0.003	0.004	0.003	
269	0.579	0.032	0.053	0.058	0.055	0.028	0.065	0.029	0.034	0.024	0.041	0.046	0.038	0.091	1.189	-1.826	0.025	0.027	0.025	

DISCUSSION

The LDA data of the preparation BBY-1 (Figure 6.3) reveal three well-defined lifetime peaks that show no pronounced broadening substantially beyond the one expected from the statistical limits and the signal/noise ratio of the measurement (Prokhorenko et al. 2000). The data from the preparation BBY-2 look similar (data not shown). The results agree well with those from the discrete global lifetime analysis (Figure 6.2). A perfect agreement is not expected, since the modeling (Figure 6.8 and Table 6.2, Table 6.3) show that the actual decays are expected to contain many, albeit small amplitude, exponentials.

No major lifetime components below the ca. 30 ps component were required in the global analysis (note that the LDA analysis for intrinsic reasons would not be sensitive for components below ca. 10 ps, i.e. for lifetimes well below the apparatus width). The ca. 1 ns component does clearly not derive from intact open PS II particles. More importantly however is the fact that it has also not been possible to include the lifetime of ca. 26-40 ps, which does have a substantial amplitude (ca. 10%), into any of the target models of various complexity (Figure 6.4). On the one hand this might hint to an origin of that lifetime different from the typical PS II complex in BBYs. One possibility would be a small amount of PS I in the BBY preparation. It is known that some PS I is located in the periphery of the grana stacks from which the BBY particles are derived (Gadjieva et al. 1999, Jansson et al. 1997, Wollenberger et al. 1994). We excluded that possibility by testing for PS I content using EPR spectroscopy.

As second argument against a PS I origin of this component is the fact that the DAS lack any indication that would point to a PS I origin, i.e. no red-shifted fluorescence nor a clear "red pigment" fluorescence is observed (Gobets and van Grondelle 2001, Jennings et al. 1998, Karapetyan et al. 1999, Melkozernov and Blankenship 2005). We have studied both PS I cores and intact PS I particles from higher plants in very detail (to be published) and do not find any similarity of the 26-40 ps DAS component with any lifetime component found in PS I particles. Thus the 26-40 ps component must also derive from intact open PS II particles.

This leaves us with two main components (ca. 150 ps and 300 ps) characterizing the fluorescence decay of intact open PS II particles, plus a smaller amplitude of a ca. 25-40 ps component whose origin can only be revealed by the theoretical modeling (*vide in-*

fra). Note that this does not exclude any small amplitudes of additional lifetimes, in particular on the short time scale below ca. 10 ps, being present in the kinetics. In fact such components are to be expected on a theoretical basis due to the various energy transfer steps (see Table 6.2 and Table 6.3) and taking into account the recent advances in our understanding of the early events in cyanobacterial PS II cores (Holzwarth et al. 2006b, Miloslavina et al. 2006). We will discuss that point further when analyzing the various models. It is interesting to note here however that an initial attempt to describe the experimental kinetics ignoring the ca. 30 ps component as a genuine PS II component led to very poor agreement with the theoretical models in all cases. For this reason we do not discuss such models any further.

Energy transfer and trapping kinetics

We will first address the important question of the characteristic (average) energy equilibration time between the antenna and the RC. This question can be answered if we assume the same mechanism of electron transfer to be present in intact BBY PS II particles as in cyanobacterial PS II cores (Holzwarth et al. 2006b).

The target models in Figure 6.4 B-D test a simplified model describing the whole antenna system as a single compartment connected to the RC, while the RC* itself and the RP compartments are connected in the same way as in PS II cores, with the first two electron transfer steps assumed to be reversible (Holzwarth et al. 2006b, Miloslavina et al. 2006). The antenna-RC energy transfer rates are 8.5 ns^{-1} for the forward and 72 ns^{-1} for the backward rate for the BBY-1 particles. This model results in calculated fluorescence lifetimes of 3.8 ps, 9.2 ps, 156 ps, and 305 ps (Figure 6.4 B). Inspection of the weighted eigenvectors (see Table 6.4) reveals that the 3.8 ps component represents a very small amplitude component that has contributions from both the rise of RP_1 (major contribution) and the antenna \rightarrow RC energy transfer. The 9 ps component derives mainly from the $\text{RP}_1 \rightarrow \text{RP}_2$ electron transfer and to a small amount again from energy transfer. The 156 ps lifetime represents primarily the main component of excited state decay (trapping) and the concomitant rise of RP_2 , with a very small contribution from the rise of RP_1 . Finally, the 305 ps lifetime represents primarily the *apparent lifetime* of electron transfer from RP_2 to Q_A , which is also seen as a contribution to the overall excited state decay due to the reversible two early electron transfer steps.

Table 6.4: Weighted eigenvectors for the compartment model Figure 6.4 B (BBY-1 particles). Also shown are the lifetimes and the excitation vector.

Compartment	Ant*	RC*	RP ₁	RP ₂	RP ₃
Excitation vector	0.084	0.07	0	0	0
Lifetimes, ps	Matrix of eigenvectors				
3.8	-0.010	0.036	-0.045	0.019	-0.000
9	0.005	-0.007	-0.036	0.040	-0.001
156	0.597	0.019	-0.039	-1.482	0.924
305	0.254	0.019	0.086	1.559	-1.901

The eigenvector matrix clearly shows that the two fast lifetimes are expected to appear in the kinetics with very small, if not negligible, amplitudes. The exact amount of the small amplitudes should depend on the relative spectral shapes of the antenna and the RC fluorescence. Of particular interest is the time dependence of the populations of the various model compartments given in Figure 6.5. These data show that the relative populations of both RC* as well as RP₁ amount to at most about 5 % after the fast initial quasi-equilibration step. Thus the system is characterized by two primarily populated compartments only, i.e. Ant* and RP₂, which has the consequence that the observed fluorescence kinetics is close to bi-exponential (*vide supra*).

The two longer-lived lifetimes of model B agree very well with the two main components from global and LDA analysis. The two short lifetimes were not resolved in the global analysis and one may ask the question whether this result is reasonable. We note that it is not unusual that more lifetime components can be resolved in target analysis than in global or LDA lifetime analysis (Holzwarth 1996) due to the much more restrictive assumptions going into a specific kinetic model. Note that despite the overall four-exponential kinetics there are only two SAES (for Ant* and RC*, *cf.* Figure 6.4 B) to be determined, which very much restricts the existence ranges for the rates, lifetimes, and SAES. Given these circumstances the result seems to be quite reasonable. We have however another important criterion to judge the validity of the model, i.e. the ratio of the obtained energy transfer rates for model B. This ratio of backward to forward energy transfer rates is about 8.5. Based on a model of isoenergetic antenna and RC excited states, this ratio implies a 8.5 times larger *effective antenna size* than RC size. Although an exact ratio is not expected to result from such an analysis, that number is reasonable given the fact that the RC comprises 6-8 (depending on whether the two peripheral Chl_z molecules are treated as belonging to the RC or not) and the antenna about 118 Chl *a*

molecules and that a substantial part of the Chl *a* molecules of the antenna have an excited state energy higher than the average RC excited states (corresponding to about 680 nm). Note that the Chl *b* molecules of the antenna do not contribute substantially to the excited state equilibrium and the *effective antenna size* due to their relatively high energy and they are thus not considered in this simple estimate. It has been shown however that a small amount of excitation resides on the Chl *b* molecules in intact thylakoids (Engelmann et al. 2005). In summary we thus consider the average rates of energy transfer between antenna and RC resulting from that simplified model as very reasonable.

The rate constants from models B-D (Figure 6.4) allow us to calculate both the average energy transfer lifetime EET as well as the average charge separation lifetime τ_{CS} , whose sum gives the total trapping lifetime $\tau_{tot\ trap}$ according to:

$$\tau_{tot\ trap} = \tau_{EET} + \tau_{CS}$$

Model B gives $\tau_{tot\ trap} = 194$ ps and $\tau_{CS} = 89$ ps, resulting in $\tau_{EET} = 105$ ps. The ratio of $\tau_{EET}/\tau_{CS} = 1.18$, implying that the total trapping dynamics is a borderline case. Thus the trapping characteristics of intact higher plant PS II is located in the transition region between trap- and diffusion-limit, but clearly excludes the full diffusion limit. In contrast, the trapping in PS II cores is strongly on the trap-limited side according to the same criteria (Holzwarth 1996, Holzwarth et al. 2006b, Miloslavina et al. 2006).

In comparison in the theoretical model for the PS II dimer (Figure 6.8, model 2) the average trapping time is 199 ps and the charge separation time 107 ps. The theoretical model gives a ratio $\tau_{EET}/\tau_{CS} = 0.87$, i.e. again a situation where the energy transfer contribution τ_{EET} to the total trapping time is quite significant, but still not dominant. Thus we can clearly exclude a strongly diffusion-limited kinetics, but the overall excited state decay is also not purely trap-limited. The theoretical modeling confirms the presence of small amplitudes of lifetimes in the range of 1-10 ps and a total of ca 15% amplitude of 2045 ps components, in agreement with the target models B-D, which always require an unconnected ca. 30 ps component of about 10% relative amplitude. The total kinetics in the theoretical model is still dominated by two main exponentials (ca. 140 and 270 ps) but two additional lifetimes (besides the very short ones below 10 ps) appear in the models with significant amplitudes (ca. 10-30 ps and 45-75 ps). Components in that lifetime range (ca. 26-37 ps) are found also in the experimental data, both in the multiexponential global analysis and the target modeling (Figure 6.2 and Figure 6.4), although it

was outside the actual target models in all cases (Figure 6.4). It was also found as a significant component in the LDA analysis (Figure 6.3). Thus the theoretical modeling clearly confirms that the ca. 26-37 ps global decay components indeed originate from intact BBY particles and not from some contamination with e.g. PS I complexes, which would indeed be hard to explain (see discussion above). These short-lived components reflect the energy equilibration processes among the various antenna parts, as can be seen easily by inspection of the eigenvector matrices in the Appendix.

The excited RC population rises with lifetimes below 10 ps. The ca. 145 ps component reflects the rise of RP_2 , while RP_1 is only very weakly populated, rising with mixed lifetimes ranging from a few ps to 145 ps. The 145 ps component is essentially identical to the main primary charge separation process. The 245 or 269 ps components (in BBY-2 and BBY-1, respectively) reflect the reduction of the Q_A , which corresponds to the electron transfer from RP_2 , to RP_1 .

Another point of interest is that the LDA data indicates that there is no significant broadening present in any of the three major lifetime components. Since the ca. 172 ps component is controlled mainly by the antenna size of the PS II particles (having contributions from both diffusion and trapping which both depend on the antenna size (Hemenger et al. 1972, Pearlstein 1982b, van Amerongen et al. 2000)), this result allows us to exclude any major size distribution in the peripheral antenna of the PS II particles in BBY preparations and would also be inconsistent with any major rate distribution in the primary charge separation rate. This result is interesting with regard to the antenna organization of PS II in the grana stacks. It excludes for example a significant random association or structure heterogeneity in the arrangement of LHC II peripheral complexes with the PS II core and functionally supports the structurally stable supercomplex model obtained by EM analysis of PS II particles from higher plants (Dekker and Boekema 2005, Ruban et al. 2003, Yakushevskaya et al. 2001), which suggests that the large majority of the PS II complexes has only one type of antenna arrangement and composition.

Comparison with cyanobacterial PS II cores

In the context of our recent studies on the mechanism and kinetics of electron transfer in cyanobacterial PS II cores from the thermophilic organism *Thermosynechococcus elongatus* (Holzwarth et al. 2006b, Miloslavina et al. 2006) and isolated D1/D2-cyt-b559 particles from higher plants (Holzwarth et al. 2006b) the question regarding any significant

differences in the electron transfer between these PS II RCs arose which can now be answered.

The analysis of model B (Figure 6.4) with free-running rates resulted in electron transfer rates for the first two electron transfer steps that were very close to those found for the cyanobacterial PS II cores, which in turn were found to be identical within the error limits with those from the isolated RCs (Holzwarth et al. 2006b). Only the backward rate from RP_2 and the rate constant of Q_A reduction were somewhat different in the two cases. In order to check this identity of electron transfer rates further, we have performed additional analyses (model C) where we fixed all the electron transfer rates to the values obtained for the cyanobacterial PS II cores (Holzwarth et al. 2006b). Since this fit did not result in a perfect fit, we also performed an additional analysis where the rate of the Q_A reduction was allowed to vary, but the other four electron transfer rates were kept fixed (model D). The latter analysis resulted in a slightly larger rate constant for the Q_A reduction than the fixed value of model C and a very good overall fit. Both of these values as well as the reverse electron transfer rate from RP_2 are significantly different from the values obtained earlier from the fluorescence kinetics analysis for cyanobacterial PS II cores (Miloslavina et al. 2006). We note however that in the latter analysis we had ignored a significant component of about 110 ps, which we could not assign at the time (Miloslavina et al. 2006).

Further comparison of these differences in the Q_A reduction rate and the second reverse electrons transfer rate, which are in fact both strongly correlated in the analysis, between all the present data for higher plant and cyanobacterial PS II reveals that the existing differences in these two rate constants can be traced to some further complexity present in the decay of RP_2 , being ignored so far in the models. Referring only to the data from cyanobacterial PS II cores similar differences seem to be already present between the transient absorption data and the fluorescence data (Holzwarth et al. 2006b, Miloslavina et al. 2006). While the ca. 110 ps component, which is very likely to derive from intact PS II cores, has been ignored so far in the modeling of the fluorescence kinetics (Miloslavina et al. 2006) the lifetime density maps of the transient absorption data (Holzwarth et al. 2006b) clearly show a relatively wide distribution of the lifetime associated with decay of RP_2 and rise of RP_3 ranging from slightly above 100 ps to about 300 ps, in good agreement with the two lifetimes observed in fluorescence. We believe that this complexity arises from either a protein relaxation in RP_2 or a heterogeneity in the rate of Q_A reduction.

Accounting for this complexity will require an extension of the kinetic models and preferentially combined analysis of all the available data, comprising fluorescence and transient absorption. This requires also further experiments. However this study of the detailed Q_A reduction kinetics is not the purpose and would be beyond the scope of the present paper and it will thus be published separately. All the other electron transfer rates seem to be nearly unaffected by that problem and we can conclude that within the error limits of the available data there exist no significant differences in the early electron transfer rates (with the possible exception of the Q_A reduction kinetics, *vide supra*) of cyanobacterial PS II cores from a thermophilic organism like e.g. *Thermosynechococcus elongatus* on the one hand and those from a higher plant PS II like e.g. spinach on the other hand. This is the case for both types of BBY preparations. The identity of the electron transfer rates for PS II in higher plants (this data) and in a cyanobacterium is quite a remarkable finding, which may be taken as a hint to rather rigid requirements for maintaining an efficient overall electron transfer mechanism in PS II RCs.

Relevance and limitations of the early ERPE model for higher plant PS II

Comparison of the simple ERPE model with the more extended target model, taking into account the extended electron transfer mechanism found recently (Holzwarth et al. 2006b, Miloslavina et al. 2006) clearly reveals the potential but also the limitations of the ERPE model (Schatz et al. 1988) for intact higher plant PS II particles. Analysis within the bi-exponential ERPE model reproduces fairly well the two main lifetimes. The shorter-lived of these two components reflects the apparent charge separation (trapping time) while the longer-lived component is mainly reflecting the apparent Q_A reduction. Note that in the simple ERPE model RP_1 stands for the $P_{680}^+Pheo^-$ RP, and RP_2 for $P_{680}^+Q_A^-$. This is still reasonable within the extended model, since both the target modeling as well as the theoretical models of the kinetics show that the relative population of the actual first RP ($Chl_{acc}^+ Pheo^-$) (Holzwarth et al. 2006b, Miloslavina et al. 2006) is very low for intact higher plant PS II, since the secondary electron transfer rate is comparably fast as the first one. Thus ignoring the first RP in the simple ERPE model is still reasonable.

Comparison of the total free energy change (taking into account also the free energy difference to the Ant^* state) for the different models reveals however that the ERPE model does not provide the proper value for the free energy difference even if the free energy difference between the unresolved antenna/RC couple is taken properly into account

(Schatz et al. 1987, Schatz et al. 1988). While the features discussed so far might suggest that the simple ERPE model can still be used at least technically to analyze the PS II kinetics, the limitations are clearly evident. First, the rate constants found for the charge separation and recombination within the ERPE model can not be reconciled easily with the molecular rates. The resulting apparent rate constant for charge separation comprises both the actual charge separation processes as well as a substantial contribution from energy diffusion in the antenna. In this point the ERPE model indeed fails to give the correct results for higher plant PS II. As a direct consequence of the assumption of rapid energy equilibration in the antenna the ERPE model also ignores the presence of lifetime components with significant amplitudes which directly reflect the limiting diffusion among the peripheral antenna complexes. Detailed analysis of the weighted eigenvector matrix for the theoretical model (see Table 6.2 and Table 6.3) reveals that the 20-45 ps components missed by the ERPE model (but also by the more extended target models) can not be assigned to a single process (none of the compartments contributes pronouncedly more to the amplitude than the other ones) but rather reflects the characteristic times for movement of the excitation through the outer antenna.

Thus the potential and the limitations for the applications of the simple ERPE model for higher plant PS II are evident: Technically one can still apply the ERPE model within certain limits to the analysis of the PS II kinetics of higher plants. It is even possible to derive some important information on relative *apparent rates* of charge separation and recombination, and also on the energetics of the total system from that analysis given the simplicity of its application. This would for example continue to be quite useful when comparing various external conditions like induced quenching, RC modifications that change the energetics etc. The most severe limitation of the ERPE model consists in the fact that the interpretation of the apparent primary charge separation and recombination rates resulting from the simple ERPE model in terms of *intrinsic molecular rates* is not possible anymore. We note however that the simplicity of the early ERPE model (i.e. a biexponential kinetics) had already broken down with the demonstration of the presence of two early radical pairs (Holzwarth et al. 2006b, Miloslavina et al. 2006). The other limitation of the ERPE model for a very detailed kinetic analysis also becomes evident: ignoring the significant additional lifetime components may lead to substantial deviations of the true kinetics from the kinetics predicted by the ERPE model. It should be noted however that the additional lifetime components which are present in the actual kinetics (20-45 ps) clearly do not derive from the more complex electron transfer scheme than assumed in the ERPE model, but rather from the energy transfer processes

among the peripheral antenna complexes. This is radically different from the situation for PS II core particles. The higher complexity of the total kinetics there does indeed derive from the presence of a more complex electron transfer scheme (Holzwarth et al. 2006b, Miloslavina et al. 2006).

The reason for all the limitations is the fact that the energy diffusion through the peripheral antenna complexes contributes significantly (about 50%) to the overall trapping. Thus in spite of the fact that the kinetics is not severely diffusion-limited the intact higher plant PS II has a significant diffusion contribution. What can be clearly excluded is a substantial transfer-to-the-trap limit, as has been suggested by some authors (Dekker and van Grondelle 2000, Vassiliev et al. 2002) (*cf.* Figure 6.9, dashed line). We have shown previously that the transfer-to-the-trap from the core antennae contributes about 9 ps to the diffusion time (Miloslavina et al. 2006) which is nearly negligible with respect to the total diffusion time of ca. 90 ps in intact higher plant PS II. Our conclusions are in good agreement with the conclusions drawn from the quenching analysis and the somewhat simpler kinetic modeling performed by Jennings et al. (Jennings et al. 2000) since at the time of the writing of that paper the details of the antenna organization of PS II were not well-known. The authors concluded that there was a 30% diffusion-limitation in the trapping kinetics, while our results point to an even higher diffusion-limitation of ca. 50%.

The energy migration time between monomeric peripheral antenna complexes found in our analysis is 18-22 ps, resulting in an intra-trimer equilibration time of ca. 12-14 ps for a single excitation. Values of ca. 30 ps for the intra-trimer equilibration have been suggested earlier (van Amerongen and van Grondelle 2001) based on data from annihilation measurements (Barzda et al. 2001) and theoretical modeling. Our modeling shows that this equilibration is in fact substantially faster than estimated earlier. Interestingly the lifetime of the energy transfer component found by Dau and Sauer (Dau and Sauer 1996) of ca. 15 ps is quite close to the ca. 11 ps intra-trimer equilibration time resulting from our analysis and can be reconciled easily within our theoretical model.

A “second generation ERPE model”

Based on the findings described in this study leading to the conclusion that the early ERPE model (Schatz et al. 1988) suffers from substantial limitations and drawbacks when applied to the dynamics in PS II from higher plants, we now proceed to propose a “second generation ERPE model” that does not suffer from these drawbacks. Besides a

more realistic description of the energy transfer processes this new model also incorporates the results of the recent findings on the electron transfer processes in the RCs of PS II (Holzwarth et al. 2006b, Miloslavina et al. 2006).

The new model is based on the kinetic scheme shown in Figure 6.7. As pointed out above for achieving better accuracy it is important to apply a dimeric rather than a monomeric PS II model. The new model keeps important elements of the early ERPE model: i) charge separation from the two first RPs is still reversible and leads back to the excited states of the RC and the antenna, and ii) the recombination reactions give rise to a fast equilibration between RPs and the excited states of the core antenna, although the kinetic scheme is more complex due to the additional RP intermediate. These features still give rise to a situation where the Q_A reduction in open RCs gives rise to one of the dominant lifetime components in the fluorescence kinetics. The differences to the old ERPE model are the consideration of the important details of the peripheral antenna organization and the ensuing limitations in the peripheral antenna energy transfer steps as well as the expanded electron transfer scheme.

We propose the following procedure for analyzing PS II kinetic fluorescence data:

1. Perform a high signal-to-noise time resolved measurement of the fluorescence kinetics and analyze it using global multi-exponential analysis or LDA methods using as many exponentials as necessary for a good fit; the individual lifetimes do not have a direct physical meaning; time-resolved spectra will be helpful in order to determine which components do derive from intact PS II;
2. Set up the kinetic scheme shown in Figure 6.7 for a dimeric PS II model; this can be done using any advanced mathematics software like e.g. MATLAB, Mathematica, etc.
3. Fit the theoretical excited state decay function resulting from the kinetic scheme either directly to the experimental fluorescence data or, if additional lifetime components are present, to the excited state decay function calculated on the basis of the multi-exponential sum function obtained from the multi-exponential analysis of the data by solving the system of linear differential equations (Beauregard et al. 1991, Holzwarth 1995, Holzwarth 1996, van Stokkum et al. 2004); choose proper excitation conditions (excitation vector); Note that the RPs are non-fluorescent when calculating the theoretical excited state decay;

4. Depending on the type of study either the peripheral inter-antenna energy transfer rate, the decay rate of excited states to the ground state (for quenching studies), or the electron transfer rates in the RC should be fitted freely, while the other rates should preferentially be kept constant at the values determined in this work.

This procedure can be adapted easily to other situations where e.g. the antenna structure of composition is expected to change etc. This analysis results in the desired information on rate constants that may have changed upon perturbing the photosystem or changing the external conditions. The model in total contains 11 rate constants, as compared to 4 rate constants for the early ERPE model (one of them, i.e. usually the excited state decay rate k_A , had to be chosen to be constant). The total number of rates is relatively large, though much smaller than required for a full-fledged theoretical description of the antenna and RC processes. It is thus advisable to have not all these 11 rates free-running in an analysis. For example, in the present work we have not modified the RC/inner core antenna energy transfer rates, but rather took the values determined from isolated PS II cores by our high resolution study (Holzwarth et al. 2006b). These rates should only be allowed to vary if there is a good reason. This reduces the number of rates to be determined to 7, which is a more reasonable number to handle and does not provide too much of a problem if high quality data are available. For better stability and narrower error limits it may be advisable however to leave those rates constant in the analysis that are not expected to change upon a change in the external conditions. Thus for a quenching experiment only the excited state decay k_A should be left free, while e.g. for a modification of RC properties the electron transfer rates should be left free. Thus it depends on the specific situation which rates should be fitted and which ones should be left constant during the analysis. It is advisable to perform in each case an analysis on the unperturbed system for a reference. The analysis in terms of the “second generation ERPE model” is necessarily more complex than the early ERPE model which required just three rate constants and one SAES spectrum to describe the total kinetics (Schatz et al. 1988). Using modern numerical software packages it is however easy to perform this analysis.

Despite the substantial increase in the number of rate constants the model presented here for the “second generation ERPE model” is still a relatively simple compartment model, as compared to a full consideration of the energy transfer processes among all chromophores in the large PS II antenna. Nevertheless it can give quite reliable results on changes of rates of inter-antenna energy transfer, quenching rates, and/or electron transfer rates. The beauty of the model is that not much information is required for the

analysis beforehand. This is in contrast to a full microscopic modeling of the energy transfer processes. Several such calculations have been performed recently for PS I particles (Brüggemann et al. 2004, Byrdin et al. 2002, Damjanovic et al. 2002, Gobets et al. 2003, Sener et al. 2002, Sener et al. 2004, Sener et al. 2005, Yang et al. 2003) but much less for PS II particles (Vasil'ev et al. 2001, Vasil'ev et al. 2004). Depending on the level of calculation a great deal of knowledge about the system and on top often many untested assumptions are usually required to perform such a microscopic quantum mechanical or excitonic modeling. In contrast, a large number of questions can be answered quite satisfactorily using much simpler compartment models that require only a small fraction of programming and computing time as compared to the full microscopic and/or quantum mechanical or exciton models.

Quite naturally the model proposed here also has its limitations: it should not be used without great consideration to answer questions regarding to the effect of specific modifications on a single or a small group of pigments in the PS II antenna, nor should it be used to predict temperature effects down to cryogenic. The latter restriction is obvious, since our model does not take into account the small but definite differences in the excited state energies of the various antenna complexes. These differences will be amplified when going to low temperatures. The model is expected to be best for temperatures relatively close to physiological temperatures. The former restriction is also self-evident, since in our compartment model we use a coarse-graining procedure for the properties of the peripheral antenna complexes. If such problems are to be addressed there will be no real shortcut possible and a full microscopic modeling taking into account in detail the properties of each antenna complex has to be performed.

Finally one may wonder whether the term “ERPE model”, as chosen here, which implies an equilibration between radical pairs and antenna excited states, is still justified, given the fact that we have explicitly demonstrated an energy transfer limitation for the peripheral antenna. We definitely believe that the term is still fully justified for several reasons: First, the electron transfer steps are reversible and lead to rapid back reaction to the excited states at least of the core antennae. Second, the meaning of “equilibration” with regard to the energy and charge transfer in photosystems is often misinterpreted. While this is an interesting topic that deserves some further detailed attention, it is not the intention of the present work to dwell much on the meaning of “equilibration kinetics” in these systems. Thus it may suffice to focus on one important point: It can easily be demonstrated by analyzing simple first order differential equations that a dynamic system after an initial perturbation (like e.g. the excitation of a photosystem using a short

laser pulse) generally only achieves real equilibrium on a time scale of the inverse rate of the slowest process(es) in the system. This fact has in the past been interpreted erroneously however in order to claim a diffusion-limitation for example in the antenna of photosystem I (Laible et al. 1994). We simply note here without specific proof that despite widespread belief, “non-equilibrium Boltzmann conditions” of the populations of antenna and/or RP compartments on a time scale of the trapping process does not necessarily imply a diffusion-limited situation. On the contrary, we have demonstrated recently for both PS I (Holzwarth et al. 2006a, Müller et al. 2003) as well as for PS II cores (Holzwarth et al. 2006b, Miloslavina et al. 2006) that the kinetics in these systems are strongly trap- and not diffusion-limited, despite the fact that Boltzmann equilibrium between antenna, RC, and RPs is not achieved in a time short compared to the charge separation process(es).

CONCLUSIONS

Based on a detailed analysis of the experimental fluorescence kinetics from BBY PS II particles from higher plants and a comparison with a theoretical antenna model, we critically evaluated the potential and limitations of the early simple ERPE model for intact higher plant PS II particles. Our comparison also takes into account the recent progress in our understanding of the electron transfer processes in the PS II RC (Holzwarth et al. 2006b, Miloslavina et al. 2006). We conclude that for some applications the ERPE model may still be useful, but care has to be taken when interpreting the resulting *apparent lifetimes* and *rate constants* in terms of *molecular rates*. In a strict sense the ERPE model does not describe the excited state kinetics of intact higher plant PS II particles correctly. Antenna equilibration is clearly not fast enough to be ignored, as was assumed intrinsically in the ERPE model. One of the consequences is a more complex excited state decay kinetics in higher plant PS II than what had been assumed when developing the ERPE model and then extended without proof to larger PS II particles. Our analysis shows that in order to fully understand the excited state dynamics of intact PS II particles a statistical approach for the antenna function as applied in the ERPE model is not sufficient and a model taking into account the structural details and the energy equilibration in the outer antenna is indeed required. We now propose a “second generation ERPE model” that does not suffer from these drawbacks. Necessarily the kinetic model is substantially more complex than the early ERPE model. However, it will not be neces-

sary for its future application to go through all the tedious analyses represented here. Rather we provide a set of energy and electron transfer parameters that represent a good starting point for an analysis. It is then possible using relatively simple data analysis methods to test in various situations, e.g. physiological adaptations like transitions, qE-quenching, photoinhibition etc., whether a change in the antenna functions or size or in the electron transfer steps in the RC takes place, and what effect these changes have on the free energy differences of the various processes. The model also allows to predict in a more reliable way than the early ERPE model what effects may be expected e.g. in fluorescence induction experiments (Lavergne and Trissl 1995, Vredenberg 2004). The application of these procedures has already led to a successful analysis of e.g. the fluorescence kinetics in intact leaves, which is very important for the understanding of qE-quenching.

Interestingly, we did not find any pronounced energy equilibration lifetime component (positive-negative amplitudes) in the experimental kinetics upon excitation into the Chl *a* pools at 663 nm. This differs from the results found by Dau and Sauer (1996) on the same type of PS II particles using an excitation wavelength of 645 nm, i.e. preferential excitation of Chl *b* in the peripheral antenna, which an initial condition that is more out of equilibrium than in the conditions of our experiment. The two observations are however in agreement and complement each other. Comparing these results we can draw the conclusion that it is possible to create a spectrally (and probably also spatially) equilibrated excited state distribution and still have overall diffusion-limited kinetics. We have in fact chosen such excitation conditions intentionally since they serve best our purpose to probe the overall degree of diffusion limitation in the PS II antenna. It can be also understood from the present data that the fact that the Stepanov relationship is fulfilled reasonably well (Dau and Sauer 1996) does not necessarily imply the absence of a partial diffusion-limitation although a fully diffusion-limited model should – in particular upon Chl *b* excitation – give rise to substantial deviation from the Stepanov relationship. However, Jennings et al. (2000) have observed that the core and RC fluorescence do not fully obey the Stepanov relationship, which is in full agreement with our finding that the energy migration through the peripheral antenna complexes adds some diffusion limitation.

Chapter 7

QUENCHING IN ISOLATED LHC II OLIGOMERS

According to the present view, the light-harvesting antenna of Photosystem II is the direct site where non-photochemical quenching (or the largest part of it) occurs, although the mechanism is still under question. Some of the hypotheses regarding the mechanism of quenching point to oligomerization and conformational changes in LHC II (*cf.* Chapter 2 for a review on the available hypotheses). These suggestions are based to a significant extent on the observation that the fluorescence of LHC II oligomers *in vitro* is strongly quenched in comparison to detergent-embedded individual complexes (Mullineaux et al. 1993, Ruban and Horton 1992).

We investigated the fluorescence decays in oligomers of the major LHC II prepared *in vitro*. We compared several different types of oligomeric LHC II preparations – lamellar aggregates isolated from wild type spinach and LHC II isolated from the *Arabidopsis npq1* and *npq2* mutants, which differ in their xanthophyll composition – *npq1* containing no zeaxanthin due to lack of Vx-deepoxidase, and *npq2*, which is deficient in Zx-epoxidase and accumulates Zx in the dark.

Analysing the quenching in isolated LHC II oligomers and in intact leaves of *Arabidopsis* (presented in the next Chapter) we found striking similarities that support the notion the formation of LHC II oligomers *in vivo* is one of the mechanisms of non-photochemical quenching.

Pigment content

The results of the pigment analysis of the different LHC II types – isolated from w.t., *npq1*, and *npq2* plants, are compared in Table 7.1. The pigment stoichiometries were similar to the published ones (Caffarri et al. 2001) for these types of LHC II. The Chl *a/b* ratio decreased from 1.36 for the w.t. to 1.35 for *npq2* and 1.33 for *npq1* mutant. Compared to the w.t. the amount of bound Car/monomer was also slightly reduced, from 4 to 3.7 in *npq2* and *npq1*. The important differences were in the XC pigments – whereas w.t. contained Vx and no Zx, the *npq1* mutant had lower amount of Vx implying that part of the Vx sites (V1) were empty or occupied by Lut. The *npq2* mutant did not contain Vx but had more than one molecule of Zx per monomer, indicating that all V1 sites and

probably some internal sites are occupied by Zx. In addition, the LHC II from *npq2* lacked Nx.

Table 7.1: Comparison of pigment composition of w.t., *npq2* and *npq1* light-harvesting complexes.

	Chl <i>a/b</i>	Car/monomer	Lut	Vx	Zx	Nx
w.t.	1.36	4	2.1	0.9	-	1.0
<i>npq1</i>	1.33	3.67	2.5	0.3	-	1.0
<i>npq2</i>	1.35	3.65	2.4	-	1.2	-

Global lifetime analysis of the fluorescence kinetics

The fluorescence kinetics of the various trimeric and oligomeric LHC II complexes were measured in the range from ~660 to ~760 nm. The full DAS of the fluorescence lifetime measurements are given in Figure 7.2. The kinetics of the trimers was characterized by either four or five exponentials. The predominant amplitude component has a long lifetime of 4.1 and 3.8 ns (spinach w.t. and *npq1*-LHC II from *Arabidopsis*, respectively) whereas the *npq2*-LHC II has a significantly shortened long lifetime of 3.5 ns. The shortest-lived exponential of 7-8 ps is an excited state equilibration.

The kinetics of the LHC II oligomers required 4-5 exponentials for a good fit. In the spectrum of the lamellar aggregates from spinach the main lifetime component is 650 ps whereas the longest component is 1.1 ns with relative amplitude of 26% (at the spectral maximum near 685 nm). The 140 ps component shows an enhanced far-red/red amplitude ratio. The DAS of the LHC II-*npq2* complex revealed a different profile. Instead of one major lifetime component, two lifetimes of 400 and 150 ps have similarly high amplitudes around 685 nm. Only one of them, the 400 ps component, shows a high far-red/red amplitude ratio. Similar to the spinach lamellar aggregates, the longest lifetime was found to be 1.2 ns, but with a much smaller amplitude. The average lifetime is the shortest-lived among all the oligomers, i.e. 284 ps. In LHC II-*npq1* oligomers the main lifetime component is 835 ps with a substantially higher far-red/red amplitude ratio than the other components. The lifetimes and the percentage of their amplitudes are combined in Table 7.2.

Table 7.2: Lifetimes τ_i (ps), relative amplitudes a_i (%), and average lifetimes at 680 nm $\tau_{av\ 680}$ (ps) of the different samples tested.

	τ_1 a_1	τ_2 a_2	τ_3 a_3	τ_4 a_4	τ_5 a_5	$\tau_{av\ 680\ nm}$
w.t. trimers	4.1 ns 84%	1.7 ns 13%	140 ps 3%	7 ps		3.6 ns
<i>npq2</i> trimers	3.5 ns 75%	1.2 ns 9%	240 ps 6%	25 ps 10%	8 ps	2.8 ns
<i>npq1</i> trimers	3.8 ns 86%	0.9 ns 11%	110 ps 4%	8 ps		3.4 ns
w.t. lamellar aggregates	1.1 ns 26%	650 ps 63%	140 ps 11%	5 ps		708 ps
<i>npq2</i> aggregates	1.1 ns 4%	400 ps 39%	150 ps 57%	8 ps		284 ps
<i>npq1</i> aggregates	3.2 ns 3%	835 ps 63%	290 ps 29%	46 ps 5%	3 ps	744 ps

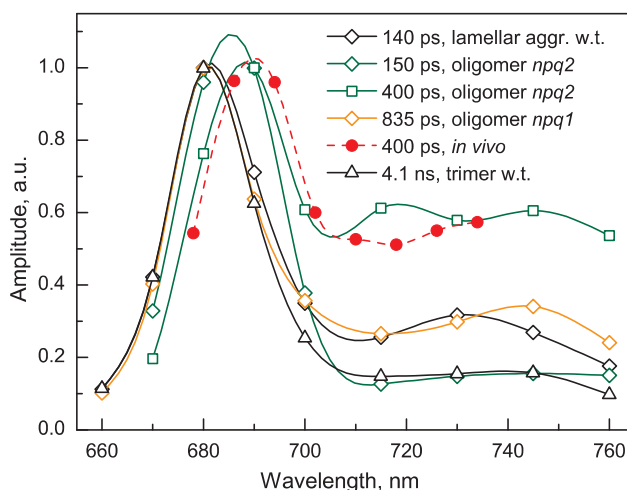


Figure 7.1: Comparison of the DAS of selected lifetime components of various in vitro oligomers and of lamellar aggregates. The spectrum of the 400 ps *in vivo* lifetime component appearing under NPQ conditions in intact *Arabidopsis* leaves is also shown (red circles). Note that the latter spectrum has been corrected for self-absorption in the optically dense plant leaf using a correction function that has been obtained from a comparison of the total fluorescence spectra from the leaf and that of isolated thylakoids from the same plant. All spectra are normalized to the maximum.

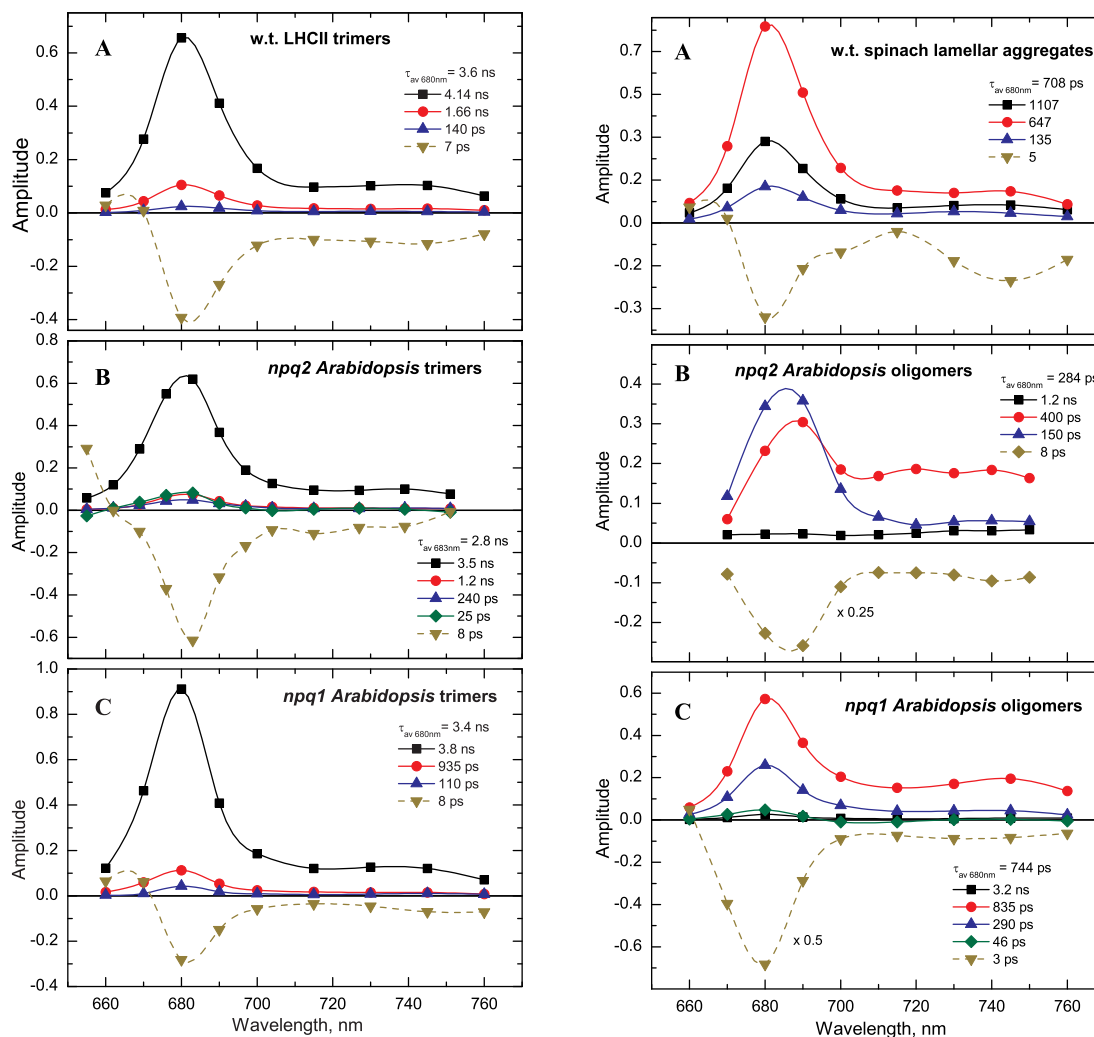


Figure 7.2: DAS obtained from global analysis of the fluorescence decays of LHC II trimers (left panels) and oligomers (right panels) from wild type (A), *npq2* (B) and *npq1* (C) mutants.

Target analysis of the kinetics

A close inspection of the kinetic data from the oligomers reveals that in particular in oligomers of LHC II-*npq1* and LHC II-*npq2* the far-red enhanced fluorescence components are formed within a few tens of ps from some of the lifetime component(s) that have spectra which are more similar to those of the trimeric species. We have thus performed a kinetic model analysis (so-called target analysis, (Holzwarth 1996)) where two emitting species are connected by a reversible process, which could either be an energy transfer process or some other process leading to a new emitting state (*cf.* Figure 7.3).

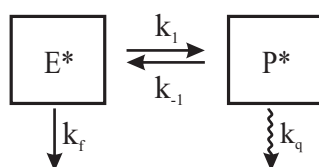


Figure 7.3: Two-state model of the fluorescence kinetics of LHCII oligomers. The rate constants k_1 , k_{-1} , and k_q were determined by global target analysis (*cf.* Table 7.3). The rate constant k_F has been varied parametrically over a range of values from which 0.3-0.4 ns⁻¹ gave the best fitting results. The states E* and P* are proposed to be a Chl-Chl exciton state formed between LHCII trimers and a Chl-Chl charge transfer (CT) state with a dominant excited state character, respectively.

This target analysis allows us to determine the rate constants of the forward and backward reactions, the decay rate of the second state, and the corresponding SAS. Indeed the fluorescence kinetics of the oligomers – except for the small amounts of very long-lived components – could be fitted very well with such a model containing two connected emitting species. If the second species was assumed to be non-emitting in the analysis, no reasonable fit to the data could be obtained. The resulting spectra are shown in Figure 7.4 and the rate constants in Table 7.3.

Table 7.3: Rate constants k_i [ns⁻¹] (*cf.* model in Figure 7.3) and lifetimes τ_i [ps] resulting from the analysis of a homogeneous oligomer model.

	k_1	k_{-1}	k_q	τ_1^*	τ_2	τ_3	τ_4
LHCII- <i>npq1</i> oligomers	47	56	3.0	10	675	220	1200
LHCII- <i>npq2</i> oligomers	16	18	4.8	27	445	180	800

*The two lifetimes indicated in bold in each case are those that result from the two-state model shown in Figure 7.3. The other two lifetimes (indicating components with small amplitudes) are required as additional independent components for a good fit.

We have ignored in this analysis some small amplitude component(s) with lifetimes of a few ps. The two connected emitting states show quite different SAS. The initially excited state has a spectrum that peaks slightly to the red (by 2-5 nm) and is slightly broader than the DAS of the long-lived component in LHC II trimers. This points to the formation of an initial emitting state in the oligomers that is different from the trimers. The far-red fluorescence intensity of this initial component (E*) – as compared to the red fluorescence amplitude – and its spectral shape are quite similar to that of the long-lived (ns) component in LHC II trimers. In contrast the fluorescence spectrum of the product state (P* in Figure 7.3) is further red-shifted in its peak to about 685 nm. The most striking feature is however a very broad and pronounced far-red tail (710-760 nm) that is responsible for the far-red enhanced steady state spectrum of the oligomers (Figure 7.6).

The SAS of the target model are quite similar for the corresponding components of the oligomers of the *npq1* and *npq2* trimers. However, the rate constants of equilibration between the two emitting states as well as the deactivation rate of the P* state differ for the two oligomers.

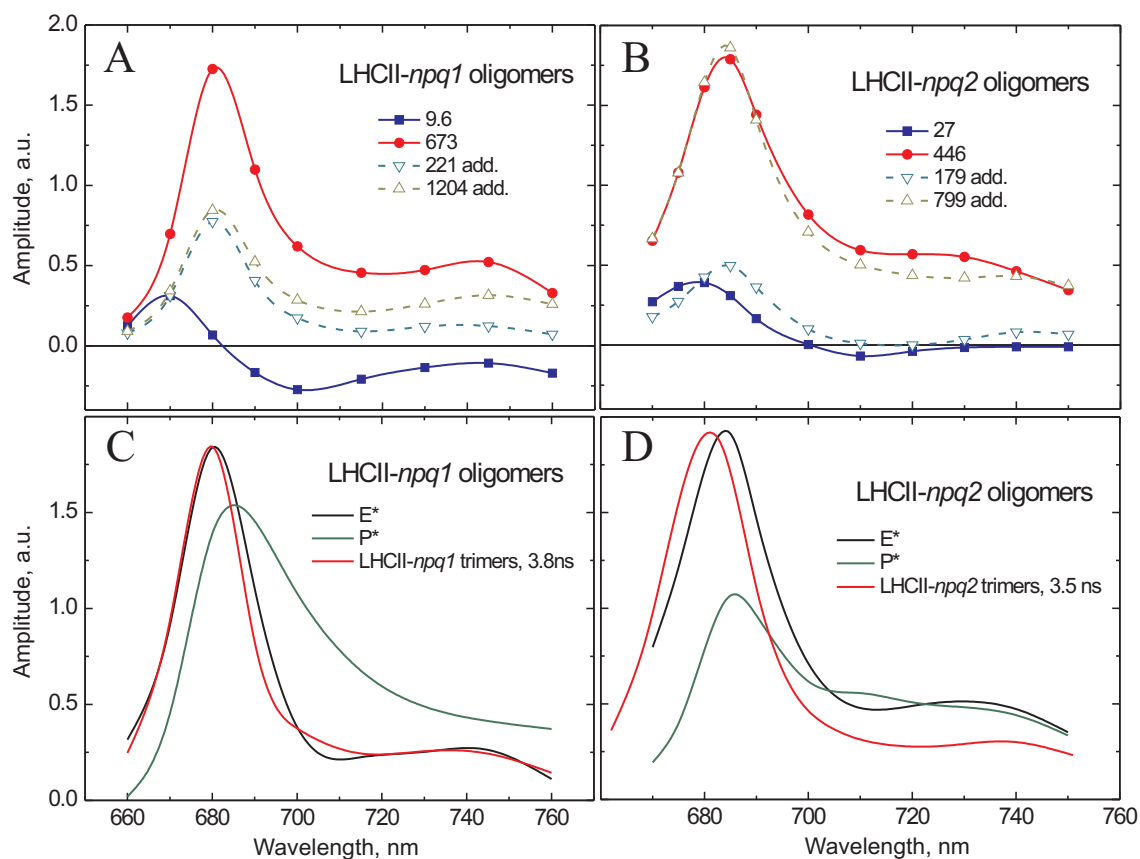


Figure 7.4: DAS (A, B) and SAS (C, D), resulting from a homogeneous CT model for the oligomers (*cf.* Figure 7.2) of *npq1* (A,C) and *npq2* (B,D) LHCII. The DAS of the long (ns) lifetime component of the corresponding LHCII trimers is also shown for comparison in red. In some cases a better fit can be obtained by a heterogeneous model having two exciton and charge-transfer states. The results of such fit are shown for *npq2* in Figure 7.5.

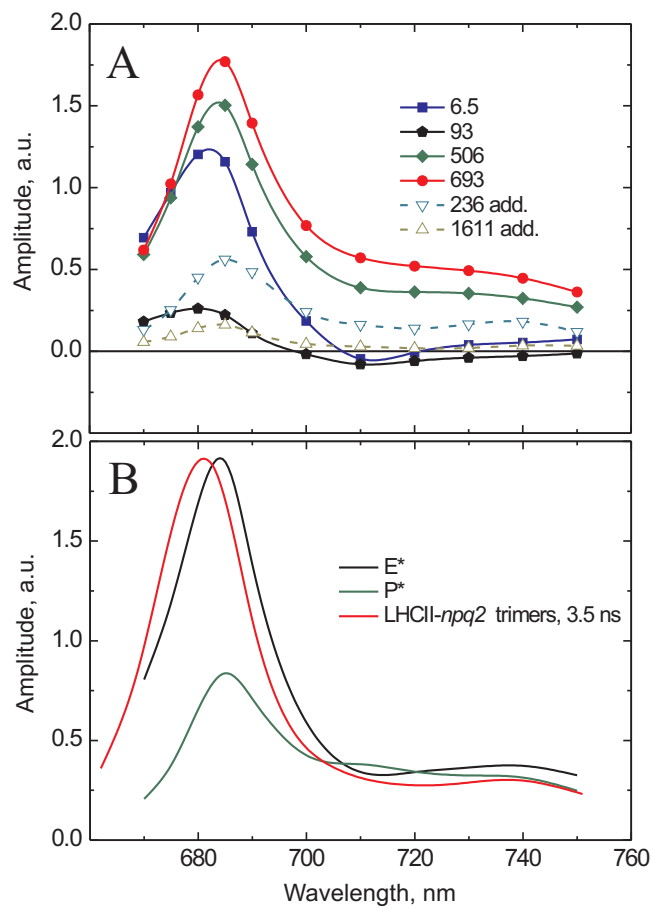


Figure 7.5: DAS (A) and SAS (B), resulting from a heterogeneous CT model for the oligomers of *npq2* LHCII. The DAS of the long (ns) lifetime component of the corresponding LHCII trimers is also shown for comparison in red.

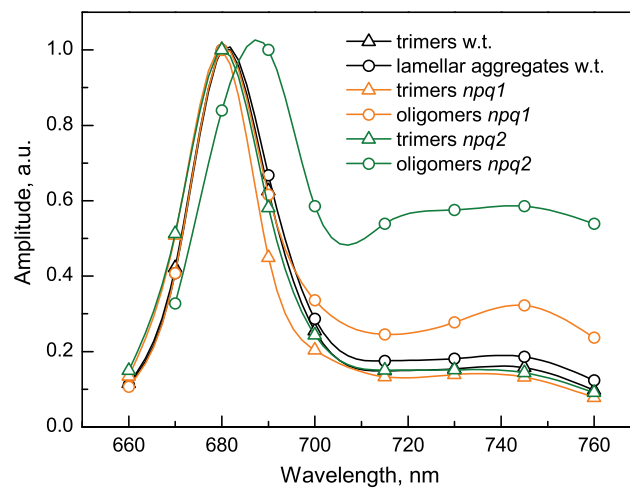


Figure 7.6: Steady state fluorescence spectra of different LHCII trimer and oligomer samples. Spectra are normalized to the maximum

DISCUSSION

We analyze the combined effect of the LHC II aggregation and the Zx presence on the fluorescence lifetime of LHC II. In contrast to previous fluorescence kinetic studies on LHC II complexes, the V1 site, which is supposed to be involved in the NPQ mechanism, is fully occupied. Thus the complexes accommodate Vx and lutein in LHC II-w.t. and LHC II-*npq1*, and Zx and lutein in LHC II-*npq2*, allowing us to directly address the question of the role of Zx bound to its physiologically relevant site (Note that in *npq2* a very small amount of Zx is found additionally in the L1 site (Mozzo et al. 2008)).

At the level of trimeric LHC II the binding of Zx leads to a slight shortening of the long (nanosecond) Chl lifetime. Because in this complex V1 is fully occupied with Zx and a small amount of Zx also binds to L1, this represents the maximal possible effect of Zx in the V1 site. This direct quenching effect of Zx is however much too small to account for the large NPQ observed *in vivo*. We do not exclude that it may enhance slightly the major part of quenching which must be due to a different effect however.

The data on LHC II *in vitro* oligomers confirm that the Chl fluorescence lifetime is drastically quenched after aggregation of the LHC II trimers. It has been reported in several different studies (Ide et al. 1987, Moya et al. 2001, Mullineaux et al. 1993, van Oort et al. 2007) that the longest lifetime of 3 to 4 ns for the trimeric LHC II is reduced to about 1 ns within the oligomers. This is in agreement with our results on the oligomers from *npq1* (which contain no Zx as did all previous LHC II aggregates) and from lamellar aggregates. However the LHC II-*npq2* oligomers containing Zx were more quenched than previously reported aggregates (average lifetime of 280 ps). Furthermore, in our data the major amplitude component(s) in these oligomers have generally shorter lifetimes than in previous studies. However, it should be noted that the mean lifetimes varied slightly between preparations, as well as measurement conditions, e.g. sample concentration (data not shown). Also, a small amount of unquenched trimers could largely affect the mean lifetime. Such variations are well-known for aggregated LHC II preparations. More important than the overall lifetimes/yields in the oligomers are the spectral features of the lifetime components.

As a new feature that has not been reported so far, some short lifetime components in oligomers show a strongly enhanced far-red/red emission ratio (Figure 7.4 and Figure 8.4) as compared to LHC II trimers. This far-red enhancement occurs both in *npq1* and

npq2 mutants, but is most pronounced in *npq2*. A similar far-red fluorescence has also been observed in LHCII crystals (Pascal et al. 2005). It was interpreted as indicating a change in Chl configuration within a trimer in the crystal leading to different emitting species. LHC II has a large fraction of Chls that are located at or close to the surface of the protein (Liu et al. 2004, Standfuss et al. 2005). While we cannot exclude the possibility of a change in the Chl-Chl interaction within a trimer upon oligomerization, we believe that it is much more likely that oligomerization leads to new Chl-Chl interactions among close-lying Chl molecules in different trimers. This is for example clearly the case in the crystals where, depending upon the crystal form, Chl pairs are created with shortest π - π (edge-to-edge) distances of about 6 Å (Liu et al. 2004) and 15 Å (Standfuss et al. 2005). While *in vitro* oligomers are clearly expected to be much less ordered and are likely somewhat heterogeneous in their relative arrangement, it is reasonable to assume that Chl-Chl pairs of similar or even shorter distances as found in crystals can be formed in such oligomers (Note that the decay lifetimes have relatively narrow distributions (Figure 7.7) signifying a small heterogeneity of the oligomers).

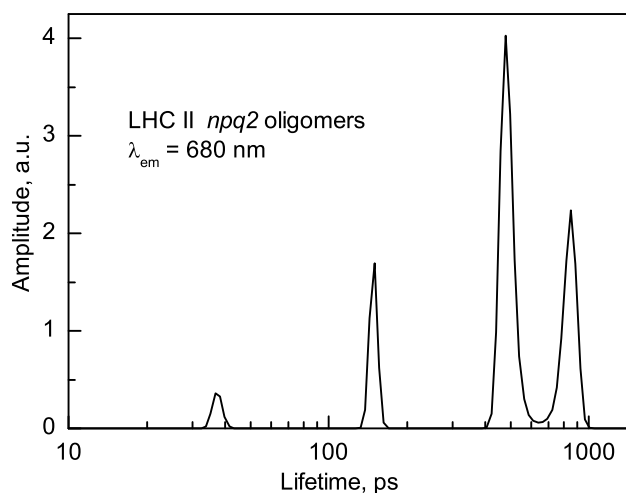


Figure 7.7: Lifetime distribution analysis of the fluorescence kinetics of LHC II-*npq2* oligomers at 680 nm. The analysis was carried out by a home-written program based on an inverse Laplace transform of the kinetic data combined with a Tikhonov regularization (Prokhorenko et al. 2000) using a set of 190 exponentials ranging from 1 ps to 1.5 ns equally spaced on a logarithmic lifetime scale as the basis function.

These new inter-trimer Chl-Chl pairs form weakly coupled exciton states, as is indicated by the slight bathochromic shift and a slight broadening of the short-lived DAS in the oligomers relative to the spectra of the trimers. Such spectral features are typical of Chl-Chl exciton states. However, the very broad and far-red enhanced fluorescence component can not be explained by a Chl-Chl exciton state alone. Strong excitonic coupling in aggregates has been excluded based on the fact that apart from a small (1-2 nm) red shift the

absorption spectrum remains the same as compared to isolated trimers (Naqvi et al. 1997). Even if we assumed formation of strongly-coupled excitonic states, this could not explain the very broad shape of the spectra in the far-red range since excitonic interactions generally lead to spectral narrowing rather than broadening (van Mourik et al. 1991). Rather the broad spectral shape and the far-red enhancement are characteristic of the formation of a charge transfer (CT) state that still maintains a pronounced excited state character, i.e. the charge is – on average – only partially translocated from the donor to the acceptor Chl. In contrast, formation of a complete radical pair state can be confidently ruled out since Chl radicals are non-fluorescent quenchers and would thus not be detected as emitting species in the time-resolved spectra. However our analysis shows clearly an emissive state, albeit with lower oscillator strength (this can be estimated from the area under the SAS) than a typical Chl excited state, pointing to its mixed exciton/CT state character.

Mixing of CT states with Chl-Chl exciton states leads to a drastic change in their spectroscopic properties including a large Stokes shift, very strong broadening, and strong vibrational tails (Ihalainen et al. 2003, Lyle et al. 1993, Renger 2004). All these effects are due to the very strong electron-phonon-coupling of these states. Such effects have been observed earlier and were shown originate from bacteriochlorophyll (BChl) and Chl excited states having strong CT character in BChl and Chl excited states in bacterial antenna systems, PSI cores from cyanobacteria (Frese et al. 2002, Palsson et al. 1996, Rätsep et al. 2000) and in LHCI (Croce et al. 2007, Ihalainen et al. 2003, Ihalainen et al. 2005a). In fact the so-called “red chlorophylls” in the PSI antenna that were proven to have strong CT character, share striking common spectroscopic features with the far-red emission spectra of the LHCII oligomers. The extremely low efficiency of hole-burning of these Chls (Ihalainen et al. 2003) has been related to the large electron-phonon coupling (Lyle et al. 1993). Interestingly, in a hole-burning study of LHCII oligomers, Pieper et al. (1999) have suggested that the low hole-burning efficiency beyond 683 nm has the same origin, i.e. strong electron-phonon coupling due to charge-transfer state character.

A comparison of the 77K fluorescence spectra of LHC II trimers and oligomers shows two new bands relative to the 682 nm fluorescence of LHCII trimers (Figure 7.8): i) the exciton emission band located at 683-684 nm and ii) the very broad far-red fluorescence peaking at 701 nm. According to the Gaussian fits of the spectra (shown as dotted curves in Figure 7.8, the bandwidth of the first component is similar to that in isolated trimers – 200 cm^{-1} – whereas the second component, which reflects the mixed exciton/charge-transfer state emission, has a bandwidth of about 600 cm^{-1} and a long tail extending to

the far-red. Detailed comparison reveals that this bandwidth is even larger than the width of the “red LHC I Chls” of 400 cm^{-1} (Croce et al. 2007). Although part of the extreme broadening may be due to inhomogeneous broadening, i.e. a heterogeneity in the spectra, this could clearly not explain the full extent of the broadening. Thus this extremely broad low temperature spectrum provides the strongest and clearest evidence that this state has CT character. The broad fluorescence component distinctly appears in LHCII with or without zeaxanthin – both at room temperature and at low temperature – but it is most pronounced in zeaxanthin-containing samples (*npq2*), possibly because zeaxanthin favours particular LHCII interactions.

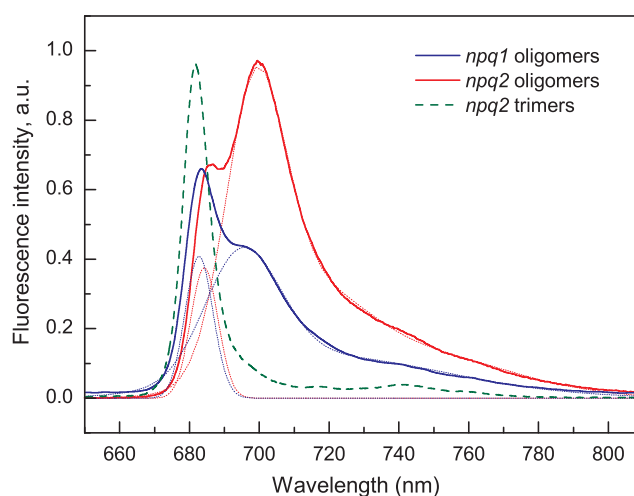


Figure 7.8: 77K fluorescence emission spectra of the trimeric *npq2*-LHC II complex and of the corresponding oligomers. Note the formation of two new emission bands upon oligomerization vs. the single 681 nm emission peak of the trimer.

The emissive character of the CT state implies a relatively moderate coupling of the Chl pairs (probably in the order of a few tens of cm^{-1}) and also a not very pronounced asymmetry between the two Chl components. This CT state is formed within 10 ps (*npq1* oligomers) or 27 ps (*npq2* oligomers) from the initial Chl-Chl exciton state at room temperature and the two states are in equilibrium with each other, implying that the energy of the CT state is in the vicinity of the exciton state energy. The CT state itself is strongly quenched with decay rates between 3 and 5 ns^{-1} (*cf.* Table 7.3). Fluorescence data alone cannot provide the final fate of the CT state. The quenching could be caused either by a pronounced coupling of the CT state to the ground state, a situation that would be quite typical for CT states, or it could be quenched by energy transfer to another low-lying state.

The far-red enhanced fluorescence of the LHCII oligomers *in vitro* derives from the emitting CT state which is the lowest energy emitting state in the system. It is striking that a nearly identical emission spectrum and lifetime (ca. 400 ps) are observed *in vivo* under NPQ conditions (Figure 7.1, Figure 8.4) as is found in the *npq2*-LHCII oligomers. Its lifetime and spectral shape differ pronouncedly from the properties of any other known higher plant antenna complex (Holzwarth 2004). We note that Gilmore et al. also resolved a ~400 ps component appearing under NPQ conditions in spinach thylakoids but did not resolve it spectrally (Gilmore et al. 1995). As this component is only present in quenching conditions, we can clearly correlate it with the formation of a new state characteristic for NPQ. We thus propose that the far-red-enhanced 400 ps fluorescence *in vivo* under NPQ conditions reflects the formation of a LHCII oligomer giving rise to an emitting CT state. This CT state plays a crucial role in the NPQ process either as a direct quencher or as a quenching intermediate. Our data suggest that Zx has a supporting effect on the formation of the quenched oligomeric state but is not strictly required. It has been shown earlier that Zx can stimulate the formation of LHCII oligomers whereas Vx functions as an inhibitor for oligomerization (Ruban et al. 1997).

NON-PHOTOCHEMICAL QUENCHING IN INTACT PLANT LEAVES

In conventional (steady-state) Chl fluorescence methods NPQ can be detected by irradiating dark-adapted leaves with high light intensity and following the fluorescence induction. NPQ is then defined as the decrease of the fluorescence of closed PS II reaction centres after a certain period of illumination. The most commonly used parameters relevant for studying NPQ are derived from the fluorescence yields registered at three different states: F_0 – fluorescence of dark-adapted leaves, where non-photochemical quenching is assumed to be zero and the PS II reaction centres are open; F_{\max} – maximal fluorescence registered after a short pulse of light, strong enough to close the PS II RCs but short enough to prevent build-up of NPQ; F_{\max}' (F_{NPQ}) – fluorescence of leaves after induction of NPQ and closure of the PS II RCs.

We designed a setup in which time-resolved fluorescence could be registered directly from intact leaves in these three conditions (see Materials and Methods). Comparing the fluorescence decays from open and closed RCs, on the one hand, and from leaves before and after induction of NPQ, on the other hand, allow us to identify and localize fluorescence components responsible for the photochemical and non-photochemical quenching separately. We used leaves of *Arabidopsis thaliana* plants of wild type and other genotypes in which parts of the machinery regulating the NPQ process are disabled: the *npq4* (*psbs-1.3*) mutant, which lacks the PsbS protein; the *L17* mutant which overexpresses PsbS (Li et al. 2002a); and the *npq1* mutant, which is deficient in the violaxanthin de-epoxidase and cannot accumulate Zx in high light (Niyogi et al. 1998). Thus we attempted to distinguish between the roles of Zx and PsbS in the components of NPQ.

RESULTS

Fluorescence decays in quenched and unquenched conditions

Figure 8.1 shows the Chl fluorescence decays of intact leaves of the four genotypes measured at 686 nm in the three conditions: F_0 (dark-adapted leaves with open RCs); F_{\max} (dark-adapted (unquenched) leaves with closed RCs); and F_{NPQ} (high-light-adapted (quenched) leaves with closed RCs). While all genotypes showed very similar kinetics in the dark-adapted states, the situation was quite different under F_{NPQ} conditions: The *PsbS* overexpressor (*L17*) showed the fastest decaying fluorescence (and thus the strongest quenching), faster than w.t., and the other two mutants exhibited substantially longer decays, i.e. less quenching.

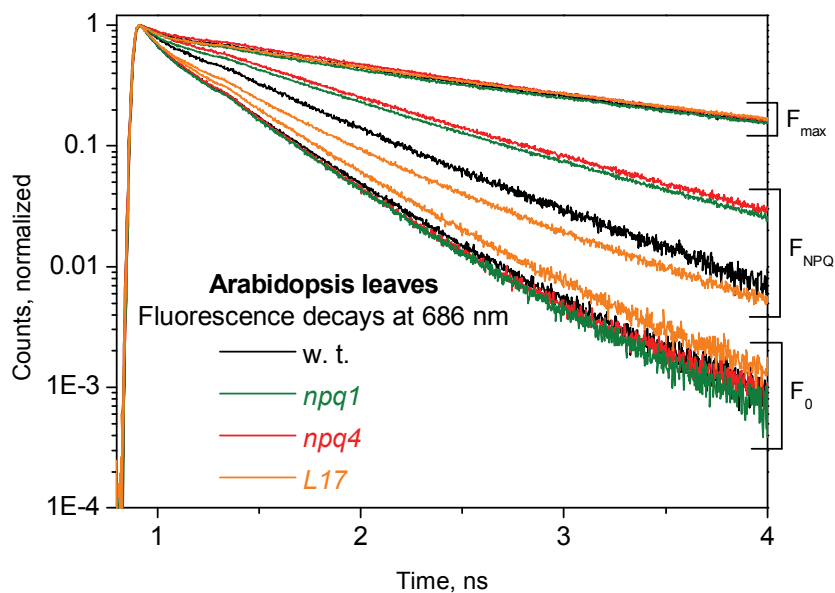


Figure 8.1: Fluorescence decays of wild-type and mutant plants. Comparison of normalized fluorescence decays (on a semilogarithmic scale) at 686 nm for high-light-adapted leaves from wild-type (w.t.), *L17*, *npq4*, and *npq1* mutant plants of *Arabidopsis* at F_{NPQ} (PS II RCs closed by light) conditions and at dark-adapted F_0 and F_{\max} conditions.

Since the average fluorescence lifetime τ_{av} is proportional to the fluorescence yield in the various states (Holzwarth 1988), we can calculate from the fluorescence decays the *NPQ* value, defined as

$$NPQ = F_{\max} / F'_{\max} - 1 = \tau_{\text{av}} / \tau'_{\text{av}} - 1$$

which is typically used to characterize the quenching capacity of a plant (Krause and Jahns 2004). Comparison of the calculated NPQ values confirms that the quenching was most pronounced in *L17* and w.t., followed by *npq4* and *npq1*. The NPQ properties found from the fluorescence lifetime measurements (Table 8.1) are thus in good agreement with the behaviour of w.t. and mutants found from steady state measurements of F_{NPQ} (Li et al. 2002a) and with fluorescence induction measurements done with a PAM fluorometer (Figure 8.2). The F_{max}/F_0 ratio describing the fluorescence intensity ratio of closed to open PS II RCs is over 5, thus proving that the F_{max} condition is really reached.

Table 8.1: Average lifetime τ_{av} [ps] of the fluorescence decays measured under the indicated conditions at 686 nm emission wavelength (excitation at 663 nm). The errors in the average lifetimes are <10 %. NPQ values were calculated from the fluorescence decays at 686 nm.

	w.t.	<i>npq4</i>	<i>npq1</i>	<i>L17</i>
τ_{av} at 686 nm, ps				
F_0	210	189	204	202
F_{NPQ}	408	498	578	245
F_{max}	1116	1061	1072	1050
NPQ	1.7	1.1	0.9	3.3
F_{max}/F_0	5.3	5.6	5.3	5.2

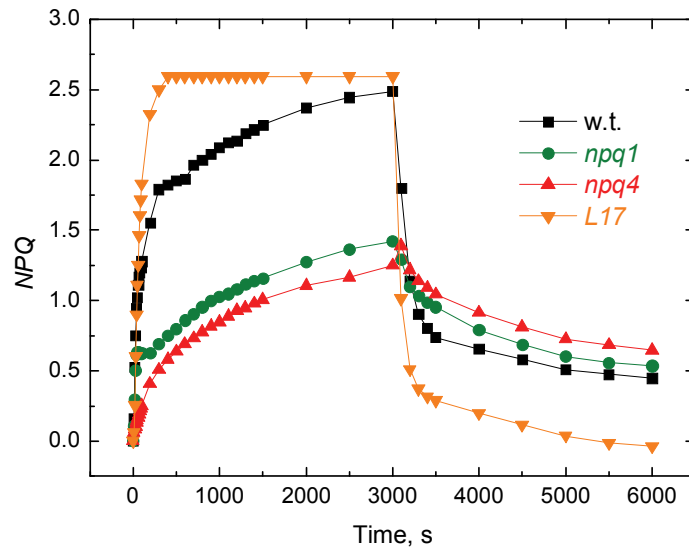


Figure 8.2: Measurement of the NPQ amount with a PAM at 20 °C. The leaves were illuminated for 50 min with $1000 \mu\text{mol photons m}^{-2}\text{s}^{-1}$ and dark-adapted for another 50 min to follow the relaxation.

Global target analysis and component separation

The fluorescence measurements were performed over the whole range of Chl fluorescence from 678 to 734 nm. Chl fluorescence originating from PS I and PS II overlaps in this range. However their lifetimes and spectral shapes differ, depending on the origin of the fluorescence (PS I or PS II, separated antenna etc.) and the state of the PS II RC (open vs. closed RCs), etc. (Holzwarth 1988, Holzwarth 1991). In addition the fluorescence kinetics also depends critically on the state of the light-adaptation and the associated reorganization of the thylakoid membrane. While the entire organization of the Chl proteins in the thylakoid membrane and the state of the RCs are reflected in the overall fluorescence kinetics, the extraction of the relevant parameters of the multi-exponential fluorescence of an entire leaf presents some difficulty. Separation of the fluorescence components deriving from PS I and PS II, and the determination of the quenching parameters in the various states is however possible by global target analysis of the fluorescence kinetics, provided that high signal-to-noise data are available over a wide wavelength range and provided the components differ in their spectral shapes and lifetimes (Holzwarth 1996).

In order to perform the target analysis we make use of the detailed knowledge that has been gained recently from kinetic studies of the isolated antenna/RC complexes (Broess et al. 2006, Holzwarth et al. 2005, Holzwarth et al. 2006a, Holzwarth et al. 2006b, Holzwarth 2008, Ihalainen et al. 2005b, Ihalainen et al. 2005a, Miloslavina et al. 2006, Slavov et al. 2008). These studies defined the principal kinetic reaction schemes underlying the fluorescence kinetics of PS I and PS II. Following these results, the target analysis of the fluorescence kinetics of the *A. thaliana* leaves was performed using the kinetic schemes shown in Figure 8.3.

In addition to the reaction schemes for PS I and PS II, which yield four and three lifetimes, respectively, additional lifetime components were added in the analysis if necessary. These procedures, performed for the data from F_{NPQ} and F_{max} conditions, allowed us to dissect the fluorescence kinetics into its contributions deriving from PS I and PS II, and to resolve the emergence of novel lifetime and spectral components appearing under high-light-adaptation conditions.

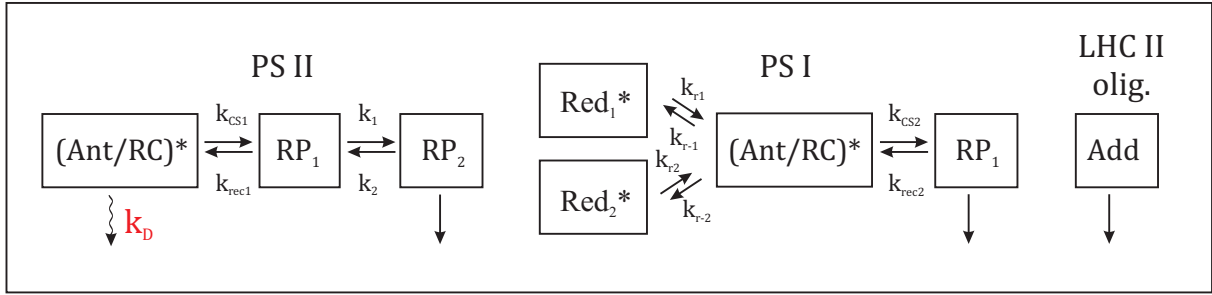


Figure 8.3: Kinetic schemes for PS I and PS II used in the global target analysis of the fluorescence decays from *A. thaliana* leaves. Where necessary additional single lifetime components were allowed in the analysis (see e.g. Figure 8.4 A and C) to represent newly appearing components that could not be fitted within the pure PS I and PS II schemes. Such component(s) are needed to describe the functionally detached LHC II oligomers. k_{CS} – rate constant of charge separation reaction, k_{rec} – rate constant of charge recombination, k_D – rate constant for energy dissipation by non-photochemical quenching.

The rate constants of the analysis are shown in Table 8.2. The k_3 rate was kept fixed to 0.9 ns^{-1} . This values were found according to our previous measurements on PS II core particles (Miloslavina et al. 2006), BBYs (Chapter 6), data on closed PS II particles (Szczepaniak et al. 2008) and the data on PS I particles (Slavov et al. 2008). Here we do not make a detailed comparison of all rates, since they reflect the photochemical energy dissipation. The rate constants associated with the PS I compartments are not expected to change considerably with illumination as it has a secondary role in NPQ after PS II and LHC II. The important rate constants that are directly connected to NPQ are k_D and the rate of decay of the additional compartment. Hence, these two rates are discussed in details further.

Table 8.2: Rate constants (ns^{-1}) resulted from the model presented in Figure 8.3 for F_{\max} and F_{NPQ} conditions for w.t. and *npq1*, *npq2*, *L17* mutants.

	PS II					PS I						add			
	k_D	k_{CS}	k_{-CS}	k_1	k_2	k_3	k_{r1}	k_{-r1}	k_{r2}	k_{-r2}	k_{CS}	k_{-CS}	k_4		
F_{\max}	w.t.	0.4	2.9	8.6	2.1	0.5	0.9	47	83	12	14	255	156	47	-
	<i>npq1</i>	0.5	2.2	9.8	2.4	1.1	0.9	55	38	13	24	173	151	101	-
	<i>npq4</i>	0.3	2.5	16.4	4.5	0.6	0.9	54	18	11	20	184	106	93	-
	<i>L17</i>	0.3	3.4	10.0	2.4	0.5	0.9	52	42	19	78	238	143	81	-
F_{NPQ}	w.t.	1.7	2.1	22.4	3.7	2.0	0.9	38	13	14	39	295	136	95.9	2.3
	<i>npq1</i>	0.5	2.4	17.3	6.2	0.5	0.9	19	44	10	28	257	122	109	1.5
	<i>npq4</i>	1.3	1.0	22.4	5.5	1.4	0.9	30	7	13	25	189	85	63	-
	<i>L17</i>	1.6	0.9	15.1	2.5	0.8	0.9	69	13	21	45	262	247	103	3.4

The rate constant k_D is the effective non-radiative and non-photochemical deactivation rate and thus a direct measure of NPQ in the PS II-attached antenna. In an unquenched PS II this rate is only 0.3-0.5 ns⁻¹, and reflects the natural non-radiative decay rate of the antenna Chls. This basic k_D was increased in high light by specific non-photochemical quenching processes about four-fold for the w.t, *L17* and the *npq4* mutant. No increase in k_D was observed for the *npq1* mutant, despite the about 20% decrease in the average lifetime of PS II (Table 8.3). Therefore this lifetime decrease can be accounted for entirely by a decrease in the antenna size of PS II under F_{NPQ} conditions. The PS II attached antenna is not quenched in the *npq1* mutant in high light.

Table 8.3: Average lifetime, τ_{av} [ps] of PS II components and of the additional compartment assigned to quenched LHC II oligomers and fraction the additional compartment amplitude relative to the total PS II fluorescence for the four *Arabidopsis* genotypes studied.

	w.t.	<i>npq4</i>	<i>npq1</i>	<i>L17</i>
τ_{av} of PS II, ps				
F_0	328	300	327	341
F_{NPQ}	559	746	1059	615
F_{max}	1282	1484	1309	1325
τ of quenched LHC II oligomers, ps	430	-	689	296
% of detached LHC II	30	-	70	52

The spectra of the different lifetime components are shown in Figure 8.4 and Figure 8.5 for the quenched (F_{NPQ}) and unquenched (F_{max}) conditions, respectively. The components corresponding to PS I and PS II as assigned by their association with the kinetic schemes shown in Figure 8.3 were present in all genotypes under all conditions. Only under F_{NPQ} conditions an additional fluorescence component (red curves in Figure 8.4) was observed, which was not present in dark-adapted leaves (neither at F_0 nor at F_{max}) and which could not be described within the PS I or the PS II kinetic schemes. This component (w.t. 430 ps, *npq1* 689 ps, *L17* 296 ps) had strongly enhanced far-red spectral emission and a maximum that was red-shifted by >5nm as compared to the regular PS II emission (Figure 8.4). No such component is present in the *npq4* mutant leaves. Its peak amplitude relative to the sum of all PS II components is 30% for w.t., 52% for *L17* and 70% for *npq1*.

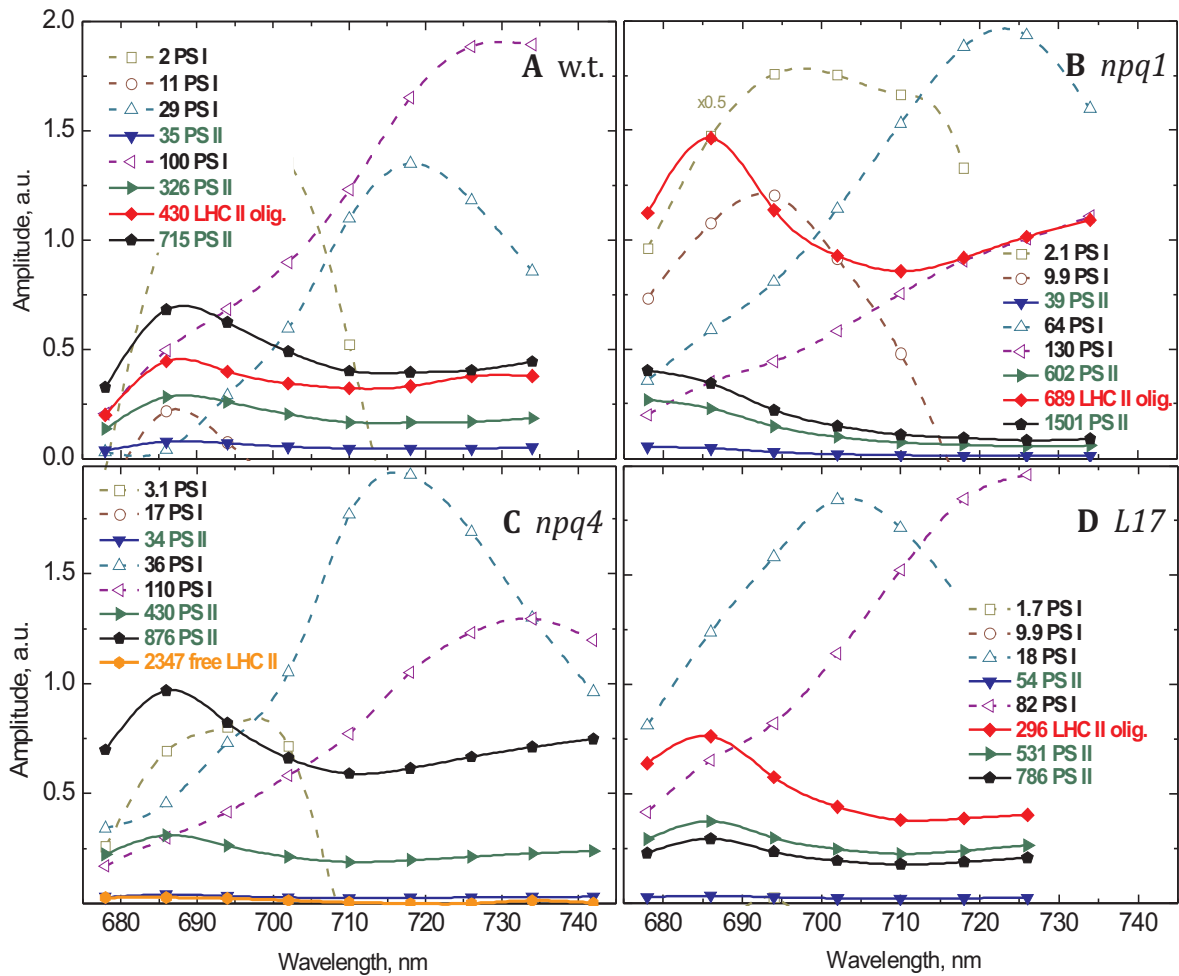


Figure 8.4: Fluorescence lifetime components of high-light-adapted plants (F_{NPQ}). DAS (Holzwarth 1996) are obtained from global target analysis of the fluorescence decays of leaves from wild-type (w.t.; A), *npq1* (B), *npq4* (C) and *L17* (D) plants under high-light-adapted (F_{NPQ}) conditions. Note that the two fastest lifetimes have negative amplitudes over most of the spectrum. Both of these components derive from PS I. Since PS I is not relevant for the present discussion only the positive amplitudes are shown for clarity of presentation.

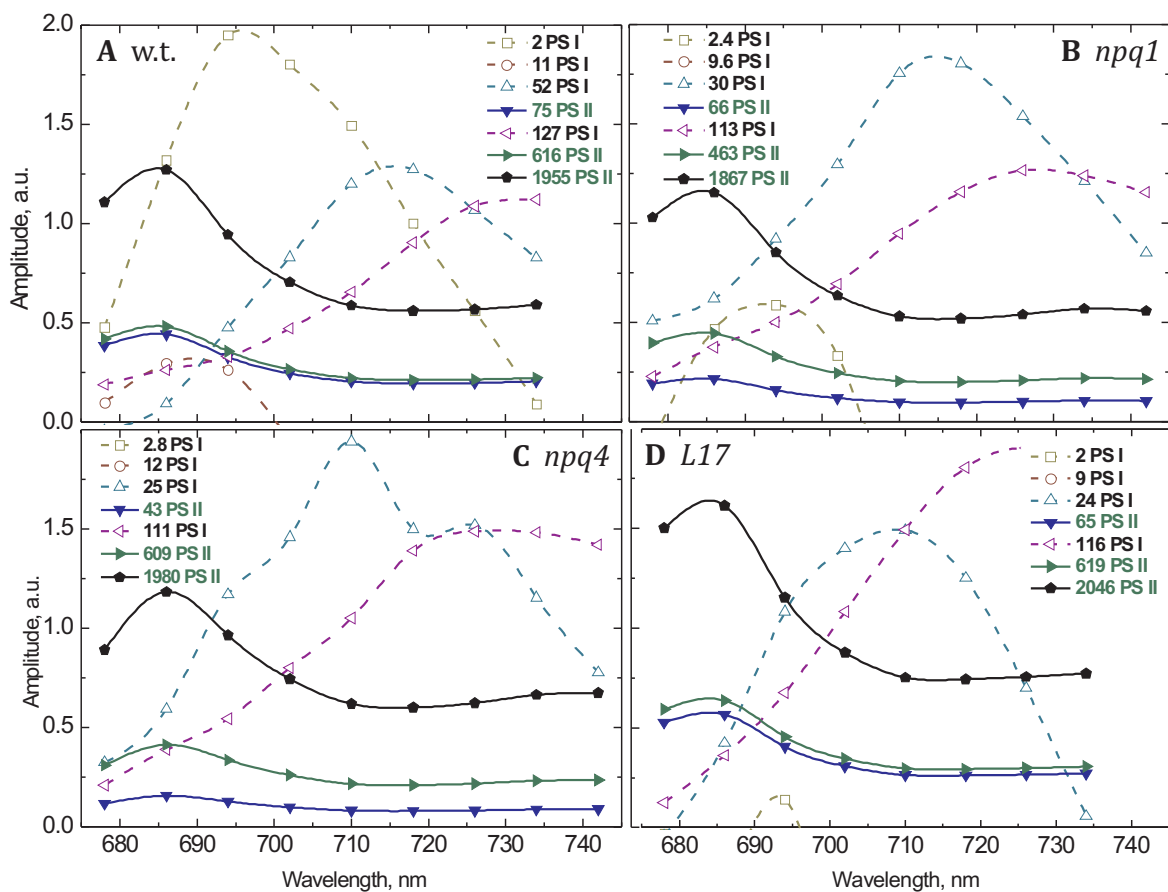


Figure 8.5: Fluorescence lifetime components of dark-adapted plants. DAS as obtained from global target analysis of the fluorescence decays of leaves from dark-adapted DCMU-incubated w.t. plants (A), *npq1* (B) and *npq4* (C) and *L17* (D) mutants under F_{\max} conditions (closed PS II RCs).

Evidence for the necessity of the additional component

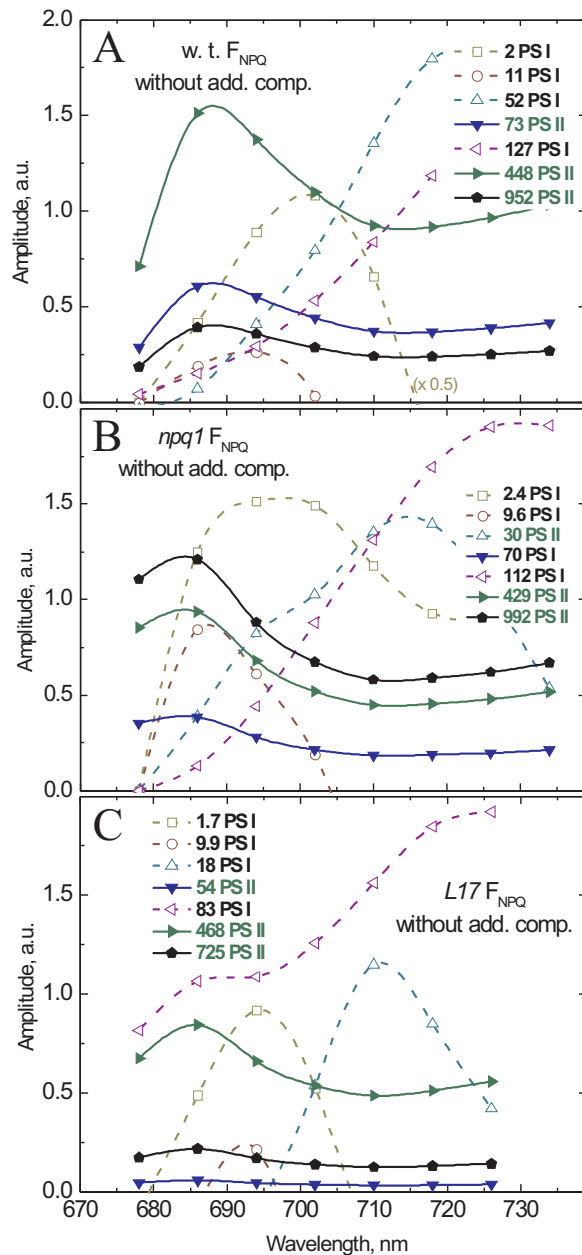
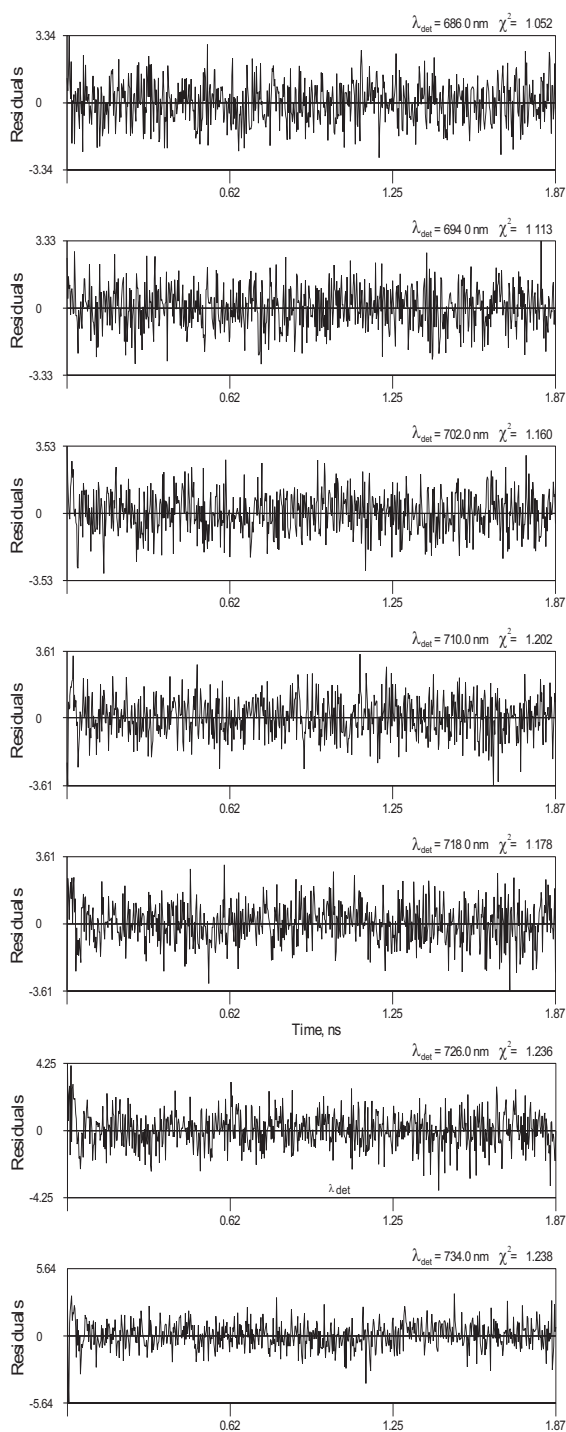


Figure 8.6: Recalculated DAS resulting from target analysis fitting of the F_{NPQ} data with the kinetic scheme that did not include additional component (detached FCP oligomers). A: wild type *Arabidopsis*, B: *npq1* mutant.

In order to check additionally the real necessity of the additional component (detached LHC II oligomers) in the target analysis of the F_{NPQ} data for *Arabidopsis* w.t. and mutants, the fit was performed also without the additional component. It included only seven compartments – three for PS II and four for PS I. For better comparison all rates were fixed to the ones resulted from the analysis of the decays in F_{max} conditions except for k_D , which was allowed to be free. The resulted DAS for w.t., *npq1*, and *L17* in Figure 8.6. The residuals of these fits are compared with those achieved from the normal fits with additional component (Figure 8.7, Figure 8.8, and Figure 8.9 for w.t., *npq1* and *L17* respectively). In all cases the fit excluding the additional component was poorer considering the deviating residuals, and unrealistic DAS (e.g. the high PS II emission of in the red region) and rate constants. Therefore the addition of the unconnected component in the analysis is justified.

w.t. with detached LHC II antenna

global $\chi^2 = 1.158$ 

w.t. without detached LHC II antenna

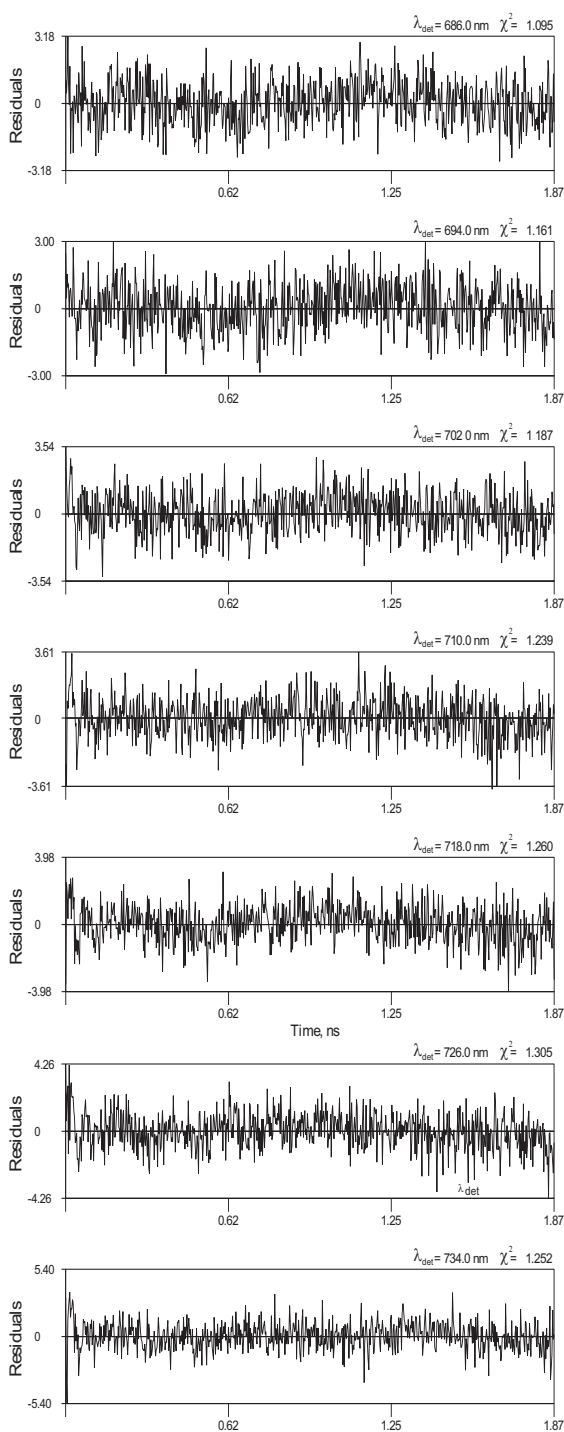
global $\chi^2 = 1.220$ 

Figure 8.7: Residuals of the fits received from target analysis of w.t. at F_{NPQ} state. Left: the fit including additional component functionally disconnected from either PS I and PS II, reflecting detached FCP oligomers. Right: the fit without additional component. It was obtained by fixing the rate constants to the solution from Fmax analysis and leaving the k_D free running.

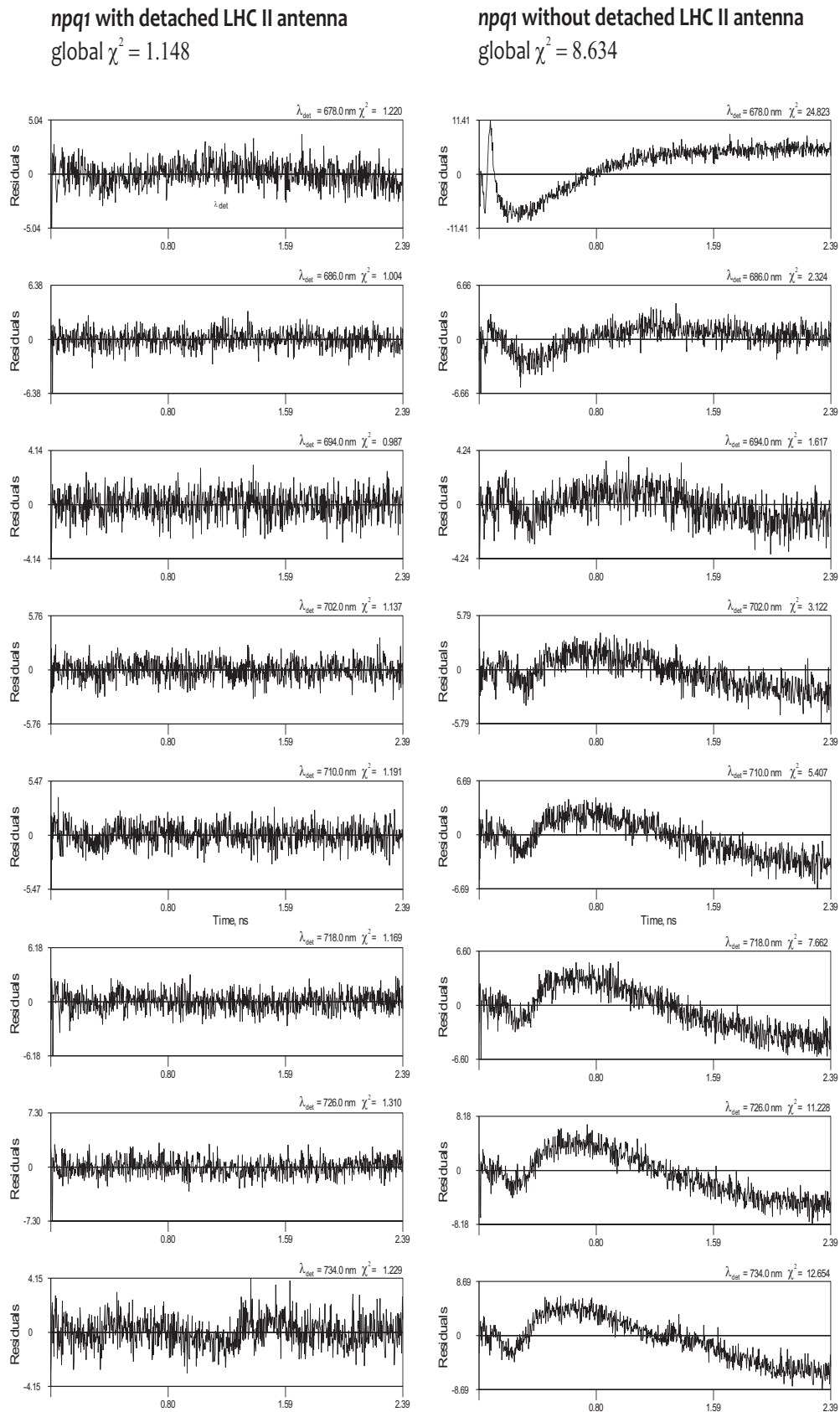


Figure 8.8: Residuals of the fits received from target analysis of *npq1* at F_{NPQ} state. Left: the fit including additional component functionally disconnected from either PS I and PS II, reflecting detached FCP oligomers. Right: the fit without additional component. It was obtained by fixing the rate constants to the solution from Fmax analysis and leaving the k_D free running.

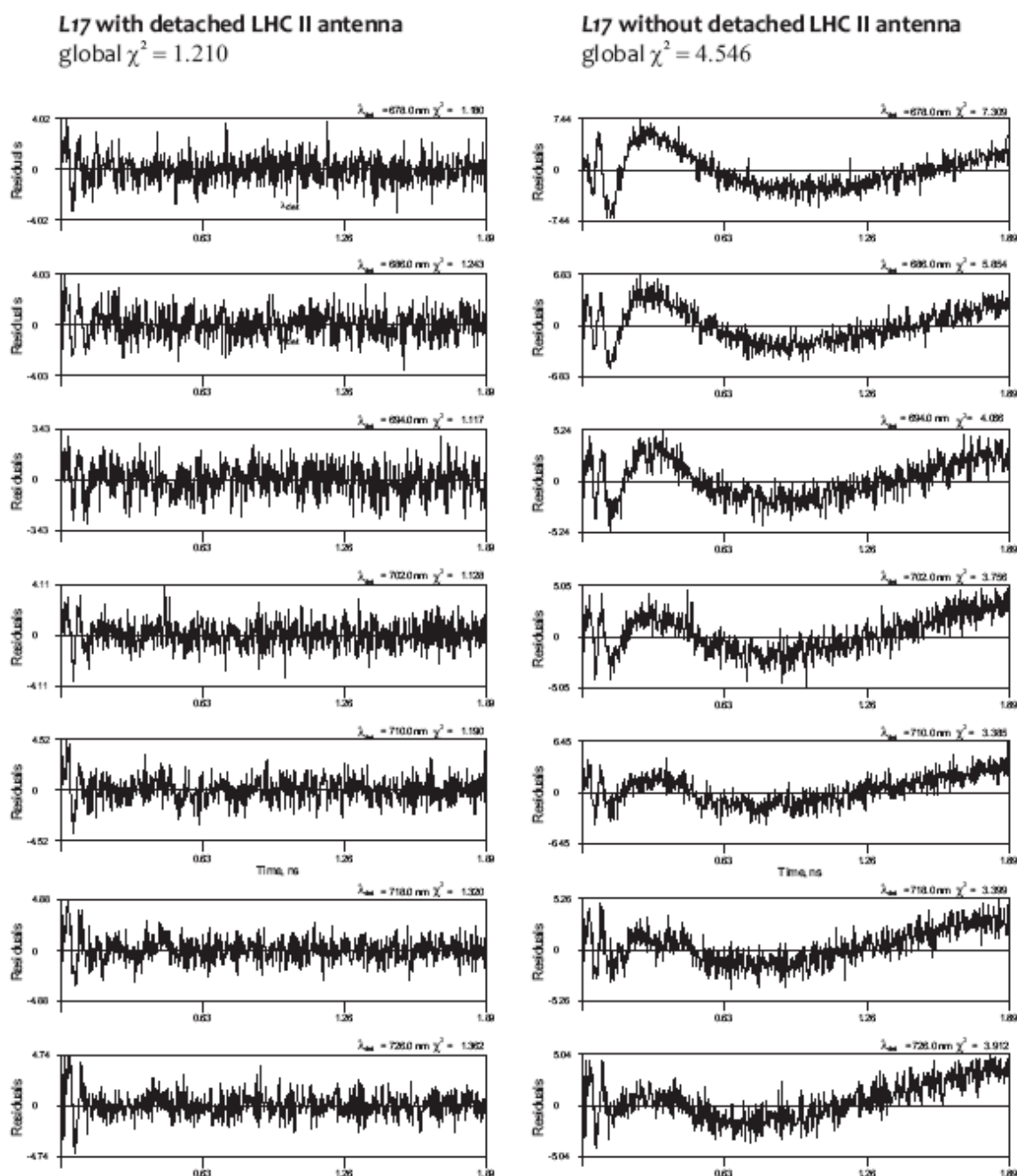


Figure 8.9: Residuals of the fits received from target analysis of *L17* at F_{NPQ} state. Left: the fit including additional component functionally disconnected from either PS I and PS II, reflecting detached FCP oligomers. Right: the fit without additional component. It was obtained by fixing the rate constants to the solution from Fmax analysis and leaving the k_D free running.

Pigment content

The effect of the irradiation used to generate NPQ on the pigment composition of the leaves was estimated by making pigment extracts from the leaves directly after measuring the fluorescence kinetics and determining their content by HPLC. The results are presented in Table 8.4 for *w.t.*, *L17*, *npq1* and *npq4*. Dark-adapted leaves were kept in

the dark for at least 10 h (F_{\max} conditions). Light-adapted leaves were illuminated for 2 h at a light-intensity of $600 \mu\text{mol m}^{-2} \text{s}^{-1}$ (F_{NPQ} conditions). All genotypes contained similar amounts of Chl *b*, Nx, Lut, β -Car, and total XC pigments, (VAZ), relative to Chl *a*. This stoichiometry was not altered by the used illumination conditions. However, upon illumination the de-epoxidation state of the VAZ pool increased from virtually zero to 60% in w.t., *L17* and *npq4* mutants. As expected, no light-induced de-epoxidation was detected in the *npq1* mutant.

Table 8.4: Pigment composition of dark-adapted and light-adapted leaves from wild-type, *L17*, *npq4*, and *npq1* plants. Nx, neoxanthin; VAZ, xanthophyll cycle pigments (violaxanthin + antheraxanthin + zeaxanthin); Lut, lutein; β -Car, β -carotene; DES, de-epoxidation state of xanthophyll cycle pigments = (zeaxanthin + 0.5 antheraxanthin) / (VAZ). Mean values \pm SD are shown.

Leaf pigments	<i>wild type</i>		<i>L17(psbsOE)</i>		<i>npq4 (psbs-1.3)</i>		<i>npq1</i>	
	dark-adapted	light-adapted	dark-adapted	light-adapted	dark-adapted	light-adapted	dark-adapted	light-adapted
Nx	33 \pm 1	34 \pm 1	33 \pm 1	33 \pm 1	33 \pm 1	34 \pm 1	34	32
VAZ	29 \pm 2	31 \pm 2	23 \pm 2	27 \pm 1	28 \pm 2	30 \pm 2	28	28
Lut	109 \pm 6	115 \pm 2	113 \pm 2	120 \pm 2	109 \pm 4	117 \pm 2	123	125
β-Car	79 \pm 5	82 \pm 1	71 \pm 4	73 \pm 6	81 \pm 4	82 \pm 4	95	93
Chl <i>a/b</i>	3.39 \pm 0.10	3.33 \pm 0.10	3.21 \pm 0.13	3.07 \pm 0.17	3.34 \pm 0.07	3.35 \pm 0.03	3.24	3.1
DEPS	0.02 \pm 0.01	0.64 \pm 0.03	0.02 \pm 0.00	0.61 \pm 0.01	0.02 \pm 0.01	0.64 \pm 0.02	0.054	0.038

DISCUSSION

Origin and differentiation of the fluorescence components

Comparison of the time-resolved fluorescence spectra measured in dark and light conditions revealed that induction of NPQ is associated with the appearance of a new red-shifted fluorescence component. We can exclude that this component originates from PS I, since the two fluorescence components related to red PS I Chls are resolved in all genotypes and remain unchanged for the various light conditions. Several observations allow us to conclude that it derives from an antenna complex that became functionally detached from PS II:

- the amplitude of PS II components decreases when the new red-shifted fluorescence appears implying a decrease in PS II antenna cross-section by a functional detachment of part of the antenna complexes
- the lifetimes of this red-shifted component do not respond to the opening or closing of the PS II RCs
- this component can neither be described within the PS II nor the PS I kinetic schemes but represents a separate and independently fluorescing entity which shows a strongly enhanced fluorescence intensity above 700 nm as compared to the typical PS II or LHC II fluorescence

While for w.t., *L17* and *npq1* upon high-light adaptation we observe a strong decrease in the relative amplitude of the PS II components and the concomitant appearance of this new fluorescing component, this was not observed for *npq4*. We thus assign the newly appearing red-shifted fluorescence under F_{NPQ} conditions to part of the major LHC II antenna (~50%) that is functionally detached from both photosystems. The associated fluorescence spectrum (Figure 8.4 A and Figure 8.4 C) is however not typical for an isolated LHC II trimer, but is reminiscent of the strongly red-enhanced fluorescence of oligomerized LHC II that is highly quenched (Figure 8.10).

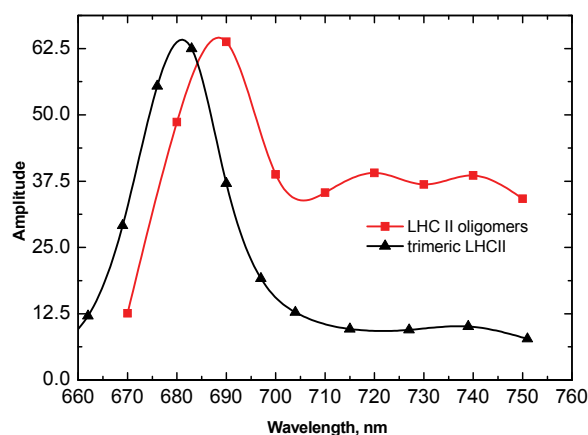


Figure 8.10: Fluorescence spectra of the main fluorescence lifetime components of isolated LHC II trimers and *in vitro* oligomers of LHC II trimers (normalized to the maximum). Note the strong enhancement in red fluorescence intensity in the oligomers.

The formation of this detached LHC II oligomers fluorescence strictly requires the presence of the PsbS protein. In its absence (*npq4* mutant) no such red-shifted fluorescence appears and the PS II antenna size, as measured by the combined amplitude of the PS II components, does not decrease upon high-light adaptation. The overexpression of PsbS

protein increases the LHC II detachment and oligomerization (judging by the shape of the component), the lifetime of it is most quenched (296 ps). Notably the excited state of these LHC II oligomers is strongly quenched even in the absence of Zx (689 ps lifetime vs. a ca. 4 ns lifetime for trimeric LHC II (see Chapter 7). Thus Zx is not obligatory for this type of antenna quenching. The presence of Zx however shortens the lifetime in the aggregate slightly – without changing the spectral shape – from 689 ps in *npq1* to 430 ps in the w.t.

Two sites and mechanisms of non-photochemical quenching

We conclude that two independent quenching sites and two different mechanisms are involved in high-light adaptation and F_{NPQ} quenching differing with respect to their requirements for PsbS and Zx (Figure 8.11). The first one (**Q1**) is localized in the major LHC II, most likely oligomers, which are functionally detached from the native PS II/RC supercomplex, thus supporting the LHC II oligomerization model of Horton and coworkers (Horton et al. 2005). Detachment of LHC II from the PS II antenna and formation of the quenched oligomers strictly requires PsbS, but not Zx. However it appears that PsbS is not in itself a quencher but functions as a catalyst or allosteric factor that enables the reorganization of the thylakoid membrane that is associated with the LHC II oligomer formation. This reorganization is known to give rise to the absorbance changes at 535 nm, which are known to be absent in the PsbS-depleted *npq4* plants (Li et al. 2002b). Interestingly in the absence of Zx, i.e. for the *npq1* mutant, the LHC II detachment and oligomer formation is strongly enhanced, in line with another recent study (Crouchman et al. 2006). We propose that the enhanced functional detachment of PS II antenna in the *npq1* mutant, as evidenced from the very small PS II amplitude and the large amplitude of the oligomer component (Figure 8.4), compensates for the lack of PS II core quenching in this mutant (*vide infra*). Most likely this enhancement is caused in *npq1* by additional functional detachment of the more strongly bound LHC II or part of the minor antenna complexes.

The second quenching site, **Q2**, is located in and connected to the PS II antenna. It is strictly dependent on the formation of Zx and thus absent in *npq1* plants. We propose that this quenching site is actually located in the minor LHCs which carry the Zx. Interestingly, the quenching rate in the *npq4* and *L17* mutants is the same as compared to the w.t. This observation provides an indication of the location of this quenching mechanism. In *npq4* plants, the PS II antenna is larger than in w.t. plants under F_{NPQ} conditions due to the absence of LHC II detachment/aggregation processes. It is further known that

the xanthophyll cycle activity is rather similar in w.t. and *npq4* plants, so that quite similar amounts of Zx are formed in both genotypes under F_{NPQ} conditions, that follow from the pigment content (Table 8.4).

If the quenching would be located in the LHC II antenna of PS II, we would expect the quenching rate k_D to be higher in *npq4* than in w.t., since the former carries a larger LHC II complement under F_{NPQ} conditions and would thus contain more quenching centres. If the Zx-dependent quenching is however located in the minor LHC antenna complexes, then a larger unquenched LHC II antenna complement would dilute the effect of the quenching centres, and a bit smaller or the same overall k_D would result. This is obviously the case in the *npq4* mutant. Our data thus strongly suggest that the Zx-dependent quenching in the PS II antenna is localized in the minor LHCs. This interpretation is well consistent with the finding that LHC II free chlorina barley mutants develop strong Zx-dependent quenching (Andrews et al. 1995).

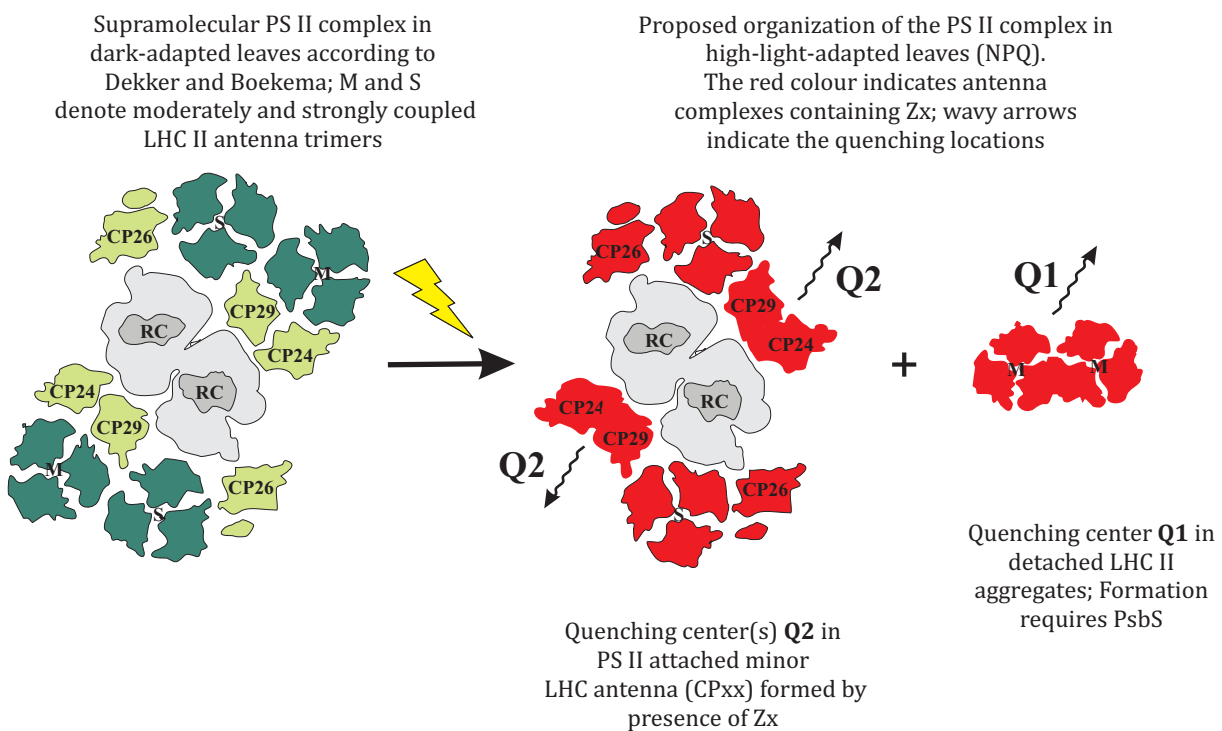


Figure 8.11: Schematic view of proposed quenching locations. Arrangement and composition of the supramolecular PS II complex in w.t. plants under dark-adapted (left-hand side) (adapted from Dekker and Boekema (2005)) and high-light F_{NPQ} (right-hand side) conditions. Binding of violaxanthin (Vx) to trimeric LHC II and minor CPs in the dark is indicated by green colour, Zx-containing LHC II and minor LHCs in the light by orange colour. The formation of quenching site Q1 requires PsbS, while the formation of the quenching site Q2 requires Zx only. We propose that interaction with PsbS causes detachment, migration and aggregation/deaggregation of LHC II depending on the lumen pH.

From the conclusions drawn above it is possible to propose a new model for the NPQ quenching as shown schematically in Figure 8.11. Starting from the supramolecular organization of PS II for dark-adapted plants as shown by Dekker and Boekema (Dekker and Boekema 2005, Yakushevskaya et al. 2003) the PS II complex reorganizes upon high-light adaptation (Figure 8.11) concomitant with the formation of two quenching centres *in vivo*: Firstly, in a fast reaction on the 10 s time scale part of the LHC II detaches from PS II and forms quenched aggregates (Q1). Next, NPQ quenching sites develop in the minor LHCs/PS II core complexes by xanthophyll conversion on a ca. 10-30 min time scale (Q2). In the *npq4* and *npq1* mutants only one of the two quenching sites can be formed in a mutually exclusive manner. Our data also suggest a role of PsbS that differs from the one assumed so far: PsbS is not a quencher in itself but enables LHC II to detach from PS II, to move within the thylakoid membrane, and to aggregate/disaggregate in response to the lumen pH change.

We cannot assign from our data any detailed photophysical quenching mechanism(s). However the Zx-dependent quenching located in the PS II-attached minor antenna complexes could well be explained by the proposed Zx cation radical formation (Ahn et al. 2008, Avenson et al. 2008, Holt et al. 2005)

For the Zx-independent quenching mechanism, operative in aggregated LHC II only, the spectral red shift provides some clues. It might be caused by some conformational modification of the LHC II complex that alters the interaction(s) of specific Chl-Chl pairs or Chl-Car pairs, as indicated also by resonance-Raman data (Robert et al. 2004). This could lead to the strengthening of Chl-Chl or Chl-Car charge transfer states which might give rise to quenching by electron transfer processes. Alternatively also an energy transfer from Chl to Car could be enhanced. Such quenching mechanism has been proposed based on crystal studies (Pascal et al. 2005). We note however that the short-lived fluorescence observed from the LHC II crystals does not show the red-shifted and red-enhanced fluorescence that we observed *in vivo*. In any case the identification of quenching locations as revealed from our data should facilitate tremendously future studies of the exact photophysical mechanism(s) of quenching.

In conclusion, PsbS enables LHC II to undergo processes that require its detachment from PS II, its movement within the thylakoid membrane, and also the aggregation/disaggregation process. PsbS thus shows many properties of a putative LHC II transport protein.

Chapter 9

QUENCHING IN MINOR ANTENNA MUTANTS

We proposed based on the time-resolved fluorescence results on intact leaves that there are two independent quenching sites formed in the PS II supercomplex regulating photosynthetic light-harvesting under high light intensities (Chapter 8). According to our model, one site (Q1) is located in the major LHC II and the other one (Q2) – in the minor or core antenna of PS II that remains attached to the PS II RC. To investigate these mechanisms in further detail we studied the fluorescence kinetics under quenched and unquenched conditions in intact leaves of *Arabidopsis thaliana* mutants, in which the genes coding for the minor antenna complexes CP26, CP29, or both, are knocked-out (de Bianchi et al. 2008).

RESULTS

Fluorescence decays in quenched and unquenched conditions

Figure 9.1 and Figure 9.2 present fluorescence decays measured by single photon counting at 686 nm on intact leaves of the knock-out mutants lacking the complexes CP24, CP26 and both together, referred as koCP24, koCP26 and koCP24/CP26, respectively. Figure 9.1 compares the fluorescence from leaves with closed PS II RCs in unquenched dark-adapted (F_{\max}) and quenched light-adapted (F_{NPQ}) state. In the dark-adapted state, the different mutants and the wild type exhibited almost identical fluorescence decay kinetics, however there were substantial differences between the light-adapted leaves. The average lifetimes for these decays together with the NPQ values are combined in the Table 9.1. In all genotypes the average lifetimes were significantly shorter in the F_{NPQ} state compared to the F_{\max} state, i.e. all mutants were able to develop non-photochemical quenching upon illumination. The extent of quenching in koCP26 and koCP24/26 was comparable to that in the w.t., however it was significantly reduced in koCP24. From these data it appears that the presence of CP24 is the most important for the quenching, whereas CP26 is not obligatory.

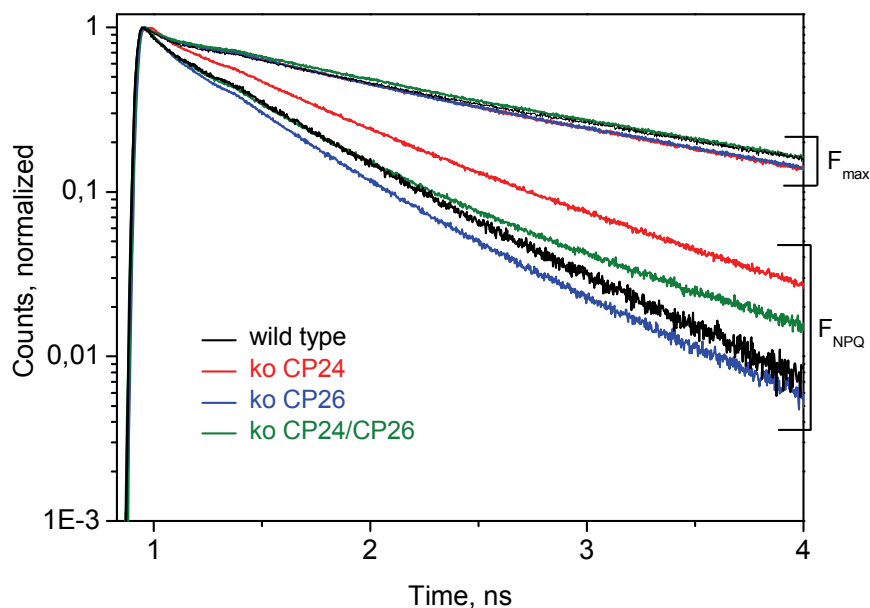


Figure 9.1: Normalized fluorescence decays (on a semilogarithmic scale) at 686 nm for w.t. and knock-out mutated intact leaves of *Arabidopsis thaliana*: koCP24, koCP26 and koCP29 in the quenched (light-adapted) F_{NPQ} and unquenched (dark-adapted) F_{\max} conditions with closed PS II reaction centres.

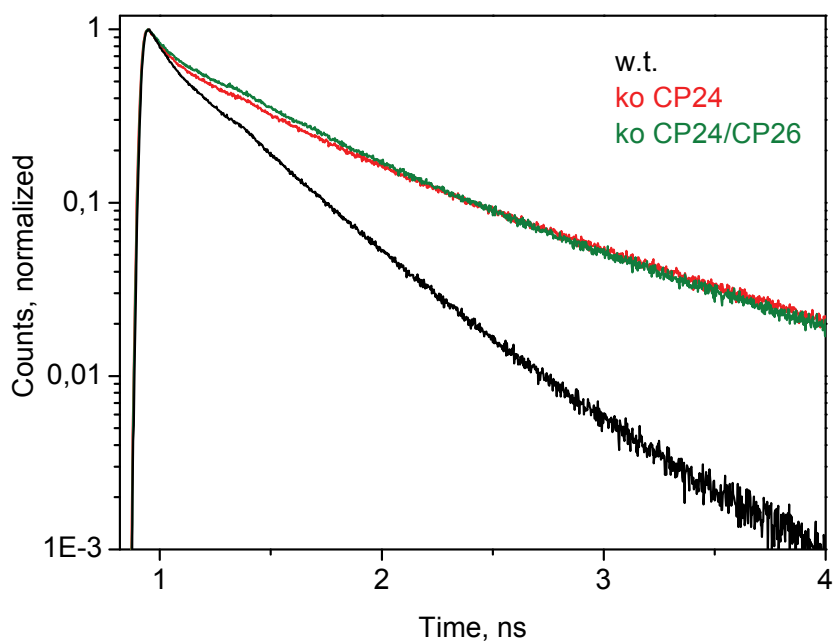


Figure 9.2: Normalized fluorescence decays (on a semilogarithmic scale) at 686 nm registered from intact *Arabidopsis thaliana* leaves of w.t. and the knock-out mutants koCP24 and koCP24/CP26 in unquenched conditions with open RCs (F_0).

Figure 9.2 compares the fluorescence decays of leaves in F_0 conditions, i.e. with open PS II RCs. The knock-out mutants decayed extremely slow in comparison to the w.t., which is in agreement with previous reports of steady-state fluorescence (de Bianchi et al. 2008, Kovács et al. 2006). The F_{\max}/F_0 ratios (Table 9.1) are twice lower for the mutants

than for the w.t. The longer fluorescence lifetimes in the dark-adapted state indicate that the organization of the photosynthetic machinery is altered by the mutations in a way that the photochemical efficiency is reduced. These changes were not correlated with the ability of the mutants to generate NPQ: e.g. in the koCP24/CP26 mutant the *NPQ* value is comparable with the w.t. whereas the efficiency of photochemistry, judged by the F_{\max}/F_0 ratio is drastically decreased.

Table 9.1: Average lifetime τ_{av} , ps of the fluorescence decays measured under the indicated conditions at 686 nm emission wavelength. The errors in the average lifetimes are <10 %. Also given are the *NPQ* values as calculated from the total fluorescence decays at 686 nm.

	w.t.	koCP24	koCP26	koCP24/26
τ_{av} at 686 nm, ps				
F_0	210	398		394
F_{NPQ}	408	507	333	420
F_{\max}	1116	967	915	1147
<i>NPQ</i>	1.7	0.9	1.7	1.7
F_{\max}/F_0	5.3	2.2		2.5

Target compartment modeling

The measured fluorescence kinetics data were analysed by global target analysis, where PS II and PS I were fitted separately. The kinetic scheme from the Chapter 8 (Figure 8.3) resulted in a good fit also here in the the unquenched dark-adapted leaves (F_{\max}). However, as previously, an additional unconnected compartment was necessary for the case of light-adapted quenched leaves (Figure 9.3 and Figure 9.4). This compartment exhibited the same features as the LHC II oligomers detached from PS II: high far-red to red amplitude ratio in the DAS accompanied by the decrease of the PS II cross-section. Formation of LHC II oligomers contributes in the Q1 site of energy dissipation that was not dependent on PsbS protein (see Chapter 8). In the double mutant koCP24/26 one more additional compartment not connected to either PS I or PS II, was necessary. Judging by its emission spectrum and long lifetime (Figure 9.3 D) it most probably arises from a small number of LHC II trimers which are energetically disconnected from the photosystems and are not quenched.

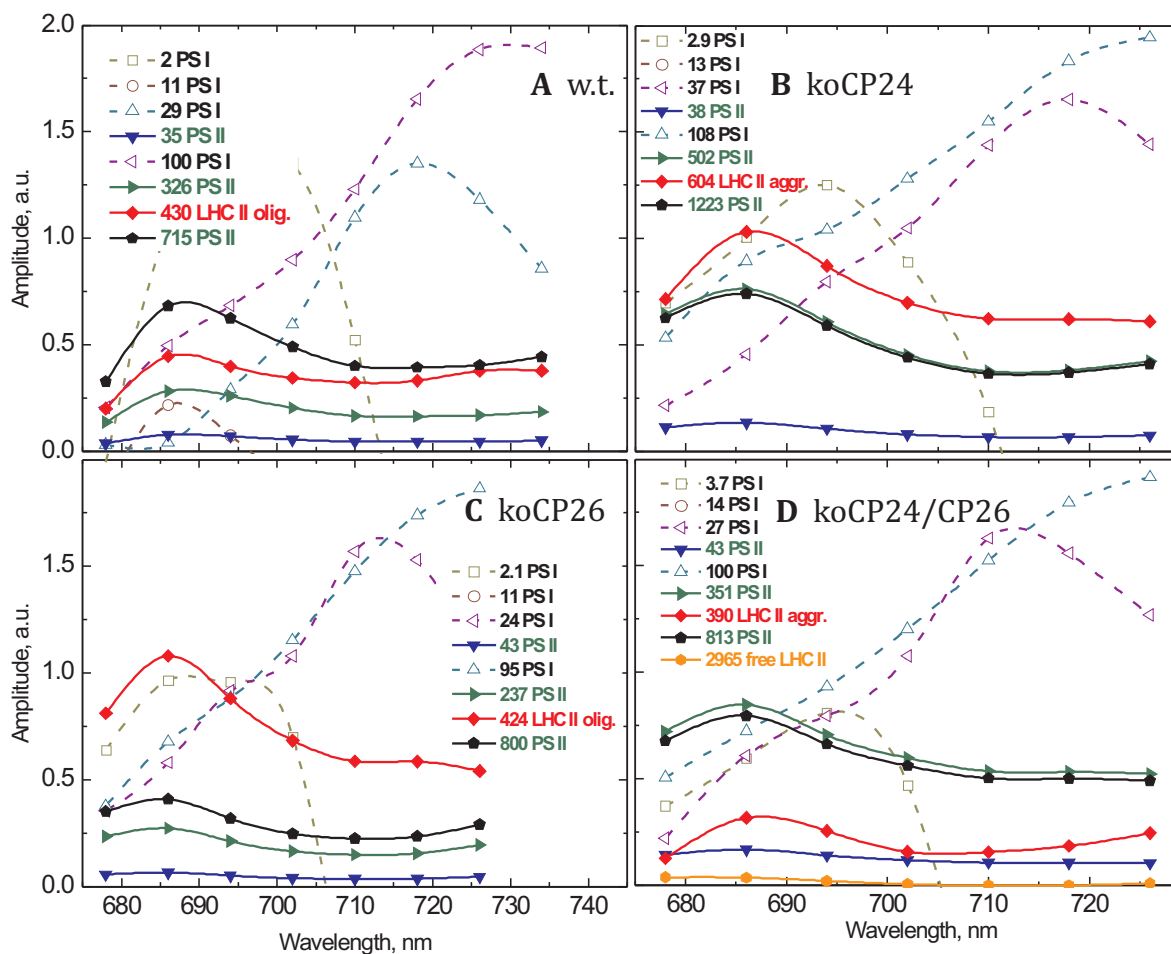


Figure 9.3: Fluorescence lifetime components of high-light-adapted plants. DAS (Holzwarth 1996) are obtained from global target analysis of the fluorescence decays of leaves from w.t. (A, discussed in Chapter 8) and knock-out mutants koCP24 (B), CP26 (C), and CP24/CP26 (D) under high-light-adapted (F_{NPQ}) conditions.

Figure 9.4 shows the DAS for the mutants and w.t. in the unquenched state. The amplitude for mutants is slightly increased towards 734 nm comparing to the w.t. which could be indicative of changes in the thylakoid membrane organization occurring in the dark in the mutants.

The second site of quenching, Q2, is revealed through the rate constant k_D (Figure 8.3), which is the average non-photochemical deactivation rate of the PS II antenna. Under illumination k_D increases four times in w.t. and *npq4*, but remains almost unchanged in the absence of Zx in the *npq1* leaves (Chapter 8), so it is strictly dependent on Zx and is localized in the PS II attached antenna: either minor antenna, where Zx is mostly bound (Bassi et al. 1993) or PS II core.

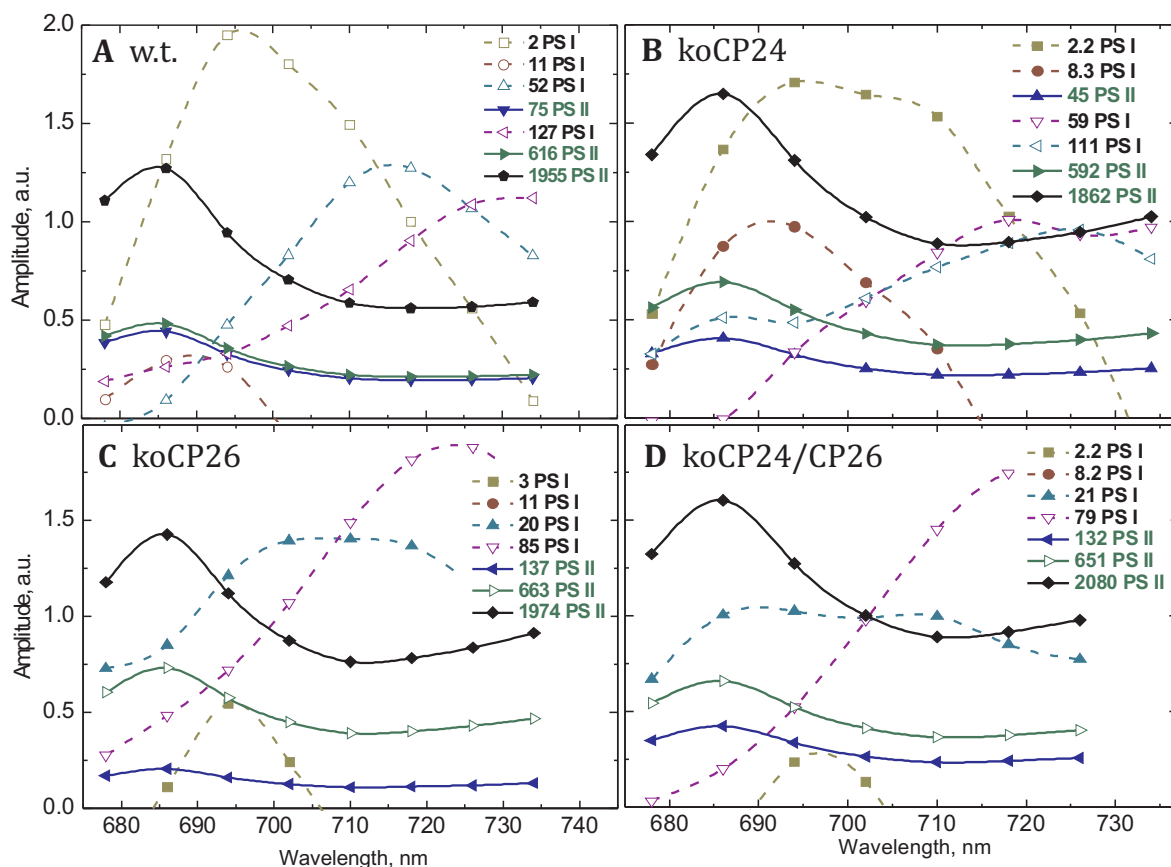


Figure 9.4: Fluorescence lifetime components of dark-adapted plants. DAS as obtained from global target analysis of the fluorescence decays of leaves from dark-adapted w.t. (A, discussed in Chapter 8) and knock-out mutants koCP24 (B), koCP26 (C) and koCP24/CP26 (D) of *Arabidopsis thaliana* plants under F_{\max} conditions (closed RCs).

The magnitude of PS II quenching can also be monitored by the lifetimes corresponding to PS II in the quenched and unquenched states. These lifetimes and the values of k_D are summarized in Table 9.2. Comparison of different genotypes shows that the average lifetime of PS II under F_{NPQ} condition for koCP24 is longer (791 ps) than that for the others (~ 520 ps). There is a good correlation between the light-induced reduction in the PS II lifetime and the increase in the non-photochemical deactivation rate constant, k_D . Because of the suppression of the light response of the k_D in the absence of the CP24, this minor antenna seems to be absolutely required for the Q2 site of quenching. It is however surprising that in the double mutant koCP24/CP26 the Q2 quenching mechanism activity is revealed.

Table 9.2: Upper part: Average lifetime, τ_{av} , of PS II components and rate constants of PS II antenna deactivation, k_D , resulting from the kinetic modelling of the different plants under high-light (NPQ) conditions. Lower part: Lifetime of the additional compartment assigned to quenched LHC II oligomers. The percentage of the LHC II amplitude at the fluorescence maximum (686 nm) calculated relative to the sum of amplitudes of all PS II and LHC II components. The number of Chl *a* correspondent to this percentage in the detached LHC II oligomers relative to the total Chl *a* in PS II/LHC II. It was assumed that w.t. PS II super-complex is in the C₂S₂M₂ state in the darkness. The number of LHC II trimers correspondent to the number of Chl *a* in detached antenna.

	w.t.	koCP24	koCP26	koCP24/26
τ_{av} of PS II, ps				
F_{NPQ}	517	791	528	525
F_{max}	1165	1274	1409	1422
k_D, ns⁻¹				
F_{NPQ}	1.8	0.8	1.7	1.7
F_{max}	0.46	0.3	0.3	0.3
τ of quenched LHC II oligomers, ps	402	604	424	390
% of detached LHCII	30	59	39	15
Chl <i>a</i> molecules in detached antenna	60	111	74	27
Detached LHCII trimers	2.5	5	3	1

Evidently, the largest part of the *NPQ* loss in the knock-out mutants, particularly koCP24, can be attributed to the changes in the k_D constant, i.e. the Q2 site of quenching. However, the mutations also affected the lifetime of the additional unconnected compartment, i.e. detached LHC II oligomers, as well as its relative amplitude (Q1 site). This indicates that the number of antenna complexes which were detached from the PS II cores was different. For a quantitative comparison the amplitude of the detached LHC II component at its fluorescence maximum (686 nm) was calculated relative to the sum of amplitudes of all PS II plus LHC II components. It is given in percentage in Table 9.2 (lower part). It can be seen that concomitantly with the suppression of the Q2 site of quenching (k_D), the absence of CP24 lead to increased amount of detached LHC II oligomers. On the contrary, in the double mutant koCP24/CP26 this number was twice lowered compared to the w.t.

The relative amount of the detached antenna can be expressed as number of Chl *a* molecules or LHC II trimers (24 Chl *a*'s) detached per PS II supercomplex (Table 9.2), since the DAS amplitude is proportional to the absorption cross-section of the excited pigments, i.e. Chl *a*. For this calculation we assume that PS II in the dark-adapted state is organized as C₂S₂M₂ supercomplexes, each containing 200 molecules Chl *a* (2 cores + 2 copies of CP24, CP26, CP29 + 4 LHCII trimers).

DISCUSSION

Based on the presented results from compartment modeling of the fluorescence kinetics, we can construct a tentative model describing the parallel action of the two discussed mechanisms of non-photochemical quenching and the high-light-induced reorganizations of PS II in the thylakoid membranes of the w.t. and the different studied mutants.

Wild type

In the w.t. both quenching sites, Q1 and Q2, are active. The fraction of LHC II oligomers detached under light conditions is 30%, corresponding, on average, to 2-3 trimers per PS II supercomplex, based on the Chl *a* content, as is shown in Table 9.2. Since moderately bound LHC IIs (M-LHC IIs) are supposed to detach easier than strongly bound (S-LHC IIs), this leads to the conclusion that in the light-adapted state the prevailing supercomplexes are of the C₂S₂ type instead of C₂S₂M₂.

The k_D , characterizing Q2 site, increases approximately four times in the quenching conditions. Further we search for the answer to the following questions: where particular the Q2 site is localized, which minor complexes play a role in this type of quenching, which mechanism is responsible for it.

koCP26

The koCP26 mutant has also both quenching sites active, as w.t. However, twice more LHC II trimers detach from PS II forming the Q1 quenching site. Taking the Chl *a* content into consideration, this corresponds to a ratio of five detached LHC II trimers per PS II supercomplex. The number tells that practically all major LHC II is detached from PS II under high light. Thus, according to our data CP26 plays the largest role in organizing the antenna subunits of the supercomplex together. However, according to the work of Dekker and Boekema (2005), CP26 is not necessary for the formation of PS II-LHC II su-

percomplexes and in its absence CP26 is not replaced by other types of LHC. The Q2 site of quenching, i.e. Zx-dependent quenching, seems to be not located in CP26 since there is no significant difference between the k_D values in light-adapted w.t. and koCP26 leaves.

koCP24

The amount of LHC II trimers detached from PS II in koCP24 mutant is only slightly larger than in w.t. and corresponds to three detached LHC II trimers per PS II. It has been shown that the organization of PS II supercomplexes in koCP24 is different than that in w.t. (de Bianchi et al. 2008, Kovács et al. 2006). In this mutant M-LHC II trimers may be lacking already in the dark, and additionally S-LHC II trimers may detach in the light-adapted state and participate in Q1 quenching.

The quenching at the Q2 site is largely suppressed in leaves lacking CP24. The light-induced increase in the non-photochemical dissipation rate k_D in these leaves is three-fold smaller than in the other mutants. Therefore the CP24 complex has a key role in the Q2 mechanism. The deletion of the *lhcb6* gene encoding CP24 reduced NPQ also in the experiments of Kovács et al. (2006), though the antisense inhibition of CP29, CP26 (Andersson et al. 2001) and Lhcb1 and Lhcb2 (Andersson et al. 2003) expression did not disrupt this function. According to Kovács et al. (2006), CP24 provides the linker for association of the M-LHC II trimer into the PS II complex, because PS II complexes deficient in the M-LHC II trimers were found mostly in koCP24. However our data suggest that the mechanism of Q2 is not a result of macroorganization of PS II, but some interaction that involves CP24, most probably the CP24-CP29 interaction. This interaction was proposed to exist by Andersson et al. (2001) since a decrease in the level of CP24 was shown in CP29 antisense lines. In the koCP24 mutant studied by (de Bianchi et al. 2008) the lack of CP24 leads to a compensatory increase in CP29 by approx. 30%. We hypothesize that small activity of the Q2 site in koCP24 can be maintained by CP29-CP29 interaction, that is however not as effective as CP24-CP29.

koCP24/CP26

When both CP26 and CP24 are lacking, the amount of detached LHC II aggregates is lowered to one trimer, and also small amounts of free, non-oligomerized LHC II appear. Electron microscopy (de Bianchi et al. 2008) has revealed that there are free LHC II clusters formed in the plastids of koCP24/CP26 already in the dark.

In contrary to koCP24, the double mutant koCP24/CP26 appears to have a fully active Q2 site (judging by k_D), as in koCP26 and w.t. Interestingly, apart from the absence of CP24 and CP26, this mutant has decreased amount of CP29 as well as of Lhcb3 protein (de Bianchi et al. 2008). At the same time the Lhcb1 and Lhcb2 content is increased (particularly Lhcb1). Hence we hypothesize that some major LHC IIs get involved in the Q2 site of quenching due to CP29-LHC II interactions.

npq1

On account of the presented analysis of the knock-out mutants, we can have further insight into the quenching process in the Zx-deficient *npq1* mutant, discussed in Chapter 8, and include it in our model scheme. The *npq1* mutant does not show any changes in k_D upon illumination – the Q2 site is not operating. However this mutant seems to counterfeit this deficiency and cope with the excessive energy via the Q1 quenching site. A much larger part of the PS II antenna (70%) is detached in the *npq1* mutant as compared to the wild type. In number of Chl *a* molecules this would be corresponds to six LHC II trimers detached. We hypothesize that together with the detachment and oligomerization of major LHC II, inactive minor LHCs may also detach and take part in the oligomerization-induced quenching. The exact amount of this can not be determined however.

NON-PHOTOCHEMICAL QUENCHING IN DIATOMS

RESULTS AND DISCUSSION

Fluorescence induction

As a reference basis for the ultrafast time-resolved fluorescence measurements, fluorescence and NPQ induction were recorded both by a PAM fluorometer (Waltz, Germany) and a Handy Pea fluorometer (Hansatech Instruments, UK) in order to characterize the different adaptation states of the algal cultures. Figure 10.1 shows the Handy Pea results for both diatoms. In contrast to the PAM fluorometer (*cf.* Materials and Methods), the Handy PEA registers direct non-modulated fluorescence using the same light source (high-intensity red LED) as actinic and excitation light. The Handy PEA has the advantage of a higher time resolution, i.e. the minimal time interval between two measured data points is 10 microseconds. This enables to monitor the fast fluorescence induction kinetics, i.e. the rise that follows the transition from fully open PS II RC to fully closed RC (at saturating light intensity). The recorded OJIP transients provide information about the electron transfer rates and efficiencies in PS II (Strasser et al. 2004).

The fluorescence induction was measured in 12 cycles consisting of 300 s actinic light intensity followed by 80 s of darkness. In the first cycle (Figure 10.1 A) the traces had the typical shape of the OJIP transient observed in algae and higher plants (Strasser et al. 1995). The F_{\max}/F_0 ratio calculated from the transients was similar for *P. tricornutum* and *C. meneghiniana* (2.7 and 2.8 respectively). It should be noted though, that these values do not necessarily reflect the maximal photochemical efficiency of PS II because the measurements were done at lower than saturating light intensity to avoid photo-damage during the relatively long measurement period. Although the amplitude of the variable fluorescence was comparable in the two diatoms, the kinetics was different. In *C. meneghiniana* the initial fluorescence rise was very rapid, with the J level (reflecting the reduction of Q_A) reached in less than 1 ms and maximal fluorescence attained in just 100 ms. In contrast, in *P. tricornutum* the J step appeared at 2 ms and the maximum at 0.5 s. The faster fluorescence rise in *C. meneghiniana* could be explained by a larger PS II

antenna size. However in this diatom the quenching formation (fluorescence decrease after the maximum) also started much earlier and proceeded with higher rate compared to *P. tricornutum*. Exponential fits of the fluorescence curves after the maximum resulted in lifetimes for quenching formation of 3.7 s and 30 s for *C. meneghiniana* and *P. tricornutum*, respectively.

The differences between the two diatoms continued with the following illumination cycles (Figure 10.1 A, dashed lines and Figure 10.1 B). In *C. meneghiniana* a fraction of the total quenching could relax during the 80 s of darkness between the cycles and it was again generated during the next cycle. These transients were absent in *P. tricornutum*, or too slow to be visible in such short time intervals. During the one-hour illumination in *C. meneghiniana* we observed a tendency for slow relaxation of NPQ (Figure 10.1 B) after the rapid initial build-up (in the first few seconds of illumination). In comparison, the NPQ continued to increase within the measurement period in *P. tricornutum*. As a result, after 1 h the fluorescence of *C. meneghiniana* was higher compared to *P. tricornutum* (relative to the dark-adapted state, F_0).

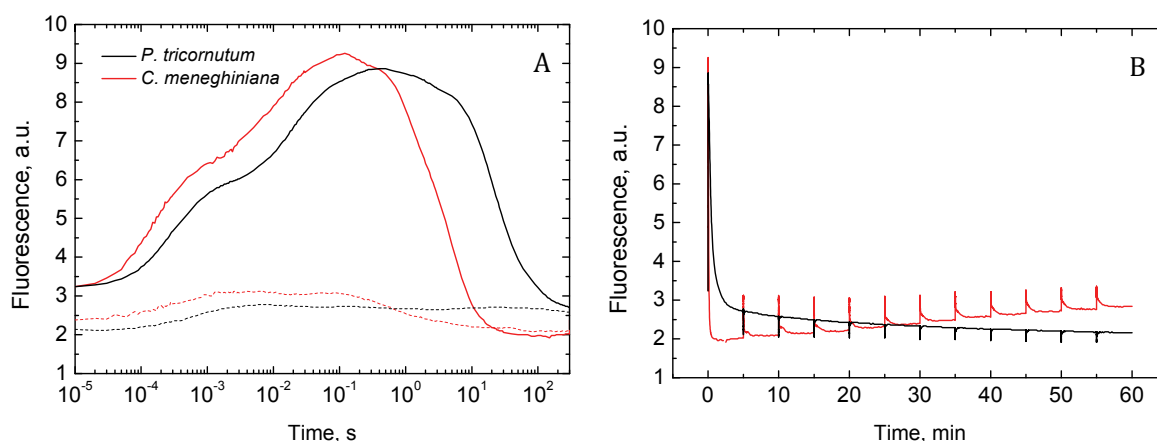


Figure 10.1: Fluorescence induction in *P. tricornutum* and *C. meneghiniana* during 1 h of constant illumination with $1000 \mu\text{mol photons m}^{-2} \text{s}^{-1}$ interrupted by 80 s of darkness every 300 s (12 cycles of 300 s light and 80 s darkness). A. First (solid lines) and second (dashed lines) illumination cycles plotted in logarithmic timescale. B. All consecutive illumination cycles.

The induction phase of NPQ measured with PAM fluorometer is shown in Figure 10.2 for *P. tricornutum* and *C. meneghiniana*. Initially a saturating pulse was applied to determine the maximal fluorescence in the dark adapted state, F_m . F_m/F_0 values of 3.7 and 3.3 were obtained for *P. tricornutum* and *c. meneghiniana*, respectively (slightly higher than the values estimated from the Handy PEA due to the higher flash intensity). After determining F_m actinic light of $600 \mu\text{mol photons m}^{-2} \text{s}^{-1}$ was applied. In *P. tricornutum* a steady-

state NPQ was established gradually during 5-6 min of actinic illumination. For *C. meneghiniana*, an almost immediate strong fluorescence quenching was typically observed, followed by a slight recovery to a constant level, as was observed in the Handy PEA measurements. In order to make sure that de-epoxidation of Ddx to Dtx was completed and NPQ remained unchanged during the ultrafast fluorescence decay measurements, cells were adapted to HL conditions as shown in Figure 10.2 for at least 30 min.

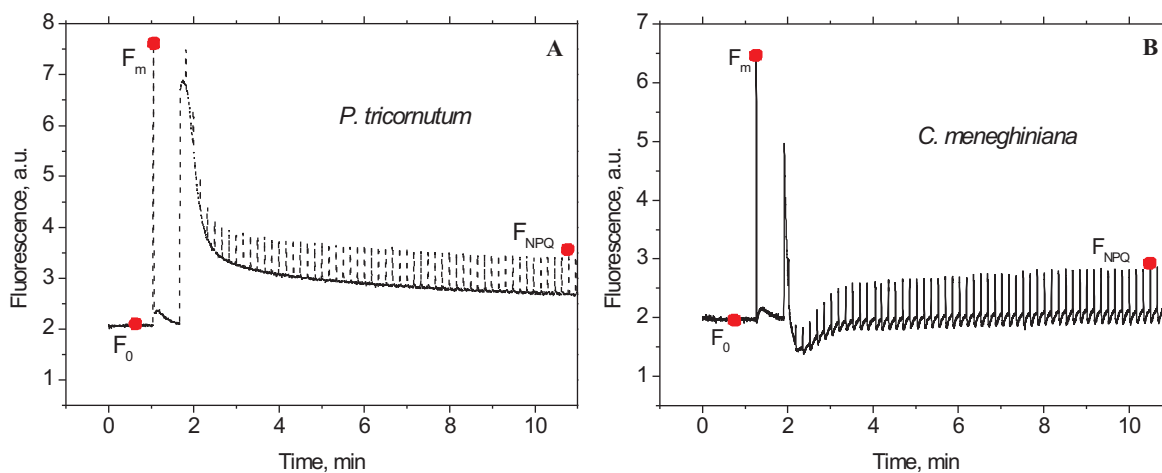


Figure 10.2: Fluorescence and NPQ induction kinetics of *P. tricornutum* (A) and *C. meneghiniana* (B) cells before and during high light illumination ($600 \mu\text{mol photons m}^{-2} \text{s}^{-1}$). Saturating light flashes were applied every 10 s in order to induce F_m' ($=F_{\text{NPQ}}$). The corresponding conditions in which lifetime measurements have been performed are indicated by red dots.

The NPQ values and the kinetics of NPQ formation in the diatoms were highly sensitive to the actinic light intensity, to a larger extent compared to *Arabidopsis*. At higher light intensity – $800 \mu\text{mol photons m}^{-2} \text{s}^{-1}$ (Figure 10.3) – there was only a very small contribution from photochemical quenching, i.e. the PS II RCs were mostly closed by the actinic irradiation. The photochemical quenching is estimated by the increase in fluorescence induced by the periodically applied saturating flashes. Under these conditions the NPQ rapidly attained steady-state level and did not further relax during the measurement period also in *C. meneghiniana*, and as a result the F_{NPQ} level was lower than F_0 .

The induction kinetics measurements performed with the two registration techniques – direct (Handy PEA) and modulated (PAM) – confirmed that *P. tricornutum* and *C. meneghiniana* largely differ in the kinetics of NPQ. While both species exhibited comparable levels of NPQ under the same light conditions, the process of NPQ formation in the latter was an order of magnitude faster. It is possible that the enzymatic activity of Ddx-

deepoxidase is higher in *C. meneghiniana* leading to faster conversion of Ddx into Dtx and activation of NPQ. Interestingly though, the initial fluorescence induction rise was also faster in this diatom, indicating that the pool of electron acceptors between the two photosystems is reduced quicker leading to a quicker closure of the PS II RCs. This could be explained either by a smaller acceptor pool or higher activity of PS II. In this respect, to gain further insight into the response of the two diatoms to the light conditions, we determined the de-epoxidation levels and the rate of oxygen evolution (as an additional test for the activity of PS II).

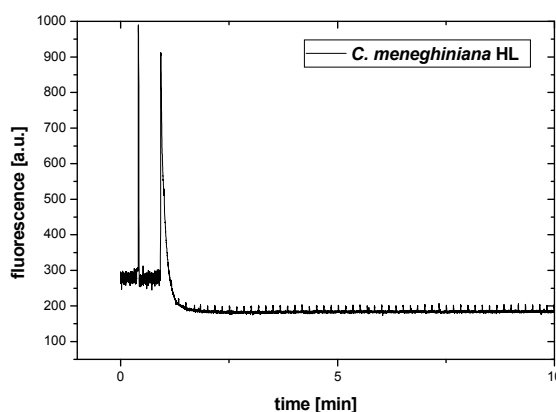


Figure 10.3: Fluorescence induction curve of a *C. meneghiniana* culture grown at $50 \mu\text{mol photons m}^{-2} \text{s}^{-1}$, and kept in growth light before measurement, illuminated with $800 \mu\text{mol photons m}^{-2} \text{s}^{-1}$ after dark-adaptation. $\text{Ddx} + \text{Dtx} = 240 \text{ mM (M Chl } a)^{-1}$, $\text{DES} = 0.4$ before onset of actinic illumination, 0.66 after 10 min of HL. NPQ after 10 min HL = 3.5 .

Oxygen evolution and de-epoxidation state

The rate of oxygen evolution of the cells was measured after 10 min (control conditions) and after prolonged, 3 h HL treatment. In control conditions the rates were 60% higher for *C. meneghiniana* ($140 \mu\text{mol O}_2 (\text{mg Chl } a)^{-1} \text{h}^{-1}$, Table 10.1) compared to *P. tricornutum* ($86 \mu\text{mol O}_2 (\text{mg Chl } a)^{-1} \text{h}^{-1}$). This result is in agreement with the faster fluorescence induction in *Cyclotella* and probably contributes to the earlier activation of NPQ in this species. In both diatoms prolonged HL treatment had almost no effect on the oxygen production, i.e. the electron transport rates. This demonstrates that the steady-state NPQ was completely based on high-energy state quenching (qE) and that photoinhibitory quenching (qI), which would have become visible as a reduction of the oxygen evolution, did not contribute to the NPQ analysed during the fluorescence decay measurements.

Because of the important role of the xanthophyll cycle, and Dtx in particular, for NPQ in diatoms, the de-epoxidation state (DES) and the size of the XC pigment pool (Ddx + Dtx)

per Chl *a* were monitored in the cells under control conditions, after HL treatment and prolonged dark incubation. *C. meneghiniana* had a higher initial DES, but during dark incubation a gradual epoxidation from Dtx back to Ddx took place. The DES decreased from an initial value of 0.14 to 0.09 within 3 hours of darkness. In *P. tricornutum*, on the contrary, a slight increase in the DES from 0.05 to 0.06 during darkness was visible. No significant changes in the XC pigment pool size took place in prolonged darkness (from 404.3 to 409.4 (Ddx+Dtx) Chl *a*⁻¹ in *P. tricornutum* and from 175.7 to 179.8 (Ddx+Dtx) Chl *a*⁻¹ in *C. meneghiniana*). In HL a sharp increase in Dtx content (a 12-fold increase in DES for *P. tricornutum* as compared to a 3.5 fold increase in *C. meneghiniana*) as well as a slight increase of the overall XC pigment pool could be observed for both species (see Table 10.1). It is important to note that the de-epoxidation of Ddx to Dtx shown here was saturated after 30 min of HL treatment, so the DES values of 0.62 for *P. tricornutum* and 0.48 for *C. meneghiniana* remained unchanged during fast fluorescence decay measurements ensuring a constant fluorescence signal.

Table 10.1: Oxygen evolution given in $\mu\text{mol O}_2$ (mg Chl *a* h)⁻¹ of cells under growth conditions (control) and after 3 hours of HL (600 $\mu\text{mol photons m}^{-2} \text{s}^{-1}$). Rates are given including dark respiration after a period of 10 min HL. Xanthophyll cycle pigment pool size (Ddt+Dtx) in mM (M Chl *a*)⁻¹ and deepoxidation state (DES) given as Dtx (Ddx+Dtx)⁻¹ in control cells and after 3 hours of HL (600 $\mu\text{mol photons m}^{-2} \text{s}^{-1}$) treatment. Pigment data are mean values of 3 measurements with S.D. below 10 %. Oxygen evolution rates show a representative measurement.

	<i>P. tricornutum</i>			<i>C. meneghiniana</i>		
	DES	Ddx+Dtx	oxygen	DES	Ddx+Dtx	oxygen
Control	0.05	404.3	86.2	0.14	175.7	140.3
3 h HL	0.62	483.5	88.9	0.48	242.4	148.6

The slight increase of the DES observed during the 3 h dark incubation of *P. tricornutum* cells is in line with data from the literature where the de-epoxidation of Ddx to Dtx during prolonged darkness as a consequence of chlororespiratory electron flow has been described (Jakob et al. 2001). From the epoxidation of Dtx to Ddx observed during darkness in *C. meneghiniana*, it appears that the establishment of a chlororespiratory proton gradient is not taking place in this alga.

Ultrafast fluorescence decay kinetics

The ultrafast fluorescence kinetics of the diatom cells were measured under unquenched (dark-adapted state) and quenched (HL-adapted state) conditions. Three different conditions were compared: a) F_0 – unquenched dark-adapted cells with open PS II RCs, b) F_{\max} – unquenched dark-adapted cells with RCs closed by DCMU, and c) F_{NPQ} – quenched HL-adapted cells with PS II RCs closed by light. The raw fluorescence decays of the two genotypes detected at 678 nm (where PS II has its maximum fluorescence) are shown Figure 10.4.

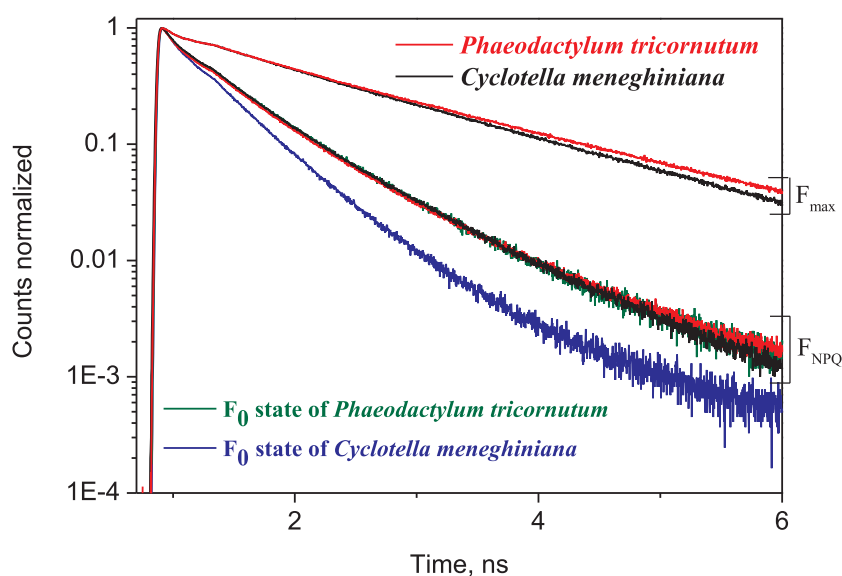


Figure 10.4: Normalized fluorescence decays (on a semilogarithmic scale) at 678 nm for *P. tricornutum* and *C. meneghiniana* at F_0 , F_{NPQ} and F_{\max} conditions.

Table 10.2: Average lifetime τ_{av} , ps of the fluorescence decays measured under the indicated conditions at 678 nm emission wavelength. The errors in the average lifetimes are <10 %. Also given are the *NPQ* values as calculated from the total fluorescence decays at 678 nm and the F_{\max}/F_0 ratio.

	<i>P. tricornutum</i>	<i>C. meneghiniana</i>
τ_{av} at 678 nm, ps		
F_0	332	295
F_{NPQ}	363	377
F_{\max}	901	803
<i>NPQ</i>	1.5	1.1
F_{\max}/F_0	2.7	2.7

C. meneghiniana and *P. tricornutum* showed very small differences in the fluorescence decays under F_{\max} conditions and essentially no differences at F_{NPQ} (cf. Figure 10.4). However, their F_0 states showed different kinetics. The F_0 of *C. meneghiniana* was similar to that of higher plants (Figure 8.1), where F_0 decays faster than F_{NPQ} . Whereas F_0 of *P. tricornutum* decayed with similar lifetime as F_{NPQ} ($\tau_{\text{av}} = 332$ ps and 363 ps, correspondently). The average lifetimes τ_{av} and NPQ values (calculated as in Chapter 8) are combined in Table 10.2. The extent of NPQ for both species was very similar, with a slightly higher value for *P. tricornutum*. The F_{\max}/F_0 ratio for both diatoms from the lifetime measurements was 2.7.

Global target analysis

The global target analysis of the time-resolved spectra was carried out using the kinetic model shown in Figure 10.5.

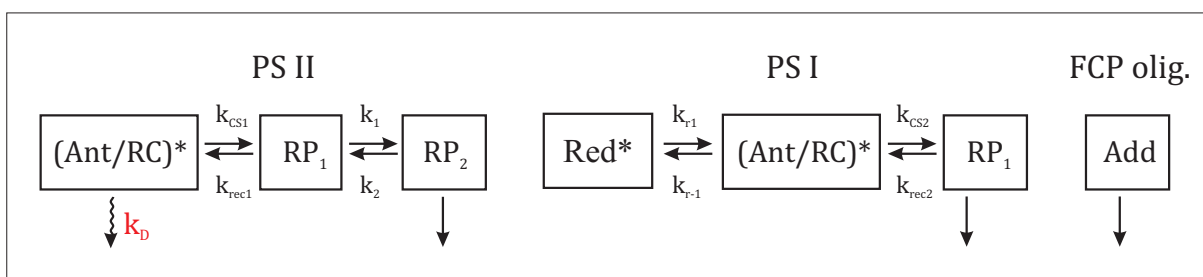


Figure 10.5: Kinetic schemes for PS I and PS II used in the global target analysis of the fluorescence decays from *P. tricornutum* and *C. meneghiniana*. The PS II and PS I scheme predicts three exponentials for the decay kinetics. For light-adapted cells one additional single lifetime component was necessary in the analysis to represent a newly appearing component that could not be fitted within the pure PS I and PS II schemes. Such component is needed to describe the functionally detached PS II antenna component, which is assigned to FCP in the oligomeric state. The rate constant for energy dissipation by non-photochemical quenching (k_D) is marked in red. k_{CS} – rate constant of charge separation reaction, k_{rec} – rate constant of charge recombination. Rate constants are given in Table 10.3

This model includes PS I and PS II compartments and is based on fluorescence lifetime and other kinetic studies on isolated PS I and PS II particles of vascular plants (cf. Chapter 8) and are found to describe the kinetics of intact cells of diatoms also very well. Only for PS I a slight adaptation in the model from vascular plant PS I is necessary: The diatoms appear to have only one red PS I antenna compartment, as can be clearly concluded from the analyses of the F_{\max} fluorescence kinetics. This is in line with recent data from the literature where the first indications for FCP complexes, which are specifically associated with either PS II or PS I are emerging (Lepetit et al. 2008). However, it appears that the PS I antenna is not as complex as in vascular plants. The global target

analysis allowed us to separate the overall fluorescence kinetics into contributions from PS II and PS I.

Detached antenna component

The same compartment model was tested for F_0 , F_{NPQ} and F_{max} conditions and in general provided excellent fits, except in the following notable cases: Under HL conditions (F_{NPQ}) an additional fluorescence component, functionally unconnected to both PS I and PS II was required. Its fluorescence spectrum (decay associated spectrum, DAS) differs from those of PS I and PS II. It has an enhanced red spectral tail, but it can neither be correlated with PS I nor with PS II. The appearance of this component correlates, however, with a corresponding decrease in the total amplitude of PS II fluorescence components (sum of the amplitudes of the three PS II DAS) relative to the PS I DAS amplitudes. It has to be noted that the exclusion as a separate compartment of the functionally uncoupled antenna fluorescence from the modelling rendered the complete fits unacceptable (see further).

Non-photochemical deactivation rate constant k_D

Within the PSII model (Figure 10.5) the most important rate constant, directly characterizing the quenching in the PS II-attached antenna is k_D , which represents the total non-radiative and non-photochemical deactivation rate of the PS II antenna. Under HL conditions both *C. meneghiniana* and *P. tricornutum* exhibited a nearly three-fold increase in k_D from 0.73-0.75 ns⁻¹ in the unquenched state to 1.9 ns⁻¹ in the quenched state (Table 10.3).

Table 10.3: Rate constants (ns⁻¹) resulted from the model presented in Figure 10.5 for F_{max} and F_{NPQ} conditions for *P. tricornutum* and *C. meneghiniana*. The most important rate for our purpose of NPQ study are k_D and the decay rate of additional component as it was already discussed in Chapter 8.

		PS II					PS I					add	
		k_D	k_{CS}	k_{-CS}	k_1	k_2	k_3	k_{r1}	k_{-r1}	k_{CS}	k_{-CS}	k_4	
F_{max}	PT	0.73	2.6	15.7	2.4	2.0	0.9	158	189	155	66.0	24.5	-
	CM	0.75	3.0	19.2	1.6	1.3	0.9	151	148	183	97.1	23.8	-
F_{NPQ}	PT	1.9	2.8	16.5	5.2	2.4	0.9	70.4	133	262	54.3	25.8	2.43
	CM	1.9	2.4	14.0	4.4	4.0	0.9	113	149	125	79.5	50.5	3.32

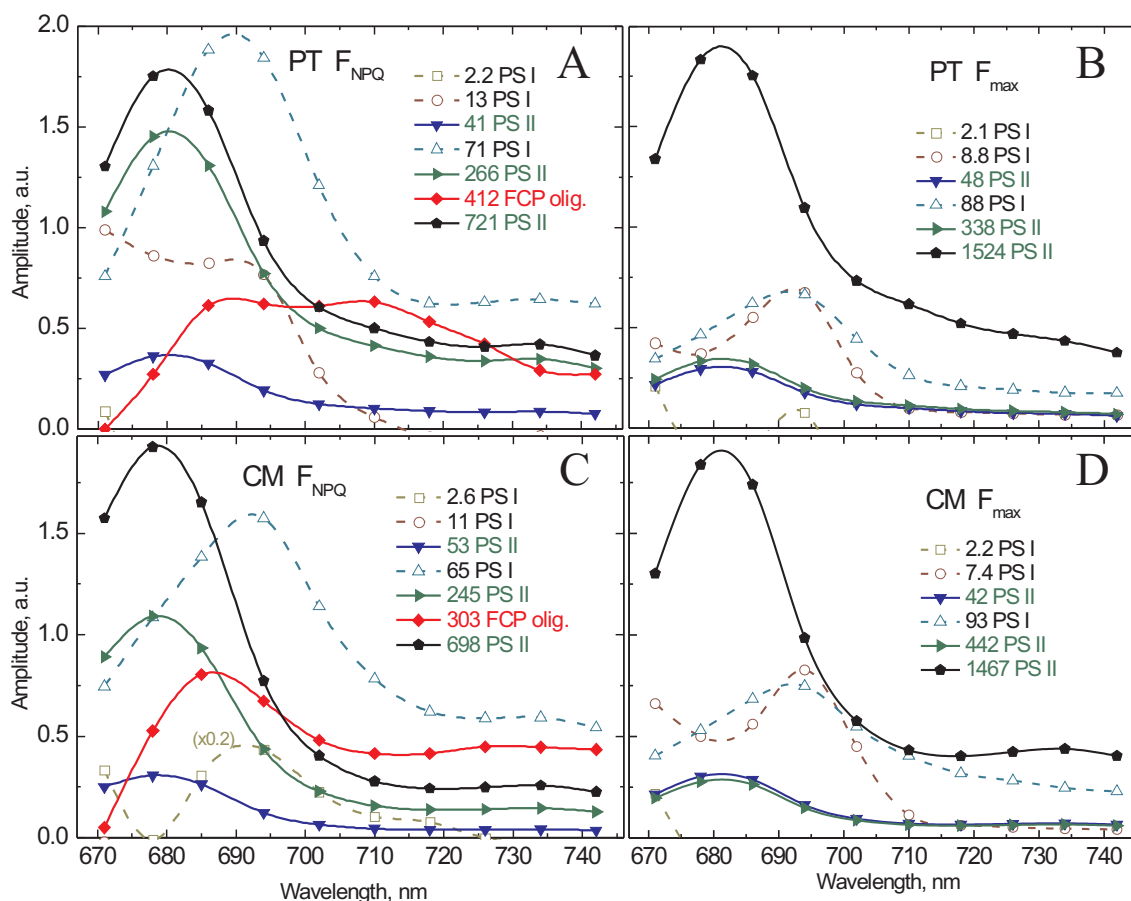


Figure 10.6: Decay-associated spectra (DAS) obtained from global target analysis of the fluorescence decays for *P. tricornutum* (A, B) and *C. meneghiniana* (C, D) under light-adapted FNPQ (A, C) and dark-adapted F_{\max} (B, D) conditions. The corresponding residual plots for the light-adapted FNPQ condition (A and C), with and without the additional detached antenna compartment, are shown in Figure 10.8 and Figure 10.9. Only fits with the additional detached antenna compartment were satisfactory as judged by the χ^2 -values and the residuals plots. Note that the amplitude scales for FNPQ and F_{\max} can not be compared directly. Note that the fast PS I components (energy transfer) are negative over most of the wavelength range. Since these components are not directly relevant for the issue discussed here we are showing only the positive amplitude for better clarity of presentation of the NPQ-relevant components. The same hold for Figure 10.7, Figure 10.10, and Figure 10.11.

The results of the global target analysis are summarized in the decay-associated spectra shown in Figure 10.6, Figure 10.10 and Figure 10.11. Figure 10.6 compares the DAS for F_{\max} and F_{NPQ} conditions. The most prominent differences between these two conditions are the shorter average lifetime under NPQ conditions (Table 10.4), which is expected, and the occurrence of the additional fluorescent antenna compartment, which appears only under HL conditions. As discussed above, this additional component is disconnected functionally from both PS II and PS I. Any models that did not allow for such an

unconnected compartment did not result in satisfactory fits (see Figure 10.7, Figure 10.8 and Figure 10.9).

Table 10.4: Average lifetime, τ_{av} , ps, of PS II compartments and of the additional compartment (assigned to FCP oligomers) resulting from the kinetic modelling of the two diatoms.

	<i>C. meneghiniana</i>	<i>P. tricornutum</i>
τ_{av} PS II, ps		
F_0	395	432
F_{NPQ}	490	467
F_{max}	1170	1188
τ of additional compartment, ps	303	412

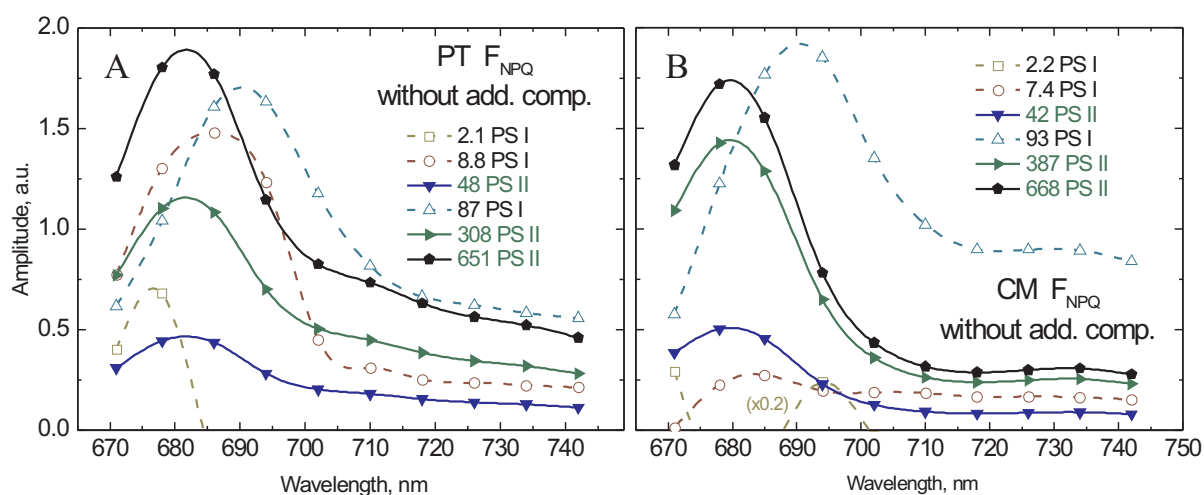


Figure 10.7: DAS for *P. tricornutum* (A) and *C. meneghiniana* (B) in F_{NPQ} state analysed with the kinetic scheme that did not include additional component (detached FCP oligomers). The residuals for the fits with and without additional component are in Figure 10.8 and Figure 10.9. For both diatoms the fit excluding detached FCPs was much poorer justifying the necessity of the additional component in the analysis.

Concomitant with the appearance of the unconnected antenna component, the relative DAS amplitudes of the PS II compartment decreased. Thus, this antenna compartment must derive from a functional detachment of part of the PS II antenna. The peak of the emission spectrum of the additional compartment was red-shifted as compared to the normal PS II emission and showed strongly enhanced emission in the long-wavelength range, resulting in a broad plateau in *C. meneghiniana* (or peaking at 710 nm in *P. tricornutum*). The relative peak amplitudes of the additional component (at 685 nm) to the sum of the three PS II amplitudes at the maximum of PS II (678 nm) was 24% for *C. meneghiniana* and 22% for *P. tricornutum*.

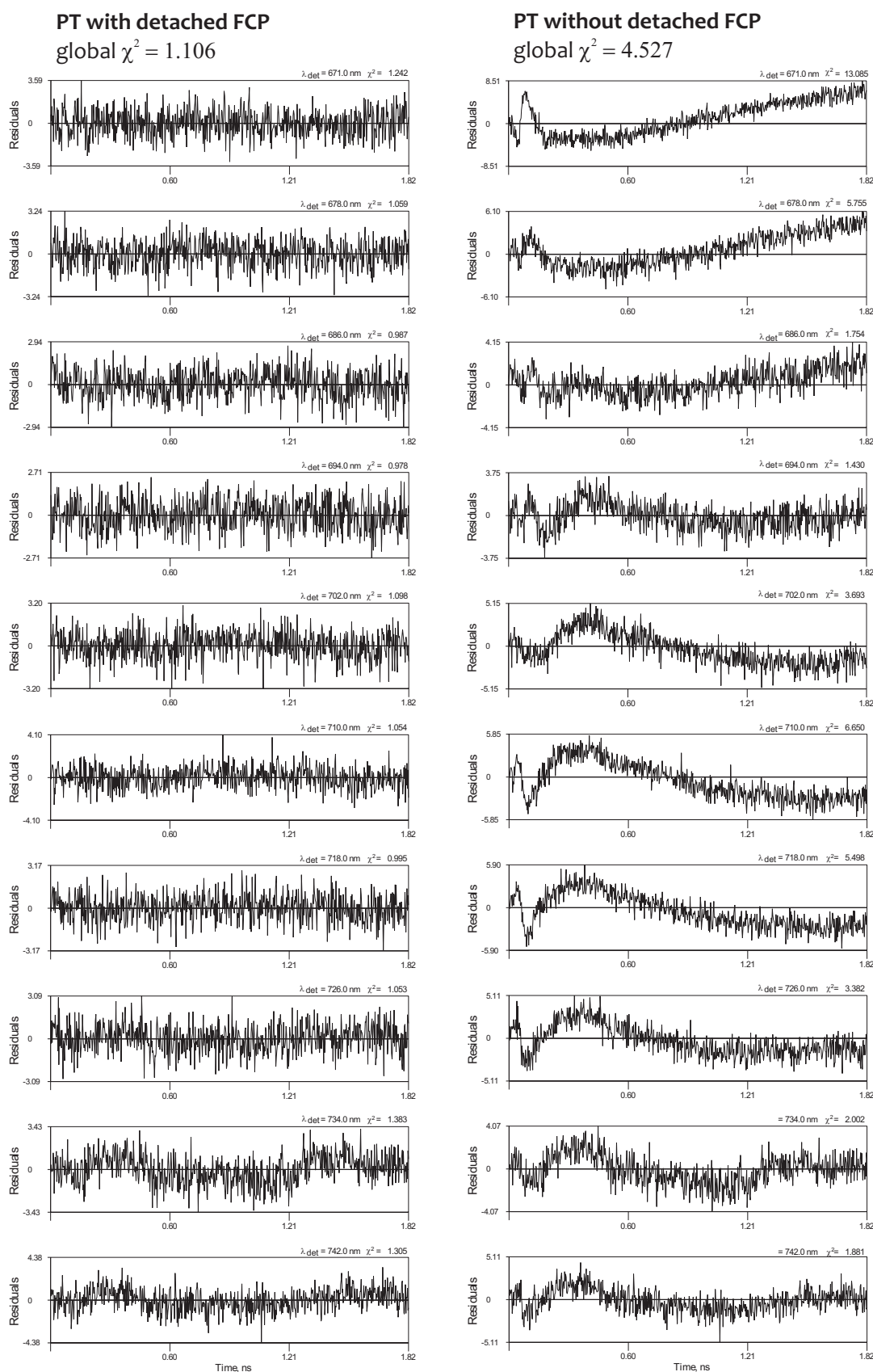


Figure 10.8: Residuals of the fits received from target analysis of *P. tricornutum* in FNPQ condition. Left: the fit with additional component, functionally disconnected from either PS I and PS II, attributed to detached FCP oligomers. Right: the fit without additional component. It was obtained by fixing the rate constants to the solution from F_{max} analysis and leaving the k_D as a variable parameter.

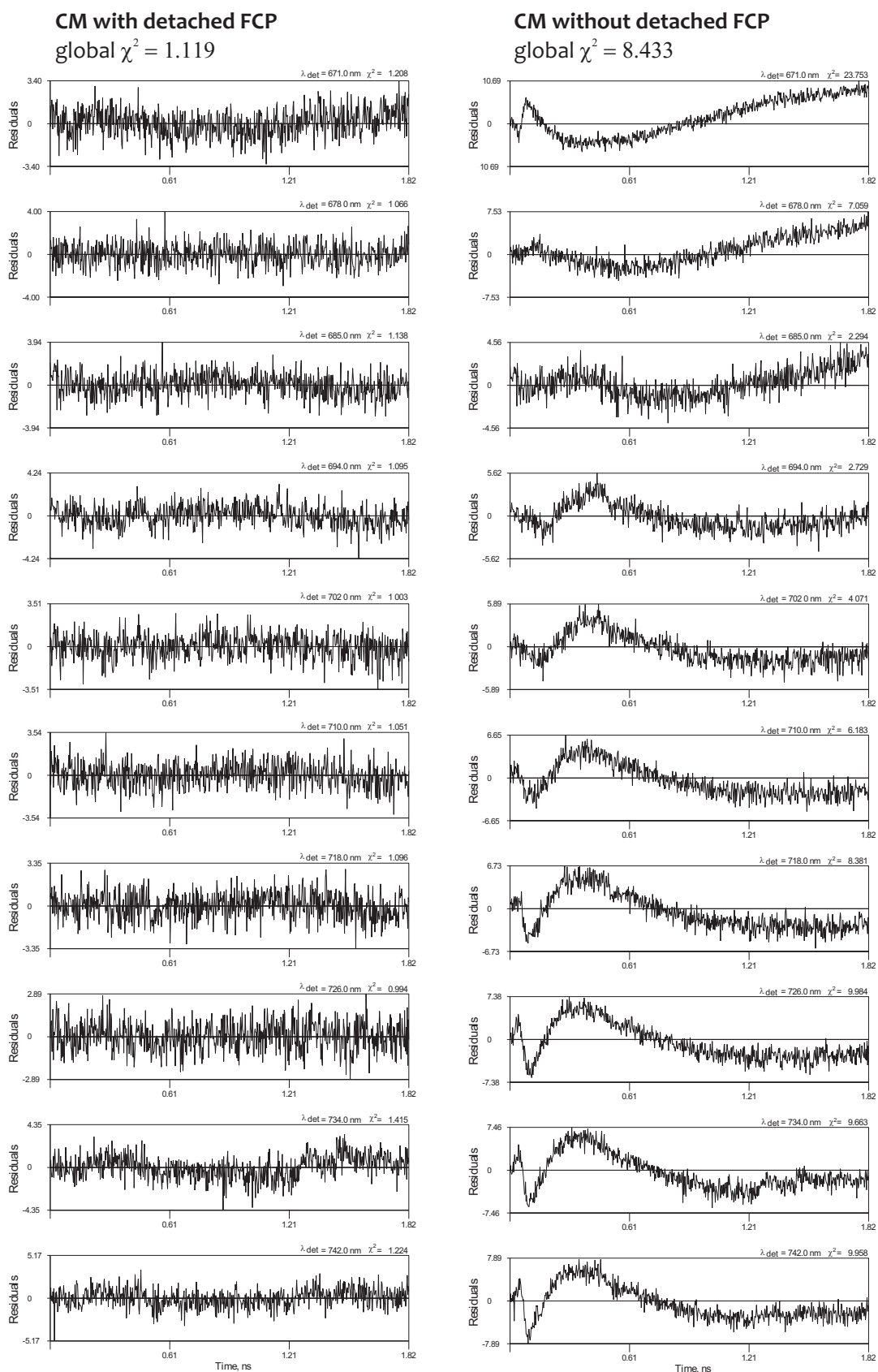


Figure 10.9: Residuals of the fits received from target analysis of *C. meneghiniana* in F_{NPQ} condition. Left: the fit with additional component, functionally disconnected from either PS I and PS II, attributed to detached FCP oligomers. Right: the fit without additional component. It was obtained by fixing the rate constants to the solution from F_{max} analysis and leaving the k_D as a variable parameter.

Species differences in the kinetics for dark-adapted diatoms with open reaction centres

For the characterization of NPQ kinetics and for comparison with literature data the ki-

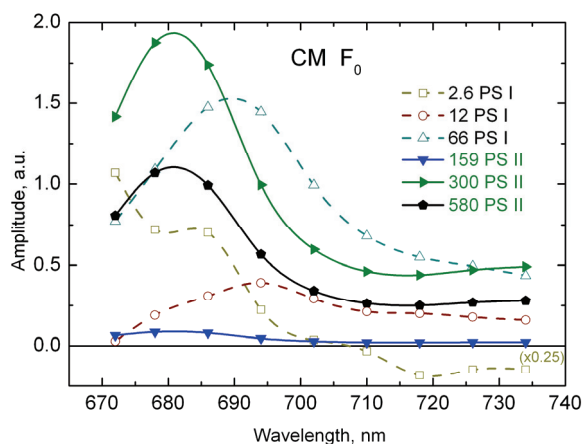


Figure 10.10: DAS of *C. meneghiniana* at dark-adapted conditions (F_0) as calculated with the target model shown in Figure 10.5. This modelling yielded good fits. See Note Figure 10.6.

netics from cells with open PS II centers are not required, since the NPQ is usually measured in a state where all PS II centers are closed. Based on our observation that *P. tricornutum* and *C. meneghiniana* showed almost identical fluorescence decays in the F_{max} and F_{NPQ} state, we nevertheless compared the kinetics of dark-adapted cells, which usually should have all PS II RCs in the open state, unless PS II is closed by non-photosynthetic processes. The target analysis for *C. meneghiniana* is shown in Figure 10.10. The average lifetime was

295 ps and the kinetics could be fitted well using the target model depicted in Figure 10.5, without requiring any additional unconnected compartment.

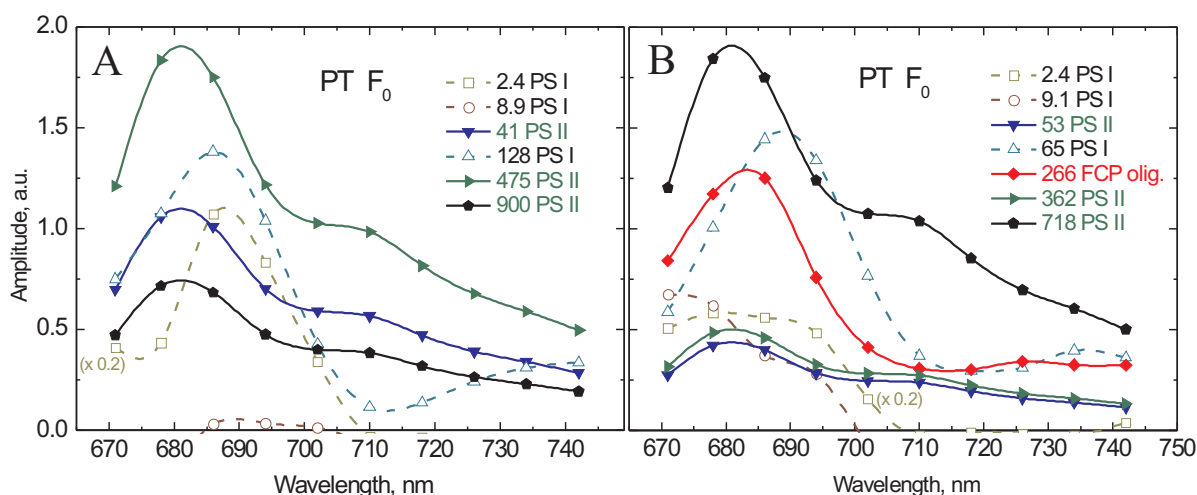


Figure 10.11: DAS of *P. tricornutum* at dark-adapted conditions (F_0) as calculated with the target model shown in Figure 10.5, with and without an additional detached antenna compartment. Both models did not yield satisfactory fits as judged by the χ^2 -values and the residuals plots (Figure 10.8 and Figure 10.9). See also Note Figure 10.6.

The analysis of the *P. tricornutum* kinetics, however, was much more difficult. The compartment scheme of Figure 10.10 did not work for *P. tricornutum* under F_0 conditions. In addition, the PS II lifetimes were rather long for PS II with open RCs. The fits were unsat-

isfactory in general and allowing for the unconnected compartment typical for the quenched state, did also not improve the quality of the fits significantly. (see DAS in Figure 10.11).

Thus, the kinetics are not in line with a (partial) NPQ in dark-adapted *P. tricornutum* cells but rather suggest that part of the PS II RCs were closed during prolonged darkness. From the literature it is known that in the dark chlororespiration can take place in diatoms (Ting and Owens 1993). Chlororespiration leads to a reduction of the PQ pool (for review see Peltier and Cournac 2002), which is in equilibrium with QA. Therefore, we suspect that in the dark-adapted *P. tricornutum* cells part of the PS II reaction centres were closed by chlororespiratory electron flow. The resulting kinetics, representing a mixture of open and closed PS II RCs, create a very complex fluorescence decay that cannot be easily analyzed. Thus, we consider the similarity of the two fluorescence decays in the F0 and FNPQ state of intact *P. tricornutum* cells at 678 nm (Figure 10.4) to be a mere coincidence. When considering the whole measured wavelength range it becomes clear that the respective kinetics differ substantially. We thus conclude that the kinetics in the quenched state (HL conditions) differs substantially from the kinetics of *P. tricornutum* cells when all PS II RCs are open.

The NPQ quenching model

We will in the following develop and propose a quenching model for diatoms. Several parts of this model are directly proven by the results of the time-resolved fluorescence data (Chapter 8). The parts we have evidence for are i) Two different locations, one in the PS II-attached antenna and the other in an antenna part that has been functionally detached from PSII during HL adaptation, are responsible for the total NPQ in diatoms. ii) The PS II-attached quenching mechanism increases the deactivation rate in the antenna of PS II by a factor of about three as compared to the unquenched state, thus protecting PS II against overexcitation. iii) The antenna part that is detached from PS II during HL adaptation is also strongly quenched as compared to isolated FCP complexes (300-400 ps lifetime for the detached antenna parts *in vivo* vs. more than 3 ns lifetimes for isolated FCP antenna complexes, data not shown). This means a quenching factor of about one order of magnitude.

While our data for the quenching locations and effects described so far are very clear, the other part of our proposed quenching model (Figure 10.12) – described in the following – still awaits further experimental verification. It has been reported that two

kinds of FCP antenna subpopulations exist and can be isolated from *C. meneghiniana* (Büchel 2003). These are a trimeric FCP (subpopulation I) and an oligomeric FCP (subpopulation II). Gundermann et al. (2008) have found that only the fluorescence of the trimeric FCP is quenched by Dtx, whereas the oligomeric FCP is insensitive in its fluorescence to Dtx accumulation. On the basis of these findings, we speculate that the quenching location described by the changes in k_D of the PSII-attached antenna takes place in the trimeric FCP, i.e. subpopulation I. This quenching does not differ significantly between *C. meneghiniana* and *P. tricornutum*. Based on our present data, we cannot provide evidence for the mechanism responsible for this quenching, but suggest that the quenching in the trimeric FCPs is caused by Dtx formation.

With respect to the oligomeric FCPs, which have also been found in the thylakoid membranes of *P. tricornutum* (Lepetit et al. 2007, Szabó et al. 2008), one may speculate that they represent the subpopulation II FCP complexes which form the quenched antenna part that becomes functionally detached from PS II. Further evidence for our present model comes from recent biochemical data (Lepetit et al. 2008) that show that different FCP subpopulations exist, which differ in their oligomerization state, their diadinoxanthin/diatoxanthin content and their DES after HL illumination. We thus propose that the PS II detached antenna compartment actually reflects oligomeric FCP complexes that are strongly quenched.

Interestingly it has been shown recently that *in vitro* oligomerization of the LHC II complex of vascular plants gives rise to a fluorescence component of similar lifetime (about 400 ps) which has a red-enhanced spectrum as compared to trimeric LHC II (*cf.* Chapter 7 and (Miloslavina et al. 2008)). The same spectrum and lifetime has been found under NPQ conditions in intact leaves of *Arabidopsis* w.t. plants and it has been concluded that in vascular plants the detachment of parts of the LHC II complex and their oligomerization represents an important part of the total NPQ (Miloslavina et al. 2008).

The shapes of the DAS components in the red region are somewhat different for the two diatoms. *P. tricornutum* has a red peak at 710 nm, while *C. meneghiniana* has a broad emission peaking around 730 nm. This suggests that there exist specific differences in the FCP oligomerization between these two diatom species. Given the differences in the FCP organization between *P. tricornutum* and *C. meneghiniana* this is very likely the case. We have summarized all these conclusions in the proposed model for NPQ in diatoms (Figure 10.12). In our model the light-induced reorganization leads to the formation of two quenching centres: The first quenching site consists of FCP subpopulation II which

detaches from PS II and forms quenched oligomers. The second site includes the conversion of the PS II-attached FCP subpopulation I into a quenching centre. The conversion of this FCP into an NPQ-active site may be triggered by the presence of Dtx. In terms of our model, *P. tricornutum* and *C. meneghiniana* show identical NPQ under steady-state conditions during HL illumination, with both quenching sites active to a comparable extent.

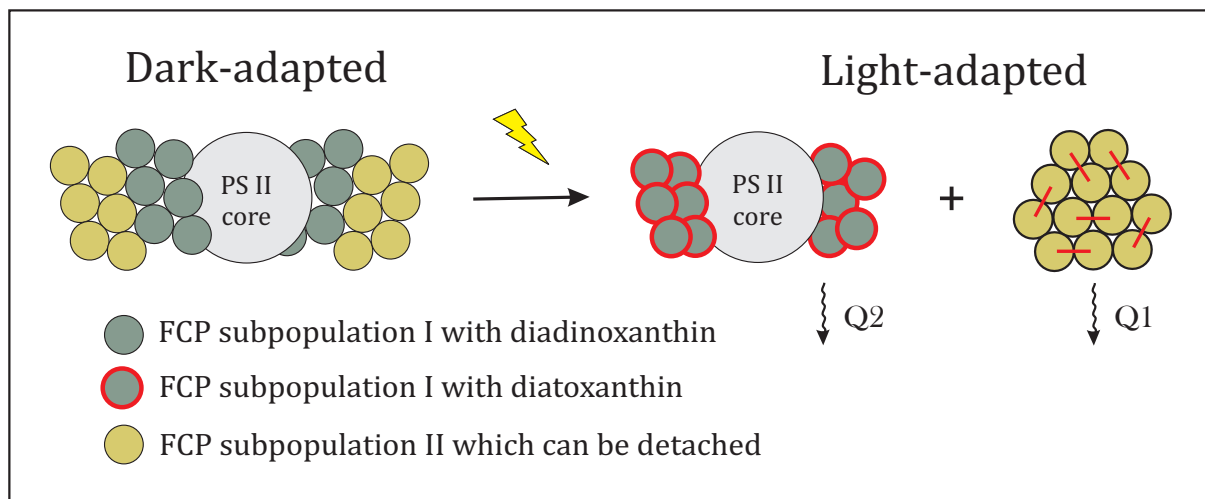


Figure 10.12: Proposed quenching model for diatoms showing the two different quenching locations Q1 and Q2. For details see the discussion. The red bars in the quenching site Q1, which are formed by oligomeric FCPs, denote the Chl-Chl interactions between FCP antenna complexes.

Comparing the data for F_{NPQ} and F_{max} conditions in Figure 10.6, we also note that the amplitude of the long-lived PS I component relative to the total amplitude of PS II components (plus detached antenna) taken at their respective maxima increases by about 20%, along with a slight decrease of the PS I lifetime (from 88 ps to 71 ps in *P. tricornutum* and from 93 to 65 ps in *C. meneghiniana*). Taking into account the uncertainties in the lifetime of about 10% it seems that these lifetime changes are significant. Two possibilities exist to explain this phenomenon: Either a change in spillover from PS II to PS I under NPQ conditions, or a state transition. In the first case we would expect some PS I spectral component with the lifetime of the PS II components. This does not seem to be the case. However we can not entirely exclude the possibility of a state transition contribution. For example, if about 10% of the FCP antenna would change its connection from PS II to PS I we could fully explain the effect. This could be physiologically relevant. Unfortunately we could not find any reliable information regarding state transitions in diatoms in the literature. This point thus remains open at the moment. It is important to note however that any of these possibilities would not affect any of the mechanisms and conclusions that we have drawn with respect to the locations of the true NPQ quenching effects.

CONCLUSIONS

Single photon counting measurements, being a precise and highly sensitive technique allowing measurements of low light signals with high signal-to-noise ratio combined with target analysis, resolved many details and provided explanations on topics that have met controversy in scientific literature – primary energy and electron transfer kinetics in PS II core particles and BBYs, in LHC II trimers and aggregates, the mechanism of non-photochemical quenching and the interplay of the many factors involved in it. This technique was for the first time thoroughly utilized for probing the ultrafast reactions *in-vivo*. These measurements and analysis were possible thanks to the preliminary studies of the kinetics of isolated complexes. The investigation of light-adapted and dark-adapted leaves led to the development of a new model of non-photochemical mechanisms that clarifies the roles of Zx and PsbS and separates their site of action. Moreover, as a surprise for us, the two-site NPQ model proved valid also for diatom cells.

The most important conclusions resulting from the experimental work are listed in the following.

1. The kinetics of energy and electron transfer in PS II particles could be successfully described in terms of the exciton/radical pair equilibrium (EPRE) model extended to include energy transfer step from the antenna into the reaction center (RC) and one additional reversible electron-transfer step or radical pair between Chl_{acc} and Pheo. By resolving this additional kinetic component it is shown that the primary reactions in intact cores and isolated RCs occur with similar rates and that the kinetics is trap-limited in both cases.
2. Considerable similarities in the early electron transfer rates of PS II reaction centres (RCs, without antenna), cyanobacterial PS II cores (with core antenna), and a higher plant PS II enriched membranes (with core and peripheral antenna) were found. The energy transfer rates scale with increase in the antenna size. Thus the dynamics of the initial photochemical steps of PS II could be implemented in the model describing the *in-vivo* fluorescence as well.

3. A second generation EPRE model was proposed that gives a more realistic structure-based description and gives good results on changes of rates of inter-antenna energy transfer. Addition of antenna to PSII core moves the kinetics to the transition region. The kinetics is not diffusion-limited – $\tau_{ET}/\tau_{CS} = 0.9-1.0$ (migration time is ~ 90 ps). The monomer-monomer equilibration time is ~ 20 ps and the equilibration time in a LHCI trimer is 12-14 ps.
4. The excited state decay kinetics in isolated LHC II oligomers in a wide spectral range was studied. It was shown that quenching in the oligomers is attained due to the formation of a new molecular state created by pigment-pigment interactions. This emissive state has a broad far-red spectrum and is assigned to a charge-transfer state formed between peripheral Chls.
5. Time-resolved fluorescence spectroscopy was applied for the first time on intact plant leaves. Common physiological parameters such as F_m/F_o and NPQ , conventionally obtained by steady-state Chl fluorescence were calculated directly from the fluorescence decays. The complete wavelength-dependent fluorescence decay kinetics in intact plants has been modelled by a target compartment analysis allowing to distinguish the contribution of the antenna and RCs of PS I and PS II to the total fluorescence emission *in vivo* and to determine the photochemical and non-photochemical rate constants.
6. Following generation of NPQ *in vivo* a new fluorescence emission component appears at the expense of the cross-section of PS II which is attributed to detachment of the peripheral PS II antenna (LHC II). This component has short lifetime and broad far-red enhanced spectrum similar to the one observed in isolated LHC II oligomers. Therefore we conclude that the detached LHC II is oligomerized and the energy is dissipated through a rapidly decaying CT state. This process in effect quenches the fluorescence of PS II and thus represents a newly discovered quenching mechanism, termed quenching site 1 (Q1). The far-red-enhanced fluorescence component this way represents a spectroscopic marker that can serve to detect the detachment and oligomerization of LHC II *in vivo*.
7. The fluorescence component ascribed to detached LHC II is not observed in plants lacking PsbS protein (*npq4* mutant) under NPQ conditions. On the other hand, its relative contribution to the total fluorescence is even stronger in plants overexpressing PsbS (*L17* mutant). We therefore conclude that the detachment and oligomeriza-

tion of LHC II is mediated by PsbS and cannot take place in its absence. It follows that the likely role of PsbS in NPQ is not direct quenching of excitations but enabling the LHC II to detach and form quenched oligomers.

8. Upon generation of NPQ the decay rate constant k_D of the antenna attached to PS II, which sums the non-photochemical energy dissipation in the antenna, is increased. The PS II-attached antenna (and mostly minor complexes) therefore represents a second quenching site (Q2).
9. Plants unable to produce Zx (*npq1* mutant) lack the capability for quenching of the PS II-antenna (Q2). Thus, the Q2 site of quenching is Zx-dependent. In these plants the quenching via Q1 (detached LHC II) is compensatory enhanced. Thus, the Q1 site and the action of PsbS are independent on XC conversion.
10. The minor antenna complex CP24 plays an important role in the Zx-dependent quenching at Q2 since this type of quenching is drastically suppressed in plants lacking CP24. Nevertheless, the Q2 site is not bound only to CP24 and is probably due to interaction with other complexes (e.g. CP29). CP26, however, is not active in Q2 site.
11. The fluorescence decay kinetics of intact diatom cells under dark- and light-adapted (NPQ) conditions can be described by a compartment model equivalent to that of higher plants. Similar to higher plants, a new, far-red enhanced fluorescence component arises upon illumination of diatoms. This unconnected component appears concomitantly with a decrease of the PS II cross-section and is therefore ascribed to detached PS II antenna (FCP). The detachment of FCP in diatoms represents one quenching site (Q1).
12. The decay rate of the PS II antenna k_D in preilluminated diatoms increases, similarly to higher plants. This represents a second quenching site (Q2). Thus, the striking similarities in the response of diatoms and higher plants to NPQ conditions lead to the conclusion that NPQ proceeds via similar mechanisms and that the two quenching sites found in higher plants are also active in diatoms.

Based on these conclusions, a new model of the non-photochemical quenching mechanism in higher plants and diatoms can be now presented. For both organisms the model is very similar. For the higher plants it includes four states (Figure 11.1): two formed in dark (1 and 4) and two in light (2 and 3).

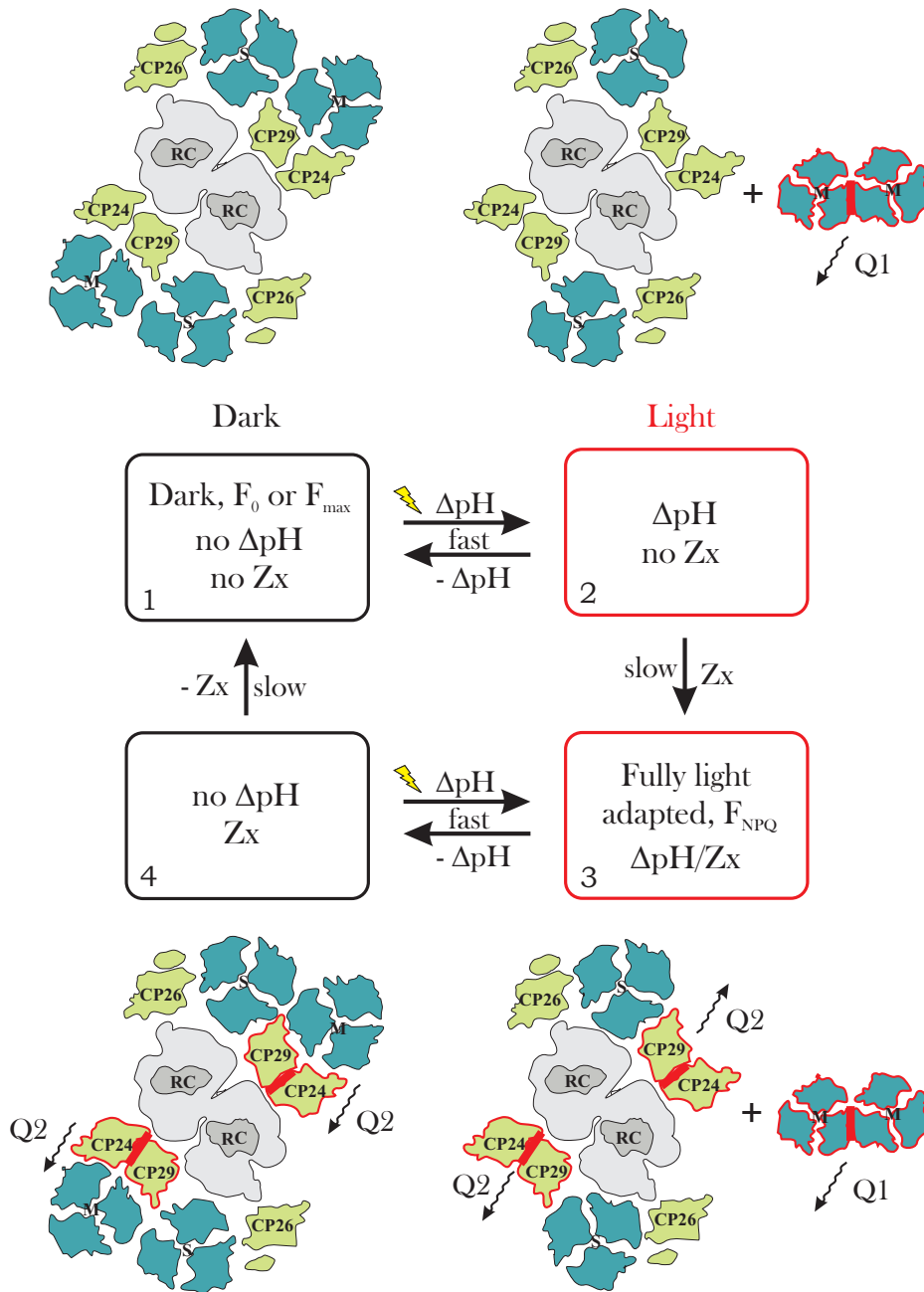


Figure 11.1: Overall scheme of the model of non-photochemical quenching mechanism in higher plants.

1. In the dark-adapted state (state 1) ΔpH is not generated across the thylakoid membrane and hence no conversion of V_x into Z_x occurs. This state corresponds to unquenched F_0 and F_{max} conditions. $C_2S_2M_2$ is the usual form of PS II supercomplexes in *Arabidopsis* plants under normal conditions (Dekker and Boekema 2005, Yakushevskaya et al. 2003)(Yakushevskaya et al. 2001).
2. Under light irradiation on a timescale of approximately 10 seconds, pH of the lumen decreases leading to protein conformational changes (Krause and Jahns 2004). The low pH activates the PsbS protein (Li et al. 2004), that according to our results medi-

ates detachment of LHC II from PS II and its oligomerization. The oligomerized complexes form Chl-Chl CT states through which the excitation energy rapidly dissipates. This is the Q1 site of NPQ active in state 2 in Figure 11.1. On this time scale Zx conversion is not yet involved. In higher plants the PsbS protein is mandatory for the light-induced antenna detachment.

3. Upon prolonged illumination, 10-30 min, additionally to Q1 site the thylakoid membrane the Vx are gets de-epoxidized. The state 3 corresponds to the F_{NPQ} state, investigated mostly in this thesis. The Zx-dependent quenching site (Q2) is located in the minor antenna complexes attached to PS II. Presence of Zx or CP24 is important for Q2.
4. The state 4 in the scheme represents the intermediate dark-adapted condition, in which the plants spend some seconds to minutes after the actinic light has stopped. At this point the transmembrane proton gradient has dissipated while the Zx amount has remained mostly unchanged. This state reflects the situation where the Q1 site of quenching (oligomerization of LHC II) is switched off while the Q2 site (Zx-dependent) is still active.

This model for the first time separates the action of PsbS and Zx. The two quenching sites can work independently from each other. One quenching site is detached peripheral major antenna LHC II oligomerization, the other – quenching in PS II-attached minor antenna.

The model is also absolutely valid for the description of NPQ in diatoms (Figure 10.12), however less information is at present available about the states 2 and 4. The Q1 site is managed by FCP subpopulation II that can detach and oligomerize like LHC II in higher plants. The Q2 site is another FCP subpopulation I that is closely attached to PS II and does not detach.

Hence, the NPQ mechanism seems to have a universal character. Within some differences the main mechanisms of quenching are preserved the same for diatoms as for higher plants.

REFERENCES

1. Adams, W.W., Demmig-Adams, B., Rosenstiel, T.N., and Ebbert, V. (2001) Dependence of photosynthesis and energy dissipation activity upon growth form and light environment during the winter. *Photosynth. Res.* 67: 51-62.
2. Ahn, T.K., Avenson, T.J., Ballottari, M., Cheng, Y.-C., Niyogi, K.K., Bassi, R., and Fleming, G.R. (2008) Architecture of a charge-transfer state regulating light harvesting in a plant antenna protein. *Science.* 320: 794-797.
3. Albertsson, P.-A. (2001) A quantitative model of the domain structure of the photosynthetic membrane. *Trends Plant Sci.* 6: 349-358.
4. Amunts, A., Drory, O., and Nelson, N. (2007) The structure of a plant photosystem I supercomplex at 3.4 Å resolution. *Nature.* 447: 58-63.
5. Andersson, J., Walters, R.G., Horton, P., and Jansson, S. (2001) Antisense inhibition of the photosynthetic antenna proteins CP29 and CP26: Implications for the mechanism of protective energy dissipation. *Plant Cell.* 13: 1193-1204.
6. Andersson, J., Wentworth, M., Walters, R.G., Howard, C.A., Ruban, A.V., Horton, P., and Jansson, S. (2003) Absence of the Lhcb1 and Lhcb2 proteins of the light-harvesting complex of photosystem II-effects on photosynthesis, grana stacking and fitness. *Plant J.* 35: 350-361.
7. Andrews, J.R., Fryer, M.J., and Baker, N.R. (1995) Consequences of LHC II deficiency for photosynthetic regulation in chlorina mutants of barley. *Photosynth. Res.* 44: 81-91.
8. Andrizhiyevskaya, E.G., Frolov, D., van Grondelle, R., and Dekker, J.P. (2004) On the role of the CP47 core antenna in the energy transfer and trapping dynamics of Photosystem II. *Phys. Chem. Chem. Phys.* 6: 4810-4819.
9. Armbrust, E.V., Berges, J.A., Bowler, C., Green, B.R., Martinez, D., Putnam, N.H., Zhou, S., Allen, A.E., Apt, K.E., Bechner, M., Brzezinski, M.A., Chaal, B.K., Chiovitti, A., Davis, A.K., Demarest, M.S., Detter, J.C., Glavina, T., Goodstein, D., Hadi, M.Z., Hellsten, U., Hildebrand, M., Jenkins, B.D., Jurka, J., Kapitonov, V.V., Kröger, N., Lau, W.W.Y., Lane, T.W., Larimer, F.W., Lippmeier, J.C., Lucas, S., Medina, M., Montsant, A., Obornik, M., Schnitzler-Parker, M., Palenik, B., Pazour, G.J., Richardson, P.M., Rynearson, T.A., Saito, M.A., Schwartz, D.C., Thamtrakoln, K., Valentin, K., Vardi, A., Wilkerson, F.P., and Rokhsar, D.S. (2004) The genome of the diatom *Thalassiosira Pseudonana*: Ecology, evolution, and metabolism. *Science.* 306: 79-86.
10. Aro, E.-M., Virgin, I., and Andersson, B. (1993) Photoinhibition of photosystem II. Inactivation, protein damage and turnover. *Biochim. Biophys. Acta.* 1143: 113-134.
11. Aro, E.M., Suorsa, M., Rokka, A., Allahverdiyeva, Y., Paakkarinen, V., Saleem, A., Battchikova, N., and Rintamaki, E. (2005) Dynamics of photosystem II: a proteomic approach to thylakoid protein complexes. *J. Exp. Bot.* 56: 347-356.
12. Avenson, T.J., Ahn, T.K., Zigmantas, D., Niyogi, K.K., Li, Z., Ballottari, M., Bassi, R., and Fleming, G.R. (2008) Zeaxanthin radical cation formation in minor light-harvesting complexes of higher plant antenna. *J. Biol. Chem.* 283: 3550-3558.

13. Barber, J. (1980) Membrane surface charges and potentials in relation to photosynthesis. *Biochim. Biophys. Acta.* 594: 253-308.
14. Barber, J. and Andersson, B. (1992) Too much of a good thing: light can be bad for photosynthesis. *Trends Biochem. Sci.* 17: 61-66.
15. Barber, J., Ferreira, K., Maghlaoui, K., and Iwata, S. (2004) Structural model of the oxygen-evolving centre of photosystem II with mechanistic implications. *Phys. Chem. Chem. Phys.* 6: 4737-4742.
16. Barber, J., Rhee, K.-H., Morris, E., Hankamer, B., Nield, J., Boekema, E., and Kühlbrandt, W. (1998) Towards the elucidation of the structure of photosystem II at high resolution. *Biophys. J.* 74: A328-A328.
17. Barzda, V., Garab, G., Gulbinas, V., and Valkunas, L. (1996) Evidence for long-range excitation energy migration in macroaggregates of the chlorophyll *a/b* light-harvesting antenna complexes. *Biochim. Biophys. Acta.* 1273: 231-236.
18. Barzda, V., Gulbinas, V., Kananavicius, R., Cervinskis, V., van Amerongen, H., van Grondelle, R., and Valkunas, L. (2001) Singlet-singlet annihilation kinetics in aggregates and trimers of LHCII. *Biophys. J.* 80: 2409-2421.
19. Bassi, R. and Caffarri, S. (2000) Lhc proteins and the regulation of photosynthetic light harvesting function by xanthophylls. *Photosynth. Res.* 64: 243-256.
20. Bassi, R., Pineau, B., Dainese, P., and Marquardt, J. (1993) Carotenoid-binding proteins of photosystem II. *Eur. J. Biochem.* 212: 297-303.
21. Bassi, R., Rigoni, F., Barbato, R., and Giacometti, G.M. (1988) Light-harvesting chlorophyll *a/b* proteins (LHCII) populations in phosphorylated membranes. *Biochim. Biophys. Acta.* 936: 29-38.
22. Beauregard, M., Martin, I., and Holzwarth, A.R. (1991) Kinetic modelling of exciton migration in photosynthetic systems. (1) Effects of pigment heterogeneity and antenna topography on exciton kinetics and charge separation yields. *Biochim. Biophys. Acta.* 1060: 271-283.
23. Becker, W. (2005) The bh TCSPC Handbook., Becker & Hickl GmbH, Berlin.
24. Berera, R., Herrero, C., van Stokkum, L.H.M., Vengris, M., Kodis, G., Palacios, R.E., van Amerongen, H., van Grondelle, R., Gust, D., Moore, T.A., Moore, A.L., and Kennis, J.T.M. (2006) A simple artificial light-harvesting dyad as a model for excess energy dissipation in oxygenic photosynthesis. *Proc. Natl. Acad. Sci. USA.* 103: 5343-5348.
25. Bergantino, E., Segalla, A., Brunetta, A., Teardo, E., Rigoni, F., Giacometti, G.M., and Szabó, I. (2003) Light- and pH-dependent structural changes in the PsbS subunit of photosystem II. *Proc. Natl. Acad. Sci. USA.* 100: 15265-15270.
26. Berthold, D.A., Babcock, G.T., and Yocum, C.F. (1981) A highly resolved, oxygen-evolving photosystem II preparation from spinach thylakoid membranes. EPR and electron-transport properties. *FEBS Lett.* 134: 231-234.
27. Bhaya, D. and Grossman, A.R. (1993) Characterization of gene clusters encoding the fucoxanthin chlorophyll proteins of the diatom *Phaeodactylum tricornutum*. *Nucleic Acids Res.* 21: 4458-4466.
28. Biesiadka, J., Loll, B., Kern, J., Irrgang, K.-D., and Zouni, A. (2004) Crystal structure of cyanobacterial photosystem II at 3.2 Å resolution: a closer look at the Mn-cluster. *Phys. Chem. Chem. Phys.* 6: 4733-4736.
29. Bilger, W. and Björkman, O. (1994) Relationships among violaxanthin deepoxidation, thylakoid membrane conformation, and nonphotochemical chlorophyll fluorescence quenching in leaves of cotton (*Gossypium hirsutum* L.). *Planta.* 193: 238-246.

References

30. Bittner, T., Irrgang, K.-D., Renger, G., and Wasielewski, M.R. (1994) Ultrafast excitation energy transfer and exciton-exciton annihilation processes in isolated light harvesting complexes of photosystem II (LHC II) from spinach. *J. Phys. Chem.* 98: 11821-11826.
31. Boekema, E.J., van Roon, H., Calkoen, F., Bassi, R., and Dekker, J.P. (1999a) Multiple types of association of photosystem II and its light-harvesting antenna in partially solubilized photosystem II membranes. *Biochemistry.* 38: 2233-2239.
32. Boekema, E.J., van Roon, H., van Breemen, J.F.L., and Dekker, J.P. (1999b) Supramolecular organization of photosystem II and its light-harvesting antenna in partially solubilized photosystem II membranes. *Eur. J. Biochem.* 266: 444-452.
33. Bonente, G., Howes, B.D., Caffarri, S., Smulevich, G., and Bassi, R. (2008) Interactions between the photosystem II subunit PsbS and xanthophylls studied *in vivo* and *in vitro*. *J. Biol. Chem.* 8434-8445.
34. Brackmann, U. (1986) *Lambdachrome Laser Dyes*, Lambda Physik GmbH, Goettingen.
35. Bratt, C.E., Arvidsson, P.-O., Carlsson, M., and Akerlund, H.-E. (1995) Regulation of violaxanthin de-epoxidase activity by pH and ascorbate concentration. *Photosynth. Res.* 45: 169-175.
36. Brettel, K. (1997) Electron transfer and arrangement of the redox cofactors in photosystem I. *Biochim. Biophys. Acta.* 1318: 322-373.
37. Broess, K., Trinkunas, G., van der Weij-de Wit, C.D., Dekker, J.P., van Hoek, A., and van Amerongen, H. (2006) Excitation energy transfer and charge separation in photosystem II membranes revisited. *Biophys. J.* 91: 3776-3786.
38. Brüggemann, B., Sznee, K., Novoderezhkin, V., van Grondelle, R., and May, V. (2004) From structure in dynamics: Modeling exciton dynamics in the photosynthetic antenna PS1. *J. Phys. Chem. B.* 108: 13536-13546.
39. Büchel, C. (2003) Fucoxanthin-chlorophyll proteins in diatoms: 18 and 19 kDa subunits assemble into different oligomeric states. *Biochemistry.* 42: 13027-13034.
40. Byrdin, M., Jordan, P., Krauss, N., Fromme, P., Stehlik, D., and Schlodder, E. (2002) Light harvesting in photosystem I: Modeling based on the 2.5Å-structure of photosystem I from *Synechococcus elongatus*. *Biophys. J.* 83: 433-457.
41. Caffarri, S., Croce, R., Breton, J., and Bassi, R. (2001) The major antenna complex of photosystem II has a xanthophyll binding site not involved in light harvesting. *J. Biol. Chem.* 276: 35924-35933.
42. Caffarri, S., Passarini, F., Bassi, R., and Croce, R. (2007) A specific binding site for neoxanthin in the monomeric antenna proteins CP26 and CP29 of Photosystem II. *FEBS Lett.* 581: 4704-4710.
43. Cinque, G., Croce, R., Holzwarth, A.R., and Bassi, R. (2000) Energy transfer among CP29 chlorophylls: Calculated Förster rates and experimental transient absorption at room temperature. *Biophys. J.* 79: 1706-1717.
44. Connelly, J.P., Müller, M.G., Bassi, R., Croce, R., and Holzwarth, A.R. (1997a) Femtosecond transient absorption study of carotenoid to chlorophyll energy transfer in the light harvesting complex II of photosystem II. *Biochemistry.* 36: 281-287.
45. Connelly, J.P., Müller, M.G., Hucke, M., Gatzert, G., Mullineaux, C.W., Ruban, A.V., Horton, P., and Holzwarth, A.R. (1997b) Ultrafast spectroscopy of trimeric light harvesting complex II from higher plants. *J. Phys. Chem. B.* 101: 1902-1909.
46. Crimi, M., Dorra, D., Bösinger, C.S., Giuffra, E., Bassi, R., and Holzwarth, A.R. (1998) Zeaxanthin-induced fluorescence quenching in the minor antenna CP29. In: (Garab, G., Ed.) *Photosynthesis*:

- Mechanism and Effects / XI. Int. Congr. Photosynthesis Budapest 1998. Kluwer Academic Publishers, Dordrecht, pp. 333-336.
47. Crimi, M., Dorra, D., Bösinger, C.S., Giuffra, E., Holzwarth, A.R., and Bassi, R. (2001) Time-resolved fluorescence analysis of the recombinant photosystem II antenna complex CP29. Effects of zeaxanthin, pH and phosphorylation. *Eur. J. Biochem.* 268: 260-267.
 48. Croce, R., Canino, G., Ros, F., and Bassi, R. (2002) Chromophore organization in the higher-plant photosystem II antenna protein CP26. *Biochemistry* . 41: 7334-7343.
 49. Croce, R., Chojnicka, A., Morosinotto, T., Ihalainen, J.A., van Mourik, F., Dekker, J.P., Bassi, R., and van Grondelle, R. (2007) The low-energy forms of photosystem I light-harvesting complexes: Spectroscopic properties and pigment-pigment interaction characteristics. *Biophys. J.* 93: 2418-2428.
 50. Croce, R., Morosinotto, T., and Bassi, R. (2006) LHCI: The antenna complex of photosystem I in plants and green algae. In: (Golbeck, J.H., Ed.) *Advances in Photosynthesis and Respiration Vol.24: Photosystem I: The Light-Driven Plastocyanin: Ferredoxin Oxidoreductase*. Springer, Dordrecht, pp. 119-137.
 51. Croce, R., Müller, M.G., Bassi, R., and Holzwarth, A.R. (2001) Carotenoid-to-chlorophyll energy transfer in recombinant major light-harvesting complex (LHC II) of higher plants. I. Femtosecond transient absorption measurements. *Biophys. J.* 80: 901-915.
 52. Croce, R., Müller, M.G., Bassi, R., and Holzwarth, A.R. (2003a) Chlorophyll *b* to Chlorophyll *a* energy transfer kinetics in the CP29 antenna complex: A comparative femtosecond absorption study between native and reconstituted proteins. *Biophys. J.* 84: 2508-2516.
 53. Croce, R., Müller, M.G., Caffarri, S., Bassi, R., and Holzwarth, A.R. (2003b) Energy transfer pathways in the minor antenna complex CP29 of photosystem II: A femtosecond study of carotenoid to chlorophyll transfer on mutant and WT complexes. *Biophys. J.* 84: 2517-2532.
 54. Croce, R., Remelli, R., Varotto, C., Breton, J., and Bassi, R. (1999a) The neoxanthin binding site of the major light harvesting complex (LHC II) from higher plants. *FEBS Lett.* 456: 1-6.
 55. Croce, R., Weiss, S., and Bassi, R. (1999b) Carotenoid-binding sites of the major light-harvesting complex II of higher plants. *J. Biol. Chem.* 274: 29613-29623.
 56. Crofts, A.R. and Yerkes, C.T. (1994) A molecular mechanism for q_E -quenching. *FEBS Lett.* 352: 265-270.
 57. Crouchman, S., Ruban, A.V., and Horton, P. (2006) PsbS enhances nonphotochemical fluorescence quenching in the absence of zeaxanthin. *FEBS Lett.* 580: 2053-2058.
 58. Dall'Osto, L., Caffarri, S., and Bassi, R. (2005) A mechanism of nonphotochemical energy dissipation, independent from PsbS, revealed by a conformational change in the antenna protein CP26. *Plant Cell.* 17: 1217-1232.
 59. Damjanovic, A., Vaswani, H., Fromme, P., and Fleming, G.R. (2002) Chlorophyll excitations in photosystem I of *Synechococcus elongatus*. *J. Phys. Chem. B.* 106: 10251-10262.
 60. Danielius, R.V., Satoh, K., van Kan, P.J.M., Plijter, J.J., Nuijs, A.M., and van Gorkom, H.J. (1987) The primary reaction of photosystem II in the D1-D2 cytochrome *b*-559 complex. *FEBS Lett.* 213: 241-244.
 61. Danielsson, R., Albertsson, P.A., Mamedov, F., and Styring, S. (2004) Quantification of photosystem I and II in different parts of the thylakoid membrane from spinach. *Biochim. Biophys. Acta.* 1608: 53-61.

References

62. Danielsson, R., Suorsa, M., Paakkarinen, V., Albertsson, P.-A., Styring, S., Aro, E.-M., and Mamedov, F. (2006) Dimeric and monomeric organization of photosystem II. Distribution of five distinct complexes in the different domains of the thylakoid membrane. *J. Biol. Chem.* 281: 14241-14249.
63. Dau, H. and Sauer, K. (1996) Exciton equilibration and Photosystem II exciton dynamics - a fluorescence study on Photosystem II membrane particles of spinach. *Biochim. Biophys. Acta.* 1273: 175-190.
64. de Bianchi, S., Dall'Osto, L., Tognon, G., Morosinotto, T., and Bassi, R. (2008) Minor antenna proteins CP24 and CP26 affect the interactions between photosystem II subunits and the electron transport rate in grana membranes of *Arabidopsis*. *Plant Cell.* 20: 1012-1028.
65. de Weerd, F.L., van Stokkum, I.H.M., van Amerongen, H., Dekker, J.P., and van Grondelle, R. (2002) Pathways for energy transfer in the core light-harvesting complexes CP43 and CP47 of photosystem II. *Biophys. J.* 82: 1586-1597.
66. Dekker, J.P. and Boekema, E.J. (2005) Supramolecular organization of thylakoid membrane proteins in green plants. *Biochim. Biophys. Acta.* 1706: 12-39.
67. Dekker, J.P. and van Grondelle, R. (2000) Primary charge separation in Photosystem II. *Photosynth. Res.* 63: 195-208.
68. DeLano, W.L. and Lam, J.W. (2005) PyMOL: A communications tool for computational models. *Abstracts of Papers Am. Chem. Soc.* 230: 254
69. Demmig-Adams, B. (1990) Carotenoids and photoprotection in plants: A role for the xanthophyll zeaxanthin. *Biochim. Biophys. Acta.* 1020: 1-24.
70. Demmig-Adams, B. and Adams, W.W. (1996) The role of xanthophyll cycle carotenoids in the protection of photosynthesis. *Trends Plant Sci.* 1: 21-26.
71. Demmig-Adams, B., Gilmore, A.M., and Adams, W.W. (1996) Carotenoids .3. *In vivo* functions of carotenoids in higher plants. *FASEB J.* 10: 403-412.
72. Durrant, J.R., Klug, D.R., Kwa, S.L., van Grondelle, R., Porter, G., and Dekker, J.P. (1995) A multimer model for P680, the primary electron donor of photosystem II. *Proc. Natl. Acad. Sci. USA.* 92: 4798-4802.
73. Engelmann, E.C.M., Zucchelli, G., Garlaschi, F.M., Casazza, A.P., and Jennings, R.C. (2005) The effect of outer antenna complexes on the photochemical trapping rate in barley thylakoid Photosystem II. *Biochim. Biophys. Acta.* 1706: 276-286.
74. Eppard, M. and Rhiel, E. (1998) The genes encoding light-harvesting subunits of *Cyclotella cryptica* (Bacillariophyceae) constitute a complex and heterogeneous family. *Mol. Gen. Genet.* 260: 335-345.
75. Falkowski, P.G. and Raven, J.A. (1997) Aquatic photosynthesis, Blackwell Science Publishers, Malden, USA.
76. Färber, A., Young, A.J., Ruban, A.V., Horton, P., and Jahns, P. (1997) Dynamics of xanthophyll-cycle activity in different antenna subcomplexes in the photosynthetic membranes of higher plants. *Plant Physiol.* 115: 1609- 1618.
77. Ferreira, K.N., Iverson, T.M., Maghlaoui, K., Barber, J., and Iwata, S. (2004) Architecture of the photosynthetic oxygen-evolving center. *Science.* 303: 1831-1838.
78. Finazzi, G., Johnson, G.N., Dall'Osto, L., Joliot, P., Wollman, F.A., and Bassi, R. (2004) A zeaxanthin-independent nonphotochemical quenching mechanism localized in the photosystem II core complex. *Proc. Natl. Acad. Sci. USA.* 101: 12375-12380.

79. Frank, H.A., Cua, A., Chynwat, V., Young, A., Gosztola, D., and Wasielewski, M.R. (1994) Photophysics of the carotenoids associated with the xanthophyll cycle in photosynthesis. *Photosynth. Res.* 41: 389-395.
80. Frese, R.N., Palacios, M.A., Azzizi, A., van Stokkum, I.H.M., Kruij, J., Rögner, M., Karapetyan, N.V., Schlodder, E., van Grondelle, R., and Dekker, J.P. (2002) Electric field effects on red chlorophylls, beta-carotenes and P700 in cyanobacterial Photosystem I complexes. *Biochim. Biophys. Acta.* 1554: 180-191.
81. Gadjieva, R., Mamedov, F., and Albertsson, P.-A. (1999) Fractionation of the thylakoid membranes from tobacco. A tentative isolation of 'end membrane' and purified 'stroma lamellae' membranes. *Biochim. Biophys. Acta.* 1411: 92-100.
82. Gatzert, G., Müller, M.G., Griebenow, K., and Holzwarth, A.R. (1996) Primary processes and structure of the photosystem II reaction center: 3. Kinetic analysis of picosecond energy transfer and charge separation processes in the D1-D2-cyt-b₅₅₉ complex measured by time-resolved fluorescence. *J. Phys. Chem.* 100: 7269-7278.
83. Gillbro, T., Sandström, A., Spangfort, M., Sundström, V., and van Grondelle, R. (1988) Excitation energy annihilation in aggregates of chlorophyll *a/b* complexes. *Biochim. Biophys. Acta.* 934: 369-374.
84. Gilmore, A.M., Hazlett, T.L., Debrunner, P.G., and Govindjee (1996) Photosystem II chlorophyll *a* fluorescence lifetimes and intensity are independent of the antenna size differences between barley wild-type and chlorina mutants: Photochemical quenching and xanthophyll cycle-dependent nonphotochemical quenching of fluorescence. *Photosynth. Res.* 48: 171-187 .
85. Gilmore, A.M., Hazlett, T.L., and Govindjee (1995) Xanthophyll cycle-dependent quenching of photosystem II chlorophyll *a* fluorescence: Formation of a quenching complex with a short fluorescence lifetime. *Proc. Natl. Acad. Sci. USA.* 92: 2273-2277.
86. Gilmore, A.M., Shinkarev, V.P., Hazlett, T.L., and Govindjee (1998) Quantitative analysis of the effects of intrathylakoid pH and xanthophyll cycle pigments on chlorophyll *a* fluorescence lifetime distributions and intensity in thylakoids. *Biochemistry.* 37: 13582-13593.
87. Gilmore, A.M. and Yamamoto, H.Y. (1991) Zeaxanthin formation and energy-dependent fluorescence quenching in pea chloroplasts under artificially mediated linear and cyclic electron transport. *Plant Physiol.* 96: 635-643.
88. Gilmore, A.M. and Yamamoto, H.Y. (1992) Dark induction of zeaxanthin-dependent nonphotochemical fluorescence quenching mediated by ATP. *Proc. Natl. Acad. Sci. USA.* 89: 1899-1903.
89. Gilmore, A.M. and Yamamoto, H.Y. (1993) Linear models relating xanthophylls and lumen acidity to non-photochemical fluorescence quenching. Evidence that antheraxanthin explains zeaxanthin-independent quenching. *Photosynth. Res.* 35: 67-78.
90. Gobets, B. and van Grondelle, R. (2001) Energy transfer and trapping in photosystem I. *Biochim. Biophys. Acta.* 1507: 80-99 .
91. Gobets, B., van Stokkum, I.H.M., van Mourik, F., Dekker, J.P., and van Grondelle, R. (2003) Excitation wavelength dependence of the fluorescence kinetics in Photosystem I particles from *Synechocystis* PCC 6803 and *Synechococcus elongatus*. *Biophys. J.* 85: 3883-3898.

References

92. Goss, R., Lohr, M., Latowski, D., Grzyb, J., Vieler, A., Wilhelm, C., and Strzalka, K. (2005) Role of hexagonal structure-forming lipids in diadinoxanthin and violaxanthin solubilization and de-epoxidation. *Biochemistry*. 44: 4028-4036.
93. Goss, R., Pinto, E.A., Wilhelm, C., and Richter, M. (2006) The importance of a highly active and Δ pH-regulated diatoxanthin epoxidase for the regulation of the PSII antenna function in diadinoxanthin cycle containing algae. *J. Plant Physiol.* 163: 1008-1021.
94. Gradinaru, C.C., Pascal, A.A., van Mourik, F., Robert, B., Horton, P., van Grondelle, R., and van Amerongen, H. (1998) Ultrafast evolution of the excited states in the chlorophyll *a/b* complex CP29 from green plants studied by energy-selective pump-probe spectroscopy. *Biochemistry*. 37: 1143-1149.
95. Gradinaru, C.C., van Stokkum, I.H.M., Pascal, A.A., van Grondelle, R., and van Amerongen, H. (2000) Identifying the pathways of energy transfer between carotenoids and chlorophylls in LHCII and CP29. A multicolor, femtosecond pump-probe study. *J. Phys. Chem. B*. 104: 9330-9342.
96. Graßes, T., Pesaresi, P., Schiavon, F., Varotto, C., Salamini, F., Jahns, P., and Leister, D. (2002) The role of Δ pH-dependent dissipation of excitation energy in protecting photosystem II against light-induced damage in *Arabidopsis thaliana*. *Plant Physiol. Biochem.* 40: 41-49.
97. Green, B.R. and Pichersky, E. (1994) Hypothesis for the evolution of three-helix Chl *a/b* and Chl *a/c* light-harvesting antenna proteins from two-helix and four-helix ancestors. *Photosynth. Res.* 39: 149-162.
98. Grinvald, A. and Steinberg, I.Z. (1974) On the analysis of fluorescence decay kinetics by the method of least-squares. *Anal. Biochem.* 59: 583-598.
99. Groot, M.-L., Frese, R.N., de Weerd, F.L., Bromek, K., Pettersson, A., Peterman, E.J.G., van Stokkum, I.H.M., van Grondelle, R., and Dekker, J.P. (1999) Spectroscopic properties of the CP43 core antenna protein of photosystem II. *Biophys. J.* 77: 3328-3340.
100. Groot, M.-L., Peterman, E.J.G., van Stokkum, I.H.M., Dekker, J.P., and van Grondelle, R. (1995) Triplet and fluorescing states of the CP47 antenna complex of photosystem II studied as a function of temperature. *Biophys. J.* 68: 281-290.
101. Grouneva, I., Jakob, T., Wilhelm, C., and Goss, R. (2008) Evidence for the existence of a fast xanthophyll cycle-independent NPQ component in diatoms. In: (Allen, J.F., Gantt, E., Golbeck, J.H., and Osmond, B., Eds.) *Photosynthesis. Energy From the Sun: 14th Int. Congr. on Photosynthesis*. Springer, pp. 1019-1022.
102. Guillard, R.R.L. and Lorenzen, C.J. (1972) Yellow-green algae with chlorophyllide C. *Journal of Phycology*. 8: 10-14.
103. Gundermann, K. and Büchel, C. (2008) The fluorescence yield of the trimeric fucoxanthin–chlorophyll–protein FCPa in the diatom *Cyclotella meneghiniana* is dependent on the amount of bound diatoxanthin. *Photosynth. Res.* 95: 229-235.
104. Haehnel, W., Nairn, J.A., and Sauer, K. (1981) Fluorescence lifetimes of *in vivo* chlorophyll studied in chloroplasts and algae. *J. Luminesc.* 24: 795-798.
105. Hager, A. (1969) Light dependent decrease of the pH-value in a chloroplast compartment causing the enzymatic interconversion of violaxanthin to zeaxanthin; Relations to photophosphorylation. *Planta*. 89: 224-243.

106. Hager, A. and Holocher, K. (1994) Localization of the xanthophyll-cycle enzyme violaxanthin de-epoxidase within the thylakoid lumen and abolition of its mobility by a (light-dependent) pH decrease. *Planta*. 192: 581- 589.
107. Hager, A. and Stransky, H. (1970a) Das Carotinoidmuster und die Verbreitung des lichtinduzierten Xanthophyllcyclus in verschiedenen Algenklassen. *Arch. Microbiol.* 72: 68-83.
108. Hager, A. and Stransky, H. (1970b) Das Carotinoidmuster und die Verbreitung des lichtinduzierten Xanthophyllcyclus in verschiedenen Algenklassen. *Arch. Microbiol.* 73: 77-89.
109. Hemenger, R.P., Pearlstein, R.M., and Lakatos-Lindenberg, K. (1972) Incoherent exciton quenching on lattices. *J. Math. Phys.* 13: 1056-1063.
110. Holt, N.E., Fleming, G.R., and Niyogi, K.K. (2004) Toward an understanding of the mechanism of nonphotochemical quenching in green plants. *Biochemistry*. 43: 8281-8289.
111. Holt, N.E., Zigmantas, D., Valkunas, L., Li, X.-P., Niyogi, K.K., and Fleming, G.R. (2005) Carotenoid cation formation and the regulation of photosynthetic light harvesting. *Science*. 307: 433-436.
112. Holzwarth, A.R. (1988) Time resolved chlorophyll fluorescence. What kind of information on photosynthetic systems does it provide? In: (Lichtenthaler, H.K., Ed.) Applications of Chlorophyll Fluorescence. Kluwer Academic, Dordrecht, pp. 21-31.
113. Holzwarth, A.R. (1991) Excited-state kinetics in chlorophyll systems and its relationship to the functional organization of the photosystems. In: (Scheer, H., Ed.) Chlorophylls. CRC Press, Boca Raton, pp. 1125-1151.
114. Holzwarth, A.R. (1995) Time-resolved fluorescence spectroscopy. In: (Sauer, K., Ed.) Methods in Enzymology. Vol.246 Biochemical Spectroscopy. Academic Press, San Diego, pp. 334-362.
115. Holzwarth, A.R. (1996) Data analysis of time-resolved measurements. In: (Amesz, J. and Hoff, A.J., Eds.) Biophysical Techniques in Photosynthesis. Advances in Photosynthesis Research. Kluwer Academic Publishers, Dordrecht, pp. 75-92.
116. Holzwarth, A.R. (2004) Light absorption and harvesting. In: (Archer, M.D. and Barber, J., Eds.) Photoconversion of Solar Energy Vol. 2: Molecular to Global Photosynthesis. Imperial College Press, London, pp. 43-115.
117. Holzwarth, A.R. (2008) Ultrafast primary reactions in the photosystems of oxygen evolving organisms. In: (Braun, M., Gilch, P., and Zinth, W., Eds.) Biological and Medical Physics, Biomedical Engineering: Ultrashort Laser Pulses in Biology and Medicine. Springer, Dordrecht, pp. 141-164.
118. Holzwarth, A.R., Haehnel, W., Ratajczak, R., Bittersmann, E., and Schatz, G.H. (1990) Energy transfer kinetics in photosystem I particles isolated from *Synechococcus sp.* and from higher plants. In: (Baltshchiffsky, M., Ed.) Current Research in Photosynthesis. II. Kluwer Academic Publishers, Dordrecht, pp. 611-614.
119. Holzwarth, A.R., Müller, M.G., Niklas, J., and Lubitz, W. (2005) Charge recombination fluorescence in photosystem I reaction centers from *Chlamydomonas reinhardtii*. *J. Phys. Chem. B*. 109: 5903-5911.
120. Holzwarth, A.R., Müller, M.G., Niklas, J., and Lubitz, W. (2006a) Ultrafast transient absorption studies on photosystem I reaction centers from *Chlamydomonas reinhardtii*. 2. Mutations around the P700 reaction center chlorophylls provide new insight into the nature of the primary electron donor. *Biophys. J.* 90: 552-565.
121. Holzwarth, A.R., Müller, M.G., Reus, M., Nowaczyk, M., Sander, J., and Rögner, M. (2006b) Kinetics and mechanism of electron transfer in intact photosystem II and in the isolated reaction center: Pheophytin is the primary electron acceptor. *Proc. Natl. Acad. Sci. USA*. 103: 6895-6900.

References

122. Holzwarth, A.R., Wendler, J., and Haehnel, W. (1985) Time-resolved picosecond fluorescence spectra of the antenna chlorophylls in *Chlorella vulgaris*. Resolution of photosystem I fluorescence. *Biochim. Biophys. Acta.* 807: 155-167.
123. Horton, P. (1996) Nonphotochemical quenching of chlorophyll fluorescence. In: (Jennings, R.C., Ed.) Light As an Energy Source and Information Carrier in Plant Physiology. New York, Plenum Press, pp. 99-111.
124. Horton, P. and Ruban, A.V. (1992) Regulation of photosystem II. *Photosynth. Res.* 34: 375-385.
125. Horton, P. and Ruban, A.V. (1999) Regulation of the structure and function of the light harvesting complexes of photosystem II by the Xanthophyll cycle. In: (Frank, H.A., Young, A.J., Britton, G., and Cogdell, R.J., Eds.) Advances in Photosynthesis Vol.8: The Photochemistry of Carotenoids. Kluwer Academic Publishers, Dordrecht, pp. 271-291.
126. Horton, P. and Ruban, A.V. (2005) Molecular design of the photosystem II light-harvesting antenna: Photosynthesis and photoprotection. *J. Exp. Bot.* 56: 365-373.
127. Horton, P., Ruban, A.V., Rees, D., Pascal, A.A., Noctor, G., and Young, A.J. (1991) Control of the light-harvesting function of chloroplast membranes by aggregation of the LHCII chlorophyll-protein complex. *FEBS Lett.* 292: 1-4.
128. Horton, P., Ruban, A.V., and Walters, R.G. (1996) Regulation of light harvesting in green plants. *Annu. Rev. Plant Physiol. Plant Mol. Biol.* 47: 655-684.
129. Horton, P., Wentworth, M., and Ruban, A.V. (2005) Control of the light harvesting function of chloroplast membranes: The LHCII-aggregation model for non-photochemical quenching. *FEBS Lett.* 579: 4201-4206.
130. Ide, J.P., Klug, D.R., Kühlbrandt, W., Giorgi, L.B., and Porter, G. (1987) The state of detergent solubilised light-harvesting chlorophyll- *a/b* protein complex as monitored by picosecond time-resolved fluorescence and circular dichroism. *Biochim. Biophys. Acta.* 893: 349- 364.
131. Ihalainen, J.A., Croce, R., Morosinotto, T., van Stokkum, I.H.M., Bassi, R., Dekker, J.P., and van Grondelle, R. (2005a) Excitation decay pathways of Lhca proteins: A time-resolved fluorescence study. *J. Phys. Chem. B.* 109: 21150-21158.
132. Ihalainen, J.A., Rätsep, M., Jensen, P.E., Scheller, H.V., Croce, R., Bassi, R., Korppi-Tommola, J.E.I., and Freiberg, A. (2003) Red spectral forms of chlorophylls in green plant PSI - a site-selective and high-pressure spectroscopy study. *J. Phys. Chem. B.* 107: 9086-9093.
133. Ihalainen, J.A., van Stokkum, I.H.M., Gibasiewicz, K., Germano, M., van Grondelle, R., and Dekker, J.P. (2005b) Kinetics of excitation trapping in intact photosystem I of *Chlamydomonas reinhardtii* and *Arabidopsis thaliana*. *Biochim. Biophys. Acta.* 1706: 267-275.
134. Ivanov, A.G., Hurry, V., Sane, P.V., Öquist, G., and Hüner, N.P.A. (2008) Reaction centre quenching of excess light energy and photoprotection of photosystem II. *Journal of Plant Biology.* 51: 85-96.
135. Jahns, P., Graf, M., Munekage, Y., and Shikanai, T. (2002) Single point mutation in the Rieske iron-sulfur subunit of cytochrome *b₆/f* leads to an altered pH dependence of plastoquinol oxidation in *Arabidopsis*. *FEBS Lett.* 519: 99-102.
136. Jakob, T., Goss, R., and Wilhelm, C. (2001) Unusual pH-dependence of diadinoxanthin de-epoxidase activation causes chlororespiratory induced accumulation of diatoxanthin in the diatom *Phaeodactylum tricorutum*. *J. Plant Physiol.* 158: 383-390.

137. Jansson, S. (1999) A guide to the Lhc genes and their relatives in Arabidopsis. *Trends Plant Sci.* 4: 236-240.
138. Jansson, S., Stefansson, H., Nyström, U., Gustafsson, P., and Albertsson, P.-A. (1997) Antenna protein composition of PS I and PS II in thylakoid sub-domains. *Biochim. Biophys. Acta.* 1320: 297-309.
139. Jennings, R.C., Croce, R., Dorra, D., Garlaschi, F.M., Holzwarth, A.R., Rivadossi, A., and Zucchelli, G. (1998) Photosystem I red spectral forms: Diffusion limited energy transfer, optical reorganisation energy and absorption cross section. In: (Garab, G., Ed.) *Photosynthesis: Mechanism and Effects*. Kluwer Academic Publishers, Dordrecht, pp. 271-276.
140. Jennings, R.C., Elli, G., Garlaschi, F.M., Santabarbara, S., and Zucchelli, G. (2000) Selective quenching of the fluorescence of core chlorophyll-protein complexes by photochemistry indicates that Photosystem II is partly diffusion limited. *Photosynth. Res.* 66 : 225-233.
141. Jolley, C., Ben-Shem, A., Nelson, N., and Fromme, P. (2005) Structure of plant photosystem I revealed by theoretical modeling. *J. Biol. Chem.* in press: 1-25.
142. Jordan, P., Fromme, P., Witt, H.T., Klukas, O., Saenger, W., and Krauß, N. (2001) Three-dimensional structure of cyanobacterial photosystem I at 2.5Å resolution. *Nature.* 411: 909-917.
143. Junesch, U. and Gräber, P. (1991) The rate of ATP-synthesis as a function of Δ -pH and $\Delta\psi$ catalyzed by the active, reduced H⁺-ATPase from chloroplasts. *FEBS.* 294: 275-278.
144. Kalituho, L., Rech, J., and Jahns, P. (2007) The roles of specific xanthophylls in light utilization. *Planta.* 225: 423-439.
145. Kamiya, N. and Shen, J.-R. (2003) Crystal structure of oxygen-evolving photosystem II from *Thermosynechococcus vulcanus* at 3.7-Å resolution. *Proc. Natl. Acad. Sci. USA.* 100: 98-103.
146. Karapetyan, N.V., Holzwarth, A.R., and Rögner, M. (1999) The photosystem I trimer of cyanobacteria: Molecular organisation, excitation dynamics and physiological significance. *FEBS Lett.* 460: 395-400.
147. Kim, S., Pichersky, E., and Yocum, C.F. (1994) Topological studies of spinach 22 kDa protein of photosystem II. *Biochim. Biophys. Acta.* 1188: 339-348.
148. Kiss, A.Z., Ruban, A.V., and Horton, P. (2008) The PsbS protein controls the organisation of the photosystem II antenna in higher plant thylakoid membranes. *J. Biol. Chem.* 283: 3972-3978.
149. Kleima, F.J., Gradinaru, C.C., Calkoen, F., van Stokkum, I.H.M., van Grondelle, R., and van Amerongen, H. (1997) Energy transfer in LHCII monomers at 77K studied by sub-picosecond transient absorption spectroscopy. *Biochemistry.* 36: 15262-15268.
150. Kovács, L., Damkjaer, J., Kereiche, S., Illoaia, C., Ruban, A.V., Boekema, E.J., Jansson, S., and Horton, P. (2006) Lack of the light-harvesting complex CP24 affects the structure and function of the grana membranes of higher plant chloroplasts. *Plant Cell.* 18: 3106-3120.
151. Kramer, D.M., Cruz, J.A., and Kanazawa, A. (2003) Balancing the central roles of the thylakoid proton gradient. *Trends Plant Sci.* 8: 27-32.
152. Krause, G.H. (1988) Photoinhibition of photosynthesis. An evaluation of damaging and protective mechanisms. *Physiol. Plant.* 74: 566-574.
153. Krause, G.H. and Jahns, P. (2004) Non-photochemical energy dissipation determined by chlorophyll fluorescence quenching: Characterization and function. In: (Papageorgiou, G.C. and Govindjee, Eds.) *Advances in Photosynthesis and Respiration Vol.19: Chlorophyll a Fluorescence: A Signature of Photosynthesis*. Springer, Dordrecht, pp. 463-495.

References

154. Krieger, A., Moya, I., and Weis, E. (1992) Energy-dependent quenching of chlorophyll *a* fluorescence: Effect of pH on stationary fluorescence and picosecond relaxation kinetics in thylakoid membranes and photosystem II preparations. *Biochim. Biophys. Acta.* 1102: 167-176.
155. Kuhl, H., Kruip, J., Seidler, A., Krieger-Liszkay, A., Bunker, M., Bald, D., Scheidig, A.J., and Rögner, M. (2000) Towards structural determination of the water-splitting enzyme-Purification, crystallization, and preliminary crystallographic studies of photosystem II from a thermophilic cyanobacterium. *J. Biol. Chem.* 275: 20652-20659.
156. Kühlbrandt, W. (1994) Structure and function of the plant light-harvesting complex, LHC II. *Curr. Opin. Struct. Biol.* 4: 519-528.
157. Külheim, C., Agren, J., and Jansson, S. (2002) Rapid regulation of light harvesting and plant fitness in the field. *Science.* 297: 91-93.
158. Laible, P.D., Zipfel, W., and Owens, T.G. (1994) Excited state dynamics in chlorophyll-based antennae: The role of transfer equilibrium. *Biophys. J.* 66: 844-860.
159. Lambrev, P., Várkonyi, Z., Krumova, S., Kovács, L., Miloslavina, Y., Holzwarth, A.R., and Garab, G. (2007) Importance of trimer-trimer interactions for the native state of the plant light-harvesting complex II. *Biochim. Biophys. Acta.* 1767: 847-853.
160. Lavaud, J. and Kroth, P.G. (2006) In diatoms, the transthylakoid proton gradient regulates the photoprotective non-photochemical fluorescence quenching beyond its control on the xanthophyll cycle. *Plant Cell Physiol.* 47: 1010-1016.
161. Lavaud, J., Rousseau, B., and Etienne, A.L. (2003) Enrichment of the light-harvesting complex in diadinoxanthin and implications for the nonphotochemical fluorescence quenching in diatoms. *Biochemistry.* 42: 5802-5808.
162. Lavaud, J., Rousseau, B., van Gorkom, H.J., and Etienne, A.L. (2002) Influence of the diadinoxanthin pool size on photoprotection in the marine planktonic diatom *phaeodactylum tricornutum*. *Plant Physiol.* 129: 1398-1406.
163. Lavergne, J. and Trissl, H.-W. (1995) Theory of fluorescence induction in Photosystem II: Derivation of analytical expressions in a model including exciton-radical- pair equilibrium and restricted energy transfer between photosynthetic units. *Biophys. J.* 68: 2474-2492.
164. Lepetit, B., Volke, D., Szabó, M., Hoffmann, R., Garab, G., Wilhelm, C., and Goss, R. (2007) Spectroscopic and molecular characterization of the oligomeric antenna of the diatom *Phaeodactylum tricornutum*. *Biochemistry.* 46: 9813-9822.
165. Lepetit, B., Volke, D., Szabó, M., Hoffmann, R., Garab, G., Wilhelm, C., and Goss, R. (2008) The oligomeric antenna of the diatom *P. tricornutum*-localization of diadinoxanthin cycle pigments. In: (Allen, J.F., Gantt, E., Golbeck, J.H., and Osmond, B., Eds.) *Photosynthesis. Energy From the Sun.* Springer, pp. 277-280.
166. Li, X.-P., Björkman, O., Shih, C., Grossman, A.R., Rosenquist, M., Jansson, S., and Niyogi, K.K. (2000) A pigment-binding protein essential for regulation of photosynthetic light harvesting. *Nature.* 403: 391-395.
167. Li, X.-P., Gilmore, A.M., Caffarri, S., Bassi, R., Golan, T., Kramer, D., and Niyogi, K.K. (2004) Regulation of photosynthetic light harvesting involves intrathylakoid lumen pH sensing by the PsbS protein. *J. Biol. Chem.* 279: 22866-22874.

168. Li, X.-P., Müller-Moule, P., Gilmore, A.M., and Niyogi, K.K. (2002a) PsbS-dependent enhancement of feedback de-excitation protects photosystem II from photoinhibition. *Proc. Natl. Acad. Sci. USA*. 99 : 15222-15227.
169. Li, X.P., Gilmore, A.M., and Niyogi, K.K. (2002b) Molecular and global time-resolved analysis of a psbS gene dosage effect on pH- and xanthophyll cycle-dependent nonphotochemical quenching in photosystem II. *J. Biol. Chem.* 277: 33590-33597.
170. Liu, Z., Yan, H., Wang, K., Kuang, T., Zhang, J., Gui, L., An, X., and Chang, W. (2004) Crystal structure of spinach major light-harvesting complex at 2.72 angstrom resolution. *Nature*. 428: 287-292.
171. Lohr, M. and Wilhelm, C. (1999) Algae displaying the diadinoxanthin cycle also possess the violaxanthin cycle. *Proc. Natl. Acad. Sci. USA*. 96: 8784-8789.
172. Lohr, M. and Wilhelm, C. (2001) Xanthophyll synthesis in diatoms: quantification of putative intermediates and comparison of pigment conversion kinetics with rate constants derived from a model. *Planta*. 212: 382-391.
173. Loll, B., Kern, J., Saenger, W., Zouni, A., and Biesiadka, J. (2005a) Towards complete cofactor arrangement in the 3.0 angstrom resolution structure of photosystem II. *Nature*. 438 : 1040-1044.
174. Loll, B., Kern, J., Zouni, A., Saenger, W., Biesiadka, J., and Irrgang, K.-D. (2005b) The antenna system of photosystem II from *Thermosynechococcus elongatus* at 3.2 Å resolution. *Photosynth. Res.* 86: 175-184.
175. Lyle, P.A., Kolaczowski, S.V., and Small, G.J. (1993) Photochemical hole-burned spectra of protonated and deuterated reaction centers of *Rhodobacter sphaeroides*. *J. Phys. Chem.* 97: 6924-6933.
176. Marquardt, D.W. (1963) An algorithm for least-squares estimation of nonlinear parameters. *J. Soc. Ind. Appl. Math.* 11: 431-441.
177. Martinez-Junza, V., Szczepaniak, M., Braslavsky, S.E., Sander, J., Nowaczyk, M., Rögner, M., and Holzwarth, A.R. (2008) A photoprotection mechanism involving the D₂ branch in photosystem II cores with closed reaction centers. *Photochem. Photobiol. Sci.* 7: 1337-1343.
178. Martinez-Junza, V., Szczepaniak, M., Braslavsky, S.E., Sander, J., Rögner, M., and Holzwarth, A.R. (2007) Triplet photocprotection by carotenoid in intact photosystem II cores. *Proceedings Photosynthesis Congress / Glasgow-England*. 001-007.
179. McCauley, S.W., Bittersmann, E., and Holzwarth, A.R. (1989) Time-resolved ultrafast blue-shifted fluorescence from pea chloroplasts. *FEBS Lett.* 249: 285-288.
180. McCauley, S.W., Bittersmann, E., Müller, M.G., and Holzwarth, A.R. (1990) Picosecond chlorophyll fluorescence from higher plants. In: (Baltscheffsky, M., Ed.) *Current Research in Photosynthesis*. II. Kluwer Academic Publishers, Dordrecht, pp. 297-300.
181. Melkozernov, A.N. and Blankenship, R.E. (2005) Structural and functional organization of the peripheral light-harvesting system in Photosystem I. *Photosynth. Res.* 85: 33-50.
182. Mewes, H. and Richter, M. (2002) Supplementary ultraviolet-B radiation induces a rapid reversal of the diadinoxanthin cycle in the strong light-exposed diatom *Phaeodactylum tricorutum*. *Plant Physiol.* 130: 1527-1535.
183. Miloslavina, Y., Szczepaniak, M., Müller, M.G., Sander, J., Nowaczyk, M., Rögner, M., and Holzwarth, A.R. (2006) Charge separation kinetics in intact photosystem II core particles is trap-limited. A picosecond fluorescence study. *Biochemistry*. 45: 2436-2442.

References

184. Miloslavina, Y., Wehner, A., Wientjes, E., Reus, M., Lambrev, P., Garab, G., Croce, R., and Holzwarth, A.R. (2008) Far-red fluorescence: A direct spectroscopic marker for LHCII oligomers forming in non photochemical quenching. *FEBS Lett.* 582: 3625-3631.
185. Mimuro, M. and Katoh, T. (1991) Carotenoids in photosynthesis: Absorption, transfer and dissipation of light energy. *Pure Appl. Chem.* 63: 123-130.
186. Morosinotto, T., Ballottari, M., Klimmek, F., Jansson, S., and Bassi, R. (2005) The association of the antenna system to photosystem I in higher plants. *J. Biol. Chem.* 280: 31050-31058.
187. Morosinotto, T., Caffarri, S., Dall'Osto, L., and Bassi, R. (2003) Mechanistic aspects of the xanthophyll dynamics in higher plant thylakoids. *Physiol. Plant.* 119: 347-354.
188. Moya, I., Silvestri, M., Vallon, O., Cinque, G., and Bassi, R. (2001) Time-resolved fluorescence analysis of the photosystem II antenna proteins in detergent micelles and liposomes. *Biochemistry.* 40: 12552-12561.
189. Mozzo, M., Dall'Osto, L., Hienerwadel, R., Bassi, R., and Croce, R. (2008) Photoprotection in the antenna complexes of photosystem II: Role of individual xanthophylls in chlorophyll triplet quenching. *J. Biol. Chem.* 283: 6184-6192.
190. Mullineaux, C.W., Pascal, A.A., Horton, P., and Holzwarth, A.R. (1993) Excitation energy quenching in aggregates of the LHC II chlorophyll-protein complex: A time-resolved fluorescence study. *Biochim. Biophys. Acta.* 1141: 23-28.
191. Munekage, Y., Takeda, S., Endo, T., Jahns, P., Hashimoto, T., and Shikanai, T. (2001) Cytochrome *b₆f* mutation specifically affects thermal dissipation of absorbed light energy in Arabidopsis. *Plant J.* 28: 351-359.
192. Murata, N., Takahashi, S., Nishiyama, Y., and Allakhverdiev, S.I. (2007) Photoinhibition of photosystem II under environmental stress. *Biochim. Biophys. Acta.* 1767: 414-421.
193. Müller, M.G. (1992) Picosekundenuntersuchungen an Photosyntheseantennen. Schriftenreihe des MPI für Strahlenchemie Nr. 65, ISSN 0932-5131.
194. Müller, M.G., Niklas, J., Lubitz, W., and Holzwarth, A.R. (2003) Ultrafast transient absorption studies on photosystem I reaction centers from *Chlamydomonas reinhardtii*. 1. A new interpretation of the energy trapping and early electron transfer steps in photosystem I. *Biophys. J.* 85: 3899-3922.
195. Müller, P., Li, X.-P., and Niyogi, K.K. (2001) Non-photochemical quenching. A response to excess light energy. *Plant Physiol.* 125: 1558-1566.
196. Nairn, J.A., Haehnel, W., Reisberg, P., and Sauer, K. (1982) Picosecond fluorescence kinetics in spinach chloroplasts at room temperature. Effects of Mg²⁺. *Biochim. Biophys. Acta.* 682: 420-429.
197. Naqvi, K.R., Melo, T.B., Bangar Raju, B., Javorfi, T., and Garab, G. (1997) Comparison of the absorption spectra of trimers and aggregates of chlorophyll *a/b* light-harvesting complex LHC II. *Spectrochim. Acta A.* 53: 1925-1936.
198. Nelson, N. and Ben-Shem, A. (2004) The complex architecture of oxygenic photosynthesis. *Nature Reviews Molecular Cell Biology.* 5: 971-982.
199. Nishiyama, Y., Allakhverdiev, S.I., and Murata, N. (2006) A new paradigm for the action of reactive oxygen species in the photoinhibition of photosystem II. *Biochim. Biophys. Acta.* 1757: 742-749.
200. Niyogi, K.K. (1999) Photoprotection revisited: Genetic and molecular approaches. *Annu. Rev. Plant Physiol. Plant Mol. Biol.* 50: 333-359.

201. Niyogi, K.K., Grossman, A.R., and Björkman, O. (1998) Arabidopsis mutants define a central role for the xanthophyll cycle in the regulation of photosynthetic energy conversion. *Plant Cell*. 10: 1121-1134.
202. Noctor, G., Rees, D., Young, A., and Horton, P. (1991) The relationship between zeaxanthin, energy-dependent quenching of chlorophyll fluorescence, and trans-thylakoid pH gradient in isolated chloroplasts. *Biochim. Biophys. Acta* . 1057: 320-330.
203. Novoderezhkin, V.I., Andrizhiyevskaya, E.G., Dekker, J.P., and van Grondelle, R. (2005) Pathways and timescales of primary charge separation in the photosystem II reaction center as revealed by a simultaneous. Fit of time-resolved fluorescence and transient absorption. *Biophys. J.* 89: 1464-1481.
204. Nuijs, A.M., van Gorkom, H.J., Plijter, J.J., and Duysens, L.N.M. (1986) Primary-charge separation and excitation of chlorophyll a in photosystem II particles from spinach as studied by picosecond absorbance-difference spectroscopy. *Biochim. Biophys. Acta*. 848: 167-175.
205. O'Connor, D.V. and Phillips, D. (1984) Time-correlated single photon counting, Academic Press, London.
206. Oudot-Le Secq, M.-P., Grimwood, J., Shapiro, H., Armbrust, E., Bowler, C., and Green, B. (2007) Chloroplast genomes of the diatoms *Phaeodactylum tricornutum* and *Thalassiosira pseudonana* : comparison with other plastid genomes of the red lineage. *Molecular Genetics and Genomics*. 277: 427-439.
207. Owens, T.G. (1986) Light-harvesting function in the diatom *Phaeodactylum tricornutum*. 2. Distribution of excitation energy between the photosystems. *Plant Physiol*. 80: 739-746.
208. Pagano, A., Cinque, G., and Bassi, R. (1998) *In vitro* reconstitution of the recombinant photosystem II light-harvesting complex CP24 and its spectroscopic characterization. *J. Biol. Chem*. 273: 17154-17165.
209. Palsson, L.-O., Dekker, J.P., Schlodder, E., Monshouwer, R., and van Grondelle, R. (1996) Polarized site-selective fluorescence spectroscopy of the long- wavelength emitting chlorophylls in isolated photosystem I particles of *Synechococcus elongatus*. *Photosynth. Res*. 48: 239-246.
210. Pascal, A., Gradinaru, C., Wacker, U., Peterman, E.J.G., Calkoen, F., Irrgang, K.-D., Horton, P., Renger, G., van Grondelle, R., Robert, B., and van Amerongen, H. (1999) Spectroscopic characterization of the spinach Lhcb4 protein (CP29), a minor light-harvesting complex of photosystem II. *Eur. J. Biochem*. 262: 817- 823.
211. Pascal, A.A., Liu, Z.F., Broess, K., van Oort, B., van Amerongen, H., Wang, C., Horton, P., Robert, B., Chang, W.R., and Ruban, A.V. (2005) Molecular basis of photoprotection and control of photosynthetic light-harvesting. *Nature*. 436: 134-137.
212. Paulsen, H., Finkenzeller, B., and Kühlein, N. (1993) Pigments induce folding of light-harvesting chlorophyll *a/b*- binding protein. *Eur. J. Biochem*. 215: 809-816.
213. Pearlstein, R.M. (1982a) Chlorophyll singlet excitons. In: (Govindjee, Ed.) Photosynthesis. Vol.1 Energy Conversion by Plants and Bacteria. Academic Press, New York, pp. 293-331.
214. Pearlstein, R.M. (1982b) Exciton migration and trapping in photosynthesis. *Photochem. Photobiol*. 35: 835-844.
215. Peltier, G. and Cournac, L. (2002) Chlororespiration. *Annual Review of Plant Biology*. 53: 523-550.
216. Pesaresi, P., Sandona, D., Giuffra, E., and Bassi, R. (1997) A single point mutation (E166Q) prevents dicyclohexylcarbodiimide binding to the photosystem II subunit CP29. *FEBS Lett*. 402: 151-156.

References

217. Peter, G.F. and Thornber, J.P. (1991) Biochemical composition and organization of higher plant photosystem II light-harvesting pigment-proteins. *J. Biol. Chem.* 266: 16745-16754.
218. Peterman, E.J.G., Gradinaru, C.C., Calkoen, F., Borst, J.C., van Grondelle, R., and van Amerongen, H. (1997) Xanthophylls in light-harvesting complex II of higher plants: Light harvesting and triplet quenching. *Biochemistry.* 36: 12208-12215.
219. Pfündel, E.E. and Bilger, W. (1994) Regulation and possible function of the violaxanthin cycle. *Photosynth. Res.* 42: 89-109.
220. Pieper, J., Irrgang, K.-D., Rätsep, M., Jankowiak, R., Schrötter, Th., Voigt, J., Small, G.J., and Renger, G. (1999) Effects of aggregation on trimeric light-harvesting complex II of green plants: A hole-burning study. *J. Phys. Chem. A.* 103: 2422-2428.
221. Plumley, F.G. and Schmidt, G.W. (1987) Reconstitution of chloroform *a/b* light-harvesting complexes: Xanthophyll-dependent assembly and energy transfer. *Proc. Natl. Acad. Sci. USA.* 84: 146-150.
222. Polivka, T. and Sundström, V. (2004) Ultrafast dynamics of carotenoid excited states-from solution to natural and artificial systems. *Chem. Rev.* 104: 2021-2071.
223. Prokhorenko, V.I. and Holzwarth, A.R. (2000) Primary processes and structure of the photosystem II reaction center: A photon echo study. *J. Phys. Chem. B.* 104: 11563-11578.
224. Prokhorenko, V.I., Steensgaard, D.B., and Holzwarth, A.R. (2000) Exciton dynamics in the chlorosomal antennae of the green bacteria *Chloroflexus aurantiacus* and *Chlorobium tepidum*. *Biophys. J.* 79: 2105-2120.
225. Provasoli, L., McLaughlin, J.J.A., and Droop, M.R. (1957) The development of artificial media for marine algae. *Arch. Microbiol.* 25: 392-428.
226. Pyszniak, A.M. and Gibbs, S.P. (1992) Immunocytochemical localization of photosystem I and the fucoxanthin-chlorophyll *a/c* light-harvesting complex in the diatom *Phaeodactylum tricorutum*. *Protoplasma.* 166: 208-217.
227. Rätsep, M., Johnson, T.W., Chitnis, P.R., and Small, G.J. (2000) The red-absorbing chlorophyll *a* antenna states of photosystem I: A hole-burning study of *Synechocystis* sp PCC 6803 and its mutants. *J. Phys. Chem. B.* 104: 836-847.
228. Remelli, R., Varotto, C., Sandona, D., Croce, R., and Bassi, R. (1999) Chlorophyll binding sites of monomeric light harvesting complex (LHCII) reconstituted *in vitro*: A mutation analysis of chromophore binding residues. *J. Biol. Chem.* 274: 33510-33521.
229. Renger, G. and Holzwarth, A.R. (2005) Primary Electron Transfer. In: (Wydrzynski, T.J. and Satoh, K., Eds.) *Photosystem II: The Light-Driven Water: Plastoquinone Oxidoreductase*. Springer Netherland, Berlin, pp. 139-175.
230. Renger, T. (2004) Theory of optical spectra involving charge transfer states: Dynamic localization predicts a temperature dependent optical band shift. *Phys. Rev. Lett.* 93: 188101-1-188101-4.
231. Robert, B., Horton, P., Pascal, A.A., and Ruban, A.V. (2004) Insights into the molecular dynamics of plant light-harvesting proteins *in vivo*. *Trends Plant Sci.* 9: 385-390.
232. Roelofs, T.A., Lee, C.-H., and Holzwarth, A.R. (1992) Global target analysis of picosecond chlorophyll fluorescence kinetics from pea chloroplasts. A new approach to the characterization of the primary processes in photosystem II α - and β -units. *Biophys. J.* 61: 1147-1163.
233. Rögner, M., Boekema, E.J., and Barber, J. (1996) How does photosystem 2 split water? The structural basis of efficient energy conversion. *Trends Biochem. Sci.* 21: 44-49.

234. Ruban, A.V., Berera, R., Illioaia, C., van Stokkum, I.H.M., Kennis, J.T.M., Pascal, A.A., van Amerongen, H., Robert, B., Horton, P., and van Grondelle, R. (2007) Identification of a mechanism of photoprotective energy dissipation in higher plants. *Nature*. 450: 575-578.
235. Ruban, A.V. and Horton, P. (1992) Mechanism of Δ pH-dependent dissipation of absorbed excitation energy by photosynthetic membranes. 1. Spectroscopic analysis of isolated light-harvesting complexes. *Biochim. Biophys. Acta*. 1102: 30-38.
236. Ruban, A.V. and Horton, P. (1994) Spectroscopy of non-photochemical and photochemical quenching of chlorophyll fluorescence in leaves Evidence for a role of the light harvesting complex of photosystem II in the regulation of energy dissipation. *Photosynth. Res.* 40: 181-190.
237. Ruban, A.V., Pascal, A.A., Robert, B., and Horton, P. (2002) Activation of zeaxanthin is an obligatory event in the regulation of photosynthetic light harvesting. *J. Biol. Chem.* 277: 7785-7789.
238. Ruban, A.V., Phillip, D., Young, A.J., and Horton, P. (1997) Carotenoid-dependent oligomerization of the major chlorophyll *a/b* light harvesting complex of photosystem II of plants. *Biochemistry*. 36: 7855-7859.
239. Ruban, A.V., Wentworth, M., Yakushevskaya, A.E., Andersson, J., Lee, P.J., Keegstra, W., Dekker, J.P., Boekema, E.J., Jansson, S., and Horton, P. (2003) Plants lacking the main light-harvesting complex retain photosystem II macro-organization. *Nature*. 421: 648-652.
240. Ruban, A.V., Young, A.J., and Horton, P. (1993) Induction of nonphotochemical energy dissipation and absorbance changes in leaves. *Plant Physiol.* 102: 741-750.
241. Salverda, J.M., Vengris, M., Krueger, B.P., Scholes, G.D., Czamoleski, A.R., Novoderezhkin, V., van Amerongen, H., and van Grondelle, R. (2003) Energy transfer in light-harvesting complexes LHClI and CP29 of spinach studied with three pulse echo peak shift and transient grating. *Biophys. J.* 84: 450-465.
242. Sapozhnikov, D.I., Krasovskaya, T.A., and Mayevskaya, A.N. (1957) Changes observed in the reflection between the main carotinoids in the plastids of green leaves exposed to light. *Dokl. Akad. Nauk SSSR*. 113: 465-467.
243. Satoh, K. and Nanba, O. (1987) Isolation of a photosystem II reaction center consisting of gamma and delta subunits (D-1 and D-2) and cytochrome b-559. *Prog. Photosynth. Res.* II: 69-72.
244. Schatz, G.H., Brock, H., and Holzwarth, A.R. (1987) Picosecond kinetics of fluorescence and absorbance changes in photosystem II particles excited at low photon density. *Proc. Natl. Acad. Sci. USA*. 84: 8414-8418.
245. Schatz, G.H., Brock, H., and Holzwarth, A.R. (1988) A kinetic and energetic model for the primary processes in photosystem II. *Biophys. J.* 54: 397-405.
246. Sener, M.K., Jolley, C., Ben-Shem, A., Fromme, P., Nelson, N., Croce, R., and Schulten, K. (2005) Comparison of the light-harvesting networks of plant and cyanobacterial Photosystem I. *Biophys. J.* 89: 1630-1642.
247. Sener, M.K., Lu, D.Y., Ritz, T., Park, S., Fromme, P., and Schulten, K. (2002) Robustness and optimality of light harvesting in cyanobacterial photosystem I. *J. Phys. Chem. B*. 106: 7948-7960.
248. Sener, M.K., Park, S., Lu, D.Y., Damjanovic, A., Ritz, T., Fromme, P., and Schulten, K. (2004) Excitation migration in trimeric cyanobacterial photosystem I. *J. Chem. Phys.* 120: 11183-11195.
249. Simidjiev, I., Barzda, V., Mustárdy, L., and Garab, G. (1997) Isolation of lamellar aggregates of the light-harvesting chlorophyll *a/b* protein complex of photosystem II with long-range chiral order and structural flexibility. *Anal. Biochem.* 250: 169-175.

References

250. Slavov, C., Ballottari, M., Morosinotto, T., Bassi, R., and Holzwarth, A.R. (2008) Trap-limited charge separation kinetics in higher plant photosystem I complexes. *Biophys. J.* 94: 3601-3612.
251. Smith, K.M. (1991) Chemistry of chlorophylls: Synthesis. In: (Scheer, H., Ed.) Chlorophylls. CRC Press, Boca Raton, pp. 115-143.
252. Snyder, A.M., Clark, B.M., Robert, B., Ruban, A.V., and Bungard, R.A. (2004) Carotenoid specificity of light-harvesting complex II binding sites: Occurrence of 9-cis-violaxanthin in the neoxanthin-binding site in the parasitic angiosperm *Cuscuta refelexa*. *J. Biol. Chem.* 279: 5162-5168.
253. Standfuss, J., van Scheltinga, A.C.T., Lamborghini, M., and Kühlbrandt, W. (2005) Mechanisms of photoprotection and nonphotochemical quenching in pea light-harvesting complex at 2.5Å resolution. *EMBO J.* 24: 919-928.
254. Strasser, R.J., Srivastava, A., and Govindjee (1995) Polyphasic chlorophyll *a* fluorescence transient in plants and cyanobacteria. *Photochem. Photobiol.* 61: 32-42.
255. Strasser, R.J., Tsimilli-Michael, M., and Srivastava, A. (2004) Analysis of the chlorophyll *a* fluorescence transient. In: (Papageorgiou, G.C. and Govindjee, Eds.) Advances in Photosynthesis and Respiration Vol.19: Chlorophyll *a* Fluorescence: A Signature of Photosynthesis. Springer, Dordrecht, pp. 321-362.
256. Stroh, M., Spunda, V., and Kurasova, I. (2004) Non-radiative dissipation of absorbed excitation energy within photosynthetic apparatus of higher plants. *Photosynthetica.* 42: 323-337.
257. Szabó, M., Lepetit, B., Goss, R., Wihelm, C., Mustárdy, L., and Garab, G. (2008) Structurally flexible macro-organization of the pigment-protein complexes of the diatom *Phaeodactylum tricornutum*. *Photosynth. Res.* 95: 237-245.
258. Szczepaniak, M., Sander, J., Nowaczyk, M., Müller, M.G., Rögner, M., and Holzwarth, A.R. (2008) Charge separation, stabilization, and protein relaxation in photosystem II core particles with closed reaction center. *Biophys. J.* In press: 000-000.
259. Takizawa, K., Cruz, J.A., Kanazawa, A., and Kramer, D.M. (2007) The thylakoid proton motive force *in vivo*. Quantitative, non-invasive probes, energetics, and regulatory consequences of light-induced pmf. *Biochimica et Biophysica Acta (BBA) - Bioenergetics.* 1767: 1233-1244.
260. Teardo, E., Polverino-De Laureto, P., Bergantino, E., Vecchia, F.D., Rigoni, F., Szabó, I., and Giacometti, G.M. (2007) Evidences for interaction of PsbS with photosynthetic complexes in maize thylakoids. *Biochim. Biophys. Acta.* 1767: 703-711.
261. Ting, C.S. and Owens, T.G. (1993) Photochemical and nonphotochemical fluorescence quenching processes in the diatom *Phaeodactylum tricornutum*. *Plant Physiol.* 101: 1323-1330.
262. Ting, C.S. and Owens, T.G. (1994) The effects of excess irradiance on photosynthesis in the marine diatom *Phaeodactylum tricornutum*. *Plant Physiol.* 106: 763-770.
263. Toth, S.Z., Schansker, G., and Strasser, R.J. (2005) In intact leaves, the maximum fluorescence level (F_M) is independent of the redox state of the plastoquinone pool: A DCMU-inhibition study. *Biochim. Biophys. Acta.* 1708: 275-282.
264. Trinkunas, G. and Holzwarth, A.R. (1996) Kinetic modeling of exciton migration in photosynthetic systems: 3. Application of genetic algorithms to simulations of excitation dynamics in three-dimensional photosystem I core antenna/reaction center complexes. *Biophys. J.* 71: 351-364.
265. Trissl, H.-W. and Wilhelm, C. (1993) Why do thylakoid membranes from higher plants form grana stacks? *Trends. Biochem. Sci.* 18: 415-419.

266. van Amerongen, H., Valkunas, L., and van Grondelle, R. (2000) Photosynthetic Excitons, World Scientific, Singapore.
267. van Amerongen, H. and van Grondelle, R. (2001) Understanding the energy transfer function of LHCII, the major light-harvesting complex of green plants. *J. Phys. Chem. B.* 105: 604-617.
268. van Grondelle, R. and Gobets, B. (2004) Transfer and trapping of excitations in plant photosystems. In: (Papageorgiou, G.C. and Govindjee, Eds.) Advances in Photosynthesis and Respiration Vol.19: Chlorophyll a Fluorescence: A Signature of Photosynthesis. Springer, Dordrecht, pp. 107-132.
269. van Leeuwen, P.J., Nieveen, M.C., van de Meent, E.J., Dekker, J.P., and van Gorkom, H.J. (1991) Rapid and simple isolation of pure photosystem II core and reaction center particles from spinach. *Photosynth. Res.* 28: 149-153.
270. van Mourik, F., Van der Oord, C.J.R., Visscher, K.J., Parkes-Loach, P.S., Loach, P.A., Visschers, R.W., and van Grondelle, R. (1991) Exciton interactions in the light-harvesting antenna of photosynthetic bacteria studied with triplet- singlet spectroscopy and singlet-triplet annihilation on the B820 subunit form of *Rhodospirillum-rubrum*. *Biochim. Biophys. Acta.* 1059: 111-119.
271. van Oort, B., van Hoek, A., Ruban, A.V., and van Amerongen, H. (2007) Aggregation of light-harvesting complex II leads to formation of efficient excitation energy traps in monomeric and trimeric complexes. *FEBS Lett.* 581: 3528-3532.
272. van Stokkum, I.H.M., Larsen, D.S., and van Grondelle, R. (2004) Global and target analysis of time-resolved spectra. *Biochim. Biophys. Acta.* 1657: 82-104.
273. Vasil'ev, S., Orth, P., Zouni, A., Owens, T.G., and Bruce, D. (2001) Excited-state dynamics in photosystem II: Insights from the x-ray crystal structure. *Proc. Natl. Acad. Sci.* 98: 8602-8607.
274. Vasil'ev, S., Shen, J.-R., Kamiya, N., and Bruce, D. (2004) The orientations of core antenna chlorophylls in photosystem II are optimized to maximize the quantum yield of photosynthesis. *FEBS Lett.* 561: 111-116.
275. Vassiliev, S., Lee, C.-I., Brudvig, G.W., and Bruce, D. (2002) Structure-based kinetic modeling of excited-state transfer and trapping in histidine-tagged photosystem II core complexes from *Synechocystis*. *Biochemistry.* 41: 12236-12243.
276. Vredenberg, W.J. (2004) System analysis and photoelectrochemical control of chlorophyll fluorescence in terms of trapping models of photosystem II: A challenging view. In: (Papageorgiou, G.C. and Govindjee, Eds.) Advances in Photosynthesis and Respiration Vol.19: Chlorophyll a Fluorescence: A Signature of Photosynthesis. Springer, Dordrecht, pp. 133-172.
277. Walters, R.G., Ruban, A.V., and Horton, P. (1994) Higher plant light-harvesting complexes LHCIIa and LHCIIc are bound by dicyclohexylcarbodiimide during inhibition of energy dissipation. *Eur. J. Biochem.* 226: 1063-1069.
278. Wehner, A., Grasses, T., and Jahns, P. (2006) De-epoxidation of violaxanthin in the minor antenna proteins of photosystem II, LHCB4, LHCB5, and LHCB6. *J. Biol. Chem.* 281: 21924-21933.
279. Wilhelm, C., Büchel, C., Fisahn, J., Goss, R., Jakob, T., LaRoche, J., Lavaud, J., Lohr, M., Riebesell, U., Stehfest, K., Valentin, K., and Kroth, P.G. (2006) The regulation of carbon and nutrient assimilation in diatoms is significantly different from green algae. *Protist.* 157: 91-124.
280. Wilhelm, C., Volkmar, P., Lohmann, C., Becker, A., and Meyer, M. (1995) The HPLC-aided pigment analysis of phytoplankton cells as a powerful tool in water-quality control. *J. Water Supply Technol.* 44: 132-141 .

References

281. Wollenberger, L., Stefansson, H., Yu, S.-G., and Albertsson, P.-A. (1994) Isolation and characterization of vesicles originating from the chloroplast grana margins. *Biochim. Biophys. Acta.* 1184: 93-102.
282. Wraight, C.A. and Crofts, A.R. (1970) Cellular Biochemistry and Metabolism Energy-dependent quenching of chlorophyll *a* fluorescence in isolated chloroplasts. *Eur. J. Biochem.* 17: 319-327.
283. Yakushevskaya, A.E., Jensen, P.E., Keegstra, W., van Roon, H., Scheller, H.V., Boekema, E.J., and Dekker, J.P. (2001) Supermolecular organization of photosystem II and its associated light-harvesting antenna in *Arabidopsis thaliana*. *Eur. J. Biochem.* 268: 6020-6028.
284. Yakushevskaya, A.E., Keegstra, W., Boekema, E.J., Dekker, J.P., Andersson, J., Jansson, S., Ruban, A.V., and Horton, P. (2003) The structure of photosystem II in *Arabidopsis*: Localization of the CP26 and CP29 antenna complexes. *Biochemistry.* 42: 608-613.
285. Yamamoto, H.Y. and Higashi, R.M. (1978) Violaxanthin De-Epoxidase. Lipid composition and substrate specificity. *Arch. Biochem. Biophys.* 190: 514-522.
286. Yang, M., Damjanovic, A., Vaswani, H.M., and Fleming, G.R. (2003) Energy transfer in photosystem I of cyanobacteria *Synechococcus elongatus*: Model study with structure-based semi-empirical Hamiltonian and experimental spectral density. *Biophys. J.* 85: 140-158.
287. Zhu, S.-H. and Green, B.R. (2008) Light-harvesting and photoprotection in diatoms: Identification and expression of L818-like proteins. In: (Allen, J.F., Gantt, E., Golbeck, J.H., and Osmond, B.R., Eds.) *Photosynthesis. Energy From the Sun: 14th International Congress on Photoynthesis.* Springer, Dordrecht, pp. 261-264.
288. Zouni, A., Witt, H.T., Kern, J., Fromme, P., Krauss, N., Saenger, W., and Orth, P. (2001) Crystal structure of photosystem II from *Synechococcus elongatus* at 3.8 Å resolution. *Nature.* 409: 739-743.

LIST OF PUBLICATIONS

1. Miloslavina, Y., Szczepaniak, M., Müller, M.G., Sander, J., Nowaczyk, M., Rögner, M., and Holzwarth, A.R. 2006. Charge separation kinetics in intact photosystem II core particles is trap-limited. A picosecond fluorescence study. *Biochemistry* 45:2436-2442.
2. Miloslavina, Y., Wehner, A., Lambrev, P.H., Wientjes, E., Reus M., Garab, G., Croce, R., and Holzwarth, A.R. 2008. Far-red fluorescence: A direct spectroscopic marker for LHC II oligomer formation in non-photochemical quenching. *FEBS Lett.* 582:3625-3631.
3. Lambrev, P., Varkonyi, Z., Krumova, S., Kovacs, L., Miloslavina, Y., Holzwarth, A.R., and Garab, G. 2007. Importance of trimer-trimer interactions for the native state of the plant light-harvesting complex II. *Biochim. Biophys. Acta* 1767:847-853.
4. Holzwarth, A.R., Miloslavina, Y., Nilkens, M., and Jahns P. 2008. Identification of two quenching sites active in the regulation of photosynthetic light-harvesting. *Science*. Submitted.
5. Miloslavina, Y., Grouneva, I., Goss, R., Wilhelm, C., and Holzwarth, A.R. 2008. On the location of non-photochemical quenching in diatoms. *BBA*, submitted.
6. Miloslavina, Y., Wehner, A., and Holzwarth, A.R. Energy transfer and charge separation kinetics in photosystem II particles from spinach. A second generation exciton/radical pair equilibrium model for photosystem II from higher plants. In preparation.

Publications not included in the thesis

7. Röger, C., Müller, M.G., Lysetska, M., Miloslavina, Y., Holzwarth, A.R., and Würthner, F. 2006. Efficient energy transfer from peripheral chromophores to the self-assembled zinc chlorin rod antenna: A bioinspired light-harvesting system to bridge the "Green Gap". *J. Am. Chem. Soc.* 128:6542-6543.
8. Röger, C., Miloslavina, Y., Brunner, D., Holzwarth, A.R., and Würthner, F. 2008. Self-assembled zinc chlorin rod antennae powered by peripheral light-harvesting chromophores. *J. Am. Chem. Soc.* 130:5929-5939.

SPECIAL THANKS

I would like to express my gratitude to Prof. Dr. Alfred R. Holzwarth for giving me the chance to work on a fascinating topic guiding me through the world of photosynthesis, for keeping me always motivated and encouraged. I also appreciate the opportunity to attend many interesting international conferences.

I am thankful to Prof. Dr. Karl Kleinermanns who agreed to be my co-supervisor and to Prof. Dr. Wolfgang Lubitz to whom I owe my place at the Max-Planck-Institut für Bioanorganische Chemie. I am especially grateful to Dr. Marc Müller, Michael Reus and Dr. Antje Werner for their support with the experimental work. My sincerest thanks go to Dr. Petar H. Lambrev for his help, proof reading and editing my thesis. I also thank Sasha Marchanka and the colleagues of my group, also the workers at the mechanical workshop, Hartmut Ulbrich and Stephan Syring. Thanks to Heike Deinert for managing our literature database and to Christopher Kley for his help.

Many parts of this work were done in collaboration with a number of other research groups. I thank my collaborators who provided the biological samples and helped with their handling. Thanks to Manuela Nilkens and Prof. Dr. Peter Jahns from HHU Düsseldorf; Silvia de Bianchi and Prof. Dr. Roberto Bassi from the University of Verona Irina Grouneva and Prof. Dr. Christian Wilhelm from the University of Leipzig; Julia Sander and Prof. Dr. Matthias Rögner from Ruhr-Universität Bochum; Dr. Petar H. Lambrev, Prof. Dr. Roberta Croce, University of Groningen; Győző Garab, Biological Research Center, Szeged.

Special regards are for my parents for understanding and for their loving support and for my sister who started everything.